輔仁學誌—理工類

中華民國九十八年十二月　　第四十三期

目　錄

FU JEN STUDIES

SCIENCE AND ENGINEERING

No.43, Dec.2009

CONTENTS

Troglitazone抑制高度醣化終產物在人類胚胎腎臟細胞所引起的反應

簡志豪、崔文慧、梁耀仁*

輔仁大學理工學院生命科學系所

摘　要

隨著生活水準的提高及飲食的過度精緻化，國人的平均壽命逐漸延長，老年人口持續增加，慢性疾病逐漸成為威脅國人健康的重要疾病。近年來，糖尿病已經成為國人的十大死因之一，另外因糖尿病所造成的併發症-糖尿腎病變，也已經成為腎病變的主要原因，約有三分之一的腎病變患者都是起因於糖尿腎病變。目前在第二型糖尿病的治療中，常利用Thiazolidinedione (TZD)來進行治療，TZD是透過刺激細胞核表面接受器peroxisome proliferator activated receptor gamma (PPAR γ)來達到治療第二型糖尿病的效果。但PPAR γ致效劑是否具有保護腎臟細胞的效果，仍舊不甚清楚。高度糖化終產物（advanced glycation end products, AGE）目前被認為是造成糖尿腎病變的主因之一。因此，在本研究中嘗試使用AGE在體外模擬糖尿腎病變的發生，接著加入PPAR γ致效劑troglitazone (TGZ)，觀察細胞的反應為何，進一步探討PPAR γ致效劑在糖尿腎病變中的相關保護機制為何。

在HEK293T細胞加入AGE後，的確會引起細胞中TNF α、IL-6的增加，而導致發炎反應的產生。此外，AGE所引起的AGE接受器（RAGE）RNA的表現量也會增加。而在加入TGZ會降低細胞激素TNF α、IL-6 的量，但並不會明顯抑制AGE向上調節的RAGE表現量。另外AGE所引起的superoxide dismutase降低，在加入TGZ後也有明顯增加的情形，推測可因而減少AGE造成氧化壓力的增加狀況。

因此，從本研究可以瞭解AGE所引起的細胞反應，可以藉由PPAR γ致效劑來減少其影響，希望可透過本研究來了解PPAR γ致效劑對於糖尿腎病變的保護機制，以期達到改善糖尿腎病變的狀況。

關鍵字：PPAR γ致效劑、高度糖化終產物、糖尿腎病變、發炎反應、接受器

* Correspondence: 梁耀仁，輔仁大學理工學院生命科學系所，台北縣新莊市中正路510號
Tel: (886)-2-29053593 Fax: (886)-2-29052193 E-mail: 071558@mail.fju.edu.tw

1.前 言

糖尿病是一種因為體內胰島素絕對或者相對不足所導致的疾病。糖尿病病人的主要特徵是為多飲 (Polydipsia)、多尿 (Polyuria)、多食 (Polyphagia) 和體重下降 (Loss of body weight)，以及血糖高、尿液中含有葡萄糖等。糖尿腎病變(diabetic nephropathy)也稱為Kimmelstiel-Wilson syndrome或者intercapillary glomerulonephritis，是糖尿病在腎臟組織所引起的糖尿病併發症。糖尿腎病變是由Clifford Wilson和Paul Kimmelstiel發現並在西元1936年所發表[1]。糖尿病所產生的腎病變通常是因為腎臟組織產生一連串不同的結構變化，例如腎臟肥大、基底膜增厚以及細胞間質的累積 [2]，而腎臟肥大更是糖尿腎病變早期病徵中的一種，主要是因為細胞間質的異常累積，以及腎臟環間膜細胞的過度增生所造成的。糖尿腎病變的病徵會被發現是因為腎絲球增厚，最後導致腎衰竭。

在之前的研究也發現糖尿腎病變的發病過程中，腎絲球的基底膜增厚與一些發炎的相關因子有關，例如Interleukin-6 (IL-6)、fibrinogen、C-reactive protein (CRP)以及serum amyloid (SAA)，其中IL-6會刺激腎間質細胞的增生，增加fibronectin 表現以及內皮細胞的通透性，而且在糖尿病鼠的實驗中發現，糖尿病鼠的腎絲球基底膜會產生較多量的IL-6和tumor necrosis factor -alpha (TNFα) [3]。也有研究指出糖尿腎病變中所引起的蛋白尿可以透過抑制Protein-kinase C (PKC)來達到減少的效果，而Protein-kinase C (PKC)則會活化糖尿病或一些細胞的傳遞反應，包括發炎因子的表現或細胞激素的增加 [4]，例如增加TNFα的表現，導致對於腎臟細胞的傷害 [5]。另外在之前的研究也有提出，糖尿腎病變初期的相關腎臟病變，TNFα對於腎臟肥大扮演著關鍵性的因素 [6]。

糖尿病中的高血糖會加速高度醣化終產物(Advanced glycation end-product, AGE)的生成與累積 [7]，導致糖尿病併發症如糖尿腎病變的產生。AGE是一類經由糖基化的產物，確信是造成糖尿腎病變的主因之一 [8]。也有研究指出長期暴露在AGE-rat血清白蛋白中的正常老鼠腎臟會出現腎絲球肥大以及腎絲球硬化的病徵 [9]。AGE主要是經由體內的葡萄糖與蛋白質上的胺基結合成Schiff base中間產物，在經過Amadori骨架成排而形成穩定的蛋白質與葡萄糖的衍生物，如果繼續進行重組則會形成不可逆的高度糖化終產物。同時AGE所造成的基底膜蛋白的交互連結，會增加基底膜對巨分子的通透性，導致蛋白尿的產生。而之前的研究發現，AGE會與其受器RAGE (receptor for AGE)結合，會加速高度糖化終產物修飾後的蛋白質的代謝，另一方面則會促進細胞激素或

生長因子的釋放與合成，也會導致細胞外間質的合成與分泌 [10]。其他研究也發現在糖尿病大鼠中的AGE會影響一氧化氮媒介的訊息傳遞，包括神經傳導、傷口癒合以及血流通透等等。因此AGE可藉由影響一氧化氮的生理功能或一氧化氮合成(nitric oxide synthase)，導致糖尿腎病變的形成。

過氧化體增殖劑活化受體(Peroxisome proliferation-activated receptors, PPAR)為一類核內轉錄因子，在其蛋白質上都含有ligand binding domain (LBD)及DNA binding domain (DBD)，因此可藉由ligand的刺激而活話PPAR進入細胞核的能力，已知有許多的脂肪酸可作為ligand而活化PPAR進入細胞核[11]，接者利用DBD與基因啟動區序列上含peroxisome proliferation response element (PPRE)結合而達到基因轉錄活化的功能，PPAR也可與核內受體retinoid X receptor (RXR)形成heterodimer進而調控基因活化。目前研究發現PPAR 家族由三種成員組成，分別為PPAR α ，PPAR β/δ ，PPAR γ [12]。PPAR γ 則有兩個isoforms: PPAR γ 1和PPAR γ 2。PPAR γ 1的分布相當普遍，而PPAR γ 2主要分布在脂肪組織、大腸及巨噬細胞中 [13]。前人研究顯示PPAR γ 的配體在許多實驗動物模式中，具有抗發炎的效果，TGZ是PPAR γ 致效劑之一，分子量為441.541 KDas，具有抗發炎以及抗糖尿病的效果，已經被用來當作二型糖尿病的治療藥劑 [14]。

2. 材料與方法

HEK293T細胞培養：

本研究所使用的HEK293T細胞是屬於人類胚胎腎細胞轉染五型腺病毒(Ad 5) DNA的細胞株。HEK293T於15公分的培養皿中使用Dulbecco's modified eagle medium (DMEM; Gibco)細胞培養液培養，內含3.7g/L NaHCO3、100 μM antibiotic-antimycotic (Gibco)、10%的胎牛血清 (Fetal bovine serum；FBS)。細胞培養於37℃、5%CO_2細胞培養箱 (CO_2 Air-Jacketed incubator；NUAIRE)中。

HEK293T細胞核醣核酸的抽取(RNA extraction)：

採用single-step method of RNA isolation的方法加以修飾。首先將適量的TRI_{ZOL}Reagent (Invitrogen) 加入細胞培養皿中，以cell lifter將細胞刮下，倒入離心管中，加入氯仿chloroform (0.2 mL cholorform/mL TRIzol Reagent)，混合均勻後，靜置於室溫中十分鐘。之後將離心管以14000 rpm，4℃，離心10分鐘。離心完後，取上清液至

另一離心管中，再加入異丙醇isopropanol (0.5 mL isopropanol/ mL TRIzol Reagent)，混合均勻後，靜置於-20℃中一小時，再以14000 rpm，4℃，離心15分鐘。倒掉上清液，加入70% 酒精Ethanol (1 mL 70% ethanol/ mL TRIzol Reagent)與pellet沖洗混合後，再以14000 rpm，4℃，離心10分鐘。去上清液後，加入27 μL的DEPC水充分溶解pellet。之後取出5 μL溶液稀釋一百倍後，利用分光光度計，來測量其OD_{260}及OD_{280}的吸光值，以判定RNA的濃度。

同步定量聚合酶連鎖反應 (Real-time quantitative PCR)：

實驗以Smart Quant Qreen Master Mix with dUTP and ROX (Protech Technology Enterprise Co.) 進行反應產物標誌，以StepOne™ Real-Time PCR System (Applied Biosystems Inc.；ABI) 偵測結果。20 μL 的混合液中內含10 μl 的Smart Quant Green Master Mix、 0.4 μL的MgCl2 (25 mM)、2 μL的Forward and Reverse Promers (1 μM)、2.5 μL 的cDNA (50 ng) 和3.1 μL 的Nuclease-Free Water。反應條件為95℃10分鐘；95℃15秒、60℃60秒共循環40次；95℃15 秒 、60℃60 秒、95℃15 秒 。所得數據為各個基因的C_t值。

數據計算方式如下(Applied Biosysterms)：

1. Ct Target-Ct Endogenous control= ΔC_t
2. ΔCt Sample- ΔCt Calibrator= $\Delta\Delta C_t$
3. 利用公式:$2^{-\Delta\Delta Ct}$ 得到所需的數值。

所使用之引子如下：

Genes	Primers		bp (base pair)
RAGE	S:5'	AAG CCC CTG GTG CCT AAT GAG3	240
	AS:5'	CAC CAA TTG GAC CTC CTC CA3'	
GAPDH	S:5'	CGA CCA CTT TGT CAA GCT CA3	228
	AS:5'	AGG GGT CTA CAT GGC AAC TG 3'	

細胞毒性試驗(Cytotoxicity studies)：

使用WST-8 Kit進行細胞毒性測試，將HEK293T細胞培養在96孔盤中，在處理藥物之前，使用PBS清洗兩次，加入不含血清的medium培養六小時後，接著加入PPAR γ 致效劑TGZ處理18小時，然後在各孔內加入10 μL 的WST-8溶液，接著在二氧化碳培養箱中培養一到四小時後，觀察其呈色反應，再利用ELISA Reader (Benchmark Plus

Microplate Reader)測量OD_{450} nm吸光值。當吸光值越低，代表對細胞毒性越強。

氧化壓力測試(oxidative stress test)：

本實驗使用Superoxide Dismutase Assay Kit (catalog no.706002，Cayman chem)。將細胞種入6cm的培養皿中，在處理藥物之前，使用PBS清洗兩次，加入不含血清的medium培養六小時後，接著加入AGE以及TGZ處理18小時，收取medium進行後續處理。首先將medium在4℃離心2000g，15分鐘，取上清液，以1(medium):5(sample buffer:50 mM Tris-HCl，pH 8.0)的方式稀釋後，置於冰上。之後在96孔盤中，每個SOD Standard well加入200 μL的diluted radicak detector(50 μL的radical detector + 19.95 mL的diluted Assay Buffer)和10 μL standard，而每個sample well則加入200 μL的diluted radicak detector和10 μL的sample。在每個well中加入20 μL的diluted xanthine oxidase (10倍稀釋)後，在室溫反應20分鐘，之後使用ELISA Reader (Benchmark Plus Microplate Reader)測其吸光值440-460nm。

酵素免疫分析(Enzyme-Linked ImmunoSorbent Assay)：

(1) TNF-α之含量測定：

利用Human TNF-α ELISA development kit (PEROTECH INC.)來測定medium中的TNF-α含量。將細胞種入6cm的培養皿中，在處理藥物之前，使用PBS清洗兩次，加入不含血清的medium培養六小時後，接著加入AGE以及TGZ處理18小時，收取medium進行後續處理。使用kit中的Capture Antibody(利用PBS稀釋至1 μg/mL)每個well加入100 μL在96孔盤中，培養過夜。之後將96孔盤中的液體移除，在每個well加入300 μL的wash buffer (0.05 % Tween-20 in PBS)洗四次後，再加入300 μL的block buffer (1% BSA in PBS)。靜置於室溫一個小時後，將液體移除，在每個well加入300 μL的wash buffer (0.05% Tween-20 in PBS) 洗四次後，在每個well加入100 μL的代測樣品或者標準液(2ng/mL to zero)，靜置於室溫最少兩小時。之後將液體移除，在每個well加入300 μL的wash buffer (0.05% Tween-20 in PBS)洗四次後，每個well加入100 μL的Detection antibody (稀釋至0.5 μg/mL)，靜置於室溫兩小時。之後將液體移除，在每個well加入300 μL的wash buffer(0.05% Tween-20 in PBS)洗四次後，每個well加入100 μL的Avidin-HRP Conjugate稀釋液 [5.5 μL Avidin-HRP Conjugate加入diluent buffer (0.05% Tween-20，0.1% BSA in PBS)補到11 mL]，靜置於室溫30分鐘，將液體移除，在每個well加入300 μL的wash buffer (0.05% Tween-20 in PBS)洗四次，利用ABTS Liquid Substrate呈色，利用ELISA Reader (Benchmark Plus Microplate Reader)測其405nm的吸光值。

(2) IL-6之含量測定：

利用Human IL-6 ELISA development kit (PEROTECH INC.)來測定medium中的IL-6含量。將細胞種入6cm的培養皿中，在處理藥物之前，使用PBS清洗兩次，加入不含血清的medium培養六小時後，接著加入AGE以及TGZ處理18小時，收取medium進行後續處理。使用KIT中的Capture Antibody (利用PBS稀釋至1 μg/ml)每個well加入100 μL在96孔盤中，培養過夜。之後將96孔盤中的液體移除，在每個well加入300 μL的wash buffer(0.05% Tween-20 in PBS)洗四次後，再加入300 μL的block buffer (1% BSA in PBS)。靜置於室溫一個小時後，將液體移除，在每個well加入300 μL的wash buffer (0.05% Tween-20 in PBS)洗四次後，在每個well加入100 μL的代測樣品或者標準液(2 ng/mL to zero)，靜置於室溫最少兩小時。之後將液體移除，在每個well加入300 μL的wash buffer (0.05% Tween-20 in PBS)洗四次後，每個well加入100 μL的Detection antibody (稀釋至0.25 μg/mL)，靜置於室溫兩小時。之後將液體移除，在每個well加入300 μL的wash buffer (0.05% Tween-20 in PBS)洗四次，之後每個well加入100 μL的Avidin-HRP Conjugate稀釋液[5.5 μL Avidin-HRP Conjugate加入diluent buffer (0.05% Tween-20，0.1% BSA in PBS)補到11mL，靜置於室溫30分鐘，將液體移除，在每個well加入300 μL的wash buffer (0.05% Tween-20 in PBS)洗四次，利用ABTS Liquid Substrate呈色，利用ELISA Reader (Benchmark Plus Microplate Reader)測其405nm的吸光值。

統計分析(Statistical analysis)：

實驗數據以平均值±平均標準誤差(mean±standard error of mean)表示。利用LSD test比較各實驗組與對照組的數據差異。當P值<0.05則表示在統計學上有顯著差異。

3. 結　果

1. PPAR致效劑或EGCG對於HEK293T細胞株的毒性影響

為了探討PPAR γ 致效劑TGZ對於細胞的影響，首先要先確定所加入的藥物PPAR γ 致效劑TGZ在高劑量下是否會對HEK293T細胞株產生毒性傷害，才能進一步進行有關HEK293T細胞的後續實驗。將HEK293T細胞培養在96孔盤中，在處理藥物之前，使用PBS清洗兩次，加入不含血清的medium培養六小時後，接著加入100 μM TGZ 18小時，再利用WST-8 KIT測試在本研究中所處理的100 μM TGZ 濃度下會不會導致HEK293T細

胞產生死亡的反應。

在本研究中所使用的TGZ的濃度為實驗中細胞用藥濃度的十倍，而如圖一所示，當TGZ為十倍劑量濃度的時候，對於所培養的HEK293T細胞株產生的細胞毒性幾乎是沒有的。

2. 處理TGZ對於AGE所引起的細胞發炎反應的影響

在先前的研究報告中有提出AGE都會引起糖尿腎病變產生相關發炎反應，因此本研究藉由觀察TNF-α以及IL-6兩種重要的發炎激素在HEK293T細胞株中量的變化。 探討在加入AGE所引起的發炎反應後，TGZ對於發炎反應的影響。將HEK293T細胞種入6well plate的培養皿中，在處理藥物之前，使用PBS清洗兩次，加入不含血清的medium培養六小時後，接著加入AGE以及10 μM TGZ處理18小時，收取medium，利用ELISA KIT分析發炎相關細胞激素TNF-α ，IL-6的表現量。

如圖二所示，加入AGE對於細胞中的TNF-α以及IL-6的表現量都有明顯增加，確定實驗中所處理的AGE可以對細胞產生發炎反應。而在加入TGZ處理後，可以看到由AGE所引起的TNF-α以及IL-6增加，都有被抑制的效果，因此我們可以知道加入AGE會引起細胞的發炎反應產生，另外透過加入TGZ處理後可以降低其發炎反應的產生。

3. TGZ對於AGE所引起的RAGE mRNA的相關表現量。

為了瞭解在處理AGE後所引起的細胞反應，是否可以透過PPAR γ 致效劑來降低其反應，因此我們利用real-time PCR來觀察處理細胞後AGE的受器RAGE的表現。進一步了解是否可以透過AGE來誘導RAGE表現，並且透過TGZ可以減少RAGE的表現量。

如圖三，在real-time PCR的結果可以看到，加入AGE會造成RAGE mRNA的增加，但經過PPAR γ 致效劑TGZ則沒有明顯抑制AGE所誘導的RAGE表現變化。

4. TGZ對於AGE所引發的氧化壓力關係

在前人的研究中有提出糖尿病的慢性併發症與氧化壓力有關，像是體內抗氧化酵素glutathione peroxidase (GSH Px)及superoxidase dismutase (SOD)均與HbA1c有呈負相關的趨勢 [15]，而且在第二型糖尿病患中也發現，具有保護避免氧化傷害的因子，如尿酸、維生素C及維生素E在血漿中的濃度均低於一般正常組 [16]，因此在本實驗中利用

SOD assay kit 測試AGE是否會引起氧化壓力的增加，而TGZ能否逆轉這反應。

如圖四，經過測試後，在AGE組中會明顯減少SOD的表現量，而TGZ處理則可回復部分AGE所減少的SOD，由於SOD在抗氧化過程中扮演重要的角色。因此推測AGE會引起細胞的氧化壓力增加，而經過TGZ處理過後，AGE所產生的氧化壓力將會有下降的趨勢。

4. 討　論

糖尿病腎病變逐漸成為已開發國家末期腎病變的主因之一，約二十％至四十％糖尿病患者會產生糖尿病腎病變，佔需要接受透析病人的四十％。糖尿病所造成的腎病變是一種慢性疾病，一但開始就無法有效的治療。在之前的研究文獻中有提出造成糖尿腎病變發生主因之一的腎絲球肥大，可能是因為高糖所引起的腎間質細胞增生，以及細胞外基質的增加所造成的 [17]，另外在高糖的環境下，也會造成細胞中PKC活化，AGE的形成以及ROS的增加等影響 [18]。所以在本研究中利用AGE處理腎臟細胞來模擬糖尿腎病變，接著利用加入PPAR γ 致效劑來觀察是否可以逆轉AGE對細胞所產生的影響。

在加入實驗濃度的TGZ之前，先測試所加入的TGZ在十倍實驗藥劑濃度下會不會對細胞造成毒殺性。在加入十倍劑量的TGZ後，對細胞的毒殺性卻沒有明顯的變化，因此確認在加入TGZ後對細胞不會產生毒殺性，透過這個結果知道我們所治療的藥物對細胞不具有毒殺性，當後續實驗能釐清TGZ造成肝臟毒性的問題後，也許未來可以有發展成為治療糖尿腎病變藥物的潛力。

在前人的研究中有發現AGE會使細胞產生發炎反應，並且產生一些發炎的前驅因子，例如TNF- α 以及IL-6等等。在研究中的實驗也發現到加入AGE後，有觀察到細胞中的TNF- α 以及IL-6都有增加的趨勢，而加入TGZ後，則會逆轉AGE的影響，這可能與產生發炎反應的相關傳導路徑有關。在一些前人的文獻有提出TZD類的藥物具有促進PPAR γ 的效果，其中TGZ也是我們研究中所使用的PPAR γ 致效劑已經被確認可以活化PPAR γ 的表現 [19]。另外在高度醣化終產物的受器RAGE方面也可以看到單獨處理AGE後，RAGE mRNA的表現量有上升的趨勢，這結果顯示AGE可能會透過RAGE來對

細胞產生影響，進行下游訊號的傳遞，不過，TGZ並未明顯降低AGE所增加的RAGE mRNA表現，代表TGZ所帶來的保護腎臟細胞作用可能並非完全透過抑制RAGE增加表現而來。在前人的文獻中提到可以透過AGE的抑制劑LR-90來抑制RAGE的表現，進一步達到抑制NF-κB所誘導的相關發炎反應以及氧化壓力的產生，在細胞或動物實驗中也發現限制RAGE的表現可以調節前發炎因子以及預防動脈粥狀硬化的發生[20]，在本實驗中，還需繼續研究TGZ所帶來的保護腎臟細胞效用，所透過的路徑為何？抑制NF-κB是可能的機制之一。不過透過本實驗結果，我們可以知道PPARγ致效劑TGZ用於治療第二型糖尿病的藥物，在AGE所引起的糖尿腎病變也具有一定的保護效果，未來透過劑型開發在腎臟表現，也許可開發成為腎臟病的用藥。

在先前的研究提到在糖尿病鼠中高血糖會引起氧化壓力的增加[21]，另外在retinal Müller cells (rMC-1) 和bovine retinal endothelial cells (BREC)中，隨著葡萄糖濃度的升高，過氧化物也會隨著葡萄糖濃度而增加[22]，在AGE方面，有文獻提到AGE可以與RAGE結合，透過NF-κB來造成體內氧化壓力的增加[23]。在本研究也發現在加入AGE後，SOD抗氧化物的減少，推測細胞內的氧化壓力有上升的趨勢，但是加入TGZ後，細胞所產生SOD增加，AGE所帶來的氧化壓力會有被抑制的效果，推斷TGZ所帶來的腎臟保護作用是與腎臟細胞的抗氧化物增加與氧化壓力減少有關。

在經過之前的研究後，可以發現到AGE所引起的細胞反應，例如發炎因子TNF-α、IL-6的增加，透過TGZ處理後，都會有降低的趨勢，因此可以確定我們所處理的藥物TGZ對於AGE是有抑制的效果。綜合以上結果，在本研究中可以得到幾個結果：1.利用AGE處理細胞會引起與糖尿腎病變相似的反應，例如細胞激素的增加以及抗氧化物的減少。2.在加入PPAR致效劑TGZ，由AGE所引起的氧化壓力增加以及發炎相關的細胞泌素都有被降低或抑制的效果。3.TGZ並沒有明顯抑制AGE所引起的RAGE表現，可見TGZ所帶來的腎臟保護效果可能是透過抑制RAGE下游訊息而來，而非直接抑制AGE接受器所致。4.希望可以透過本研究，對於糖尿腎病變的相關保護或治療機制可以有進一步的了解，在未來也可以透過TGZ來提供糖尿腎病變治療或保護的另一種選擇。

圖一：100 μ M TGZ處理並不會明顯造成HEK293細胞死亡。

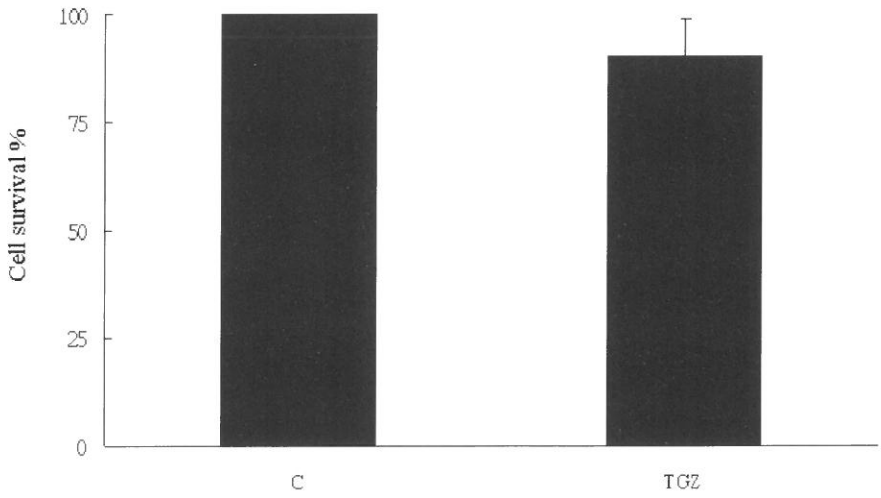

圖二：在HEK293細胞中，TGZ處理明顯降低AGE誘導增加的IL-6與TNF-α分泌。
*p < 0.01與對照組相比；+ p < 0.05與AGE組相比

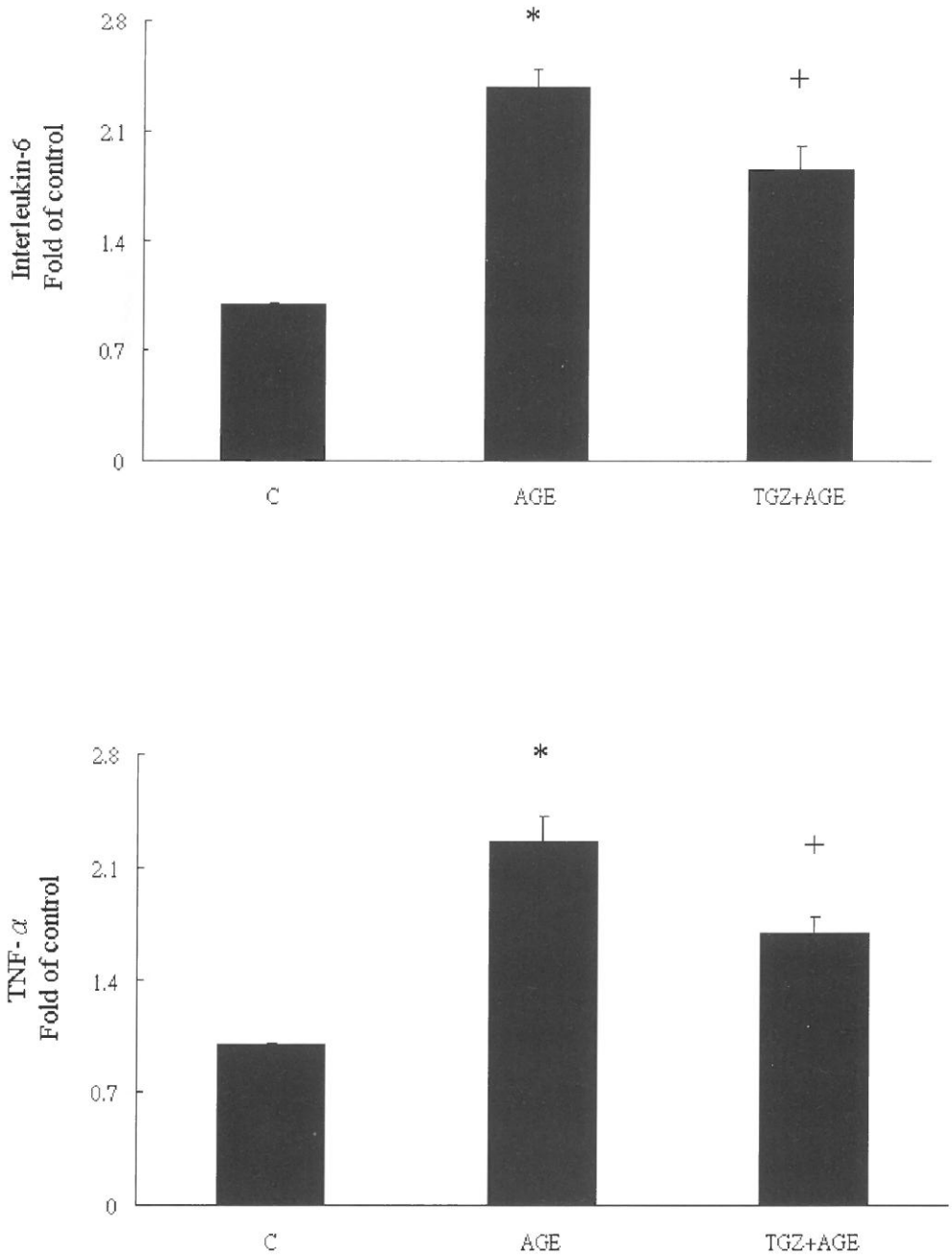

*p < 0.01與對照組相比

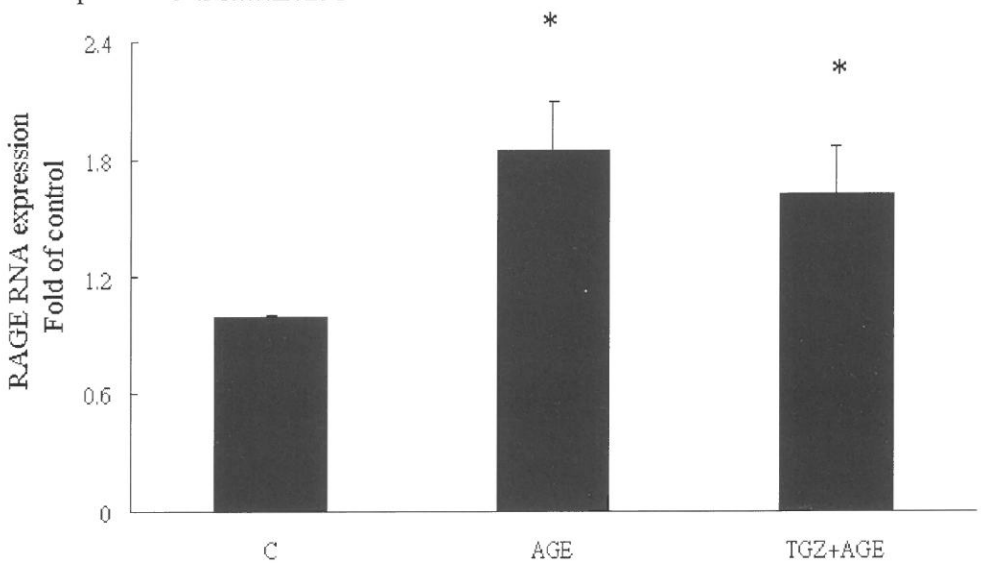

*p < 0.01與對照組相比；+ p < 0.05與AGE組相比

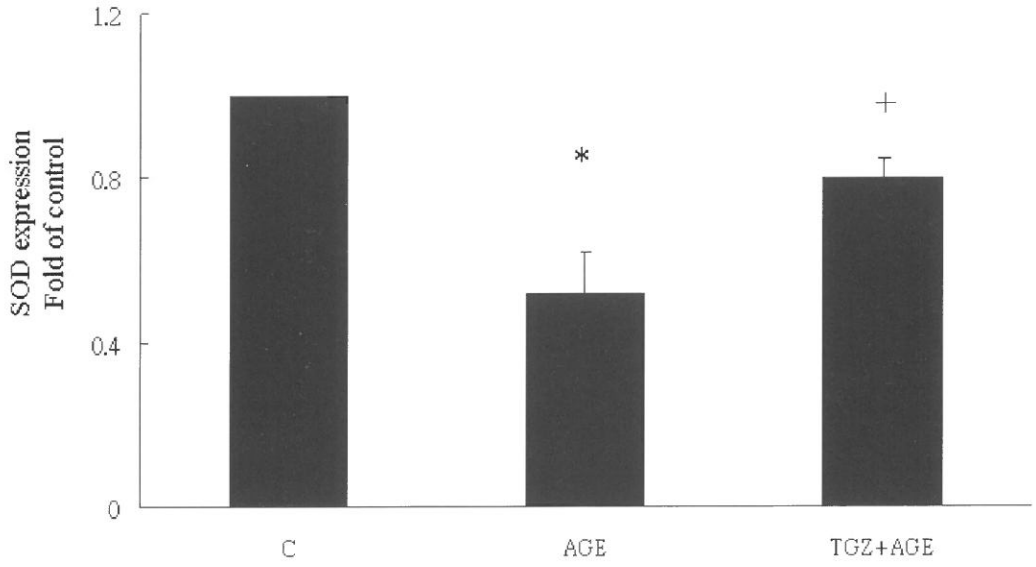

參考文獻

[1] Kimmelstiel P, Wilson C. (1936). Intercapillary lesions in the glomeruli of the kidney. Am J Pathol 12, pp. 83-97.

[2] Mauer SM, Steffes MW, Ellis EN, Sutherland DE, Brown DM, Goetz FC. (1984). Structural-functional relationships in diabetic nephropathy. J Clin Invest 74, pp. 1143-1155.

[3] Dalla Vestra M, Mussap M, Gallina P et al. (2005). Acute-phase markers of inflammation and glomerular structure in patients with type 2 diabetes. J Am Soc Nephrol 16, pp. S78-82.

[4] Kelly DJ, Chanty A, Gow RM, Zhang Y, Gilbert RE. (2005). Protein kinase C beta inhibition attenuates osteopontin expression, macrophage recruitment, and tubulointerstitial injury in advanced experimental nephropathy. J Am Soc Nephrol 16, pp. 1654-1660.

[5] Ortiz A, Gonzalez-Cuadrado S, Bustos C et al. (1995). Tumor necrosis factor as a mediator of glomerular damage. J Am Soc Nephrol 8, pp. 27-34.

[6] Dipetrillo K, Coutermarsh B, Gesek FA. (2003). Urinary tumor necrosis factor contributes to sodium retention and renal hypertrophy during diabetes. Am J Physiol Renal Physiol 284, pp. F113-F121.

[7] Brownlee M, Vlassara H, Cerami A. (1984). Nonenzymatic glycosylation and the pathogenesis of diabetic complications. Ann Intern Med 101, pp. 527-37.

[8] Simm A, Munch G, Seif F, Schenk O, Heidland A, Richter H, Vamvakas S, Schimzel R. (1997). Advanced glycation endoproducts stimulate the MAP-kinase pathway in the tubulus cell line LLC-PK1. FEBS Lett 410, pp. 481-484.

[9] Iwashima Y, Eto M, Horiuchi S, Sano H. (1999). Advanced glycation end product-induced peroxisome proliferator-activated receptor £^ gene expression in the cultured mesangial cells. Biochem Biophys Res Commun. 264, pp. 441-448.

[10] Webster L, Abordo EA, Thornalley PJ, Limb GA. (1997). Induction of TNF alpha and IL-1 beta mRNA in monocytes by methylglyoxal- and advanced glycated endproduct-modified human serum albumin. Biochem Soc Trans 25, pp. 250.

[11] Wahli W, O. Braissant B. (1995). Peroxisome proliferator -activated receptors: transcriptional regulators of adipogenesis, lipid metabolism and more. Chem. Biol 2, pp. 261-266.

[12] Kota BP, Huang TH, Roufogalis BD. (2005). An overview on biological mechanisms of PPARs. Pharmacol Res 51, pp. 85-94.

[13] Fajas L, Fruchart JC, Auwerx J. (1998). Transcriptional control of adipogenesis. Curr Opin Cell Biol 10, pp. 165-173.

[14] Kim EK, Kwon KB, Koo BS, et al. (2007). Activation of peroxisome proliferator-activated receptor-γ protects pancreatic β-cells from cytokine-induced cytotoxicity via NF-£eB pathway. Int J Biochem Cell Biol. 39, pp. 1260-1275.

[15] Ruiz OS, Robey RB, Qiu YY, Wang LJ, Li CJ, Ma J, Arruda JA. (1999). Regulation of the renal Na-HCO(3) cotransporter. XI. Signal transduction underlying CO(2) stimulation. Am J Physiol 277, pp. F580-586.

[16] Sridulyakul P, Chakraphan D, Patumraj S. (2006). Vitamin C supplementation could reverse diabetes-induced endothelial cell dysfunction in mesenteric microcirculation in STZ-rats. Clin Hemorheol Microcirc 34, pp. 315-321.

[17] Luo P, TAN Z, Zhang Z, Li H, Mo Z. (2008). Inhibitory effects of salvianolic acid B on the high glucose-induced mesangial proliferation via NF-kappaB-dependent pathway. Biol Pharm Bull 31, pp. 1381-1386.

[18] Xia L, Wang H, Munk S, et al. (2007). Reactive oxygen species, PKC-beta1, and PKC-zeta mediate high-glucose-induced vascular endothelial growth factor expression in mesangial cells. Am J Physiol Endocrinol Metab 293, pp. E1280-1288.

[19] Staels B, Fruchart JC. (2005). Therapeutic roles of peroxisome proliferator-activated receptor agonists. Diabetes 54, pp. 2460-2470.

[20] Figarola JL, Shanmugam N, Natarajan R, Rahbar S. (2007). Anti-inflammatory effects of the advanced glycation end product inhibitor LR-90 in human monocytes. Diabetes 56, pp. 647-655.

[21] Caldwell RB, Bartoli M, Behzadian MA, et al. (2005). Vascular endothelial growth factor and diabetic retinopathy: role of oxidative stress. Curr Drug Targets 6, pp. 511-524.

[22] Du Y, Miller CM, Kern TS. (2003). Hyperglycemia increases mitochondrial superoxide in retina and retinal cells. Free Radic Biol Med 35, pp. 1491-1499.

Received September 25 ,2009
Revised December 5 ,2009
Accepted December 23 ,2009

Troglitazone attenuated effects of advanced glycation end products in human embryonic kidney cells

Jhin-Hao Jian, Wen-Huei Tsui, Yao-Jen Liang*

Department and Institute of Life Science, Fu-Jen Catholic University, Taipei, Taiwan.

Abstract

According to the improvement of life standard and over-delicate diet, the average life span is increasing in this world. Old age population is increasing and chronic diseases have become an important issue which threaten the national health. Recently, diabetes has become one of the top ten leading causes of death. The complication-diabetic nephropathy has gained attention of many researchers. About one-third patients with nephropathy are due to diabetic nephropathy. At the present time, we usually use Thiazolidinedione (TZD) to treat the type II diabetic patients. Pharmacological mechanism of TZD is regulating peroxisome proliferator activated receptor gamma (PPAR γ). PPAR £^ agonist has been reported to promote the delivery of glucose and insulin secretion. Therefore, we tried to use advanced glycation end products (AGE, the one of the leading causes of diabetic nephropathy) to stimulate kidney cells in this study. We detect the response of kidney cells after PPAR γ agonist troglitazone (TGZ) treatment. The mechanism of PPAR γ agonist in the treatment of diabetic nephropathy were discussed.

The HEK293T cells treated with AGE both significantly increased pro-inflammatory cytokines TNF α and IL-6 secretions and TGZ treatment significantly attenuated these effects. The AGE receptor (RAGE) induced by AGE did not decrease significantly by TGZ. However, AGE-induced superoxide dismutase decreased was reversed by TGZ treatment. Therefore, this study identified that PPAR γ agonist decreased the AGE-induced kidney cell inflammation and oxidative stress. This study provides important insights into the molecular mechanism of TGZ attenuation of kidney cell inflammation and may serve as therapeutic modality to treat patients with diabetic nephropathy.

Key Words : PPAR γ agonist, advanced glycation end products, diabetic nephropathy, inflammation, receptor of AGE

* Correspondence: Yao-Jen Liang, Department and Institute of Life Science, Fu-Jen Catholic University School 510 Chung-Cheng Road, Hsinchuang, Taipei, Taiwan, ROC
Tel: (886)-2-29053593 Fax: (886)-2-29052193 E-mail: 071558@mail.fju.edu.tw

Evaluating a Simulated Annealing technique used to find the m.l.e.'s of exponential power distribution with type II censoring Data

Sy-Mien Chen and Hong-Mei Liao

Department of Mathematics
and
Institute of Mathematics
Fu-Jen Catholic University,
Taipei, Taiwan, R.O.C.
March 19, 2010

Abstract

An explicit form of the maximum likelihood estimator of an exponential power distribution is analytically impossible to get. In this research, statistical simulation along with Simulated Annealing method is conducted to study the performance of the maximum likelihood estimator of exponential power distribution based on type II censoring data.

keywords: Maximum likelihood estimator; Simulated Annealing.

1. Introduction

In recent years, more and more studies show that normal distribution may not be a proper model to use in real life. There are many studies about the robustness for non-normality in the literature, for instance, Huber (1981) and Hamperet *et al* (1986).

Subbotin (1923) proposed the Exponential Power (EP) distribution (also known as the generalized random error distribution) with a location parameter μ, a positive scale parameter σ, and a positive shape parameter p, where the density function

Corresponding author : Tel : (02)290-52451
E-mail address : math1013@mail.fju.edu.tw

$$f_{EP}(x;\mu,\sigma,p) = \frac{1}{2p^{\frac{1}{p}}\sigma\Gamma(1+\frac{1}{p})} e^{-\frac{1}{p}|\frac{x-\mu}{\sigma}|^p}, \tag{1}$$

for $-\infty < x < \infty$, $-\infty < \mu < \infty$, $\sigma > 0, p > 0$. The location parameter, in this case, the mean of the distribution is

$$\mu = E[X] = \int_{-\infty}^{\infty} xf(x)dx,$$

the scale parameter which measures the variability of the distribution is defined by

$$\sigma = \{E[|X-\mu|^p]\}^{\frac{1}{p}} = \left\{\int_{-\infty}^{\infty} |x-\mu|^p f(x)dx\right\}^{\frac{1}{p}}.$$

The variance

$$Var(X) = \sigma^2 p^{\frac{2}{p}-1}.$$

The shape parameter p determines the shape of the curve, which describes both leptokurtic ($0 < p < 2$) and platykurtic ($p > 2$) distributions. In particular, one has Laplace distribution when $p = 1$, the normal distribution for $p = 2$ and the uniform distribution as $p \to \infty$.

The cumulative distribution function (cdf) of EP(μ, σ, p) is defined as follows:

$$F_{EP}(x;\mu,\sigma,p) = \int_{-\infty}^{x} \frac{1}{2p^{\frac{1}{p}}\sigma\Gamma(1+\frac{1}{p})} e^{-\frac{1}{p}|\frac{t-\mu}{\sigma}|^p} dt$$

$$= \frac{1}{2}\int_{-\infty}^{x} \frac{1}{p^{\frac{1}{p}}\sigma\frac{1}{p}\Gamma(\frac{1}{p})} e^{-\frac{1}{p}|\frac{t-\mu}{\sigma}|^p} dt$$

$$= \begin{cases} \frac{1}{2}\left[1 - \int_0^{|\frac{x-\mu}{\sigma}|^p} \frac{1}{p^{\frac{1}{p}}\Gamma(\frac{1}{p})} z^{\frac{1}{p}-1} e^{-\frac{z}{p}} dz\right] & \text{if } x < \mu \\ \frac{1}{2}\int_0^{\infty} \frac{1}{p^{\frac{1}{p}}\Gamma(\frac{1}{p})} z^{\frac{1}{p}-1} e^{-\frac{z}{p}} dz + \frac{1}{2}\int_0^{|\frac{x-\mu}{\sigma}|^p} \frac{1}{p^{\frac{1}{p}}\Gamma(\frac{1}{p})} z^{\frac{1}{p}-1} e^{-\frac{z}{p}} dz & \text{if } x > \mu \end{cases}$$

$$= \begin{cases} 0.5 - s & \text{if } x < \mu \\ 0.5 + s & \text{if } x > \mu \end{cases} \qquad (2)$$

where $s = \frac{1}{2}\int_0^{|\frac{x-\mu}{\sigma}|^p} \frac{1}{p^{\frac{1}{p}}\rho(\frac{1}{p})} z^{\frac{1}{p}-1} e^{-\frac{z}{p}} dz$, is proportional to the cdf of the two-parameter Gamma distribution Gamma $(\frac{1}{p},p)$ with $-\infty < x < \infty$, $-\infty < \mu < \infty$, $\sigma > 0, p > 0$, and $\Gamma(x)$ is the Gamma function.

The hazard function of EP(μ , σ , p) is defined by:

$$h(x) = \frac{f(x)}{1 - F(x)} = \frac{e^{-\frac{1}{p}|\frac{x-\mu}{\sigma}|^p}}{\int_x^{\infty} e^{-\frac{1}{p}|\frac{x-\mu}{\sigma}|^p} dt}.$$

Let *sign* be the sign function such that *sign*(k) = + when $k > 0$, and sign(k) = – when $k < 0$. Then

$$h'(x) = -\frac{e^{-\frac{1}{p}|\frac{x-\mu}{\sigma}|^p} \cdot |\frac{x-\mu}{\sigma}|^{p-1} \cdot sign(\frac{x-\mu}{\sigma})}{\sigma \cdot \int_x^{\infty} e^{-\frac{1}{p}|\frac{x-\mu}{\sigma}|^p} dt} + \left(\frac{e^{-\frac{1}{p}|\frac{x-\mu}{\sigma}|^p}}{\int_x^{\infty} e^{-\frac{1}{p}|\frac{x-\mu}{\sigma}|^p} dt}\right)^2.$$

It can be shown numerically that $h'(x) > 0$, hence the hazard function is increasing.

Box (1953), Tuner(1960), Vianelli (1963) (used the name the normal distribution of order p instead), Azzalini (1986), Bottazzi and Secchi (2006) and Zhu and Zinde-Walsh (2009) are authors among those who discussed the exponential power distribution and some extention. Lunetta (1963) derived the probability density function of EP distribution by solving a particular differential equation, and it has been applied to the GARCH models by Nelson (1991) to forecast the risks of futures.

Agrò (1995) discussed the maximum likelihood estimator for a complete data. Agrò (1999) also considered the EP distribution via the parameter orthogonality and conditional profile likelihood. Mineo (2004) compared four different approaches to estimate the structure parameter of a EP distribution which based on the log-likelihood function, the profile log-likelihood function, the conditional profile log-likelihood function and an index of kurtosis. Further more, Mineo and Ruggieri (2005) presented the normal package, which is a very useful tool for dealing with the exponential power distribution under the statistical environment R.

In the current paper, the MLE of EP distribution based on censored type II data will be discussed in section two. In section three, a simulation study is carried. The conclusion is given in section four.

2. The MLE for EP(μ, σ, p)based on type II censoring data

Let $\mathbf{X} = (X_1, X_2, ..., X_n)$ be a random sample from EP(μ, σ, p), and denote $\theta = (\mu, \sigma, p)$, then the likelihood function based on a complete sample $\mathbf{X}$ is

$$L(\theta;\mathbf{X}) = \left[2p^{\frac{1}{p}} \sigma\Gamma(1+\frac{1}{p}) \right]^{-n} \exp\left(-\frac{1}{p\sigma^p} \sum_{i=1}^{n} |x_i - \mu|^p \right),$$

and the log-likelihood function can be expressed as

$$l(\theta;\mathbf{X}) = -n\log\left[2p^{\frac{1}{p}} \sigma\Gamma(1+\frac{1}{p}) \right] - \frac{1}{p\sigma^p} \sum_{i=1}^{n} |x_i - \mu|^p .$$

By differentiating the log likelihood function with respect to μ, σ and p and set to zero, one has the following estimating equations:

$$\frac{\partial l}{\partial \mu} = -\frac{1}{\sigma^p} \sum_{i=1}^{n} |x_i - \mu|^{p-1} sign(x_i - \mu) = 0$$

$$\frac{\partial l}{\partial \sigma} = -\frac{n}{\sigma} + \frac{1}{\sigma^{p+1}} \sum_{i=1}^{n} |x_i - \mu|^p = 0$$

$$\frac{\partial l}{\partial p} = \frac{n}{p^2}\left[\log p + \Psi(1+\frac{1}{p}) - 1 \right] + \frac{1}{p\sigma^p}\left[\frac{1}{p} \sum_{i=1}^{n} |x_i - \mu|^p + \log\sigma \sum_{i=1}^{n} |x_i - \mu|^p - \sum_{i=1}^{n} |x_i - \mu|^p \log|x_i - \mu|^p \right] = 0$$

where $\Psi(\cdot)$ is the digamma function

$$\Psi(x) = \frac{d\ln\Gamma(x)}{dx} = \frac{\Gamma'(x)}{\Gamma(x)} .$$

It is clear that the MLE of σ, the power deviation of order p (Vianelli (1963)), is

$$\sigma = \left(\frac{\sum_{i=1}^{n} |x_i - \hat{\mu}|^{\hat{p}}}{n} \right)^{\frac{1}{\hat{p}}},$$

where $\hat{\mu}$ and $\hat{p}$ are the MLE of μ and p, respectively. However, as we can see from the estimating equations above, neither $\hat{\mu}$ nor $\hat{p}$ can be solved explicitely, and one way out will be based on some numerical methods.

Let I(θ) be the Fisher information matrix with elements $-E\left[\frac{\partial^2 logf(x,\theta)}{\partial\theta_i\theta_j}\right]$ for $i, j = 1, 2, 3$. In order to derive the asymptotic covariance matrix of $\hat{\theta}$, Agrò (1995) computed the inverse matrix $I^{-1}(\theta)$ of the maximum likelihood estimators $\hat{\mu}$, $\hat{\sigma}$ and $\hat{p}$. Agrò also derived the consistency, asymptotic normailty and efficiency for the likelihoo estimators under EP distribution.

However, in medical science or industrial science, one is always interested in knowing if the treatments or products are acceptable. But the truth is that in real life we may not have full but only partial data on hand. In this section, we would like to study the maximum likelihood estimation of those parameters in EP(μ , σ , p) distribution when we only have Censored Type II data.

Again, let $\mathbf{X} = (X_1, X_2, ..., X_n)$ be a random sample from EP(μ , σ , p). Now, let $\mathbf{Y} = (Y_1, Y_2, ..., Y_r) = (X_{(1)}, X_{(2)}, ..., X_{(r)})$ consists of a type II censoring data of size r from $\mathbf{X}$ and let $\theta = (\mu, \sigma, p)$. Then the log-likelihood function $l(\theta ; \underline{y})$ is

$$l(\theta;\underline{y}) = \ln\frac{n!}{(n-r)!} - r\ln\left[2p^{\frac{1}{p}}\sigma\Gamma(1+\frac{1}{p})\right] - \frac{1}{p\sigma^p}\sum_{i=1}^{n}|y_i-\mu|^p + (n-r)\ln[1-F(y_r)],$$

where $-\infty < y_1 < y_2 < ... < y_r < \infty, -\infty < \mu < \infty, \sigma > 0, p > 0.$

By differentiating with respect to μ , σ , and p respectively, the partial derivatives of the log-likelihood function are as following:

$$\frac{\partial l}{\partial\mu} = \frac{1}{\sigma^p}\sum_{i=1}^{r}|y_i-\mu|^{p-1}\ sign\,(y_i-\mu)$$
$$-\frac{n-r}{1-F(y_r)}\int_{-\infty}^{y_r}\frac{e^{-\frac{1}{p}\left|\frac{x-\mu}{\sigma}\right|^p}}{2p^{\frac{1}{p}}\sigma^2\Gamma(1+\frac{1}{p})}\left|\frac{t-\mu}{\sigma}\right|^{p-1}sign\left(\frac{t-\mu}{\sigma}\right)dt\ ;$$

$$\frac{\partial l}{\partial \sigma} = -\frac{r}{\sigma} + \frac{1}{\sigma^{p+1}} \sum_{i=1}^{r} |y_i - \mu|^p - \frac{n-r}{1-F(y_r)} \int_{-\infty}^{y_r} \frac{e^{-\frac{1}{p}\left|\frac{x-\mu}{\sigma}\right|^p}}{2p^{\frac{1}{p}}\sigma^2\Gamma(1+\frac{1}{p})} + \frac{e^{-\frac{1}{p}\left|\frac{x-\mu}{\sigma}\right|^p}}{2p^{\frac{1}{p}}\sigma^3\Gamma(1+\frac{1}{p})} \left|\frac{t-\mu}{\sigma}\right|^{p-1} (t-\mu)\, sign\left(\frac{t-\mu}{\sigma}\right) dt \;;$$

$$\frac{\partial l}{\partial p} = \frac{r}{p^2}\left[\ln p + \Psi(1+\frac{1}{p}) - 1\right] + \frac{1}{p\sigma^p}\left[\frac{1}{p}\sum_{i=1}^{n} |y_i - \mu|^p + \ln\sigma \sum_{=1}^{n} |y_i - \mu|^p - \sum_{=1}^{n} |y_i - \mu|^p \ln|y_i - \mu|\right]$$

$$- \frac{n-r}{1-F(y_r)}\left\{\int_{-\infty}^{y_r} \frac{e^{-\frac{1}{p}\left|\frac{x-\mu}{\sigma}\right|^p}}{2p^{\frac{1}{p}}\sigma\,\Gamma(1+\frac{1}{p})} \cdot \frac{1}{p^2}\left(\ln p - 1 + \Psi(1+\frac{1}{p})\right)\right.$$

$$\left. + \frac{e^{-\frac{1}{p}\left|\frac{x-\mu}{\sigma}\right|^p}}{2p^{\frac{1}{p}}\sigma\,\Gamma(1+\frac{1}{p})} \left|\frac{t-\mu}{\sigma}\right|^p \cdot \left[\frac{1}{p^2} - \frac{1}{p}\ln\left|\frac{t-\mu}{\sigma}\right|\right] dt\right\}. \qquad (3)$$

By setting the partial derivatives equal zero, one can get the maximum likelihood estimators for each parameter if they do exist. Unfortunately, the expression above are too complicated and it is even much worse than while one has complete data. Since it is hopeless to solve the system of estimating equations analytically, a simulation study along with the simulated annealing method will be carried out to study MLE of θ.

3. Simulation study

3.1 Parameter setting

Since there is no explicit form of the MLE for parameters in EP(μ, σ, p), consider

Monte Carlo approach (Robert and Casella (2004), we apply the Simulated Annealing technique to find the optimum solution of the system of estimating equations (3).

Simulated Annealing (SA) technique was introduced by Kirkpatrick (1983) and it has been shown that SA method can deal with the optimization problem successfully. The fundamental idea of SA is that to change its temperature. As the temperature falls, the step length does too, and the algorithm closes in on the global optimum, so the optimal point can be reached. In a maximization problem, all uphill moves are accepted and the downhill moves may be accepted with a probability. The accepted probability is also increasing in temperature, as the temperature declines to zero, a poor solution will never be accepted, so SA allows one to escape from the local optimum. A simple algorithm about SA is given below:

At iteration t the algorithm is at $((\mu^{(t)}, \sigma^{(t)}, p^{(t)}), l(\mu^{(t)}, \sigma^{(t)}, p^{(t)}))$:

1. simulate $u = (u_1, u_2, u_3)$ where
   $u_1 \sim$ Uniform$(g_1(t), k_1(t))$,
   $u_2 \sim$ Uniform$(g_2(t), k_2(t))$,
   $u_3 \sim$ Uniform$(g_3(t), k_3(t))$,
   and,
   $g1(t) = \max\{\mu^{(t)} - r, 0\}$, $k_1(t) = \mu^{(t)} + r$,
   $g2(t) = \max\{\sigma^{(t)} - r, 0\}$, $k_2(t) = \sigma^{(t)} + r$,
   $g3(t) = \max\{p^{(t)} - r, 0\}$, $k_3(t) = p^{(t)} + r$.
2. Accept $(\mu^{(t+1)}, \sigma^{(t+1)}, p^{(t+1)}) = u$ with probiblity $\rho^{(t)} = \min\{\exp(\frac{l(u)-l((\mu^{(t)}, \sigma^{(t)}, p^{(t)}))}{Wt}), 1\}$, take $(\mu^{(t+1)}, \sigma^{(t+1)}, p^{(t+1)}) = (\mu^{(t)}, \sigma^{(t)}, p^{(t)})$ otherwise.
3. Update W_t to W_{t+1}.

In this simulation study we take the temperature function $W(t) = \frac{1}{100 \ln(1+t)}$, and r = 0.5.

To generate a random sample $\mathbf{X} = (X_1, X_2, \ldots, X_N)$ from EP(μ, σ, p), we first generate a random sample $\mathbf{Z} = (Z_1, Z_2, \ldots, Z_N)$ from Gamma$(\frac{1}{p}, p)$, then $\mathbf{X}$ can be gotten based on the transformation $Z_i = \left|\frac{X_i - \mu}{\sigma}\right|^p$, $i = 1, 2, \ldots, N$.

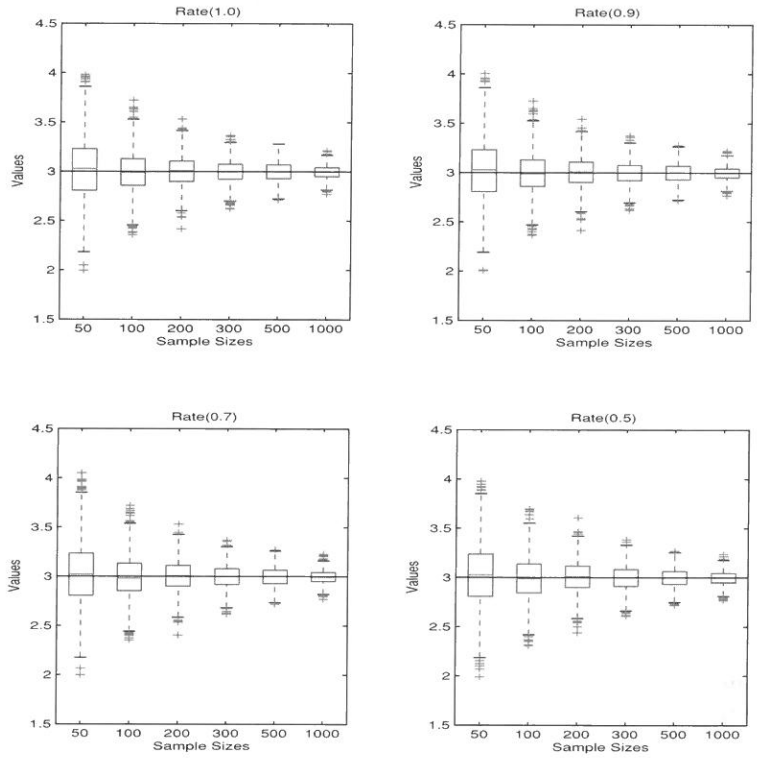

Figure 1: The boxplot of μ given that σ = 2, p = 1.5 (true value μ = 3)

In the simulation, we consider the sample size N = 50, 100, 200, 300, 500, 1000. For each sample size, the process will be repeated 1000 times. In order to see the effect of censoring, we consider the censored rates 100%, 90%, 70% and 50%. The censored rate lower than 50% is rare, so we won't consider any of them in this research. About the parameters, we choose the location parameter μ = (–3,–2,–1, 0, 1, 2, 3), the scale parameter σ = (1, 2, 3), and the shape parameter p = (1.5, 2, 2.5, 3).

Hazard function plays an important role in applied field, so we would like to check its MLE too. By the invariance property of the MLE, we can get the MLE of the hazard function easily once we had the MLE of unknown parameters. In this simulation study, we consider $h(0.5)$.

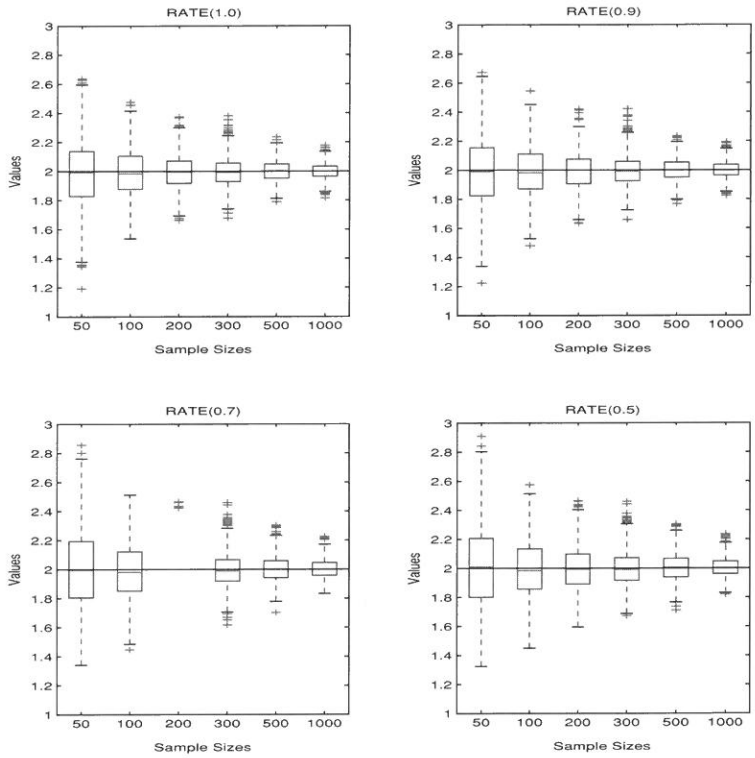

Figure 2: The boxplot of σ given that $\mu = 3, p = 1.5$ (true value $\sigma = 2$)

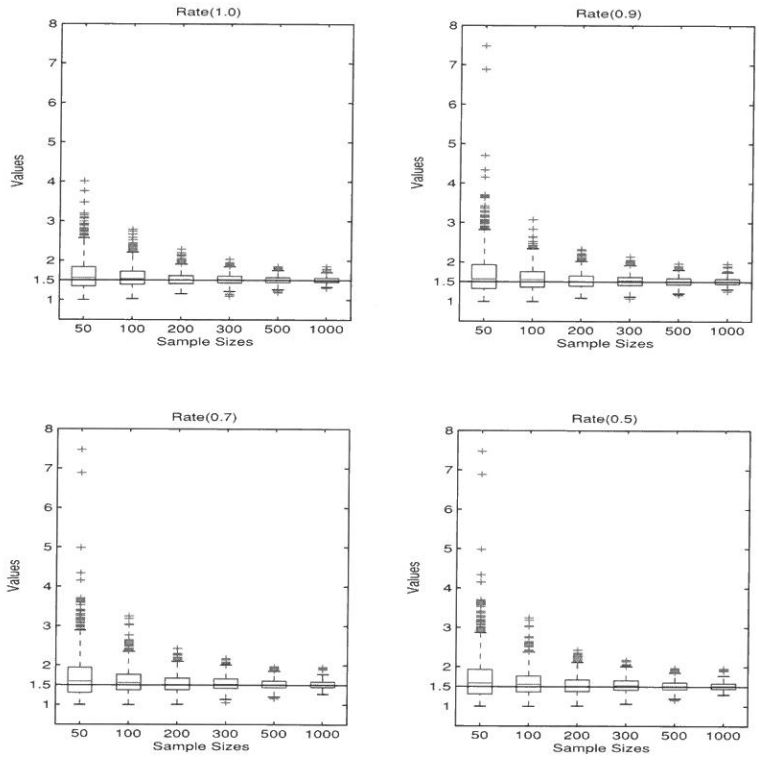

Figure 3: The boxplot of $\hat{p}$ given that $\mu = 3$, $\sigma = 2$ (true value $p = 1.5$)

3.2 Simulation results

3.2.1 When there is only one unknown parameter

While there is only one unknown parameter, the boxplots of estimators $\hat{\mu}$, $\hat{\sigma}$, and $\hat{p}$ are given in Figure 1 ~ Figure 3, respectively. The variability of the sampling distribution of each estimator is reduced as the sample size increased for all unknown parameters.

When the sample size is small to moderate, the sampling distribution of $\hat{\mu}$ and $\hat{\sigma}$ are only slightly skewed to the right regardless the censored rate, the location of the median of a box is about the place of the true value. For large sample, say 1000, the sampling distribution

of $\hat{\mu}$ and $\hat{\sigma}$ are quite symmetric about their means. But for $\hat{p}$, the asymmetry exists even for large sample. The interquartile range are reduced rapidly as the sample size increases, which indicates that the sample size plays a very important role to the estimation, same thing happened to the censored rate. On the other hand, even it seems that the censored rate doesn't lead to huge change, the interquartile range do increase when censored rate is reduced.

Some results are given in Table 1 ~ Table 3. Each table contains the bias, the standard error (se) and the root mean square error (rmse) of the estimator of the corresponding unknown parameter. From tables, we can see that the bias of $\hat{\mu}$ and $\hat{\sigma}$ are unstable, fortunately the amounts are generally small. As the sample size is large enough, the bias of $\hat{\sigma}$ is almost 0. The bias of $\hat{p}$ is decreased when the sample size is increased or when the censored rate is increased, and it seems to be larger than the bias caused by $\hat{\mu}$ and $\hat{\sigma}$. The standard error and the root mean square error are decreased when the sample size is augmented, but is increased when the censored rate becomes small for all the three estimators.

On the other hand, the bias, the standard error, and the root mean square error of $\hat{\sigma}$ and $\hat{p}$ are larger when the true value are larger, but this does not happen to $\hat{\mu}$. For fixed sample size and censored rate, the standard error of $\hat{\sigma}$ is proportional to the true value of σ which indicates that one needs quite large sample to get a more precise estimator. But the rate of increasing is slow when N is huge. The standard error of $\hat{p}$ performs similar to the standard error of $\hat{\sigma}$.

Additionally, Table 4 is the bias and standard error of the estimated hazard function for the case when there is only one unknown parameter. For each unknown parameter, we choose two combinations of the other two fixed parameters. Under the cases of unknown μ and σ, the bias of the estimated hazard functions are still unstable, but its value are very small and are even reduced to zero in some situation. For unknown p, the results of bias is different from those mentioned above, it is decreasing when the sample size is increasing or when the censored rate is increasing.

On the other hand, when we focus on the standard error, we can see that for all of three parameters, they have similar results, i.e. they always decrease when we take bigger sample

size or bigger censored rate. By the way, we found that an interesting result for unknown p case, the standard error of the estimated hazard function is smaller than the other two cases, and the fact is different to the standard error of the likelihood function.

3.2.2 When there are two unknown parameters

When we consider the situation for two unknown parameters, the effect of sample size is evident, but not the censored rate. The scatter plots of estimators are given in Figure 4 ~ Figure 6. The red dots in each subplot are the true values of the corresponding parameters. When the censored rate decreases, the scatter plot spreads in a bigger range. When the sample size increases (from $N = 50$ to $N = 1000$), the estimator is getting closer and closer to the true value.

In Figure 4, the plots of ($\hat{\mu}$ (3), $\hat{\sigma}$ (2)) spread like circles, so a conjecture is that the two estimators $\hat{\mu}$ and $\hat{\sigma}$ are uncorrelated, this can be verified by computing the correlation coefficients ρ between $\hat{\mu}$ and $\hat{\sigma}$. From Table 5, we can see that all the correlation coefficients ρ are quite small, especially for large censored rate, so at least we are sure that these two estimators do not have linear relation between them even for small sample size.

Figure 5 is the scatter plots of $\hat{\sigma}$ and $\hat{p}$. It seems that $\hat{\sigma}$ and $\hat{p}$ have positive correlation between them. From Table 6, the correlation coefficients are within 0.56 ~ 0.83. It is interested to see from Figure 6 that there is no linear trend between $\hat{\mu}$ and $\hat{p}$. But from Table 7, the correlation coefficients between them are almost all negative even though they are quite small.

In Table 5 ~ Table 7, the bias, the standard error, the correlation coefficient ρ between two estimators, and the sum of their root mean square error, which is named as srmse are given. From tables, different combinations of unknown parameters have similar results as the case when only one parameter is unknown. For instance, larger sample size leads to smaller srmse, and the same thing happened to larger censored rate.

Again the effect of the sample size is more significant than that of the censored rate. Regardless the value of μ, the srmse is larger for large σ and p. As we can see that while both p and σ are small, the srmses are smaller, but become larger when both increase. For all censored rates or sample sizes, the sum of the root mean square error increases as both σ and

p increasing simultaneously.

The bias and the standard error of the estimated hazard function for two parameters are given in Table 8, we choose two cases for each combination of two parameters with one fixed. The sample size and the censored rate also play an important role, they lead to larger bias and larger standard error when both the size and rate are bigger, the pattern is more significant for the standard error, but for the bias, it is almost decreasing to zero when the sample size is 1000. It is worth to pay attention that for combinations of true value (3, 2, 1.5), we have three combinations with one different known parameter fixed, the cases which with unknown p seems to lead the bigger bias than the (μ , σ) unknown case.

3.2.3 When there are three unknown parameters

In practice, the situation of all unknown parameters are more common, i.e, three unknown parameters in our case. The simulation results are similar to the case while one or two parameters are unknown. The standard error and the sum of the root mean square error decrease for larger sample size and larger censored rate, and these results are as we expected, because it is affected by three parameters simultaneously, the values is more obvious. In general, the bias and the standard error of $\hat{p}$ is bigger than those of $\hat{\sigma}$ and $\hat{\mu}$, but it is decreasing dramatically when sample size is 1000.

The bias and the stansard error of the estimator of three unknown parameters and the hazard function are given in Table 9. As we can see from the table, the bias caused by $\hat{h}$ (0.5) are almost all negative, which tells us that the maximum likelihood estimation of the hazard function underestimates the true hazard, however, they are very small especially for larger sample size and larger censored rate. Besides, the pattern of bias caused by $\hat{h}$ (0.5) is more regular than the bias of estimated parameters, it is not up and down.

The standard errors for $\hat{\mu}$ and $\hat{\sigma}$ are not large especially for large sample size, which means the precision can be improved by increasing the sample size. However, for $\hat{p}$, the precision is still hard to improve. Even though $\hat{p}$ may be not as good as we expected, the estimated hazard function performs quite well with small bias and standard error even for small sample size.

Furthermore, we also wonder whether the smaller sample size can affect the simulation, and we find that when sample size is taking 30, the solution of our case also can be tolerated, but when the sample size is reduced to 10, the simulation results seem to be not so good, and at the moment, under the situation of three unknown parameters, the effect of censored rate is more obvious than it under the bigger sample size.

4. Conclusion

In this research, we study the performance of the maximum likelihood estimator of unknown parameters and the hazard function while we only have type II censoring data. In order to see the effect of the censored rate, we choose three censored rates to compare with the complete data.

Except the effect of the sample size, we also study the effect of the true value of the unknown parameters. From the simulation results, we conclude that the accuracy increases with sample size, and the effect of the sample size is much more significant than the censored rate. But in real life, it is sometimes unrealistic to increase the sample size indefinitely, so other factors may be needed to put into consideration. For EP distribution, when the censored rate decreases, the outcome of estimation is not good, it spreads in a bigger range, and has bigger bias and standard error.

Besides, different value of parameters also lead to different simulation results, i.e. different value of σ and p affect the performance of the $\hat{\sigma}$, $\hat{p}$. From the simulation, we see that $\hat{\sigma}$ and $\hat{p}$ are positive correlated no matter we choose which sample size. However, the location parameter μ has non-significant effect to the EP distribution, i.e. the performance of $\hat{\mu}$ is consistent regardless the true value of μ.

Similar to Agrò (1995), the Fisher information matrix can be expressed but in an ugly form hence is not given here. Due to the horrible expression of the matrix, it is not possible to

check if the regularity conditions can be satisfied. However, numerical methods may be helpful to get a clearer picture of the bound of the asymptotic variance of mles' and we will leave the problem to further research.

Table 1: When parameter μ is unknown, with σ = 2, p = 3

		$\mu = 0$			$\mu = 1$			$\mu = 2$			$\mu = 3$		
N	Rate	bias	se	rmse	bias	se	rmse	bias	se	rmse	bias	se	rmse
50	1.0	-.0089	.2354	.2356	.0070	.2319	.2321	.0135	.2356	.2361	.0105	.2330	.2333
	0.9	-.0103	.2439	.2441	.0073	.2358	.2359	.0128	.2470	.2472	.0103	.2408	.2411
	0.7	-.0047	.2577	.2577	.0125	.2542	.2544	.0213	.2613	.2622	.0163	.2542	.2548
	0.5	-.0011	.2655	.2655	.0167	.2623	.2629	.0225	.2657	.2667	.0159	.2623	.2628
100	1.0	-.0025	.1670	.1670	-.0036	.1652	.1653	.0002	.1676	.1676	.0059	.1676	.1678
	0.9	-.0043	.1709	.1709	-.0021	.1685	.1686	-.0010	.1729	.1730	.0085	.1718	.1720
	0.7	-.0040	.1817	.1818	.0027	.1817	.1818	-.0024	.1836	.1836	.0108	.1855	.1858
	0.5	.0004	.1892	.1891	.0053	.1881	.1883	.0027	.1863	.1862	.0134	.1879	.1883
200	1.0	.0073	.1149	.1153	.0057	.1192	.1192	-.0013	.1221	.1219	-.0004	.1187	.1189
	0.9	.0082	.1187	.1192	.0067	.1217	.1217	.0004	.1249	.1250	-.0009	.1233	.1233
	0.7	.0098	.1281	.1285	.0089	.1311	.1313	.0025	.1323	.1322	.0011	.1345	.1347
	0.5	.0137	.1315	.1324	.0102	.1334	.1338	.0058	.1353	.1355	.0026	.1393	.1392
300	1.0	.0011	.0980	.0979	-.0032	.0954	.0956	-.0027	.0985	.0983	.0037	.0917	.0918
	0.9	.0013	.0995	.0995	-.0026	.0975	.0973	-.0029	.0995	.0994	.0041	.0949	.0948
	0.7	.0030	.1077	.1078	-.0017	.1058	.1060	-.0018	.1054	.1054	.0072	.1020	.1021
	0.5	.0059	.1114	.1114	.0009	.1086	.1088	0	.1077	.1077	.0102	.1054	.1059
500	1.0	-.0026	.0693	.0697	.0013	.0768	.0768	.0003	.0721	.0720	-.0010	.0755	.0758
	0.9	-.0016	.0714	.0711	.0003	.0781	.0783	.0000	.0748	.0750	-.0012	.0775	.0776
	0.7	-.0010	.0748	.0750	.0008	.0843	.0842	.0017	.0794	.0796	.0010	.0825	.0825
	0.5	.0008	.0775	.0774	.0031	.0849	.0849	.0039	.0819	.0820	.0021	.0854	.0854
1000	1.0	.0026	.0539	.0535	-.0013	.0529	.0526	.0019	.0529	.0529	.0004	.0529	.0533
	0.9	.0024	.0548	.0551	-.0019	.0548	.0549	.0024	.0539	.0543	.0003	.0548	.0548
	0.7	.0023	.0592	.0595	-.0008	.0583	.0584	.0026	.0583	.0587	-.0003	.0583	.0585
	0.5	.0031	.0616	.0614	.0003	.0600	.0602	.0043	.0600	.0599	.0012	.0592	.0594

able 2: When parameter σ is unknown, with μ = 0, p = 2

		σ = 1			σ = 2			σ = 3		
N	Rate	bias	se	rmse	bias	se	rmse	bias	se	rmse
50	1.0	-.0057	.0990	.0990	-.0021	.1982	.1982	-.0073	.3035	.3036
	0.9	-.0064	.1063	.1065	-.0032	.2159	.2159	-.0018	.3175	.3175
	0.7	-.0077	.1208	.1210	.0002	.2371	.2371	-.0024	.3413	.3413
	0.5	-.0037	.1229	.1228	.0033	.2419	.2419	.0068	.3501	.3502
100	1.0	-.0036	.0686	.0690	-.0010	.1442	.1443	.0030	.2175	.2175
	0.9	-.0038	.0728	.0727	.0006	.1562	.1561	.0054	.2330	.2330
	0.7	-.0032	.0812	.0811	.0004	.1709	.1710	.0131	.2516	.2519
	0.5	-.0006	.0831	.0830	.0000	.1726	.1725	.0168	.2583	.2588
200	1.0	-.0003	.0500	.0501	-.0030	.1030	.1032	.0016	.1466	.1465
	0.9	.0000	.0539	.0543	-.0024	.1109	.1107	.0012	.1559	.1558
	0.7	.0006	.0592	.0594	-.0036	.1212	.1212	.0004	.1688	.1688
	0.5	.0024	.0608	.0612	-.0017	.1253	.1255	.0040	.1741	.1742
300	1.0	.0031	.0424	.0420	-.0013	.0812	.0811	-.0002	.1257	.1256
	0.9	.0029	.0447	.0447	-.0016	.0849	.0849	.0007	.1345	.1347
	0.7	.0034	.0500	.0500	.0025	.0954	.0957	-.0019	.1480	.1480
	0.5	.0042	.0520	.0523	.0044	.0990	.0992	.0019	.1526	.1526
500	1.0	-.0003	.0316	.0318	-.0038	.0640	.0645	-.0005	.0943	.0941
	0.9	-.0002	.0346	.0340	-.0035	.0700	.0700	-.0013	.1010	.1008
	0.7	.0001	.0374	.0376	-.0015	.0775	.0775	-.0031	.1122	.1123
	0.5	.0013	.0387	.0389	.0003	.0806	.0808	-.0004	.1166	.1166
1000	1.0	.0005	.0224	.0225	-.0021	.0447	.0445	-.0009	.0678	.0680
	0.9	.0009	.0245	.0242	-.0018	.0469	.0472	-.0005	.0735	.0732
	0.7	.0005	.0265	.0267	-.0011	.0539	.0540	.0008	.0819	.0816
	0.5	.0017	.0283	.0276	.0005	.0557	.0560	.0035	.0854	.0854

Table 3: When parameter p is unknown, with $\mu = 3$, $\sigma = 1$

		$p = 1.5$			$p = 2$			$p = 2.5$			$p = 3$		
N	Rate	bias	se	rmse	bias	se	rmse	bias	se	rmse	bias	se	rmse
50	1.0	.1528	.4781	.5019	.2044	.5801	.6151	.2283	.7251	.7601	.2987	.8185	.8713
	0.9	.1995	.5997	.6321	.2888	.8448	.8928	.3615	1.0211	1.0832	.4559	1.1490	1.2362
	0.7	.2274	.6256	.6657	.3255	.8976	.9548	.4047	1.0754	1.1490	.5106	1.2597	1.3592
	0.5	.2304	.6231	.6644	.3284	.8959	.9542	.4036	1.0747	1.1480	.5094	1.2585	1.3577
100	1.0	.0515	.2443	.2496	.0723	.3151	.3233	.1183	.4083	.4250	.1260	.5168	.5320
	0.9	.0731	.3017	.3103	.1078	.4020	.4162	.1810	.5768	.6045	.1959	.6777	.7055
	0.7	.0892	.3254	.3373	.1191	.4422	.4579	.1982	.6007	.6326	.2219	.7181	.7516
	0.5	.0907	.3254	.3379	.1193	.4434	.4591	.2003	.6013	.6338	.2239	.7192	.7533
200	1.0	.0225	.1616	.1631	.0331	.2131	.2157	.0734	.2860	.2952	.0555	.3234	.3281
	0.9	.0304	.1962	.1985	.0458	.2569	.2610	.1022	.3657	.3797	.0860	.4225	.4311
	0.7	.0385	.2078	.2114	.0605	.2814	.2879	.1193	.3872	.4051	.0947	.4494	.4594
	0.5	.0421	.2090	.2133	.0633	.2828	.2899	.1241	.3887	.4081	.0983	.4527	.4632
300	1.0	.0129	.1338	.1342	.0298	.1729	.1754	.0369	.2117	.2148	.0480	.2676	.2718
	0.9	.0176	.1572	.1581	.0322	.2062	.2086	.0568	.2773	.2830	.0698	.3565	.3632
	0.7	.0263	.1685	.1706	.0350	.2154	.2182	.0712	.2978	.3063	.0731	.3838	.3907
	0.5	.0283	.1700	.1723	.0382	.2156	.2189	.0745	.3003	.3094	.0757	.3856	.3929
500	1.0	.0157	.1010	.1020	.0117	.1311	.1315	.0216	.1732	.1745	.0269	.1997	.2016
	0.9	.0210	.1187	.1204	.0099	.1575	.1579	.0329	.2112	.2136	.0425	.2655	.2689
	0.7	.0264	.1281	.1308	.0134	.1738	.1742	.0384	.2261	.2294	.0473	.2827	.2867
	0.5	.0280	.1285	.1315	.0175	.1761	.1769	.0402	.2285	.2321	.0490	.2839	.2880
1000	1.0	.0044	.0671	.0671	.0109	.0927	.0933	.0080	.1158	.1161	.0150	.1389	.1397
	0.9	.0082	.0819	.0825	.0092	.1131	.1136	.0148	.1407	.1415	.0209	.1780	.1792
	0.7	.0102	.0889	.0894	.0131	.1225	.1231	.0170	.1517	.1526	.0271	.1908	.1927
	0.5	.0116	.0906	.0911	.0157	.1237	.1247	.0185	.1536	.1547	.0294	.1916	.1939

Table 4: The bias and standard error of the estimated hazard function $\hat{h}$ (0.5) when only one parameter is unknown

		μ						σ			p		
true (μ , σ , p)		(−3, 2, 3)			(3, 2, 3)			(0, 1, 2)			(0, 2, 2)		
N	Rate	bias	se	rmse	bias	se	rmse	bias	se	rmse	bias	se	rmse
50	1.0	.0093	.1947	-.0003	.0225	.0282	.1598	.0072	.0583	-.0035	.0094	.0008	.0037
	0.9	.0069	.2026	-.0002	.0233	.0326	.1743	.0088	.0642	-.0041	.0109	.0012	.0046
	0.7	.0032	.2133	-.0007	.0245	.0417	.2033	.0095	.0711	-.0046	.0113	.0015	.0050
	0.5	.0003	.2185	-.0006	.0253	.0361	.2046	.0089	.0722	-.0047	.0114	.0014	.0050
100	1.0	.0023	.1411	-.0002	.0163	.0146	.1072	.0038	.0421	-.0014	.0063	.0006	.0028
	0.9	.0024	.1443	-.0004	.0167	.0160	.1123	.0039	.0457	-.0018	.0074	.0009	.0035
	0.7	-.0013	.1515	-.0006	.0181	.0174	.1253	.0048	.0502	-.0022	.0078	.0010	.0037
	0.5	-.0063	.1546	-.0008	.0183	.0141	.1280	.0050	.0508	-.0023	.0078	.0010	.0037
200	1.0	-.0005	.1021	.0002	.0116	.0053	.0764	.0026	.0298	-.0006	.0043	.0004	.0020
	0.9	.0001	.1045	.0003	.0121	.0056	.0828	.0027	.0320	-.0008	.0052	.0005	.0025
	0.7	-.0009	.1110	.0001	.0132	.0056	.0898	.0035	.0352	-.0010	.0054	.0006	.0027
	0.5	-.0024	.1135	0	.0136	.0034	.0922	.0031	.0363	-.0011	.0055	.0006	.0027
300	1.0	.0003	.0817	-.0003	.0090	-.0013	.0628	.0014	.0231	-.0003	.0036	.0002	.0016
	0.9	.0007	.0840	-.0003	.0093	-.0006	.0672	.0016	.0243	-.0005	.0042	.0003	.0020
	0.7	.0004	.0902	-.0006	.0100	-.0005	.0750	.0008	.0274	-.0007	.0045	.0004	.0022
	0.5	-.0008	.0933	-.0009	.0103	-.0013	.0782	.0003	.0283	-.0008	.0045	.0004	.0022
500	1.0	.0009	.0596	.0001	.0074	.0023	.0483	.0018	.0184	-.0004	.0027	.0001	.0013
	0.9	.0008	.0618	.0002	.0076	.0025	.0515	.0018	.0200	-.0005	.0032	.0002	.0016
	0.7	.0006	.0666	0	.0081	.0026	.0572	.0014	.0222	-.0007	.0034	.0003	.0018
	0.5	-.0003	.0685	-.0002	.0084	.0008	.0591	.0010	.0231	-.0007	.0034	.0002	.0018
1000	1.0	-.0007	.0441	-.0001	.0052	.0002	.0340	.0009	.0127	-.0001	.0018	.0001	.0009
	0.9	-.0009	.0457	0	.0054	-.0002	.0363	.0009	.0134	-.0002	.0022	.0001	.0011
	0.7	-.0008	.0495	0	.0057	.0005	.0401	.0008	.0154	-.0002	.0024	.0001	.0012
	0.5	-.0019	.0511	-.0001	.0058	-.0011	.0413	.0003	.0159	-.0003	.0024	.0001	.0012

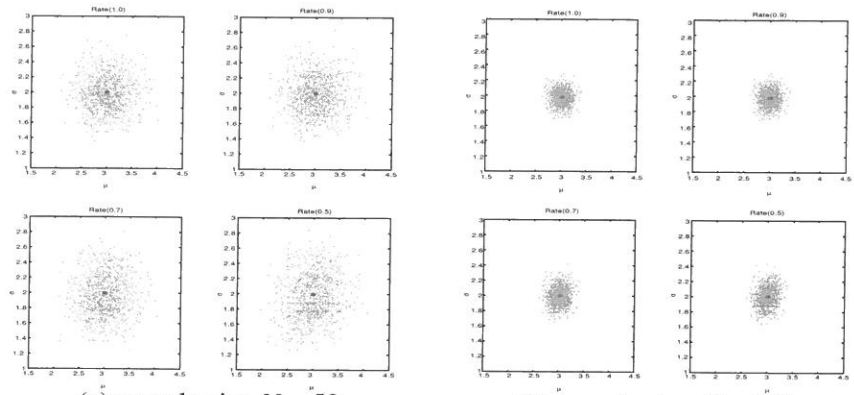

(a) sample size $N = 50$ (b) sample size $N = 300$

Figure 4: The scatter plot of $\hat{\mu}$ (3), $\hat{\sigma}$ (2), with $p = 1.5$

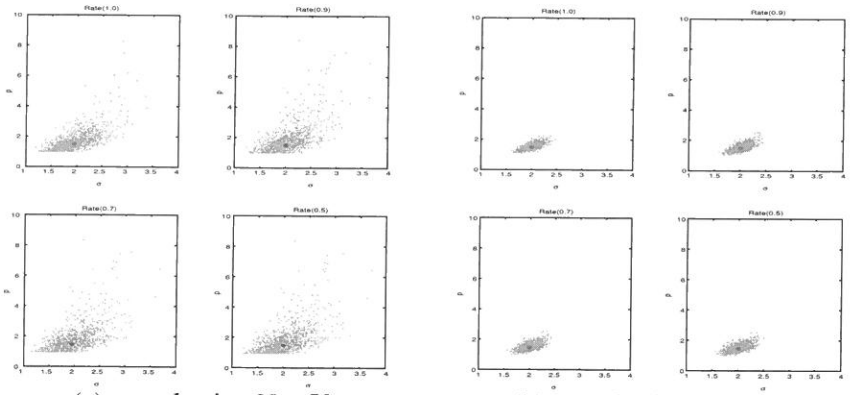

(a) sample size $N = 50$ (b) sample size $N = 300$

Figure 5: The scatter plot of $\hat{\sigma}$ (2), $\hat{p}$ (1.5), with $\mu = 3$

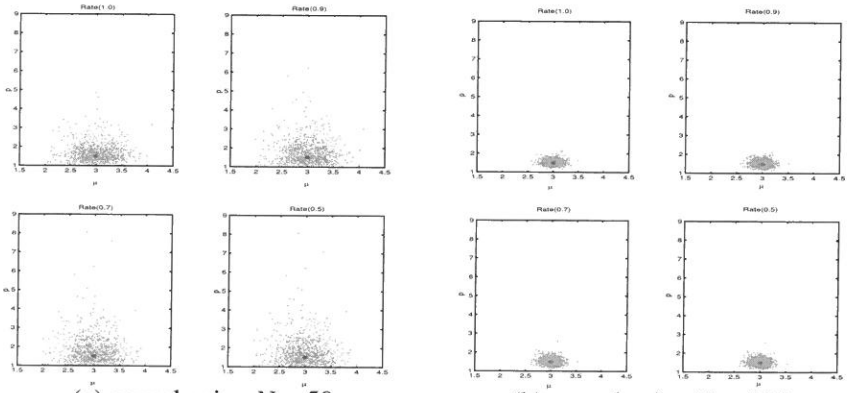

(a) sample size $N = 50$ (b) sample size $N = 300$

Figure 6: The scatter plot of $\hat{\mu}$ (3), $\hat{p}$ (1.5), with $\sigma = 2$

Table 5: When parameters μ and σ are unknown, with $p = 1.5$

N = 1000		σ = 1				σ = 2				σ = 3			
μ	Rate	1.0	0.9	0.7	0.5	1.0	0.9	0.7	0.5	1.0	0.9	0.7	0.5
0	bias($\hat{\mu}$)	.0006	.0005	.0007	.0006	-.0011	-.0008	-.0007	-.0013	.0023	.0018	.0016	.0002
	se($\hat{\mu}$)	.0332	.0332	.0346	.0346	.0686	.0686	.0693	.0714	.0975	.0980	.0995	.1030
	bias($\hat{\sigma}$)	-.0019	-.0022	-.0015	-.0006	.0016	.0014	.0029	.0062	.0027	.0014	.0028	.0039
	se($\hat{\sigma}$)	.0265	.0283	.0316	.0361	.0548	.0574	.0640	.0714	.0775	.0806	.0922	.1025
	ρ	.0000	.1066	.0913	.2402	.0266	.0508	.1127	.1961	-.0132	.0253	.1090	.1896
	srmse	.0592	.0612	.0656	.0706	.1233	.1260	.1333	.1435	.1747	.1789	.1918	.2056
1	bias($\hat{\mu}$)	.0008	.0008	.0009	.0002	.0000	.0005	.0008	-.0003	-.0005	-.0007	-.0002	-.0016
	se($\hat{\mu}$)	.0346	.0346	.0361	.0361	.0700	.0700	.0714	.0735	.1020	.1020	.1044	.1072
	bias($\hat{\sigma}$)	-.0001	.0001	.0003	.0007	-.0034	-.0033	-.0015	.0011	-.0031	-.0035	.0003	.0014
	se($\hat{\sigma}$)	.0265	.0283	.0300	.0346	.0490	.0529	.0616	.0700	.0781	.0819	.0949	.1030
	ρ	.0000	.0000	.0925	.1601	-.0292	-.0270	.0909	.1750	-.0251	-.0120	.0909	.1630
	srmse	.0605	.0624	.0661	.0706	.1190	.1229	.1331	.1435	.1797	.1841	.1990	.2102
2	bias($\hat{\mu}$)	.0004	.0004	.0006	.0002	-.0005	-.0002	-.0006	-.0012	.0065	.0062	.0057	.0048
	se($\hat{\mu}$)	.0316	.0332	.0332	.0346	.0686	.0686	.0693	.0714	.1054	.1058	.1072	.1100
	bias($\hat{\sigma}$)	-.0016	-.0019	-.0009	-.0002	-.0002	-.0006	-.0005	.0025	-.0069	-.0079	-.0083	-.0062
	se($\hat{\sigma}$)	.0265	.0283	.0300	.0346	.0520	.0548	.0624	.0707	.0787	.0854	.0970	.1063
	ρ	.0000	.0000	.1005	.1667	.0281	.0533	.0925	.1584	.0362	.0553	.1347	.1881
	srmse	.0581	.0599	.0636	.0689	.1205	.1233	.1317	.1421	.1849	.1915	.2047	.2167
3	bias($\hat{\mu}$)	-.0016	-.0015	-.0017	-.0025	-.0007	-.0007	-.0020	-.0028	-.0014	-.0015	-.0019	-.0032
	se($\hat{\mu}$)	.0361	.0361	.0374	.0374	.0671	.0671	.0686	.0707	.1025	.1025	.1034	.1077
	bias($\hat{\sigma}$)	-.0021	-.0022	-.0026	-.0023	-.0018	-.0036	-.0055	-.0034	.0033	.0030	.0038	.0057
	se($\hat{\sigma}$)	.0245	.0265	.0300	.0346	.0500	.0539	.0616	.0686	.0781	.0819	.0938	.1025
	ρ	.0000	.0000	.0891	.1543	.0000	.0277	.1183	.2269	.0125	.0238	.0824	.1631
	srmse	.0606	.0625	.0674	.0721	.1181	.1209	.1302	.1407	.1806	.1849	.1972	.2102

Table 6: When parameters σ and p are unknown, with $\mu = 3$

$N = 1000$		$\sigma = 1$				$\sigma = 2$				$\sigma = 3$			
p	Rate	1.0	0.9	0.7	0.5	1.0	0.9	0.7	0.5	1.0	0.9	0.7	0.5
0	bias($\hat{\sigma}$)	.0011	.0015	.0006	-.0005	-.0028	-.0028	-.0048	-.0064	.0039	.0049	.0021	-.0010
	se($\hat{\sigma}$)	.0011	.0011	.0012	.0013	.0022	.0023	.0023	.0025	.0034	.0035	.0036	.0037
	bias($\hat{p}$)	.0064	.0127	.0084	.0074	.0058	.0089	.0066	.0053	.0095	.0159	.0110	.0091
	se($\hat{p}$)	.0031	.0035	.0036	.0037	.0030	.0035	.0037	.0037	.0030	.0036	.0037	.0038
	ρ	.7152	.6918	.6257	.5746	.6930	.6513	.5824	.5684	.7264	.6511	.5846	.5765
	srmse	.1335	.1492	.1527	.1579	.1671	.1837	.1899	.1949	.2060	.2258	.2319	.2375
1	bias($\hat{\sigma}$)	.0029	.0026	.0019	.0008	-.0004	-.0005	-.0020	-.0039	.0021	.0016	-.0015	-.0042
	se($\hat{\sigma}$)	.0010	.0011	.0011	.0012	.0022	.0022	.0023	.0024	.0032	.0033	.0033	.0035
	bias($\hat{p}$)	.0185	.0216	.0191	.0181	.0132	.0179	.0154	.0131	.0127	.0143	.0120	.0108
	se($\hat{p}$)	.0044	.0053	.0054	.0055	.0046	.0054	.0055	.0056	.0045	.0053	.0054	.0055
	ρ	.7714	.7169	.6632	.6470	.7642	.7295	.6868	.6870	.7421	.7146	.6679	.6682
	srmse	.1759	.2052	.2086	.2119	.2159	.2432	.2484	.2545	.2432	.2733	.2773	.2835
2	bias($\hat{\sigma}$)	.0007	.0008	.0001	-.0010	-.0025	-.0016	-.0039	-.0056	.0074	.0080	.0062	.0032
	se($\hat{\sigma}$)	.0010	.0010	.0010	.0011	.0022	.0023	.0024	.0024	.0032	.0032	.0033	.0034
	bias($\hat{p}$)	.0179	.0293	.0247	.0222	.0092	.0238	.0199	.0173	.0212	.0317	.0277	.0265
	se($\hat{p}$)	.0061	.0071	.0072	.0073	.0062	.0075	.0075	.0076	.0062	.0070	.0071	.0072
	ρ	.7902	.7717	.7279	.7009	.7988	.7566	.7177	.7082	.8073	.7610	.7274	.7140
	srmse	.2245	.2595	.2628	.2662	.2649	.3098	.3140	.3159	.2969	.3259	.3312	.3353
3	bias($\hat{\sigma}$)	.0014	.0017	.0009	.0002	.0012	.0019	-.0008	-.0024	.0074	.0072	.0057	.0031
	se($\hat{\sigma}$)	.0009	.0010	.0010	.0010	.0020	.0021	.0022	.0023	.0031	.0032	.0032	.0033
	bias($\hat{p}$)	.0340	.0538	.0478	.0486	.0329	.0479	.0430	.0414	.0387	.0490	.0438	.0421
	se($\hat{p}$)	.0077	.0095	.0096	.0096	.0078	.0092	.0094	.0095	.0080	.0094	.0095	.0096
	ρ	.8385	.7888	.7360	.7443	.8107	.8015	.7649	.7589	.8308	.7836	.7473	.7385
	srmse	.2754	.3374	.3403	.3415	.3128	.3618	.3714	.3753	.3548	.4021	.4076	.4115

Table 7: When parameters μ and p are unknown, with $\sigma = 2$

$N = 1000$		$p = 1.5$				$p = 2$			
μ \ Rate		1.0	0.9	0.7	0.5	1.0	0.9	0.7	0.5
0	bias($\hat{\mu}$)	-.0012	-.0010	-.0021	-.0029	.0002	-.0007	-.0016	-.0026
	se($\hat{\mu}$)	.0678	.0678	.0693	.0707	.0632	.0640	.0663	.0678
	bias($\hat{p}$)	.0071	.0115	.0129	.0128	.0062	.0132	.0166	.0175
	se($\hat{p}$)	.0671	.0831	.0917	.0927	.0938	.1153	.1277	.1300
	ρ	-.0440	-.1242	-.1732	-.1677	.0169	-.0677	-.1653	-.1701
	srmse	.1356	.1521	.1615	.1640	.1570	.1796	.1953	.1989
1	bias($\hat{\mu}$)	-.0019	-.0019	-.0029	-.0038	-.0019	-.0019	-.0029	-.0038
	se($\hat{\mu}$)	.0656	.0663	.0671	.0693	.0656	.0663	.0671	.0693
	bias($\hat{p}$)	.0077	.0131	.0142	.0136	.0077	.0131	.0142	.0136
	se($\hat{p}$)	.0700	.0883	.0954	.0970	.0700	.0883	.0954	.0970
	ρ	.0218	-.0683	-.1250	-.1191	.0218	-.0683	-.1250	-.1191
	srmse	.1356	.1552	.1635	.1673	.1356	.1552	.1635	.1673
2	bias($\hat{\mu}$)	.0018	.0019	.0008	.0001	.0018	.0019	.0008	.0001
	se($\hat{\mu}$)	.0686	.0686	.0693	.0707	.0686	.0686	.0693	.0707
	bias($\hat{p}$)	.0049	.0092	.0105	.0105	.0049	.0092	.0105	.0105
	se($\hat{p}$)	.0728	.0889	.0985	.1010	.0728	.0889	.0985	.1010
	ρ	.0200	.0164	-.0440	-.0280	.0200	.0164	-.0440	-.0280
	srmse	.1414	.1580	.1683	.1722	.1414	.1580	.1683	.1722
3	bias($\hat{\mu}$)	-.0009	-.0010	-.0023	-.0037	-.0012	-.0021	-.0027	-.0036
	se($\hat{\mu}$)	.0678	.0678	.0686	.0693	.0624	.0632	.0656	.0678
	bias($\hat{p}$)	.0074	.0130	.0157	.0154	.0100	.0168	.0183	.0187
	se($\hat{p}$)	.0742	.0889	.0990	.1005	.0949	.1166	.1285	.1300
	ρ	.0596	.0664	.0000	-.0144	-.0169	-.0949	-.1662	-.1474
	srmse	.1420	.1578	.1686	.1708	.1578	.1811	.1956	.1994

Table 7: (continued) When parameters μ and p are unknown, with $\sigma = 2$

$N = 1000$		$p = 1.5$				$p = 2$			
μ	Rate	1.0	0.9	0.7	0.5	1.0	0.9	0.7	0.5
0	bias($\hat{\mu}$)	-.0008	-.0021	-.0034	-.0055	.0021	.0016	.0009	-.0022
	se($\hat{\mu}$)	.0566	.0574	.0608	.0624	.0539	.0566	.0608	.0624
	bias($\hat{p}$)	.0151	.0251	.0273	.0275	.0168	.0231	.0262	.0280
	se($\hat{p}$)	.1212	.1523	.1649	.1670	.1400	.1766	.1997	.2037
	ρ	.0437	-.0686	-.1695	-.1726	.0265	-.1501	-.2798	-.2987
	srmse	.1790	.2121	.2279	.2322	.1944	.2343	.2618	.2680
1	bias($\hat{\mu}$)	-.0008	-.0012	-.0008	-.0025	-.0007	-.0009	-.0016	-.0044
	se($\hat{\mu}$)	.0557	.0574	.0608	.0624	.0529	.0548	.0600	.0616
	bias($\hat{p}$)	.0172	.0227	.0179	.0181	.0163	.0204	.0207	.0221
	se($\hat{p}$)	.1200	.1546	.1661	.1673	.1421	.1863	.2064	.2098
	ρ	.0150	-.1239	-.2078	-.2201	.0133	-.1470	-.2746	-.2939
	srmse	.1769	.2136	.2278	.2310	.1957	.2417	.2671	.2728
2	bias($\hat{\mu}$)	-.0005	-.0005	-.0017	-.0038	.0008	.0004	.0000	-.0029
	se($\hat{\mu}$)	.0583	.0608	.0624	.0656	.0539	.0566	.0616	.0648
	bias($\hat{p}$)	.0155	.0184	.0192	.0200	.0203	.0276	.0294	.0297
	se($\hat{p}$)	.1183	.1453	.1600	.1606	.1418	.1822	.2074	.2107
	ρ	.0145	-.1132	-.1902	-.2089	-.0131	-.1843	-.3286	-.3369
	srmse	.1780	.2069	.2236	.2274	.1967	.2406	.2715	.2773
3	bias($\hat{\mu}$)	.0007	.0000	-.0017	-.0038	.0006	.0006	-.0001	-.0016
	se($\hat{\mu}$)	.0574	.0592	.0624	.0648	.0529	.0539	.0583	.0608
	bias($\hat{p}$)	.0120	.0213	.0243	.0243	.0161	.0210	.0226	.0223
	se($\hat{p}$)	.1233	.1572	.1720	.1729	.1382	.1780	.2002	.2032
	ρ	.0000	-.1183	-.2234	-.2320	.0684	-.0730	-.2227	-.2346
	srmse	.1811	.2176	.2362	.2394	.1918	.2333	.2598	.2653

Table 8: The bias and standard error of the estimated hazard function $\hat{h}(0.5)$ when two parameters are unknown

unknown				(μ, σ)		(μ, p)				(σ, p)			
true	(μ, σ, p)	(3, 1, 1.5)		(3, 2, 1.5)		(3, 2, 1.5)		(3, 2, 3)		(3, 2, 1.5)		(3; 1; 3)	
N	Rate	bias	se	bias	se	bias	se	bias	se	bias	se	bias	se
50	1.0	-.0002	.0129	-.0005	.0209	.0033	.0225	.0016	.0265	.0030	.0170	.0007	.0039
	0.9	-.0004	.0133	-.0006	.0210	.0039	.0235	.0040	.0296	.0039	.0186	.0010	.0048
	0.7	-.0004	.0136	-.0011	.0212	.0049	.0246	.0061	.0315	.0036	.0188	.0011	.0049
	0.5	.0000	.0140	-.0008	.0215	.0053	.0249	.0072	.0326	.0034	.0190	.0011	.0051
100	1.0	-.0001	.0091	-.0003	.0144	.0014	.0139	.0001	.0163	.0019	.0121	.0002	.0025
	0.9	-.0003	.0093	-.0004	.0144	.0018	.0143	.0013	.0181	.0023	.0128	.0005	.0032
	0.7	-.0002	.0097	-.0005	.0146	.0023	.0149	.0028	.0198	.0019	.0130	.0007	.0035
	0.5	-.0002	.0100	-.0002	.0147	.0026	.0151	.0039	.0209	.0018	.0133	.0007	.0035
200	1.0	-.0003	.0066	-.0003	.0102	.0009	.0099	-.0005	.0120	.0009	.0086	.0002	.0021
	0.9	-.0003	.0067	-.0003	.0102	.0014	.0104	-.0002	.0127	.0011	.0090	.0004	.0026
	0.7	-.0004	.0072	-.0004	.0103	.0016	.0108	.0005	.0144	.0008	.0091	.0004	.0027
	0.5	-.0001	.0075	-.0001	.0104	.0017	.0109	.0010	.0149	.0006	.0094	.0004	.0028
300	1.0	.0002	.0054	.0003	.0084	.0005	.0082	.0001	.0095	.0009	.0068	.0001	.0017
	0.9	.0002	.0057	.0003	.0084	.0006	.0085	.0005	.0104	.0011	.0073	.0002	.0021
	0.7	.0002	.0061	.0003	.0085	.0007	.0088	.0007	.0115	.0008	.0074	.0003	.0023
	0.5	.0005	.0064	.0005	.0085	.0008	.0088	.0013	.0120	.0006	.0076	.0003	.0023
500	1.0	-.0001	.0044	-.0001	.0062	.0004	.0065	.0002	.0075	.0005	.0052	.0001	.0013
	0.9	-.0001	.0045	-.0002	.0062	.0005	.0067	.0006	.0079	.0006	.0056	.0002	.0017
	0.7	.0000	.0048	-.0002	.0062	.0005	.0070	.0008	.0091	.0004	.0057	.0002	.0018
	0.5	.0001	.0050	.0000	.0063	.0007	.0070	.0012	.0095	.0004	.0059	.0002	.0018
1000	1.0	.0000	.0030	.0000	.0044	.0003	.0044	.0000	.0052	-.0001	.0035	.0000	.0009
	0.9	.0000	.0031	.0000	.0044	.0003	.0044	.0000	.0054	.0000	.0037	.0000	.0012
	0.7	-.0001	.0033	.0000	.0044	.0005	.0046	.0001	.0061	-.0001	.0038	.0001	.0013
	0.5	.0000	.0035	.0001	.0044	.0005	.0047	.0002	.0064	-.0002	.0039	.0001	.0013

Table 9: Unknown parameters with true value (μ , σ , p) = (3, 1, 1.5)

		μ		σ		p			hazard	$\hat{h}(0.5)$
N	Rate	bias($\hat{\mu}$)	se($\hat{\mu}$)	bias($\hat{\sigma}$)	se($\hat{\sigma}$)	bias($\hat{p}$)	se($\hat{p}$)	srmse	bias($\hat{h}$)	se($\hat{h}$)
50	1.0	.0011	.1694	.0298	.1895	.4084	1.2755	1.7005	-.0016	.0160
	0.9	-.0034	.1744	.0374	.1992	.7649	1.9854	2.5047	-.0034	.0181
	0.7	-.0103	.1694	.0222	.2007	.7237	1.9369	2.4394	-.0040	.0180
	0.5	-.0117	.1664	.0147	.2078	.6986	1.9435	2.4408	-.0041	.0179
100	1.0	-.0031	.1136	.0121	.1192	.1295	.4077	.6612	-.0007	.0103
	0.9	-.0036	.1136	.0143	.1265	.2164	.7389	1.0107	-.0018	.0111
	0.7	-.0079	.1145	.0065	.1288	.2177	.7244	1.0001	-.0024	.0117
	0.5	-.0084	.1153	-.0006	.1367	.2015	.7244	1.0040	-.0026	.0119
200	1.0	-.0061	.0768	.0008	.0837	.0491	.2488	.4141	-.0003	.0069
	0.9	-.0061	.0768	.0000	.0854	.0651	.3022	.4721	-.0008	.0074
	0.7	-.0070	.0775	-.0006	.0894	.0688	.3027	.4780	-.0009	.0080
	0.5	-.0071	.0787	-.0063	.0970	.0618	.3122	.4940	-.0012	.0081
300	1.0	-.0023	.0608	.0041	.0656	.0349	.1975	.3277	0	.0054
	0.9	-.0019	.0616	.0042	.0686	.0498	.2532	.3883	-.0004	.0059
	0.7	-.0027	.0616	.0030	.0707	.0542	.2575	.3956	-.0006	.0063
	0.5	-.0030	.0632	-.0015	.0768	.0462	.2602	.4044	-.0008	.0065
500	1.0	-.0010	.0469	.0002	.0520	.0177	.1453	.2452	-.0002	.0041
	0.9	-.0010	.0469	.0002	.0529	.0302	.1844	.2866	-.0005	.0044
	0.7	-.0009	.0469	.0006	.0566	.0319	.1865	.2927	-.0005	.0048
	0.5	-.0015	.0480	-.0027	.0608	.0263	.1895	.3001	-.0006	.0048
1000	1.0	.0012	.0332	-.0009	.0387	.0067	.1010	.1734	-.0002	.0030
	0.9	.0019	.0332	-.0013	.0387	.0089	.1221	.1944	-.0003	.0032
	0.7	.0015	.0332	-.0016	.0412	.0104	.1249	.1997	-.0003	.0035
	0.5	.0015	.0346	-.0031	.0447	.0067	.1273	.2070	-.0004	.0036

References

[1] Agrò, G., "Maximum Likelihood Estimation for the Exponential Power Function Parameters", *Communications in Statistics-Simulation and Computation*, 24(2),523-526, (1995).

[2] Agrò, G., "Parameter Orthogonality and Conditional Profile Likelihood: The Exponential Power Function Case" , *Communications in Statistics Theory and Methods*, 28(8) 1759-1768, (1999).

[3] Azzalini, A. "Futher Result on a Class of Distributions which includes the Normal Ones" , *Statistica XLVI*, 199-208, (1986).

[4] Bottazzi, G. and Secchi, A., "Maximum Likelihood Estimation of the Symmetric and Asymmetric Exponential Power Distribution, " LEM Papers Series, Laboratory of Economics and Management (LEM), Sant' Anna chool of Advanced Studies, Pisa, Italy, (2006/19).

[5] Box, G.E.P, "A Note on Regions for Test of Kurtosis", *Biometrika*, 40, 465, (1953).

[6] Hampel, F. R., Ronchetti, E. M., Rousseeuw, P. J. and W.A., Robust Statistics-The Approach Based on Inflence Functions, Wiley, 1986 (republished in paperback,2005)

[7] Huber, P. J., Robust Statistics, Wiley, (1981).

[8] Kirkpatrick, S., Gelatt, C.D. and Vecchi,M.P. (1983) "Optimization by simulated annelaing". Science 220, 671-680, (1983).

[9] Lunetta, G.,"Di una Generalizzazione dello Schema della Curva Normale", *Annali della Facolta di Economià e Commercio di Palermo*,17, 237-244, (1963).

[10] Mineo, A. M., "On the estimation of the structure parameter of a normal distribution of order p" , *Statistica (Bologna)*, 63, no.1, 109-122, (2004).

[11] Mineo, A.M. and Ruggieri, M., "A Software Tool for the Exponential Power Distri bution: The normalp package", *Journal of Statistical software*, 12(4), (2005).

[12] Mineo, A.M., *The normalp package*. URL http://CRAN.R-project.org/, (2007).

[13] Nelson, D.B., "Conditional Heteroskedasticity in Asset Returns: A new Approach", *Econometrica* 59(2), 347-370, (1991).

[14] Robert, C.P. and Casella, G., Monte Carlo Statistical Methods, second edition, Springer, (2004).

[15] Subbotin, M.T., "On the Law of Frequency of Errors", *Matematicheskii Sbornik*, 31, 296-301, (1923).

[16] Turner, M.C., "On Heuristic Estimation Methods", *Biometrics*, 16,299,(1960).
Vianelli, S., "La Misura della Variabilita Condizionata in uno Shema Generale delle
[17] Curve Normali di Frequenza", *Statistica*, 23, 447-474,(1963).
[18] Zhu, D. and Victoria Zinde-Walsh, "Properties and Estimation of Asymmetric Exponential Power Distribution", Journal of Econometrics, 48, pp.86-99,(2009).

Received September 29 ,2009
Revised December 11 ,2009
Accepted December 22 ,2009

模擬冶金法運用在型II資料下對廣義誤差分佈之參數估計

陳思勉　廖虹媚

輔仁大學數學系及數學研究所

摘　要

對於一個三參數廣義誤差分佈EP(μ, σ, p)其參數之最大概似估計氏的表示法無法具體的呈現出來.本文透過統計模擬及冶煉法討論在型II設限資料下最大概似估計氏的表現.

圖字分類作業與語意促進效果

高玉靜
輔仁大學心理學系

摘　要

本研究主要利用Stroop干擾作業典範，進行中文圖字分類作業與語意促進效果之探究。實驗結果發現：在語意關連部分一致與完全不一致的情境下，參與者在對字分類作業上之正確率與正確反應時間要較其在對圖分類作業上之表現佳，顯示出字優效果；另語意促進效果僅在圖分類作業中得到證實，故此實證分析結果傾向支持雙重編碼理論。

關鍵字：Stroop干擾作業典範、圖字混合刺激、語意促進、雙重編碼理論

Phone: +886 2 2905 2129
Email: 078148@mail.fju.edu.tw

1.緒　論

Stroop實驗典範為研究閱讀歷程之經典，其乃導源於Stroop之叫色實驗，在Stroop叫色實驗中，受試者被要求叫出色字的顏色，實驗操弄之情境有二：一為和諧（congruent）情境，即字的顏色與其所指稱者一致，比如：用紅色寫「紅」字，另一則為不和諧（incongruent）情境，即字的顏色與字所指稱者不相符合，比如：用藍色寫「紅」字；研究結果顯示：受試者在色字不和諧的情境下，反應時間與錯誤率皆要較在和諧情境下為高，對此，研究者之解釋是：文字的閱讀已經自動化，故當刺激之顏色與所指稱者和諧時，二者不會相互干擾，但是，當刺激之顏色與所指稱者不和諧時，則會形成競爭，而產生干擾效果。

承襲此種干擾作業之原型，有研究者進一步將之轉化成「字-字」、「圖-圖」或「圖-字」等型態（Glaser & Glaser,1982；Glaser & Glaser,1989；La Heij, Van der Heijden, & Schreuder,1985），從其研究結果可發現：當作業任務為閱讀文字時，無干擾效果產生；但若作業任務為分類時，則無論是「字-字」或「圖-圖」刺激皆會有干擾效果（Glaser & Glaser,1989），而就「圖-字」等結合兩種形式之刺激來看，在進行語文處理時容易被圖形分心物所干擾，但進行圖形分類時卻不會受到分心字之影響（Smith & Magee,1980；Glaser & Dungelhoff,1984）；Arieh與Algom（2002）之研究亦顯示參與者在圖字分類作業之表現呈現圖優效果，也就是說，當要求參與者將注意力置於圖形而忽略干擾字，以對目標圖形進行分類時，參與者受干擾字之影響較小，相對的，要求參與者注意目標字、忽略干擾圖形，以進行對文字之分類時，干擾圖形對參與者作業表現之影響較大。

對於上述圖優現象，國外學者傾向以共同編碼假定加以解釋，所謂之共同編碼假定圖形和文字刺激經處理後會被轉譯成抽象形式，如圖1所示（Amrhein,1994），且圖形觸接抽象語意系統要快於文字，由於分類作業不太涉及語言學的處理，而文字刺激之處理在到達抽象編碼前需要經過語言學處理程序，因此，圖形在觸接抽象語意系統具有優先性（Theios & Amrhein,1989；Glaser,1992）。

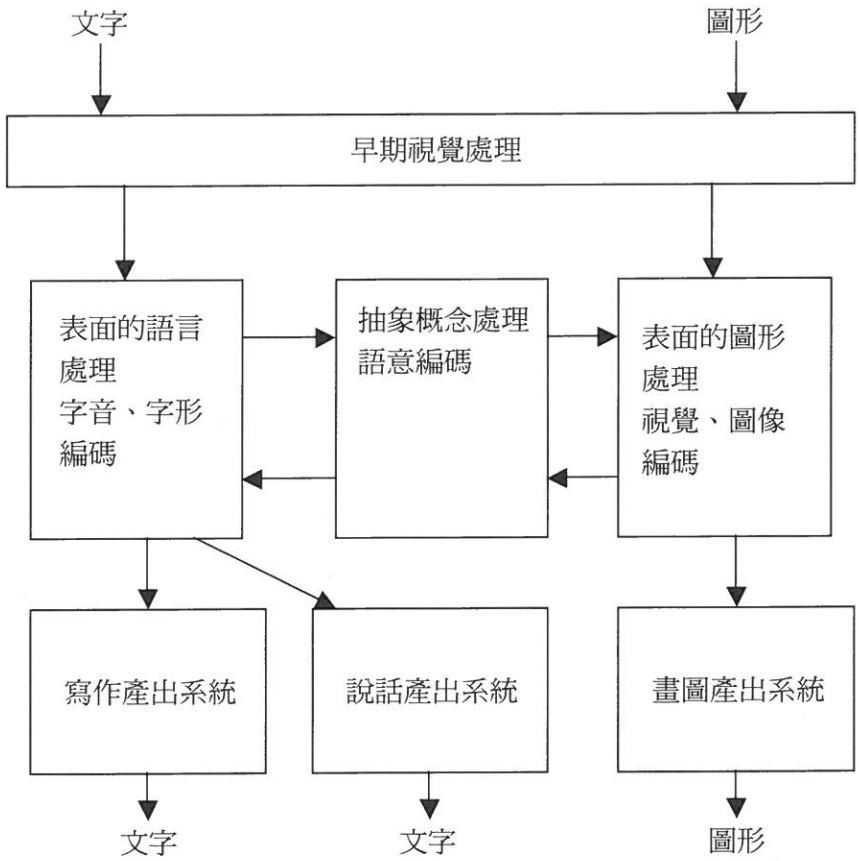

圖1. 共同編碼模式圖
資料來源：Temporal invariance for picture-word translation: evidence from drawing-writing and naming-reading tasks by P. C. Amrhein, 1994, *Memory and Cognition*, 22, 443.

相對於共同編碼模式，Paivio主張人類擁有兩種不同但有互動關係的訊息處理系統，一為語文系統，另一為視覺系統；文字由語文系統加以編碼處理，儲存在語文記憶區，視覺圖像訊息則由視覺系統編碼，儲存在視覺記憶區，並且同時與其對應之語文系統產生參照連結，如圖2所示（Amrhein,1994）。Glaser（1992）認為雙元編碼假

定無法預測分類的字圖差異，因為高層次的區別較抽象，其應被儲存在由文字觸接要較圖形為快之語文系統，倘若只有一個語文形式之內在表徵，則對圖分類應該較對字分類要花費較長的時間，這是因為圖形刺激必須被轉為文字碼，而文字刺激不需要經歷此歷程所致。

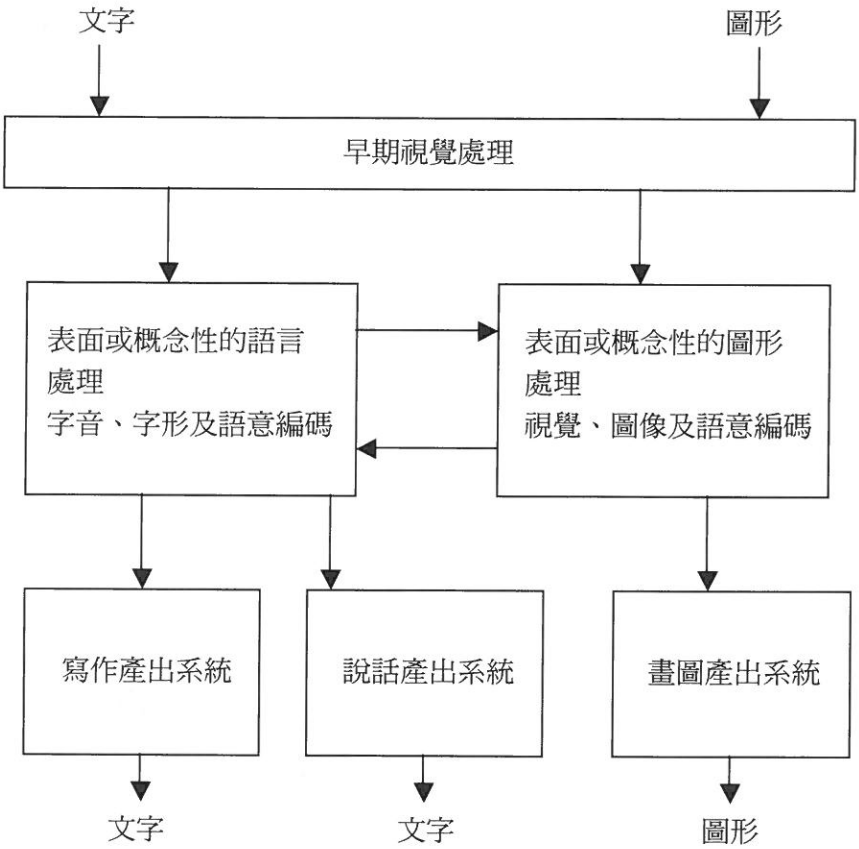

圖2. 雙重編碼模式圖
資料來源：Temporal invariance for picture-word translation: evidence from drawing-writing and naming-reading tasks by P. C. Amrhein, 1994, *Memory and Cognition*, 22, 443.

由於以往圖字分類研究結果所產出之脈絡仍不脫西方拼音符號表徵系統之外，而中文屬於意符表徵系統，其結構當與拼音文字系統不同，李文玲、張厚粲（1993）之研究便曾指出中文是介在圖畫與英文間之一種符號系統。是故，研究者想瞭解以中文字為刺激之圖字整合型干擾作業，能否再次驗證共同編碼論所解釋之圖優效果。

此外，刺激中分心物與目標物之配對，常會影響干擾量，通常刺激物之目標成份與分心成份間在基礎層次完全符合，則會產生促發效果，而目標項為圖形時較目標項為文字時容易被促發（Glaser & Glaser,1989）；然若分散注意項與目標項是不一致的，其配對將導致Stroop之抑制效果，Mayhis（2002）的研究指出當文字置於不和諧的物體圖形中時，受試者對字分類的速度要比當文字置於中性非物圖形中時要慢；然在叫圖作業中，則顯示出目標項較容易受到來自相同上層類別之分心項干擾甚於來自不同上層類別者（Glaser & Dungelhoff,1984；Glaser & Glaser,1989）。

換言之，語意干擾與促進效果可能分別出現在不同的處理層級，當要求參與者叫名時，涉及較基礎的處理層級，因而若干擾項與目標項同屬某一語意類別，會使得目標項之辨識延遲；但在要求參與者分類時，則直接涉及到語意層級的處理，在此，干擾項雖然在知覺層次與目標項不同，但因與目標項同屬一語意類別，故不會干擾作業表現，Roelofs（2001）曾指稱無論是對圖形或文字之分類，皆會呈現出語意促進效果，即將狗圖案歸為動物類時，語意相關之干擾字「貓」相較於無關字「樹」能促進反應發生，同樣的，當分類目標為文字，干擾目標為圖形時亦然。

基於上述，本研究提出了以下兩個待答問題：
問題一：在中文脈絡下之圖字分類作業，是否同樣會呈現出圖優效果？
問題二：在中文脈絡下之圖字分類作業，是否會呈現語意促進效果？

2.方　法

受試者

40位政治大學教育系的學生，因修課要求而參與本項實驗，所有受試者之原始視力或矯正後視力均正常。

實驗設計

本研究採用完全受試者內設計，主要操弄的是作業類型（分成對圖分類與對字分類兩個水準）以及刺激語意關連（分成完全一致、部分一致與不一致三個水準）兩個因子。

其中，對圖分類作業意指對內含文字的「圖形」刺激進行語意類別判斷，而對字分類作業則是對外圍圖形的「文字」刺激進行語意類別判斷；此外，所謂的完全一致（complete congruent）意指圖字刺激中之圖形與文字在基礎層次（basic level）皆完全一致，比方說：在冰箱的圖形輪廓中內含文字「冰箱」，部分一致（partial congruent）則是指圖字刺激之圖形與文字在基礎層次不相同，但卻同屬於某一上層語意類別，比如：兔子的圖形輪廓中內含文字「魚」，二者在基礎層次並不一致，但卻同屬於動物類，而不一致（incongruent）則指圖字刺激中之圖形與文字在基礎層次與上層語意類別層次完全不一致，比如：在汽車的圖形輪廓中內含「檯燈」二字，其不僅在基礎層次不相同，在語意類別亦各自分屬於交通運輸工具以及電器類。

所有實驗參與者均接受48個嘗試次，其中，對圖分類有6個練習嘗試次，18個正式嘗試次，而對字分類亦有6個練習嘗試次與18個正式嘗試次。為了能平衡不同分類作業進行先後順序所導致之反應偏向影響，有半數之受試者先作圖形分類作業，接著才作文字分類，另外半數受試則恰好相反，即先對文字進行分類，之後，再對圖形加以分類，而上述各區段中之嘗試呈現順序是隨機的。

刺激材料

本實驗之圖形刺激材料取自汪曼穎（1997）建立之物體輪廓圖形常模，在上述常模中，共提供了13類、132個常見之物體輪廓圖形及其「客觀複雜度」、「主觀複雜度」、「叫名正確性」、「叫名一致性」、「熟悉度」及「心像一致性」之評估

資料，研究者乃基於研究需要隨機從中選取48個物體圖形，並利用PhotoImpact7.0製成本實驗所需之圖字刺激（參考圖3），所有刺激之大小皆為200×200像素，而其中文字之字形為新細明體、字體大小為40。

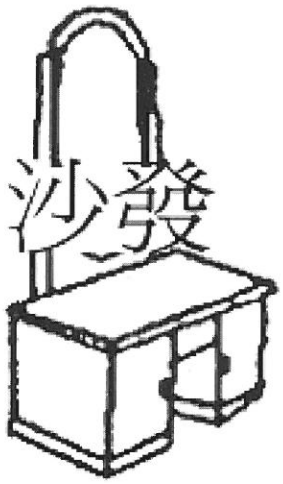

圖3. 本實驗所採用之圖字刺激範例

為了配合本實驗變項之操弄，除了將圖字刺激的配對依據其語意關連性均分為完全一致、部分一致與不一致之外，作答反應的設計為「是」與「否」各佔一半，而具有不同語意關連性之圖字刺激在反應為「是」與為「否」中之出現頻率皆相等，茲將對圖分類作業與對字分類作業之圖字刺激設計，分列於表1及表2。

表1

對圖分類作業之圖字刺激設計

練習嘗試：請判斷以下「圖形」是否為「動物」？			
正確反應	圖形	內含文字	語意關連性
是	兔子	兔子	完全一致
是	大象	駱駝	部份一致
是	魚	球	不一致
否	手套	手套	完全一致
否	削鉛筆機	滑鼠	部份一致
否	大衣	鍋子	不一致
正式嘗試：請判斷以下「圖」是否為「家電用品」？			
正確反應	圖形	內含文字	語意關連性
是	冰箱	冰箱	完全一致
是	電視	電鍋	部份一致
是	電話	蠟燭	不一致
是	熨斗	熨斗	完全一致
是	音響	檯燈	部份一致
是	洗衣機	溜冰鞋	不一致
是	吹風機	吹風機	完全一致
是	吸塵器	電風扇	部份一致
是	果汁機	釘書機	不一致
否	企鵝	企鵝	完全一致
否	月亮	風車	部份一致
否	火箭	牙刷	不一致
否	豎琴	豎琴	完全一致
否	水桶	茶壺	部份一致
否	顯微鏡	拖鞋	不一致
否	望遠鏡	望遠鏡	完全一致
否	梳妝台	沙發	部份一致
否	打火機	紅綠燈	不一致

進一步針對圖形分類作業中之圖形輪廓加以分析，汪曼穎（1997）曾提到可辨認程度高為良好圖形的重要條件，據此其提供了一些指標：高叫名正確性（>90%）、高熟悉度（>3.5）、高心像一致性（>3.5）；此外，其亦指出若研究作業重視反應速度，則應將叫名一致性納入考量。基於上述，本實驗所使用之刺激圖形在叫名正確性部分皆高於90%（介於95.2%-100%），而在熟悉度部分，除了企鵝（3.41）、火箭（3.04）以及豎琴（3.09）外，其餘皆高於3.5（介於3.63到4.78之間），就心像一致性而言，除了手套（3.29）與企鵝（3.26）外，其餘皆高於3.5（介於3.54到4.78之間），因而，在圖形的辨認方面堪稱良好，然在叫名一致性的部分，就略有限制，如：大衣（36.60%）、火箭（48.8%）、電視（50%）與梳妝台（51.2%）在此向度上之得分較低。

表2
對字分類作業之圖字刺激設計

練習嘗試：請判斷以下「圖形」是否為「文具」？			
正確反應	圖形	內含文字	語意關連性
是	圓規	圓規	完全一致
是	剪刀	書	部份一致
是	原子筆	衣櫃	不一致
否	木屐	木屐	完全一致
否	帳篷	雪人	部份一致
否	斧頭	滑板	不一致
正式嘗試：請判斷以下「文字」是否為「交通運輸工具」？			
正確反應	圖形	內含文字	語意關連性
是	飛機	飛機	完全一致
是	公車	帆船	部份一致
是	汽車	書桌	不一致
是	機車	機車	完全一致
是	火車	公車	部份一致
是	帆船	電鍋	不一致
是	纜車	纜車	完全一致

表2（續）
對字分類作業之圖字刺激設計

正式嘗試：請判斷以下「文字」是否為「交通運輸工具」？			
是	腳踏車	汽車	部份一致
是	直升機	皮箱	不一致
否	杯子	杯子	完全一致
否	天秤	榔頭	部份一致
否	鋼琴	茶壺	不一致
否	郵筒	郵筒	完全一致
否	螃蟹	鴕鳥	部份一致
否	蝴蝶	剪刀	不一致
否	照相機	照相機	完全一致
否	手電筒	縫紉機	部份一致
否	三角板	手槍	不一致

實驗程序

實驗時，受試者維持在距離螢幕70公分處。在實驗嘗試中，先在電腦螢幕正中央呈現凝視點，呈現時間為1000毫秒，之後，在原凝視點位置呈現圖字刺激，刺激出現的時間為2000毫秒，所有圖字刺激中之圖形與文字皆為黑色，而背景則為白色。

受試者在實驗中被要求忽略干擾字（或圖），而將注意力集中於圖形（或文字），並判斷目標刺激是否屬於某一語意類別，當作答反應為「是」時，按下「Z」鍵，當反應為「否」時，則按「/」鍵。

有半數的受試者在實驗一開始，先進行6個嘗試次之對圖分類練習，每個嘗試皆給予回饋，接著，才進入對圖分類之正式嘗試（共18個嘗試次），此時便不再給予回饋，在完成對圖分類作業後，緊跟著便進行對字分類，同樣先進行6個練習嘗試（有回饋）後，進入正式嘗試次（不給回饋）；而另外半數之受試者則是先完成對字分類作業之練習嘗試與正式嘗試後，才進行對圖分類。無論受試者先作何種作業，其所接受的刺激皆相同，並且所有嘗試皆為隨機呈現。

3.結　果

本研究分別以受試者在正式嘗試中之反應正確率及反應時間資料為依變項進行2(分類作業類型)×3(語意關連性)之二因子重複量數變異數分析。

由於正確率僅在交互作用項違反了球形假設（Mauchly's W=.819,p=.022），且在經過對數轉換後仍有違反球形假設現象（Mauchly's W=.706,p=.001），而反應時間未違反球形假設（Mauchly's W=.963,p=.486），因此，本研究將直接採用原始資料進行變異數分析，有違反球形假設的部分，則採用校正後的檢定結果。

就反應正確率而言，結果呈現出「分類作業類型」與「語意關連性」之交互作用效果（$F_{(2,78)}$ =8.346，p<.01），參見圖4。進一步針對此交互作用效果進行單純主要效果檢定與事後比較（參見表3），就分類作業類型之單純主要效果而言，研究發現：在語意關連為不一致之情境時，對圖分類之反應正確率（65.37%）明顯較對字分類（82.48%）為低（p<.01）；另就語意關連性之單純主要效果而言，在對圖形分類的條件下，刺激語意關連完全一致時之正確率要較語意關連部分一致時之正確率高（二者的正確率分別為90.77%與81.57%，p<.01），亦較語意關連不一致時之正確率（65.37%）要高（p<.001），此外，語意關連部分一致時較語意關連不一致時之反應正確率要高（p<.001），然在對字分類的情境下，各種語意關連條件間則無顯著差異。

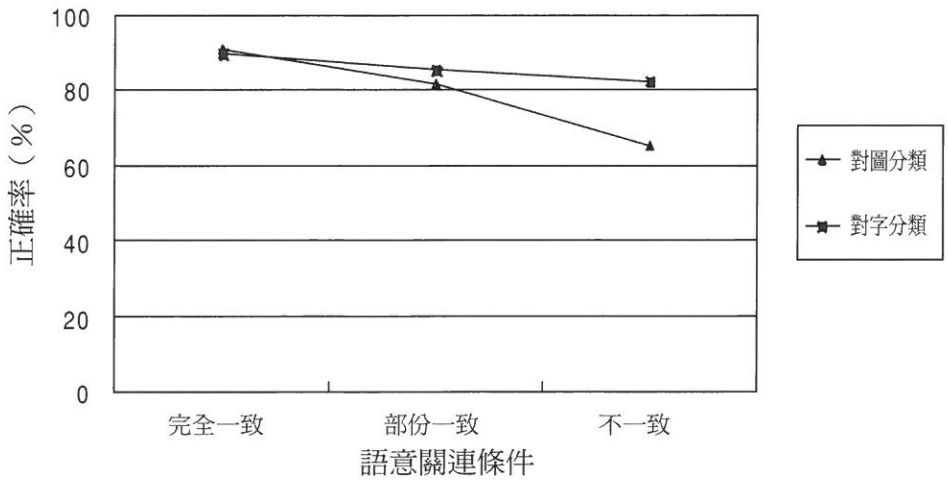

圖4. 作業類型與語意關連對反應率的交互作用效果

表3
不同分類作業與語意關連性對反應正確率單純主要效果檢定之變異數分析摘要

變異來源	SS	df	MS	F	事後比較結果
分類作業類型					
在語意完全一致的條件下	.003	1	.003	.123	
在語意部分一致的條件下	.029	1	.029	.871	
在語意不一致的條件下	.585	1	.585	11.377**	字> 圖
語意關連性					
在對圖分類的條件下	1.323	2	.661	24.971***	一致>部分 一致>不一致 部分>不一致
在對字分類的條件下	.100	2	.050	2.861	

p<.01,*p<.001

另就反應時間而言，本實驗結果亦呈現出「分類作業類型」與「語意關連性」之交互作用效果（$F_{(2,78)}$ =14.189，p<.001），參見圖5。進一步針對此交互作用效果進行單純主要效果檢定與事後比較，發現：就分類作業之單純主要效果而言，在語意關連為部分一致時，對圖分類之正確反應時間明顯要較對字分類時為長（反應時間差異為162.623毫秒，p<.001），在語意關連為完全不一致時，對圖分類的反應時間亦明顯要較對字分類的反應時間長（反應時間差異為214.032毫秒，p<.001），在語意關連完全一致的情境下，對圖與對字分類作業的反應時間則無差異存在；此外，在對圖形分類情境下，不同語意關連性間之差異達到顯著（$F_{(2,78)}$ =19.912,p<.001），經LSD事後考驗，得知其單純主要效果來自於在對圖形分類時，刺激之語意關連完全一致較部分一致、不一致之正確反應時間明顯要短（語意完全一致較部分一致的反應時間短164.782毫秒，p<.001；語意完全一致較完全不一致的反應時間短179.864毫秒，p<.001），而在對字分類情境下，各種語意關連條件間並無顯著差異存在。

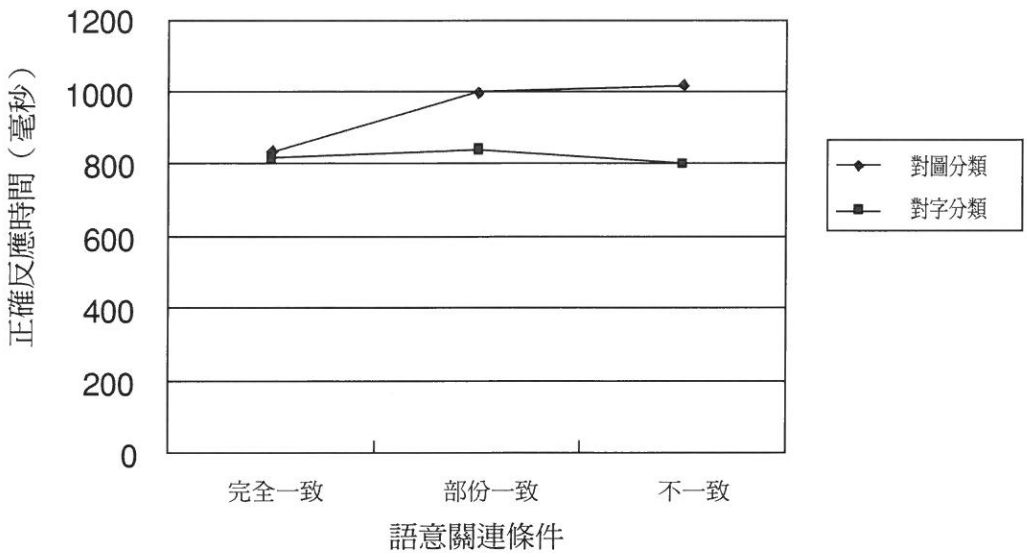

圖5. 作業類型與語意關連對反應時間的交互作用效果

4.討　論

研究結果顯示：無論是在反應正確率以及正確反應時間，對文字分類皆有較對圖形分類為佳之表現，亦即本研究並未在中文化分類作業中發現圖優效果。此與李文玲、張厚粲（1993）實驗一之研究結果不一致，然研究者以為此乃是由於其所設計之分類作業，每次僅呈現一種形式（或圖形、或中文字、或英文字）之刺激，在辨識與語意決定歷程未受到干擾效果介入所致；此外，就圖形分類之正確率而言，當目標項與干擾項間之語意關連完全一致或部分一致時，皆較之二者不一致時有明顯的優勢表現，此證實了語意促進效果之存在，但在正確反應時間上，目標項與干擾項間語意關連完全一致會較部分一致或不一致來得迅速，此與叫圖作業之反應組型較為相似，然對文字分類而言，則完全未發現語意促發效果。綜合以上，本研究傾向支持雙重編碼假定，也就是說，在處理圖形刺激時，必須經歷語文訊息處理歷程以提取相對應之抽象語意碼，此正可說明對文字進行語意類別判斷會比對圖形類別進行判斷要快之因，同時，干擾文字在語文系統中觸接語意要較目標圖形來得迅速些，因此，其瓜分了圖形處理時所需之認知資源，而造成對圖形類別進行判斷之干擾；反之，當目標項為文字時，在干擾圖形尚未與之競爭認知資源之前，即完成了抽象語意觸接工作，是故，文字分類作業不會受圖形分散注意項之干擾。

參考文獻

[1] 李文玲、張厚粲。圖畫與中、英文字詞識別加工的比較。*心理學報*，1，24-30。（1993）。

[2] 汪曼穎。常見物體之輪廓圖形的知覺及語意特性評估研究。*中華心理學刊*，2，157-172。（1997）。

[3] Amrhein, P. C. Temporal invariance for picture-word translation: evidence from drawing-writing and naming-reading tasks. *Memory and Cognition*, 22, 442-454. (1994).

[4] Arieh, Y., & Algom, D. Processing picture-word stimuli: the contingent nature of picture and of word superiority. *Journal of Experimental Psychology: Learning, Memory, and Cognition*, 28, 221- 232. (2002).

[5] Glaser, M. O., & Glaser, W. R. Time course analysis of Stroop phenomenon. *Journal of Experimental Psychology: Human Perception and Performance*, 8, 875-894. (1982).

[6] Glaser, W. R. Picture naming. *Cognition*, 42, 61-105. (1992).

[7] Glaser, W. R., & Dungelhoff, F. -J. The time course of picture-word interference. *Journal of Experimental Psychology: Human Perception and Performance*, 10, 640-654. (1984).

[8] Glaser, W. R., & Glaser, M. O. Context effects in Stroop-like word and picture processing. *Journal of Experimental Psychology: General*, 118, 13-42. (1989).

[9] La Heij, W., Van der Heijden, A. H. C., & Schreuder, R. Semantic priming and Stroop-like interference in word-naming task. *Journal of Experimental Psychology: Human Perception and Performance*, 11, 62-80. (1985).

[10] Smith, M. C., & Magee, L. E. Tracing the time course of picture-word processing. *Journal of Experimental Psychology: General*, 109, 373- 392. (1980).

[11] Theios, J., & Amrhein, P. C. Theoretical analysis of the cognitive processing of lexical and pictorial stimuli: reading, naming, and visual and conceptual comparisons. *Psychological Review*, 96, 5-24. (1989).

[12] Mayhis, K. M. Semantic interference from objects both in and out of a scene context. *Journal of Experimental Psychology: Learning, Memory, and Cognition*, 28, 171-182. (2002).

[13] Roelofs, A. Set size and repetition matter: comment on Caramazza and Costa (2000).*Cognition*, 80, 283-290. (2001)

Received October 13 ,2009
Revised December 11 ,2009
Accepted December 27 .2009

Picture-Word Difference in Categorizing and Semantic Facilitation

Yu-Jing Gao
Department of Psychology, Fu Jen Catholic University

Abstract

The Stroop interference paradigm was used to explore the difference in categorizing the picture or the word of picture-word compounds and the effect of semantic facilitation. The type of task in categorizing and semantic relatedness of distractors has a significant interaction effect on the rate of correct responses and latencies. The effect of word superiority was found while partially congruent and fully incongruent stimuli were presented. Besides, the semantic facilitation effect was obtained in picture categorizing. These results could be explained by the dual-code theory.

Key Words : Stroop interference paradigm, picture-word compounds, semantic facilitation, dual-code theory

Phone: +886 2 2905 2129
Email: 078148@mail.fju.edu.tw

Using Multithreading with Blocking on Multi-Core Processors

Joseph M. Arul[1], Fu-Hsin Chen, Tsung-Yun Chen, Ming-Yan Tu and Da-Lun Luo

Department of Computer Science and Information Engineering,
Fu Jen Catholic University, Hsin Chuang 242, Taipei, Taiwan.

Abstract

In the 21th century, computers are built with not just one level cache, but even up to three level cache memories. There is an on-chip and off-chip cache. Even the note book computers come with dual core processors. Cache is an effective way to eliminate the performance gap between processor speed and memory access. However, how to use cache efficiently has been an important issue. Several researches on adjustable cache have been investigated recently. Among many techniques, blocking is a well known and effective way, which can reduce cache miss and give good performance of program execution. Now, multithreading has been intertwined with the multi-core to switch rapidly from one core to another core. Due to data locality, multithreading can also reduce cache misses. Since multi-core processors are becoming the mainstream of the computer market, how to use multi-core processor and get better cache performance as well better execution time is an issue. Hence, this paper will combine multithreading with blocking technique and observe the improvement of cache miss which will ultimately lead to better performance of the execution of a program. Several common benchmarks were chosen to execute on a multi-core processor using OpenMP compiler. When a sequential program is executed using hyper-threading on a multi-core processor, the cache performance improvement is only about 2% and the execution of the program improves slightly. In addition, when blocking technique is used, the cache performance improvement is about 6%.This leads to better execution performance of these benchmarks. While this technique improves cache performance, the performance improvement of the overall execution of a program on a multi-core processor is obvious.

Keywords **:** Multithreading, Multi-core, Cache, Blocking, OpenMP.

[1] Corresponding author: Joseph M. Arul, email: arul@csie.fju.edu.tw,
Ph: (02)2905-3896 Fax: (02)2902-3550

1. Introduction

The performance gap between processor and memory has been a critical bottleneck in achieving maximum program performance. The processor performance improvement speed is much faster than memory. Hence, how to reduce the performance gap between processor speed and memory access has been an important issue. There are many techniques proposed to alleviate the gap and tolerate the memory latency. Among them, the utilization of cache has been proven to be a useful way [1-3]. Cache can hold the data needed for the processor to perform execution. Accessing cache takes much less time than accessing memory for processor. If the data needed for the processor is in the cache, the processor will use it without accessing memory again. Due to cache, the performance gap between processor and memory can be reduced.

Since cache is effective in reducing the gap, how to use cache efficiently has been an important issue. Blocking has been proved to be a useful way to reduce cache misses [4-7]. Generally, if we need to access an array, we will access the entire array. But when the array is too large and it has to be reused many times, lots of cache misses will occur. Instead of operating on entire matrix, blocking is performed on submatrices. Only needed portion of the matrix is accessed at a time. The portion is small enough to stay in cache and it will be used to the maximum amount of time. A lot of cache misses can be eliminated. So, this can lead to low cache misses.

Nowadays, multi-core processor has become the mainstream of computer market. There are many researches that are related to multi-core architecture [7-10]. In the multi-core architecture, there are many execution cores in it. The cores can execute simultaneously and much work can be done at the same time. This can lead to high throughput. In a multi-core architecture, multithreading is extremely important because every core needs at least a thread to operate. Multiple cores need multiple threads so that the cores can be fully utilized. Because of the popularity of multi-core processors, the use of multithreading becomes more important than before. This paper presents not only using multithreading, but how to use it efficiently by improving the cache performance. Using multithreading with a blocking methodology on a multi-core processor can lead to a better cache performance and execution time. This research

mainly explores the usage of blocking on a multithreaded multi-core architecture.

The reminder of this paper is organized as follows. In section 2, we will present the background and related work. In section 3, we will discuss the multithreading issues with a blocking methodology in detail. In section 4, we will present the experimental environment and experimental results. Section 5 will present the conclusion and the future work.

2. Background and Related Research

Blocking is a technique that can utilize temporal locality. There are some studies using this technique. Lam et. al. [4] optimized cache performance via blocking. They used cache interference to discover the behavior of cache. Using a fixed blocking factor and tailoring the blocking factor lead to different cache interference misses. Using a fixed blocking factor for a given cache size causes relatively high cache interference misses. Tailoring the block size for different matrix sizes and cache parameters can get a better cache interference misses. Based on the experimental results, they have showed that the performance of the cache is highly dependent on the problem size and the block size. It is more effective to tailor the block size according to the problem size and cache size.

In [5], an algorithm is presented to choose the best problem-size dependent tile sizes. When we input the cache size, the cache line size, the column length and the row length, we can get the best tile size as the output. The sizes of the tile submatrices are small enough to remain in the cache for reuse. This can utilize the data locality to improve the cache performance. On a direct-mapped cache, it gives better performance than other algorithms. On higher set associativity caches, it also performs well when matrices are large in comparison to the cache size.

Park et. al. [6] provide a theoretical analysis for the TLB and cache performance of block data layout. A lower bound analysis for TLB performance is presented. The lower bound where N means that we are accessing an N by N Matrix and the Pv represents the page size of

the TLB. They showed that block data layout achieves this bound ($2\ (N^2/\sqrt{Pv})$). Block data layout improves TLB misses by a factor of O(B), where B is the block size of block data layout. Because of temporal locality and reduced capacity misses, block data layout with tiling can improve overall memory hierarchy performance. Hence, using blocking technique is an efficient way to reduce cache misses. For this part, we have discussed how to choose the appropriate blocking size that is needed when applying blocking technique. In the next part we will discuss multithreading that is another way to reduce cache miss.

2.1 Multithreading

There are some studies that are related to cache performance on multithreading. These studies discuss how to use multiple threads efficiently to get low cache miss rate. Kwak et. al. [11] presented a Multithreaded Virtual Processor (MVP) model. The processor integrates the multithreaded programming paradigm and a modern superscalar processor. It is capable of fast context switching and threads scheduling. Based on MVP, they showed that multithreading can tolerate memory latency and utilize data locality. Data locality means that a thread brings the data into cache; other threads may use it later. Thus, multithreading execution gets lower cache miss rates than serial execution.

Based on trace-driven simulation, Chen et. al. [12] evaluated three scheduling schemes. They are round-robin (switch-on-instruction), round-robin (switch-on-miss) and priority scheduling (MRU-priority). Their experimental results show that priority scheduling has the best cache performance. They also studied the effect of multithreading degree on cache performance. According to the experimental results, they suggest that cache size and set associativity should be increased with the multithreading degree. In this part we can see that multithreading can improve cache performance because of data locality. How to use multithreading efficiently to utilize data locality is an important issue. Nowadays, multi-core processors become more and more popular. On a multi-core processor multiple threads need to execute. So, how to use multithread on a multi-core processor efficiently is another important issue. In the next part, we will discuss the multi-core architecture.

2.2 Multi-Core Architecture

Gepner et. al. [9] discussed some innovative designs on Intel multi-core processor, like

Intel Advanced Smart Cache and Intel Smart Memory Access. Former multi-core processors used separate L2 cache. However, it led to bad CPU performance. A New multi-core processor uses shared L2 cache and it increases the efficiency of cache to processor core data transfers and inter-processor communication. Figure 1 shows the layout of different dual-core CPU L2 cache organization. Intel Advanced Smart Cache adopts shared L2 cache. Data is stored in one location of the cache and each core can access it. When one core needs less cache, the other core can increase their usage of L2 cache. Thus, it can share better the L2 cache. This can reduce cache misses. As to Intel Smart Memory Access, it speculatively loads data into the execution cores for instructions that are about to be executed before previously stored instructions are executed. This can improve execution throughput because it maximizes the available system-bus bandwidth and hides latency to the memory subsystem.

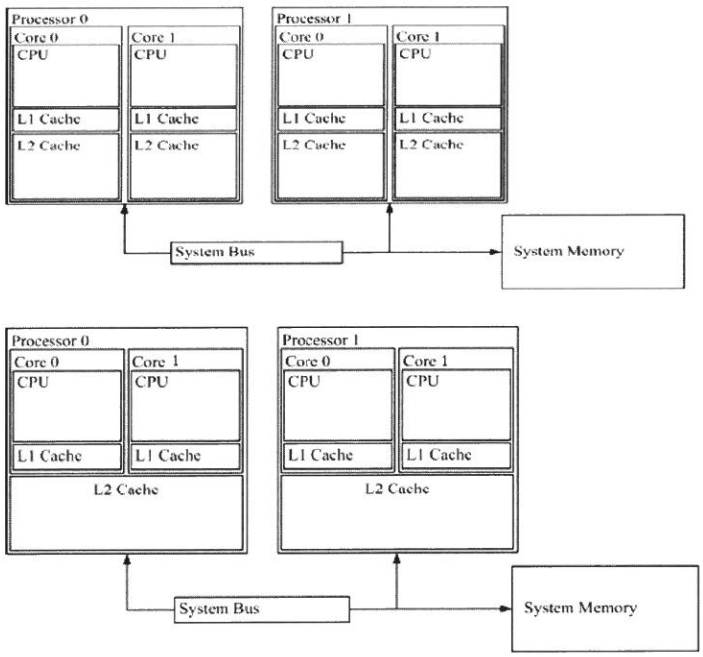

Figure 1. Dual Socket System with Different Dual-Core CPU L2 Cache Organization (figure taken from [9])

3. Multithreading with Blocking on Multi-Core Processor

Multi-core processors have become the mainstream of the computer market. There are two or more independent cores in a single processor. A process with one thread is not capable of fully utilizing multi-core processors. Multithreading is suitable for multi-core processors. Multiple threads can use the cores at the same time. In this chapter, we will discuss how to use multithreading with blocking technique to reduce cache misses and get the best performance on multi-core processors. In Multi-core architectures, these cores have their own hardware resources and execution sets. They can execute simultaneously. Figure 2 shows a dual-core processor architecture. The core 1 and core 2 execution units can execute simultaneously. In order to fully utilize the multi-core processor the program must be divided into two or more threads and can be simultaneously fed into multiple cores. If we have two or more threads, then each core has its own thread to process. By multithreading, the dual-core processor can really be utilized.

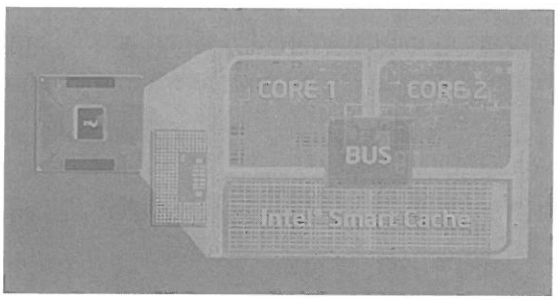

Figure 2. A Dual-Core Processor Architecture (figure taken from [13])

3.1 Multithreading with Blocking on Multi-Core Processor

Multithreading can utilize data locality to reduce cache misses. But when the cache is not big enough to hold the later data needed, data locality can not be utilized. We illustrate this situation with figure 3. There are two threads. Thread 1 accesses the elements with shadow. Thread 2 accesses the elements with bias. If the cache is not big enough to hold all the elements of B matrix, cache misses may occur while thread 2 needs the elements of B matrix. Thus, data locality is not utilized.

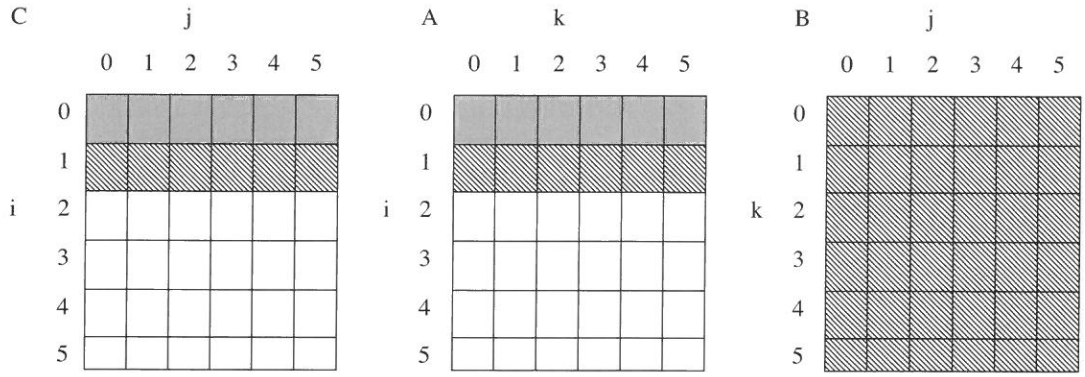

Figure 3. The Process of Multithreaded Matrix Multiplication

If we use multithreading with blocking technique, data locality can be ensured. We can vary the blocking factor to ensure that the reused data remains in the cache. Figure 4 shows the process of Multithreading with Blocking Matrix Multiplication. In each step, the submatrix of B matrix remains in the cache until it is not needed any more. Thread 1 brings the submatrix into the cache. Thread 2 can use it without fetching again. So, blocking technique can ensure the data locality of multithreading. Hence, our main purpose of our research is to implement blocking in all the OpenMP benchmarks that are run using multithreading and see the effect of cache misses as well as the impact on overall execution.

4. Benchmarks Used for the Experiments

In order to apply the blocking methodology to improve the performance of various programs as well as to show the cache performance improvement using blocking methodology, we used several benchmarks that are commonly used in various data structures.

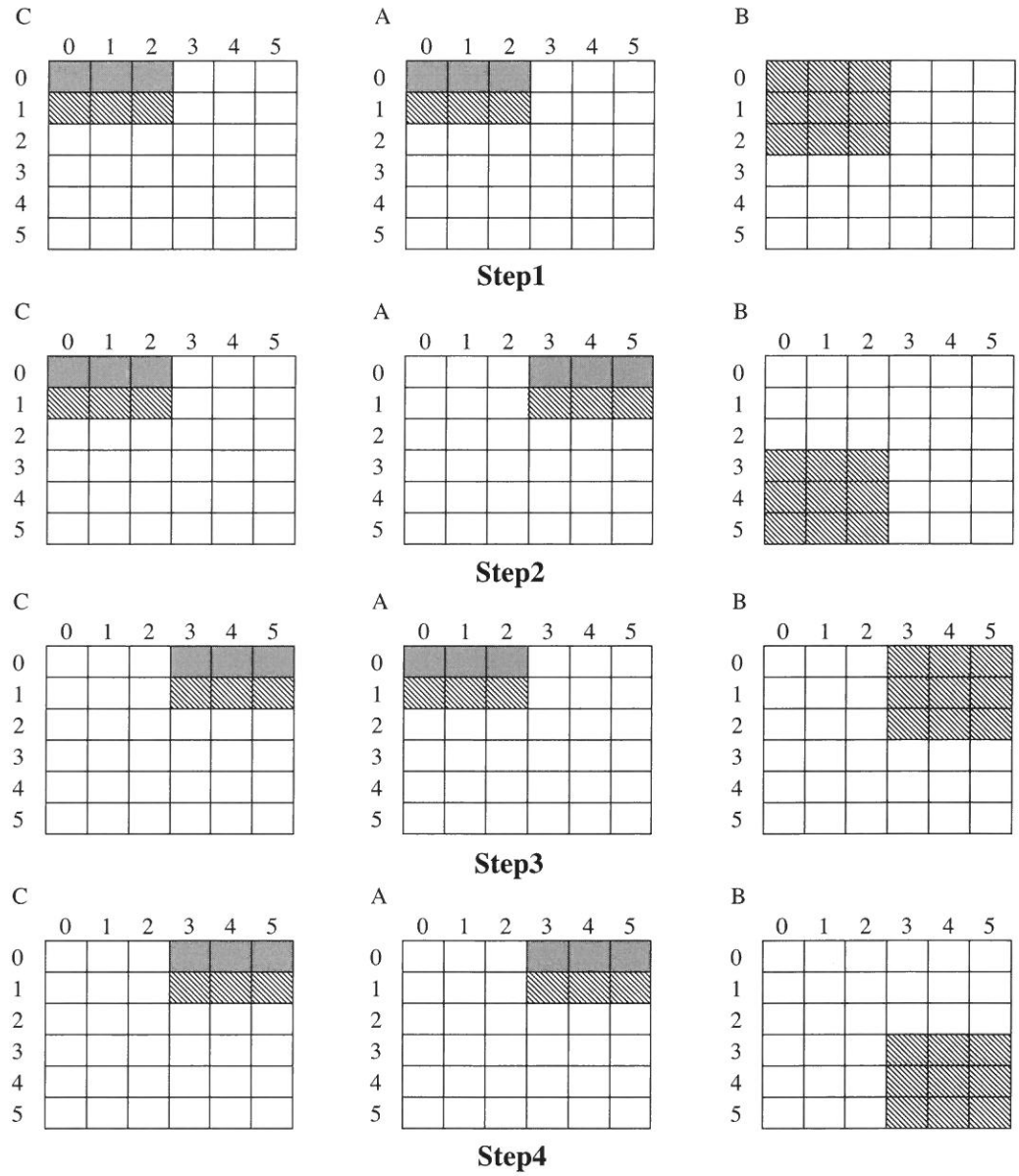

Figure 4. The Process of Multithreading with Blocking Matrix Multiplication

When we improve the cache performance of each program, we also show that the execution time of each program has also significantly been improved. The benchmarks used for comparisons are matrix multiplication, string matching, linear search, base conversion, and a program that calculates the power of n. We used OpenMP compiler to parallelize each program using hyperthreading and implemented on a Dual core machine. Every program had its serial version, parallelized version using multithread and multithread with blocking paradigm. In the following sections we describe each benchmark and its results using the above three different ways. Each benchmark shows a gradual improvement in execution time as well as cache miss rates. All the programs show that blocking method in a multithreaded environment has significantly improved cache performance. Here we describe the matrix multiplication program and its results. Figure 5 and 6 show matrix multiplication's multithread and multithread with a blocking methodology pseudocode.

```
#pragma omp parallel for   /*multithreadeb command*/
for  ( i = 0 ; i < N ; i++ )
    for  ( j = 0 ; j < N ; j++ )
        for  ( k = 0 ; k < N ; k++ )
            C[i][j] = C[i][j] + A[i][j] * B[k][j] ;
```

Figure 5. The Code for Multithreaded Matrix Multiplication

```
for  ( jj = 0 ; jj < N ;  jj = jj + BB )
    for  ( kk = 0 ; kk < N ;  kk = kk + BB )
        #pragma omp parallel for   /*multithreadeb command*/
        for  ( i = 0 ; i < N ; i++ )
            for  ( j = jj ; j < min ( jj + BB , N ) ; j++ )
                for  ( k = kk ; k < min ( kk + BB , N ) ; k++ )
                    C[i][j] = C[i][j] + A[i][j] * B[k][j] ;
```

Figure 6. The Code for Multithreaded Matrix Multiplication with Blocking

4.1 Experimental Results

The processor we used for our experimentation is Intel(R) Core(TM)2 CPU E6600 2.4GHz. The two cores share the L2 cache. We conduct our experiment on L2 cache. After compilation for various benchmarks, the programs were run on the above processor. When the programs were executed, Pintool [14] was used to dynamically collect the memory references. These memory references were stored in a file containing all the hex address values. Finally, the memory reference files were used into DineroIV [15] to analyze the cache performance of these benchmarks. We observed that 32 byte block size and a 4-way set associative had the best performance. So, block size 32 was set and a 4-way set associative was used.

Table 1. Comparison of Matrix Program's Cache Performance of Different Sizes.

Matrix Multiplication Data Cache									
Problem Size	Serial			Multithread			Multithread + Block		
	Fetches	*Misses*	*Rate (%)*	*Fetches*	*Misses*	*Rate (%)*	*Fetches*	*Misses*	*Rate (%)*
128	17392610	19468	**0.11**	17513189	21282	**0.12**	6370246	24423	**0.38**
256	135424780	16952320	**12.51**	135829800	16997447	**12.51**	46931921	446395	**0.95**
512	1077313391	134959016	**12.52**	1079966108	135343202	**12.53**	369407429	3400999	**0.92**

In the following pages we present the results of the experiments such as Matrix multiplication, string matching, linear search, base conversion, and power of n. Data miss rates of these programs and execution time with different data sizes are shown below. All these programs show similar results. We conclude that blocking mechanism not only improves cache performance of these programs, but also contributes to the execution time better than the one without blocking mechanism. Even though several benchmarks were tested, due to lack of space, only a few are mentioned here.

Table 1 presents the cache performance of matrix multiplication. Since we did not use trace reduction, our computer was not capable of getting the cache performance of 1024 by 1024 matrix. But the execution time of 1024 by 1024 matrix will be presented later. From Table 1 we can note that the miss rate of multithreaded matrix multiplication is very similar to that of serial paradigm. As we can see from the table, the cache performance of blocked

version has been improved significantly from roughly**12.5%** to **0.9%**. Except for the 128 by 128 matrix size, the miss rate of multithreaded matrix multiplication with blocking is much less compared with serial and multithreaded paradigm. It could be that the 128 by 128 matrix size is too small to show the cache benefits of blocking and multithreading. Table 1 shows that the multithreading with blocking paradigm gets the lowest miss rate. Table 2 shows not only the cache performance, but also indicates a way to improve the execution time. Table 2 presents the execution time of matrix multiplication. From table 2 we can clearly see that multithreading with blocking paradigm gets the least execution time. For example the matrix size of 1024 x 1024 takes only **1.44** secs as opposed to the multithreaded version which is about **8.45** secs.

Table 2. Comparison of Matrix Program's Execution Time for Different Data Size.

Matrix Multiplication Execution Time			
Problem Size	**Serial**	**Multithread**	**Multithread + Block**
128	0.009548	0.005056	**0.001723**
256	0.110528	0.056740	**0.013143**
512	1.536550	0.750327	**0.176759**
1024	17.094374	8.451998	**1.437403**

Table 3. Comparison of String Matching's Cache Performance for Various Sizes.

Matrix Multiplication Data Cache									
Problem Size	**Serial**			**Multithread**			**Multithread + Block**		
	Fetches	*Misses*	*Rate (%)*	*Fetches*	*Misses*	*Rate (%)*	*Fetches*	*Misses*	*Rate (%)*
100000	4134668	477934	**11.56**	4280891	379074	**8.86**	6370246	278818	**6.46**
200000	7859691	952934	**12.12**	8081612	754537	**9.34**	46931921	553893	**6.78**
400000	15309680	1902935	**12.43**	15696529	1504211	**9.58**	369407429	1103883	**7.02**
800000	30209673	3802935	**12.59**	30945246	3003953	**9.71**	369407429	2203895	**7.11**

Table 3 presents the cache performance of the string matching program. From table 3, we note that multithreading can improve the cache performance of a serial program about **3%** whatever the problem size is. Multithreading with the blocking paradigm can improve the

cache performance of serial program about **6%**. When we improve the cache performance of a program, we naturally also improve the execution time which in turn improves the performance of a program. From Table 3 we can clearly see that the cache performance improvement of multithreading with blocking paradigm is twice that of multithreaded paradigm. This program is popularly used in online dictionaries.

Table 4. Comparison of String Matching's Execution Time for Various Sizes.

Matrix Multiplication Execution Time			
Problem Size	**Serial**	**Multithread**	**Multithread + Block**
100000	0.001245	0.001192	**0.000805**
200000	0.003130	0.003010	**0.002105**
400000	0.007723	0.007445	**0.004219**
800000	0.019572	0.017044	**0.007815**

Table 4 presents the execution time of the string matching program. From table 4 we can see that multithreading improves the execution time of the serial program slightly. But the multithreaded with the blocking paradigm can improve the execution time of the serial paradigm more significantly. Hence, multithreading should be complemented with the blocking paradigm for all the loops in a program. In this program, for different data size, the improvement remains constant which is shown by the three lines. For this program we varied the data size upto 800,000 to see the improvement in execution time as well as the cache performance.

Table 5 presents the cache performance of the linear search program. From table 5 we can note that the average miss rate of serial program is about **7%**. The average miss rate of multithreaded paradigm is about **5%**. The average miss rate of multithreading with the blocking paradigm is about **0.14%**. Blocking technique improves the cache performance of multithreaded program significantly which is seen clearly in this program too. The miss rate improvement of multithreading with the blocking paradigm is about **3.5** times that of multithreaded program. Table 6 presents the execution time of linear search program. From table 6 we can see that multithreading improves the execution time of the serial program. But multithreading with the blocking paradigm can improve the execution time of the serial program further. When the problem size becomes large, the improvement of the execution

time becomes significant too. This program shows that for all different data size, the cache miss rate is not even **1%**. There is a big gap between multithreaded version and the blocking with the multithreaded paradigm.

Table 5. Comparison of Linear Search's Cache Performance for Various Sizes.

Matrix Multiplication Data Cache									
Problem Size	Serial			Multithread			Multithread + Block		
	Fetches	*Misses*	*Rate (%)*	*Fetches*	*Misses*	*Rate (%)*	*Fetches*	*Misses*	*Rate (%)*
100000	181417930	12628370	**6.96**	201915389	10125086	**5.01**	185042971	254043	**0.14**
200000	362418607	25253367	**6.97**	403370340	19681038	**4.88**	369627975	504043	**0.14**
300000	543418653	37878365	**6.97**	604887981	30458880	**5.04**	554192301	754032	**0.14**
400000	724418439	50503365	**6.97**	806383008	47490273	**5.89**	738798457	1004033	**0.14**

Table 6. Comparison of Linear Search's Execution Time for Various Sizes.

Matrix Multiplication Execution Time			
Problem Size	Serial	Multithread	Multithread + Block
100000	0.083141	0.046225	**0.030477**
200000	0.190912	0.107605	**0.061583**
300000	0.286340	0.175128	**0.094208**
400000	0.381265	0.257105	**0.124107**

Table 7 presents the cache performance of base conversion program. From table 7 we can note that the average miss rate improvement of multithreaded program is below **1%** compared to the serial program. But the average miss rate improvement of multithreading with blocking paradigm is about **5%**. The improvement is very significant.

Table 7. Comparison of Base Conversion's Cache Performance for Various Sizes.

Matrix Multiplication Data Cache									
Problem Size	Serial			Multithread			Multithread + Block		
	Fetches	*Misses*	*Rate (%)*	*Fetches*	*Misses*	*Rate (%)*	*Fetches*	*Misses*	*Rate (%)*
100000	2509842	265428	**10.58**	2694708	267073	**9.91**	1200215	66154	**5.51**
200000	4609830	527928	**11.45**	4820598	529901	**10.99**	1980340	128989	**6.51**
300000	6709819	790428	**11.78**	7060424	792465	**11.22**	2660681	191494	**7.2**
400000	8809823	1052932	**11.95**	9218576	1054971	**11.44**	3400320	254002	**7.47**

Table 8 presents the execution time of base conversion program. From figure 7 we can see that multithreading improves the execution time of serial program. But the multithreading with the blocking paradigm can improve the execution time of serial program further. When the problem size becomes large, the improvement of execution time becomes significant.

Table 8. Comparison of Base Conversion's Execution Time for Various Sizes.

Matrix Multiplication Execution Time			
Problem Size	**Serial**	**Multithread**	**Multithread + Block**
100000	0.003731	0.002670	**0.000861**
200000	0.007526	0.005208	**0.001582**
300000	0.011472	0.007919	**0.002299**
400000	0.015622	0.011117	**0.003459**

Table 9 presents the cache performance of the program calculating power of n. From table 9 we can note that the average miss rate improvement of multithreaded program is below **2%**. The average miss rate improvement of multithreaded with the blocking paradigm is about **4%** as compared to the serial version. The improvement is more significant. Figure 8 shows the results. Table 10 presents the execution time of the program calculating power of n. From figure 8 we can see that multithreading improves the execution time of the serial program. But multithreading with the blocking paradigm can improve the execution time of the serial paradigm further. When the problem size becomes large, the improvement of execution time becomes significant.

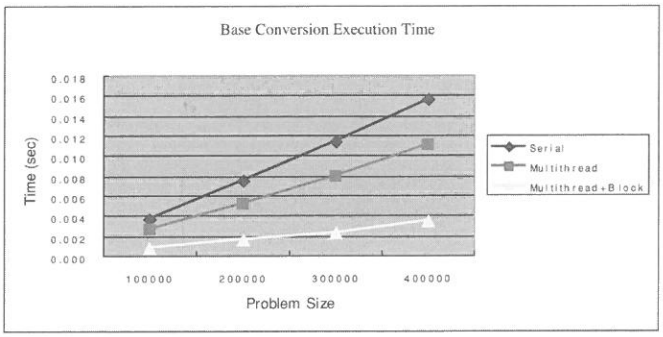

Figure 7. Execution Time of Base Conversion Program

Table 9. Comparison of Power of N Program's Cache Performance for Various Sizes.

Matrix Multiplication Data Cache									
Problem Size	Serial			Multithread			Multithread + Block		
	Fetches	*Misses*	*Rate (%)*	*Fetches*	*Misses*	*Rate (%)*	*Fetches*	*Misses*	*Rate (%)*
100000	30656695	3877932	**12.65**	31554647	3558401	**11.28**	31863483	2753906	**8.64**
200000	60906735	7752932	**12.73**	62667309	7313792	**11.67**	63204638	5503893	**8.71**
300000	91156046	11627938	**12.76**	93755112	10057455	**10.73**	94513591	8253919	**8.73**
400000	121409272	15502935	**12.77**	124859109	13094156	**10.49**	125918926	11003971	**8.74**

Table 10. Comparison of Power of N Program's Execution Time for Various Sizes.

Power of N Program on Execution Time			
Problem Size	**Serial**	**Multithread**	**Multithread + Block**
100000	0.020251	0.017411	**0.009997**
200000	0.046448	0.033713	**0.019858**
300000	0.065522	0.051711	**0.028532**
400000	0.090450	0.071136	**0.039090**

From all the experiments presented above in this paper, it is obvious that multithreading and using dual core improve the performance of the serial programs. However, using the blocking methodology improves the cache performance of all these programs and thus it improves the overall execution time of each program for various data size.

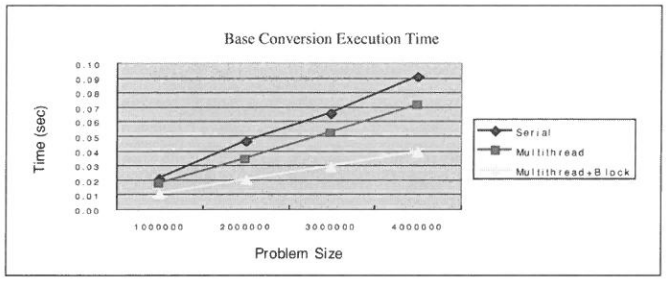

Figure 8. Execution Time of Power of N Program

5. Conclusion and Future Work

All the benchmark results show that using multithread on multi-core processors can improve the execution time of the serial program. But the cache performance improvement by multithreading is improved slightly. The average cache miss rate improvement by multithreading is about **2%**. If we use multithreading with the blocking methodology, the average cache miss rate improvement can be **6%**. The improvement is more significant. Because of low miss rate, multithreading with a blocking methodology can also reduce the execution time of the serial program further. According to our experiment, we can conclude that on multi-core processors, using multithread with a blocking methodology can get a lower cache miss rate and a better execution time than only using multithreading. Besides, based on our experiments, we find that when we are accessing a matrix, accessing the 16 by 16 submatrices can give the best cache performance. While we are accessing an array, accessing 200 elements of the array at a time can give the best cache performance.

In this research, because we do not use trace reduction technique, which is a technique used to eliminate unnecessary memory reference, the memory reference file is very big. The memory reference file of 800 by 800 matrix multiplication is about 200 GB. So we can not conduct our experiment on complicated programs. All the benchmarks tested were relatively simple. In the future, we plan to use trace reduction technique so that more complicated benchmarks can be tested. We believe that if we conduct our experiments on more complicated benchmarks, the improvement of miss rate and execution time will be more

significant. Besides, we plan to find a formula or an algorithm that can compute the best blocking size according to the core number, thread number, cache size and problem size.

References

[1] Tien-Fu Chen. and J, L. Baer, "Reducing memory latency via non-blocking and prefetching caches," ACM SIGPLAN notices, Vol. 29, No. 9, 1992, pp. 51-61.

[2] K, Öner, and M, Dubois, "Effects of memory latencies on non-blocking processor/cache architectures," In Proc. of the 7th Int'l. Conf. on Supercomputing, 1993, pp. 338-347.

[3] A. Naz, K. Kavi, W. Li and P. Sweany. "Tiny split data caches make big performance impact for embedded applications", the Journal of Embedded Computing (Special Issue on Embedded Single-Chip Multi-core Architectures from System Design to Application Support), Vol.2, No.2, 2006, pp. 207-219.

[4] M, Lam, E. Rothberg, and M.Wolf, "The Cache Performance and Optimizations of Blocked Algorithms," Proc. Fourth Int'l Conf. Architectural Support for Programming Languages and Operating Systems, 1991, pp. 63-74.

[5] S. Coleman and K. McKinley, "Tile Size Selection Using Cache Organization and Data Layout," Proc. SIGPLAN notices, Vol. 30, No.6, 1995, pp. 279-290.

[6] N. Park, B. Hong, and V. Prasanna, "Analysis of memory hierarchy performance of block data layout," Proc. of the Int. Conf. on Parallel Processing, 2002, pp. 35.

[7] J. Parkhurst, J. Darringer, and B. Grundmann. "From single core to multi-core: preparing for a new exponential," In ICCAD '06: Proc. of the 2006 IEEE/ACM international Conf. on Computer-aided design, 2006, pp. 67-72.

[8] R. Noronha, and D. Panda, "Improving Scalability of OpenMP Applications on Multi-core Systems Using Large Page Support," IEEE Int. Symposium On Parallel and Distributed Processing, 2007, pp. 1-8.

[9] P. Gepner and M. Kowalik, "Multi-Core Processors: New Way to Achieve High System Performance, " Proc. of the Int. Symposium on Parallel Computing in Electrical Engineering (PARELEC'06), 2006, pp. 9-13.

[10] A. Kayi, Y. Yao, T. El-Ghazawi, and G. Newby, "Experimental Evaluation of Emerging

Multi-core Architectures," IEEE Int. Symposium on Parallel and Distributed Processing, 2007, pp. 1-6.

[11] H. Kwak, B. Lee, A. Hurson, Suk-Han Yoon, and Woo-Jong Hahn, "Effects of Multithreading on Cache Performance," *IEEE Transactions on Computers,* vol. 48, no. 2, 1999, pp. 176-184.

[12] Yunn-Yen Chen, Jih-Kwon Peir, and Chung-Ta King, "Performance of Shared Cache on Multithreaded Architectures," Proc. of the 4th Euromicro Workshop on Parallel and

[13] Distributed Processing (PDP '96), 1996, pp. 541- 548.

[14] Intel Website. http://www.intel.com/technology/computing/dual-core/

[15] Intel Pin. http://rogue.colorado.edu/pin/

J. Edler and M. D. Hill. http://pages.cs.wisc.edu/~markhill/DineroIV/

Received October 16 ,2009
Revised December 13 ,2009
Accepted December 27 ,2009

使用多執行緒與區塊資料存取於多核心處理器上

周賜福 陳福新 陳琮云 涂明彥 羅大倫
輔仁大學資訊工程系

摘 要

在二十一世紀，電腦擁有不只單一階層的快取，而是最多達三階層的快取記憶體。包含晶片上與晶片外的快取。就算是筆記型電腦，也擁有雙核心的處理器。快取是個有效解決處理器速度與記憶體存取時間差的方法，如何有效率地運用快取一直是個討論的重點。最近有數篇研究在探討快取調校。在眾多技術中，區塊資料存取(blocking)是個廣為人知且有效的方法，它可以降低快取失誤進而提昇程式執行效能。現在，多執行緒也與多核心處理器結合，以達到在不同核心中快速轉換的效果。由於多執行緒有資料區域性，它亦可降低快取失誤。而如今，多核心處理器已成為市場上的主流，如何有效率的運用多核心處理器以提昇其效能，亦是一個重要的課題。因此，在此篇論文中，我們將結合區塊資料存取與多執行緒這兩個技術，觀察在多核心處理器上可獲得多少快取及執行時間的效能改善。我們在實驗中使用OpenMP編譯器，在多核心處理器上測試多個標準程式。在多核心處理器上以超執行緒執行循序處理程式時，可改善約2%的快取失誤率，程式的執行效能只有些微的改善。但結合區塊資料存取後，可改善約6%的快取失誤率，這可更進一步改善測試程式的執行效能。這個技術不只可改善快取效能，在多核心處理器上，程式整體執行效能的改善亦非常明顯。

關鍵字：多執行緒，多核心，快取，區塊資料

μzBox：音樂辨識與管理系統[1]

尤姿文、徐嘉連[2]
輔仁大學資訊工程學系

摘　要

在內涵式音樂資訊查詢（content-based music information retrieval）的研究領域中，基於網際網路的發展與MP3音樂大為盛行，音樂資料量越來越龐大，且有許多不知名的音樂物件，如何提供查詢音樂資訊與管理的服務是一個重要的研究主題。

在這篇論文裡面，我們提供音樂辨識與管理系統(Music Identification Management System) 軟體，命名此系統為μzBox，音樂物件辨識可利用此系統得到音樂資訊，並且編輯音樂資訊及音樂分類。我們使用音樂物件格式為MP3和WAVE格式。

音樂辨識（Music identification）關鍵之一是如何擷取音樂物件中的特徵，本論文擷取特徵參數為梅爾刻度式倒頻譜參數（Mel-scale frequency cepstrums coefficients，MFCC），採用Bisecting *K*-means clustering來分群音樂特徵參數，而得數個群集，並從數個群集中挑選音樂參考特徵，作為音樂物件之間相似比對依據，使用*k*-nearest neighbor classifier（*k*-NN）演算方法計算音樂物件之間的相似度，將查詢相似歌曲的音樂資訊回傳給使用者。最後，本論文並根據所提之演算法實作系統，來評估查詢的命中率。

關鍵字：內涵式音樂資訊查詢(Content-based music information retrieval)、音樂辨識(Music Identification)、音樂特徵(Music feature)、梅爾刻度式倒頻譜係數(Mel-scale frequency cepstrums coefficients，MFCC)、Bisecting *K*-means clustering、*k*-nearest neighbor classifier。

---

1 本論文研究為輔仁大學補助研究、計畫編號：409731044039
2 論文通訊作者：Email: alien@csie.fju.edu.tw

1. 序　論

內涵式音樂資訊查詢(content-based music information retrieval)的研究領域，是這幾年來迅速發展研究相關的議題，音樂物件的分析有兩類格式，分別為symbolic類型和digital audio類型。

symbolic類型主要格式為MIDI檔，將音樂旋律的音高(pitch)或音頻(frequency)轉換成數值或符號來代表音樂物件特徵，以字串(string)的方式呈現，藉由字串比對演算法(string matching algorithm)得到相似的音樂。

另一個研究音樂類型為數位音訊(digital audio)，也就是MP3或WAVE格式。因此，在這音樂物件中含有大量的特徵資訊，特徵通常都以時間的形式(time series pattern)來表達，如何從音樂物件中取出具有代表性的特徵參數也是一個很重要研究，例如最常使用的特徵有音高(pitch)、節奏(rhythm)、音色(timbre)等等，就數位音訊(digital audio)分析的角度來說，若這些音樂物件的特徵保存越多，則音樂可以分析就越準確。

近期，音樂特徵(Music feature)的擷取與應用發展，提供許多查詢音樂服務給使用者，例如：彈奏查詢(query by tapping)、範例查詢(query by example)、關鍵字查詢(query by keyword)、哼唱系統(query by humming)等等研究領域，而我們欲提供查詢與整理硬碟中的音樂物件、編輯音樂物件的音樂資訊，進而整理與分類音樂物件，我們稱之為音樂辨識與管理系統(Music Identification and Management System)，命名此系統為μzBox。

本篇論文，音樂物件格式為數位音訊(digital audio)類型，我們利用音色(timbre)來保存音樂物件的特徵，採用梅爾刻度式倒頻譜係數(Mel-scale frequency cepstral coefficients，MFCC)來分析音樂物件，並且建立音樂物件的音樂資訊。

1.1 研究動機

由於網際網路迅速發展，且MP3音樂在數位音樂世界中大為盛行，因此下載許多音樂在硬碟中，且加上科技的發展，使得儲存裝置的容量越來越大，而我們儲存在硬碟中的音樂資料量越來越龐大，如何有效率整理硬碟中的音樂資料量，在整理這些音樂物件時，音樂辨識(Music identification)變成一個很重要的課題。

這幾年來，在「內涵式音樂資訊查詢(Content-based music information retrieval)」的多媒體研究領域中，音樂資訊查詢與搜尋的技術越來越受重視，近來相關研究主題有關鍵字查詢(query by keyword)、範例查詢(query by example)、彈奏查詢(query by tapping)、哼唱系統(query by humming)等等研究領域。傳統的查詢方式，需使用者提供歌名、歌手名稱、關鍵字或者音符來查詢，但近來的研究都朝著音訊方面查詢歌曲資訊，例如哼唱系統(query by humming)，需使用者哼唱一段旋律或給一段音樂。以上這些搜尋方式雖然很方便，但有時在操作上對使用者來說會有困難，當使用者不記得音樂資訊時，往往就無法提供有效的查詢。利用音符或哼唱旋律辨識音樂資訊，這對於沒有音樂背景或者不懂得樂理的使用者來說，在查詢上更加困難，因為使用者有可能不知如何哼唱這首歌曲的旋律或哼唱旋律時不準確，造成音高相同但節奏不同而導致查詢不正確或找不到音樂。因此，使用者的硬碟中，若有一堆不知名的歌曲或沒有音樂資訊時，使用上列的方式查詢會相當耗時間，且會很辛苦在整理音樂資料與音樂資訊，有鑑於此，如果我們提供一個音樂辨識與管理系統(Music Identification Management System) 軟體，對於硬碟中的音樂物件作進一步查詢音樂資訊，且修改檔名及分類，便於使用者在音樂收藏與整理上，因而變得容易又快速。

1.2 問題描述

本研究目的主要是針對硬碟中音樂物件的音樂資訊查詢，系統自動整批寫入音樂資訊且作為音樂分類的依據，也就是幫我們整理硬碟中的音樂。我們將提供一個音樂辨識與管理系統(Music Identification Management System)軟體，命名此系統為 μzBox。

本研究音樂物件格式為MP3或WAVE，音樂物件的資訊可能不詳或不完整，利用音樂辨識(Music Identification)的功能，搜尋出最相似歌曲的音樂資訊(music information)，其包含歌曲曲目(song number)、歌曲名稱(title)、演唱歌手(artist)、專輯名稱(album)、歌曲時間長度(duration)、出版年份(year)、歌曲語言(language)、歌曲類別(genre)、作曲家(composer)、作詞家、(songwriter)、候選相似歌曲(candidate similar song)的音樂資訊，此系統可將重覆歌曲(redundant songs)移除。系統在同一時間辨識很多首音樂物件，發現某幾首音樂物件辨識的音樂資訊為相同，則視為這些音樂物件為重覆歌曲。音樂分類(music classification)根據音樂辨識(Music Identification)得到音樂資訊來分類，依歌手(artist)、專輯名稱(album)、出版年份(year）來整理。因此，μzBox系統主要分成兩大部分，第一部份為音樂辨識與管理(Music Identification Management)，將使用者給予的音樂物件進行資料庫查詢相似比對，將相似的音樂資訊

回傳給使用者，其可選擇更改原路徑音樂的檔名(file name)與音樂資訊(music information)，以及刪除重覆歌曲(redundant song)，且可將整理好的音樂檔案搬移或另存指定的位置，使用者在整理音樂物件時，可以選擇如何音樂分類。第二部分是音樂資料庫建置，目前這部分我們需要自己建置，未來可藉由網際網路架設sever端，由大家提供音樂物件及音樂資訊。

這篇論文的內容組織如下：第二章為相關產品與相關論文，第三章是我們的系統架構，而第四章是我們的研究方法包括MFCC特徵擷取，使用Bisecting *K*-means clustering產生特徵參數群集，群集經音樂特徵(Music feature)縮減而得音樂參考特徵參數，則音樂物件之間相似比對使用*k*-nearest neighbor classifier方法，第五章是我們實驗設定與結果。最後，第六章則是本篇論文的結論與未來工作。

2. 相關研究

針對內涵式音樂資訊查詢(content-based music information retrieval)，有許多研究相關的議題，我們分成相關軟體與相關論文等研究，探討他們使用的方法與成果。

2.1 相關軟體

在音訊辨識上，Gracenote被稱為音樂界的搜尋引擎，因為Gracenote擁有一個全世界最龐大的數位音樂資料庫，[Gra]目前資料庫中擁有七百多萬首歌曲，八千萬Tracks，以及六百多萬張CD的曲目、歌手、歌曲分類、專輯、年代與歌詞...等相關資訊，共有80種語言，Gracenote提供一個應用這個資料庫的SDK應用程式介面，給各家音樂設備廠商，讓他們的產品可以透過軟體或是硬體的方式來使用Gracenote的資料庫。Gracenote的音訊辨識簡稱為MusicID，MusicID的辨識技術有兩種，分別為Track ID技術和CDDB技術。

Gracenote的Track ID技術，利用音樂本身音訊指紋辨識和數位文件編碼記錄檔，在數位編碼有一段特別記錄這些資訊，使用Track ID技術的軟體有Sony Ericsson Walkman手機、Apple線上音樂商店、Tune up、Winamp、foobar等軟體。

我們利用Tune up軟體，查詢不同位元率的音樂物件，針對查詢同一首歌曲給不同的音訊品質和移除音樂物件中的ID3 Tag，而發現MP3位元率品質大於128Kbps時，整體

查詢歌曲準確度為六成二左右，如果音樂中的ID3 Tag存在，整體查詢準確度會提高，大約八成左右，由此可知它是同時利用音樂本身音訊指紋辨識和數位文件編碼記錄檔。另有查詢部分歌曲，從歌曲開始切一段查詢，此時整體查詢準確度五成；而從音樂中間任意切一段或切副歌查詢時，皆無法找到音樂資訊，由此可知它的音訊指紋只儲存前面一部分。

Gracenote的CDDB技術[Kat04][Mic04]，每一張CD都有獨立的disc ID，因此當原版CD放入時就可以認到disc ID，而回傳相同disc ID的CD專輯名稱、每一軌的歌名及其他資訊，我們將CD每一軌重新編排或者任意抓取CD某幾首時，就無法找到CD的資訊，由此可知它是辨別CD的長度與每一軌順序，使用此技術的軟體有iTunes和Windows Media Player。

其他音樂查詢相關產品有liveplasma、Pandora、Musicovery等等，他們皆是以關鍵字查詢方式，搜尋相似的歌曲，給予使用者聆聽，並得知音樂資訊，分別有不同的查詢方式。在[Liv]的liveplasma當中，使用了Flash的技術，由使用者輸入想要查詢的歌手名字、或者電影的名稱、導演、演員，找出跟使用者所輸入的同類型音樂或電影，並顯示出彼此之關係，也可以利用當中的Last Maps查看之前曾經查詢過的記錄。在[Pan]中的Pandora，使用者只需要輸入關鍵字，系統會自動找出在資料庫當中與關鍵字相似的音樂，使用者可以透過試聽，並作進一步的喜好篩選。在[Mus]中的Musicovery，使用者只需要先選擇想要搜尋的歌曲年代、類型或者使用者的心情，系統會自動找出最符合的歌曲開始播放，並顯示出與其有類似曲風的歌曲給予使用者試聽。

2.2 相關論文

近年來，有鑑於梅爾刻度式倒頻譜係數(Mel-scale frequency cepstral coefficients，MFCC)在語音辨識(Speech Recognition)所帶來的成效，在內涵式音樂資訊查詢(Content-based music information retrieval)的相關研究上，許多研究[Jea04][Jea02]嘗試以音樂物件的MFCC來當作音樂物件的特徵之一，其中[Ant00]的研究結果更指出MFCC具有保留音樂物件的音色特性，用於辨別樂器(instrument)準確率達80.6%。MFCC是一種倒頻譜係數(Cepstral Coefficients)，當音訊訊號在時域中的波形透過傅利葉轉換，便會在頻域中形成頻譜，接著將頻譜的能量頻譜(Energy spectrum)取對數值再做逆向傅利葉轉換回到時域，此時會在時域中形成一個倒頻譜，最後將倒頻譜通過倒濾波器所得到的新參數就是所謂的倒頻譜係數。倒頻譜係數被視為是一種很有效的參數，因為倒頻譜係數具有

分離發音腔道模型與激發訊號的特性，可以更準確地計算發音腔道參數，進而掌握語音頻譜特性，所以被廣為使用[王04]。除此之外，根據研究[楊00]發現，人耳並非對全頻域都有相同的敏感度，人類對於低頻聲音的感知能力較強，約呈線性關係；而對於高頻聲音的感知能力則較弱，約呈對數關係，所以在考慮這些特性下，梅爾倒頻譜係數就是其中一種以較細緻的方式來取出的倒頻譜係數。

內涵式音樂資訊查詢(Content-based music information retrieval)的相關研究上，有Query by tapping、Query by Humming等查詢方式，使用音訊格式有MP3、WAVE或MIDI等來深入探討，早期都以MIDI資料庫格式為主有[Jan00][Ghi95][Kos99]，清華大學資訊工程學系張智星教教授超級點歌王[Sup]，使用音高追蹤方式查詢，主要方法是使用動態時間扭曲(Dynamic Time Warping)來做加速比對。近期MP3音樂在數位音樂世界中大為盛行，在內涵式音樂資訊查詢(Content-based music information retrieval)以MP3格式為主，針對壓縮MP3音訊格式的文獻有[Liu02a][Liu02b][Tsu06]，使用多項位濾波器係數向量(PCV)來當作MP3的特徵值，計算每一個音框的音高及音量，用來判斷MP3音訊能量的高低起伏，再利用不同分類法進行比對，比對的準確率皆可達八成以上。其中[Kyu05]是數位音訊(digital audio)格式，音訊格式來自原版CD、錄音帶和MP3格式，使用多種特徵參數包含頻譜參數、MFCC、LPC等六種參數，特徵參數共擷取54維度，使用K-means方法來訓練這些特徵參數，並使用漸進式挑選(Sequential Forward Selection, SFS)來降低維度，使查詢速度加快，最後利用歐幾里得距離方式比對，其準確度約八成四以上。

3. 系統架構

在這一個章節，分別介紹我們的系統架構和流程，以及我們設計的系統介面功能。

3.1 系統流程

目前，μzBox系統主要分成兩大部份，第一部份為音樂資料庫建置，第二部份為音樂辨識與管理(Music Identification Management)，μzBox系統架構如圖一所示。

音樂資料庫的部分由我們事先建置於μzBox系統中，音樂資料庫建置流程如圖二所示，音樂資料庫的音樂來源為原版CD Audio，每首音樂分別擷取MFCC特徵作為音樂

辨識(Music Identification)的依據，並且建立音樂物件的音樂資訊。系統另一部分為音樂辨識與管理(Music Identification Management)，音樂辨識(Music Identification)的檔案格式可為MP3和WAVE兩種，歌曲的音樂特徵建立方式與音樂資料庫相同，則音樂相似比對使用k-nearest neighbor classifier方法，計算與音樂資料庫的相似度值，並將相似度值最高的音樂資訊回傳給使用者，也可觀看其他候選相似歌曲的音樂資訊，則辨識而得的音樂，其選修改檔名，最後使用者可指定音樂依分類方式來搬移或另存檔案。

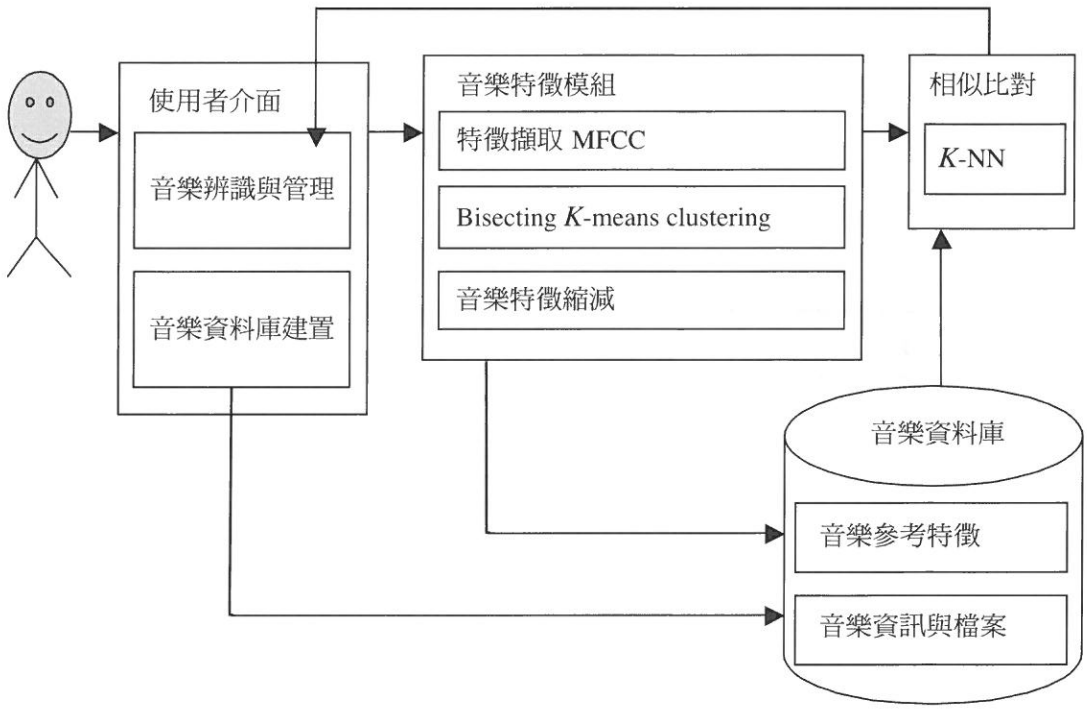

圖一：μzBox系統架構

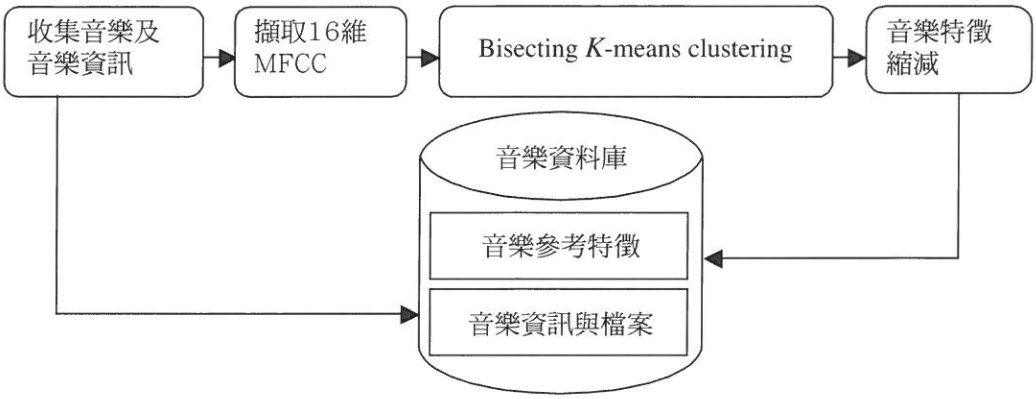

圖二：音樂資料庫建置流程

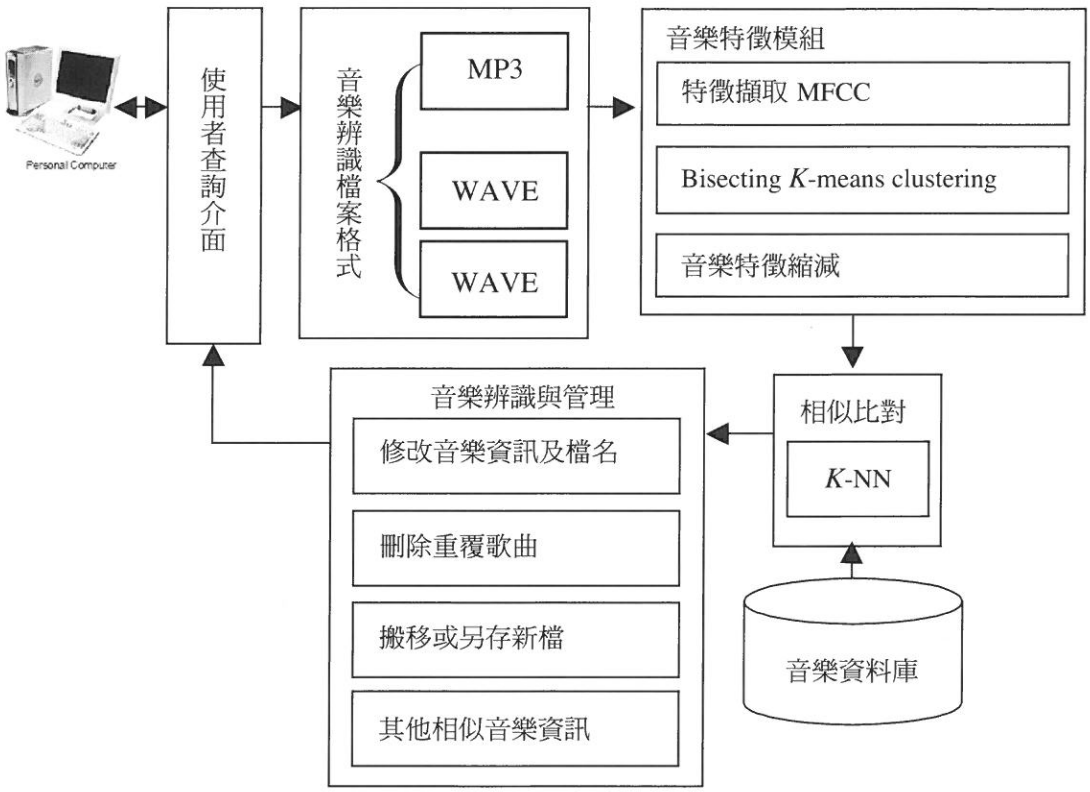

圖三：音樂辨識與管理(Music Identification Management)流程

3.2 系統介面

μzBox系統介面主要分成兩部份，第一部份為音樂辨識與管理(Music Identification Management)，第二部份為音樂資料庫建置，分別為圖四和圖五，下列針對這兩部份的功能作介紹。

第一部份為音樂辨識與管理(Music Identification Management)，如圖四所示，功能介紹分別如下：

- A功能為讀檔，接受音樂格式為MP3或WAVE，在I視窗展示，分別有檔名、歌名、演唱者、專輯、歌曲時間、歌曲年代、檔案大小、檔案目錄。
- B功能為辨識音樂物件的音樂資訊，可選擇I視窗哪些音樂物件要辨識，經系統辨識而得音樂資訊，展示在J視窗。
- C功能為刪除重覆歌曲，辨識而得到相同的音樂資訊，我們將同首音樂資訊的音樂物件視為一群，使用者可選這群哪一首要刪除或由系統自動保留一首。
- D功能為改檔名與修改音樂資訊，可選擇I視窗哪些音樂物件要修改，修改為對應J視窗的音樂資訊。
- E功能為搬移或另存檔案，可選擇I視窗哪些檔案要搬移或另存，系統將依照使用選擇音樂分類方式歸類。
- F功能為顯示該首其他相似歌曲。
- G功能為設定檔名的編輯方式與該首辨識相似的歌曲數目。
- H功能為播放音樂，點選I或J視窗的歌曲。

第二部份音樂資料庫建置，如圖五所示，功能介紹分別如下：

- A功能為讀取音樂檔，接受音樂格式為WAVE和MP3，如果音樂物件有音樂資訊系統則會自動紀錄，沒有音樂資訊使用者需自我編輯，且系統將建立音樂參考特徵至資料庫。
- B功能為編輯或修改已建立資料庫歌曲的音樂資訊。
- C功能為刪除資料庫中的音樂參考特徵與音樂資訊。
- D功能是設定我們演算法的Bisecting K-means clustering和k-nearest neighbor classifier中的參數，實驗我們演算法中的最佳參數設定。
- E功能是播放資料庫的音樂，為F視窗的歌曲。
- F功能是顯示資料庫歌曲的音樂資訊畫面。

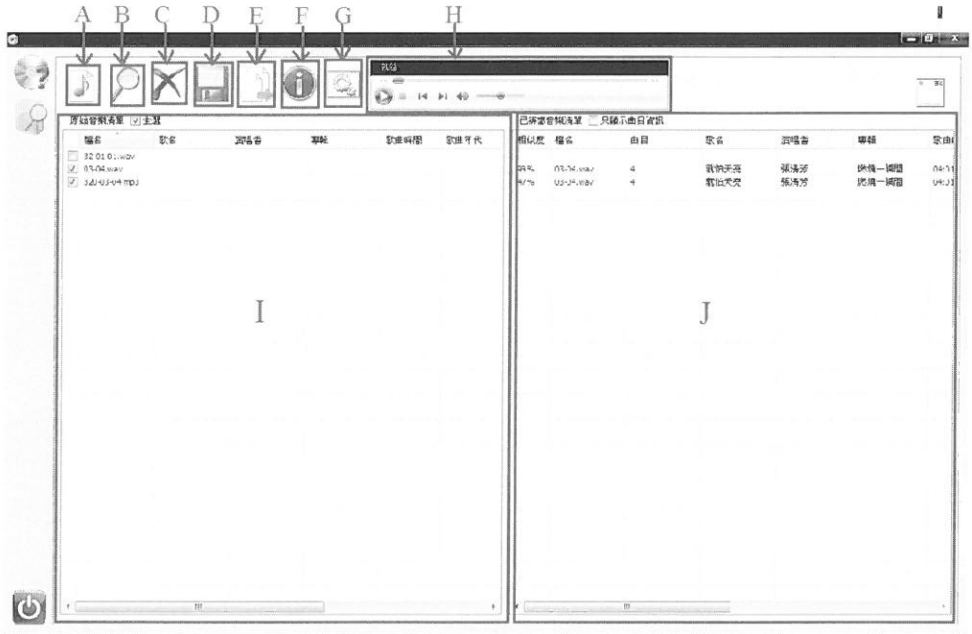

圖四：音樂辨識與管理(Music Identification Management)介面

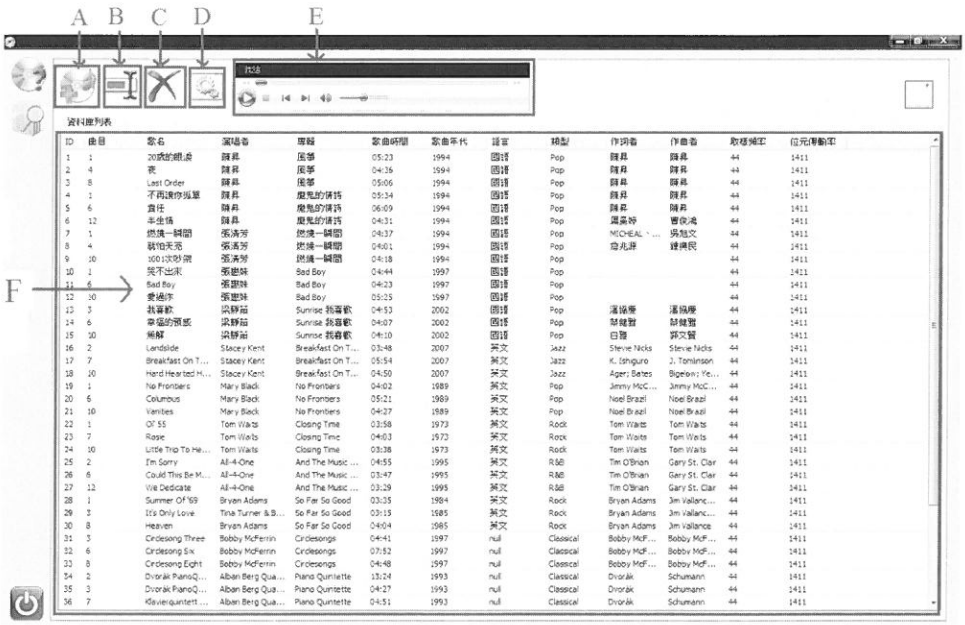

圖五：音樂資料庫建置介面

4. 方法的介紹

在這一個章節，分別介紹我們如何擷取音樂特徵(Music feature)，我們擷取特徵參數為梅爾刻度式倒頻譜係數(Mel-scale frequency cepstral coefficients，MFCC)，每個音框擷取16維度的MFCC特徵參數，使用*k*-NN[Hig93][Hsu00][Tou74][Gos96]作為比對的依據，查詢的音樂參考特徵與資料庫中的所有音樂參考特徵進行徹底找尋最近鄰居，但如此一來相當花費時間和記憶體空間，因此我們採用Bisecting K-means clustering分群，將歌曲全部的特徵進行分群，而從數群中選出代表音樂參考特徵向量，其代表該首音樂參考特徵，作為音樂之間相似度比對的依據，比對方法為k-nearest neighbor classifier(簡稱為k-NN)。

4.1 特徵擷取(Feature extraction)

特徵參數的擷取在音訊處理上是一個非常重要技術，如何正確擷取音樂的特徵，對於之後歌曲辨識有極大的相關性。因此，如何找出一組可代表每首歌聲的特徵參數來做識別，且又不易受環境干擾，並能具有鑑別（discriminative）的特徵參數。對數位音訊(digital audio)處理而言，倒頻譜（cepstrums）優點是將頻譜上的高低頻分開，只要取前面幾項特徵參數，就可代表音訊的特性，使得辨識率提高。因此，在語音研究上，線性預估編碼導出的倒頻譜係數(linear predictive coding derived cepstrum coefficients，LPCC) [Hig93][Vel88] 和梅爾刻度式倒頻譜係數(Mel-scale frequency cepstrums coefficients，MFCC) [Jua93][Mam96]皆廣泛被使用的特徵參數。在過去幾年研究發現，MFCC辨識效果比LPCC能力較佳，MFCC考慮到人類聽覺系統的特性，對低頻的聲音感知較強，而對高頻的聲音感知能力較弱，所以MFCC在求取特徵參數時，以低頻的聲音為取較多，而高頻的聲音為取較少，針對不同語音和背景，都會有不錯的辨識率，且在音樂辨識 (Music Identification)方面也廣泛被應用，因此我們採用特徵參數為MFCC。

首先，將數位音訊(digital audio)轉成WAVE格式，取樣率以44100kHz、16bits、單聲道。一般數位訊號是屬於時變性（time-varying）的信號，其波形變化非常快速。特徵參數沿著時間軸變化，因此，數位音訊(digital audio)利用短時域的特性去分析，就可得到所需的特徵參數，不過從頻率領域（frequency domain）上來看數位訊號，可發現頻譜（spectrum）是隨時間作緩慢變化，因此，數位音訊(digital audio)在短時距內是穩定的，被視為『短時間穩定』（short time stationary）訊號，對數位音訊(digital audio)

作『短時距處理』（short time processing）。這方法是假設在一短時距中，其特性是固定的，且將有助於分析音樂訊號，通常這個段短時距稱為一個音框（frame），以一個音框（frame）為切割音訊的單位，求出此時的音樂特徵參數。

本論文擷取MFCC特徵參數主要有下列幾個步驟，如圖六所示。我們將整首音樂訊號切割成許多音框，每個音框長度為1024點，每個音框擷取16維度的MFCC特徵參數，音框之間重疊(overlapping) 50%，其以向量表示為$F_i = (e_{i,1}, x_{i,2}, \cdots, x_{i,16})$，其中$F_i$為第$i$個音框，$e_{i,1}$為能量，$x_{i,2}$為梅爾倒頻譜，$c = 2, \cdots, 16$。整首音樂特徵向量以序列表示為$S = <F_1, F_2, \cdots>$。

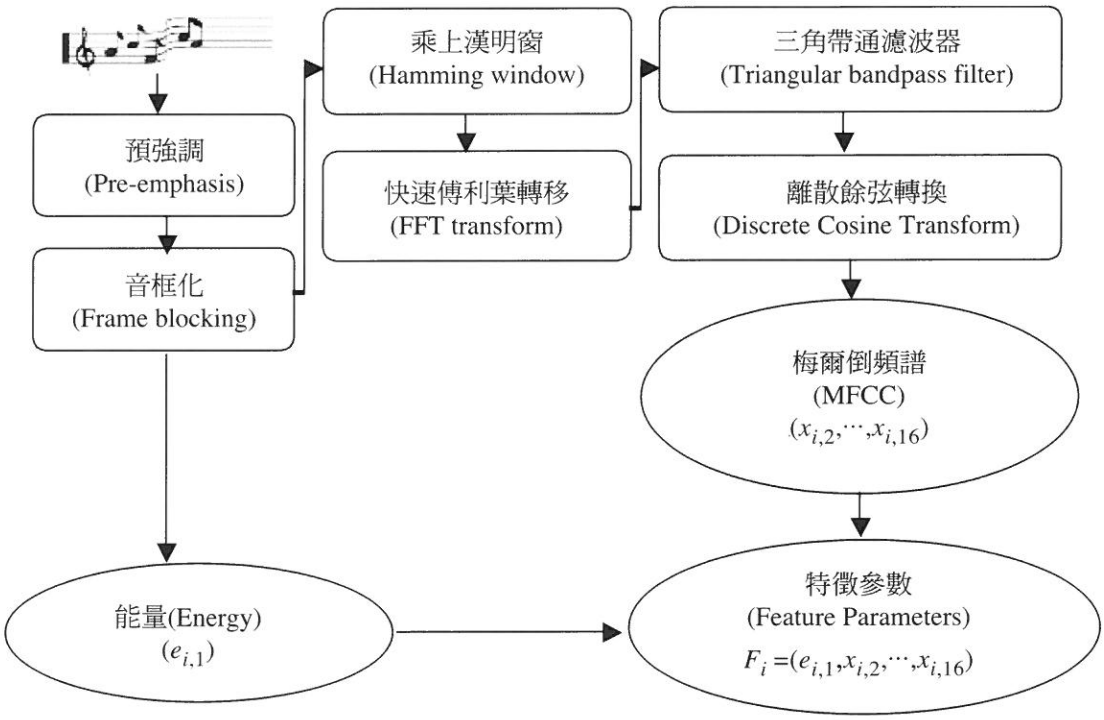

圖六：特徵參數擷取流程

(1)**預強調**（Pre-emphasis）

數位音訊(digital audio)通過一個一階高通濾波器$H(Z)=1-aZ^{-1}$，其中 介於0.9和1.0之間，在此取a=0.95。以時域的運算式來表示，預強調後的訊號為$y(n)-ax(n-1)$，以突顯高頻聲音的部分。

(2)**音框化**（Frames blocking）

音框取樣點為1024個，涵蓋時間約為23ms左右，為了避免音框之間的特性變化太劇烈，讓兩個相鄰的音框之間重疊區域，也就每次音框每次位移512個取樣點後再取1024個取樣點當下一個音框。

(3)**乘上漢明窗**（Hamming window）**及通過低通濾波器**（Low-pass filter）

針對每一個音框乘上漢明窗，可消除兩端的音框不連續性，如此可避免分析時受到兩端音框的影響，將音框通過低通濾波器，可去除異常高頻的雜訊。假設音框化的訊號為$y(n)$，乘上漢明窗後為$y'(n)=y(n)\times W(n)$，此漢明窗$W(n)$定義如下：

$$W(n)=\begin{cases}0.54-0.46\times\cos\left(\dfrac{2\pi n}{N-1}\right), & 0\le n\le N-1\\ 0, & \text{otherwise}\end{cases}$$

(4)**快速傅利葉轉換**(Fast Fourier Transform，FFT)

由於數位音訊(digital audio)在時域(Time domain)上的變化很難看出它的特性，所以通常將它轉成頻域(Frequency domain)上的能量分佈來觀察，因此計算短時距能量，代表音量的高低，乘上漢明窗後，刪掉所處理的聲音一些細小雜訊，且每個音框必需要再經過FFT轉換才可得到在頻譜上的能量分布，我們稱為短時距能量。短時距能量為：

$$E_k(n)=\sum_{n=0}^{N-1}x^2(n)e^{\frac{j2\pi n}{N}},0\le n\le N$$

(5)**三角帶通慮波器**(Triangular band-pass filter)

將能量頻譜乘以一組20個等頻寬三角帶通慮波器，求得每一個濾波器輸出的對數

能量(Log energy)，而梅爾頻譜(Me-frequency)和一般頻譜 f 的對應關係式：

$$Mel(f)=1125\times\ln(1+\frac{f}{700})$$

(6)**離散餘弦轉換**(Discrete Cosine Transform，DCT)

將20個對數能量E_K帶入離散餘弦轉換，求出梅爾倒頻譜 (Mel-scale cepstrum) 參數，在此取L為15階，就可以得到15維的梅爾倒頻譜係數。離散餘弦轉換公式為：

$$C_m=\sum_{k=1}^{M}E_K\cos[m(k-\frac{1}{2})\frac{\pi}{M}],m=1,\cdots,L$$

4.2 Bisecting *K*-means clustering

我們使用Bisecting *K*-means clustering [Sav04][Sav01]來分類資料群，並縮減資料量。分類群集有很多種，其中最常見是階層式群集法(Hierarchical clustering)與分割式群集法(Partitional clustering)兩大類，而Bisecting *K*-means clustering就是結合這兩大類演算法的優點。Bisecting *K*-means clustering是一種分裂式階層群集法，其將群集作二分法，所採用的計算方式與分割式群集法中的*K*-means很相似，並皆以群集重心(cluster mean)來表示一個群，唯一不同的地方是不必事先給定群集個數，而是給定繼續分裂門檻值(th_SE)，然後藉著反覆地修正每一個群集重心與群集相似度，達到分群的目的。因此，本論文使用Bisecting *K*-means clustering分群，將音樂特徵參數分成數個群集。首先我們先定義演算法中所使用到的符號與參數，如下表一：

表一：Bisecting *K*-means clustering **符號與參數定義**

符號	定義
S	輸入的整首歌曲MFCC特徵參數序列，表示為$S=<F_1,F_2,\cdots>$
M	輸出的各群的MFCC特徵參數集合，表示為$M=\{C_1,C_2,\cdots\}$
th_loop	停止參數群集分裂參數，當迴圈已執行th_loop次數，即停止分群
th_SE	停止參數群集分裂參數，當每個群集的SE值，均小於th_SE，即停止分群
SE_i	C_i群集內相似度（intra-cluster distance），以squared error來代表（*SE*值愈小，代表群集內的音樂特徵向量愈集中、愈相似）。

Bisecting K-means Clustering演算法

輸入：音樂特徵向量為$S=<F_1,F_2,\cdots>$

參數th_loop

參數th_SE

輸出：$M=\{C_1,C_2,\cdots\}$

BEGIN

將$S=<F_1,F_2,\cdots>$視為第一個群集C_1, *i.e.*,$M=\{C_1\}$，並計算SE_1；t = 1；

while {(t < th_loop) && NOT(每一個群集C_i的SE_i值，都小於th_SE)} **do**

令C_k為$M=\{C_1,C_2,\cdots\}$中，SE值最大的群集；

以C_k為資料集，呼叫K-means (K = 2)，並得到兩個子群集C_x ,C_y ；

$M= M - \{C_k\}+\{C_x,C_y\}$ ； $t = t + 1$；

end-of-while

return M；

END

請參考範例一，我們使用二維資料集的序列來說明Bisecting K-means clustering演算法的過程，並搭配圖形來表示。

範例一： 輸入一個資料集

S=<(3,6),(3,5),(6,8),(7,9),(2,5),(8,6),(4,5),(3,4),(9,6)>，

而且參數設定如下：th_loop = 8、th_SE = 1。

步驟一： 將整個資料集視為一群（如圖七，所有點投在二維平面）。

S=<(3,6),(3,5),(6,8),(7,9),(2,5),(8,6),(4,5),(3,4),(9,6)>=C_1, $M=\{C_1\}$

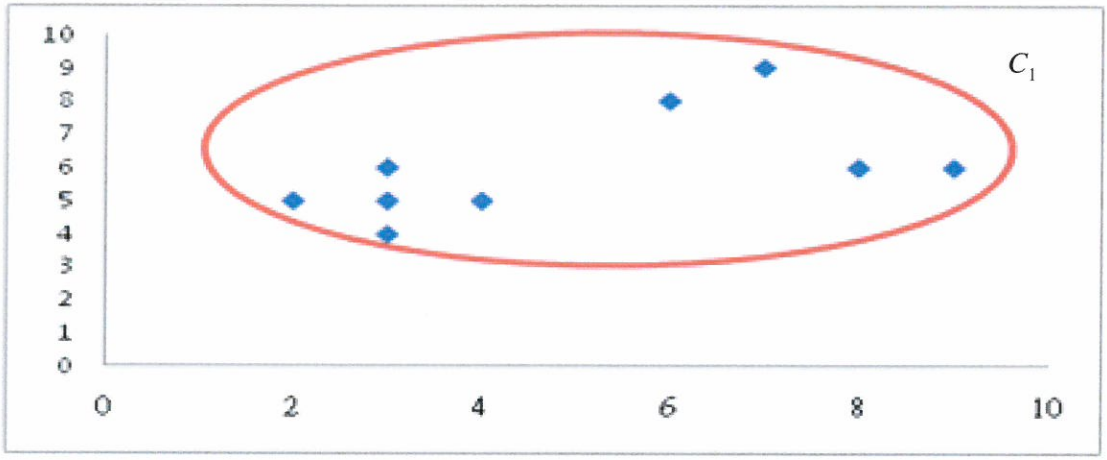

圖七：演算法執行開始，所有資料集在二維平面的示意圖

步驟二：因為M中，只有一個群集，所以，將C_1 執行二分的步驟呼叫K-means (K=2) algorithm， 將C_1 分為兩群C_x 與C_y。

C_x=<(3,6),(3,5),(2,5),(4,5),(3,4)>， SE_x=0.8

C_y=<(6,8),(7,9),(8,6),(9,6)>， SE_y=2.9375

M={C_x,C_y}（為說明方便，我們將各群集，更名為：M={C_1,C_2}）

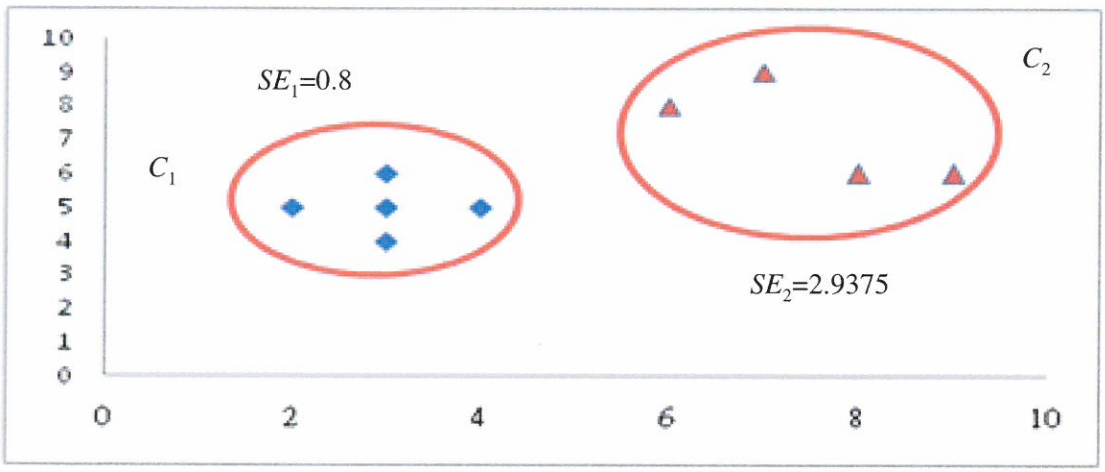

圖八：資料集分成兩群的示意圖

步驟三：在M所包含的數個群集中，C_2的SE為最大，故將C_2依照K-means algorithm，再分為兩群C_x與C_y。

C_x=<(6,8),(7,9)>，SE_x=0.5

C_y=<(8,6),(9,6)>，SE_x=0.25

M={C_1,C_x,C_y}

此時，每群的SE值皆小於1，因此輸出為M

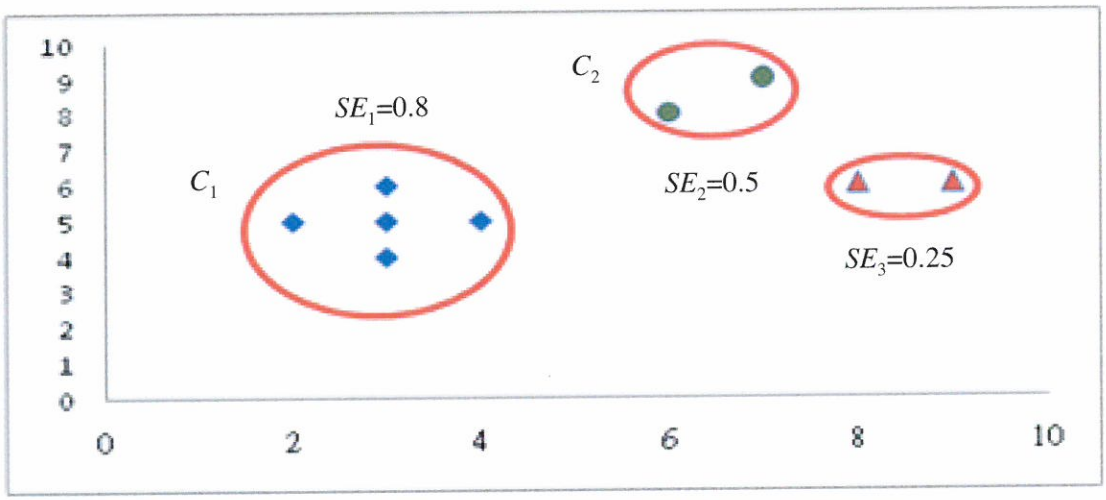

圖九：資料集分成三群示意圖

4.3 音樂特徵縮減(Music feature reduction)

特徵縮減（feature reduction）在圖形識別的過程中，降低辨識所花費得時間，還可減少記憶體所佔的空間，音樂特徵序列經Bisecting K-means clustering訓練得數個群集，再依每群大小比例，選離中心點最近的幾點，其為一連串音樂參考特徵向量。將每首歌曲的音樂參考特徵向量標上所屬的歌曲代號標籤，音樂資料庫有每首歌的音樂資訊、音樂及音樂參考特徵，音樂參考特徵以集合表示為DB={R_1,R_2,⋯,R_n}，其中n= $|DB|$ 。每首音樂特徵(Music feature)以集合表示為R={P_1,P_2,⋯,P_f}，其中f_n=$|R|$，P_i∈{F_1,F_2,⋯}。

音樂特徵縮減演算法步驟如下：

輸入：$M=\{C_1,C_2,...\}$。

輸出：音樂的代表特徵向量以集合表示為$R=\{P_1,P_2,\cdots,P_{fn}\}$。

- 步驟一：依每群大小的比例挑選音樂特徵(Music feature)向量，降低特徵比例我們簡稱為Reduce Rate(RR)，其挑選與群集重心最近距離的音樂特徵向量數個。
- 步驟二：最後挑選出的音樂特徵(Music feature)表示為$R=\{P_1,P_2,\cdots,P_{fn}\}$，即音樂參考特徵。

範例二：以RR=1/3來挑選範例一中所得出的$M=\{C_1,C_2,C_3\}$：
分別挑選$C_1=\{(3,6),(3,5)\}$、$C_2=\{(6,8)\}$、$C_3=\{(8,6)\}$，最後可得這資料集為$R=\{(3,6),(3,5),(6,8),(8,6)\}$，其代表資料集的參考特徵。

4.4 *k*-nearest neighbor classifier

k-nearest neighbor classifier，簡稱為*k*-NN[Hsu00] [Tou74][Gos96]，它的基本觀念，就是將每一資料點找最接近的鄰居判斷資料點屬於哪一類，在語音和圖形識別上常作為辨識的方法之一，利用投票方式來決定辨識者所屬的類別，也就是找最近的鄰居點來決定本身的類別。

本論文使用*k*-NN分類法來識別歌曲，利用*k*-NN (k >1)對查詢參考特徵向量，進行周圍前*k*個最近的鄰居投票，票數最高的鄰居即為所屬的歌曲，音樂資料庫被識別到的歌曲與測試歌曲很相似。

步驟一：

擷取查詢歌曲的MFCC特徵參數，由Bisecting *K*-means clustering分群，且音樂特徵(Music feature)經特徵縮減得到音樂參考特徵，此音樂參考特徵集合作為比對的依據。

步驟二：

利用「歐幾里得距離」(Euclidean distance)方法，計算查詢歌曲的音樂參考特徵與資料庫所有音樂參考特徵之間的最小距離，其累計查詢歌曲的音樂參考特徵是屬於資料庫哪一首歌曲，得票數最多代表兩者之間越相似，則候選相似歌曲排序越前面，代表相似度值越高。計算歌曲之間的相似度，使用歐幾里得距離公式如下式4-4-1。

$$d_{ij}=[(x_i-x_j)^T(x_i-x_j)]^{1/2}$$，其中和 $x_j \in DB$。 (4-4-1)

步驟三：

將音樂參考特徵中每一點與資料庫進行投票，找距離最近的點，k為$R=\{P_1,P_2,\cdots,P_{fn}\}$中每一個參考特徵點的投票數，也就是每個特徵點找$k$個最近鄰居點，以總投票數來決定$R=\{P_1,P_2,\cdots,P_{fn}\}$最相似歌曲，則總投票數$=f_n \times k$。

步驟四：

將$R=\{P_1,P_2,\cdots,P_{fn}\}$進行投票，最後統計投中音樂資料庫各歌曲的票數，稱為相似度(Similarity)，相似度(Similarity)公式如下4-4-2：

$$Similarity\ (\%) = \frac{\text{音樂資料庫各首被投中票數}}{f_n \times k} \times 100\% \qquad (4\text{-}4\text{-}2)$$

以下我們用一個簡單的範例，並搭配圖形來表示，說明k-NN演算法完整的執行過程。

範例三：資料庫有四個類別共19點，一筆資料有兩個查詢點分別為A、B兩點，結果如下：

圖十：A點查詢示意圖

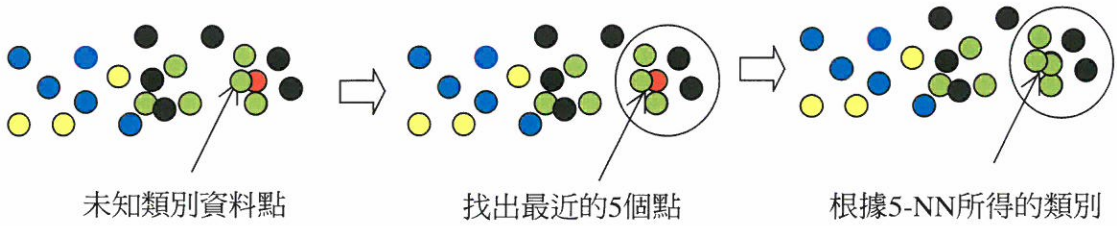

圖十一：B點查詢示意圖

從圖十得知，A點最近五點分別為黑色圈一票和綠色圈四票，而圖十一得知B點最近五點分別為黑色圈兩票和綠色圈三票，則最後A、B兩點所得為黃色圈為零票、黑色圈為三票、藍色圈為零票，綠色圈為七票，下列根據式二而得結果如下：

- ：Similarity=0/10
- ：Similarity=3/10
- ：Similarity=0/10
- ：Similarity=7/10

所以，此筆查詢為 。

5. 系統實驗

本章節描述我們系統實驗部份，撰寫的程式軟體是Microsoft Visual Studio 2008，使用C++程式語言，所使用的電腦配備是Intel Core2 Duo，3.0GHz CPU，4GB memory size，作業系統Microsoft Windows XP。

5.1 實驗資料

我們資料庫的音樂是來自十五張原版CD專輯，分成三類型歌曲，有國語歌、英文歌、輕音樂三種，各有五張專輯，每張專輯任意取三首歌曲來當作資料庫，共有四十五首歌曲，使用Win DAC[Win]軟體擷取CD Audio，當作我們音樂資料庫識別的依據。

測試音樂檔案有完整、前十秒、十五秒、二十秒和副歌部分來當作查詢，其分別擷取不同位元率的MP3品質，使用Blaze MediaConvert[Mys]軟體轉檔，分別為32 Kbps、64 Kbps、80 Kbps、128 Kbps、320Kbps作為測試歌曲，各類的查詢數量皆為音樂資料庫的四十五首歌曲。計算該次全部查詢音樂的正確命中率，正確命中率公式如下5-1-1：

$$\text{正確命中率 (\%)} = \frac{\left| \text{找到歌曲} \cap \text{查詢歌曲} \right|}{\left| \text{查詢歌曲} \right|} \times 100\% \qquad (5\text{-}1\text{-}1)$$

5.2 實驗結果

首先，我們探討Bisecting *K*-means clustering的*SE*參數分群效果，*SE*值越小分裂次數越多，在分群上所耗費的時間越久，為了避免設定*SE*值太小而無法停止群集分裂，因此我們觀察當while執行*h*=100次時，群集的分裂幾乎呈現收斂狀態，因此我們設定群集最大分裂次數為100次，*SE*值設定不佳，會影響挑選每群的音樂參考特徵向量，相對的，命中率結果也會有差異。下圖十二是探討Bisecting *K*-means clustering的訓練群集個數中，*SE*值影響查詢Top-1正確命中率。從圖十二來看，對於不同MP3不同位元率品質，群集分裂門檻值設定為*SE*=13的正確命中率最佳。

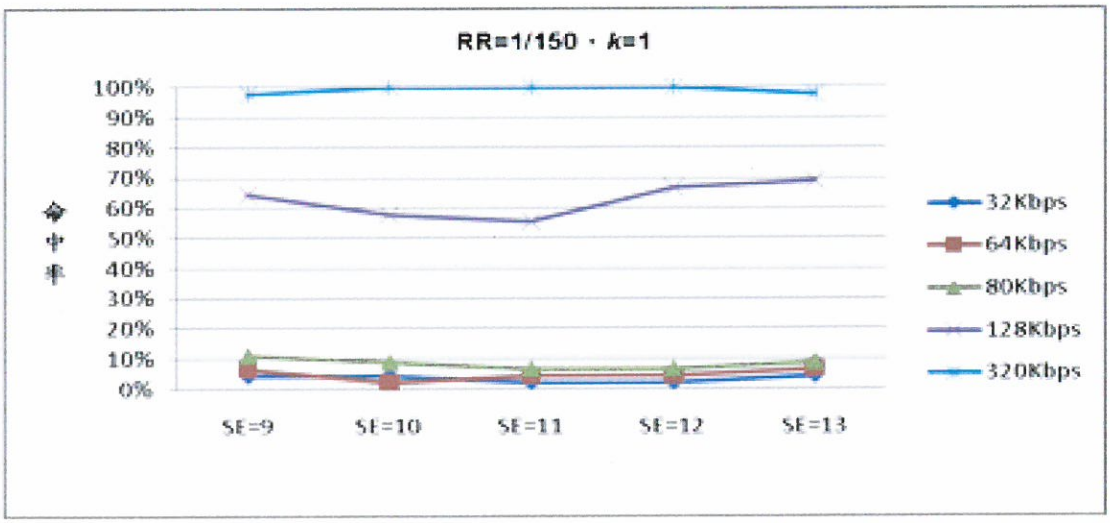

圖十二：探討Bisecting *K*-means clustering中，*SE* 值影響查詢Top-1正確命中率

k-NN(*k* >1)的優點主要是比較公平，尤其當音樂資料庫的歌曲越多，查詢特徵向量周圍的鄰居會更加混亂，藉由多人投票來決定所屬歌曲會比較具有可信度，而缺點是所花的時間比1-NN還要久，且對於每一個音樂參考特徵點均需對音樂資料庫所有的音樂參考特徵點作徹底比對，而找出最相似的歌曲。如此一來，不但需要較大的記憶體來儲存比對資料，且計算相似距離時需花費較多時間，因此資料庫的音樂參考特徵向量點越多，比對的時間就越久。圖十三探討*k*=1時，對於MP3不同位元率品質正確命中率最高。由圖十三可得知*k*-NN中，每個特徵向量投票數*k*查詢Top-1正確命中率，且*k*=1的命中率對於MP3不同位元率品質最好，查詢時間也較快，因此選擇*k*=1的結果最好。

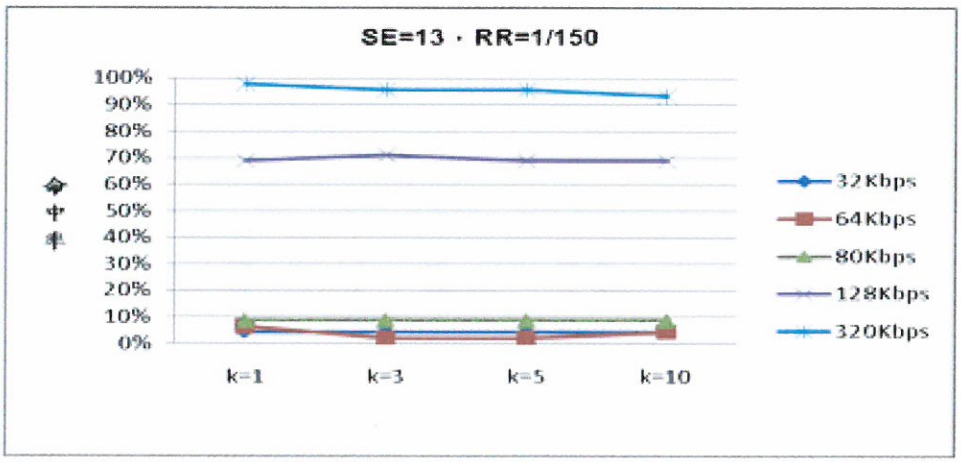

圖十三：探討*k*-NN中，每個特徵向量投票數k查詢Top-1正確命中率

從上列圖十二和圖十三，我們演算法參數的設定為*SE*，RR=1/150，*k*=1，我們分別探討MP3不同位元率品質、查詢時間長度與查詢位置的正確命中率，下圖十四至圖十八是MP3不同位元率品質的正確命中率，其分別為32Kbps、64Kbps、80Kbps、128 Kbps、320 Kbps；查詢時間長度在不同MP3位元率品質的正確命中率，時間分別為前10秒、15秒、20秒、副歌、整首歌曲。從圖十四至十八的實驗結果，發現位元率品質越佳查詢正確命中率約高，尤其320 Kbps正確命中率為100%，位元率低於128Kbps Top-1正確命中率較不佳，但一般我們存放硬碟中的MP3位元率品質至少有128Kbps以上，基於這樣的情況，Top-10內的正確命中率高達九成以上，幾乎接近100%。

圖十九得知，查詢時間長度越長正確命中率越高，且任意一段音樂查詢正確命中率也是不錯的，尤其當位元率達128 Kbps以上，查詢完整的歌曲準確度可達100%，因此很符合我們硬碟中的音樂查詢音樂資訊。

圖二十是針對查詢不同格式及長度所花的查詢時間，由圖二十得知MP3和WAVE的查詢時間幾乎差不多，因此不因查詢檔案格式不同而查詢時間較為久，本系統查詢一般MP3長度只要一分半就可完成，且查詢歌曲長度與查詢時間等速成長，從此處可見我們查詢速度算還滿快的。

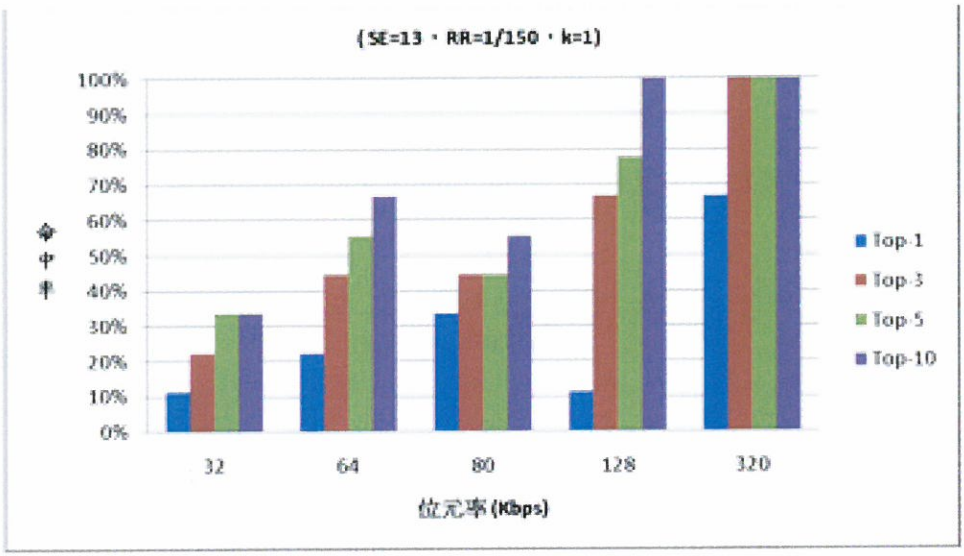

圖十四：查詢前十秒，Top-10內的正確命中率

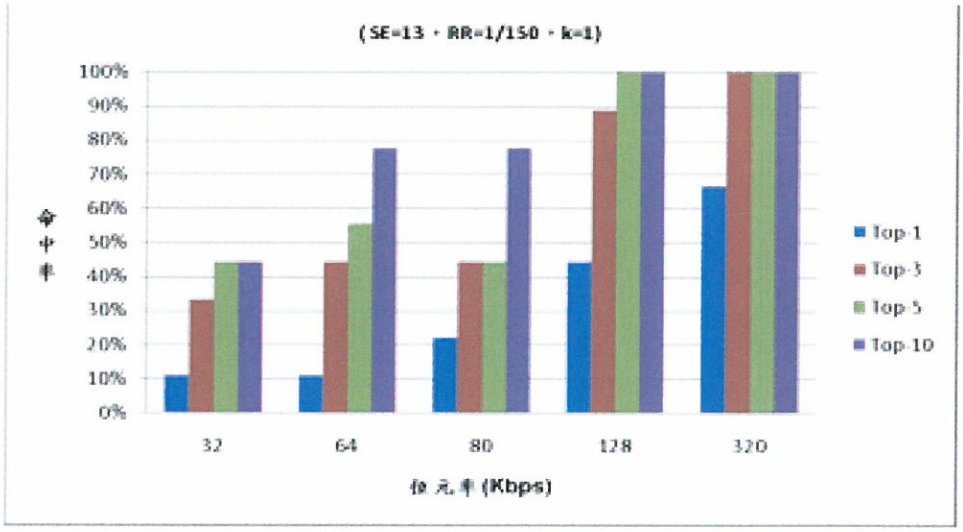

圖十五：查詢前十五秒，Top-10內的正確命中率

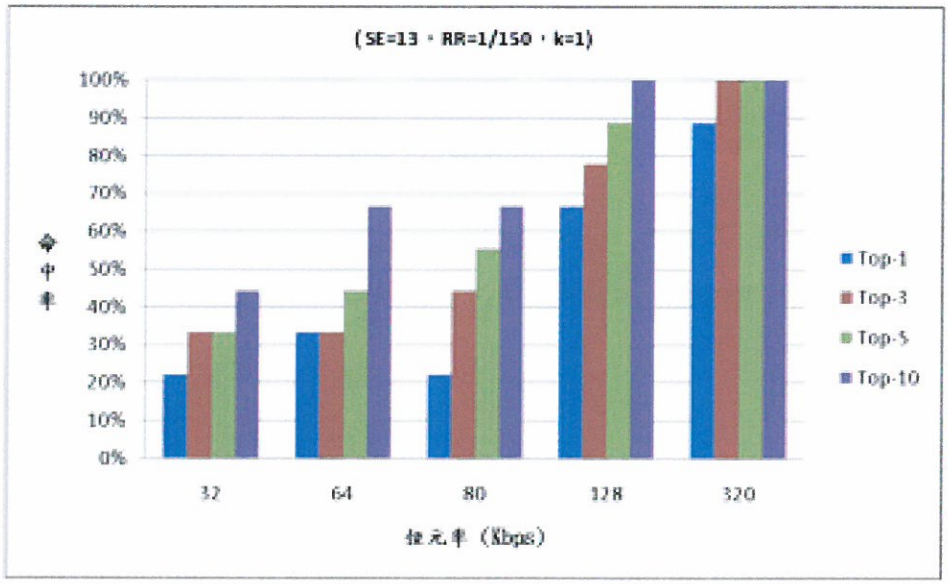

圖十六：查詢前二十秒，Top-10內的正確命中率

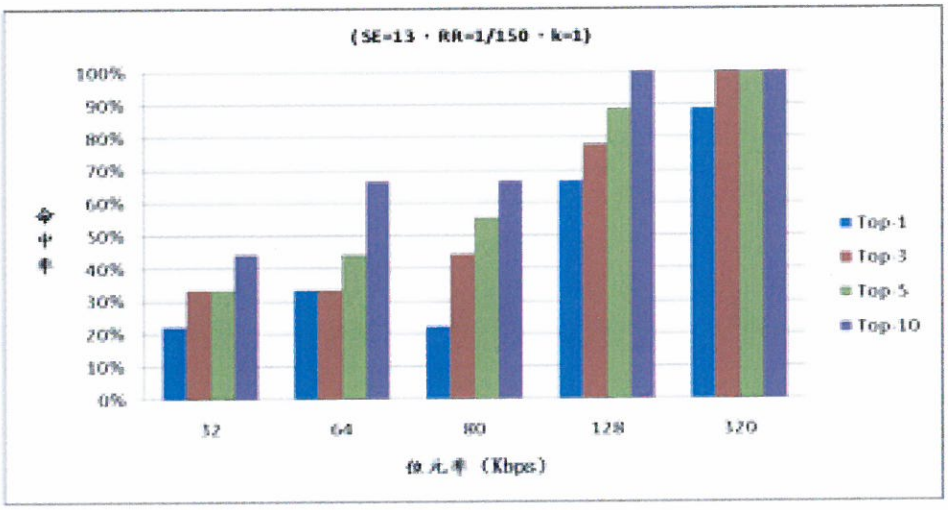

圖十七：查詢副歌，Top-10內的正確命中率

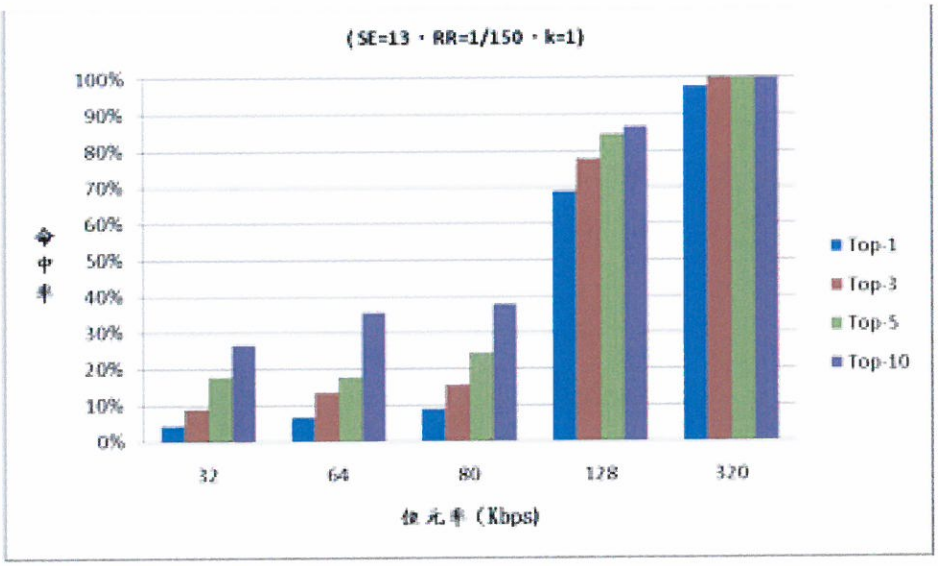

圖十八：查詢整首，Top-10內的正確命中率

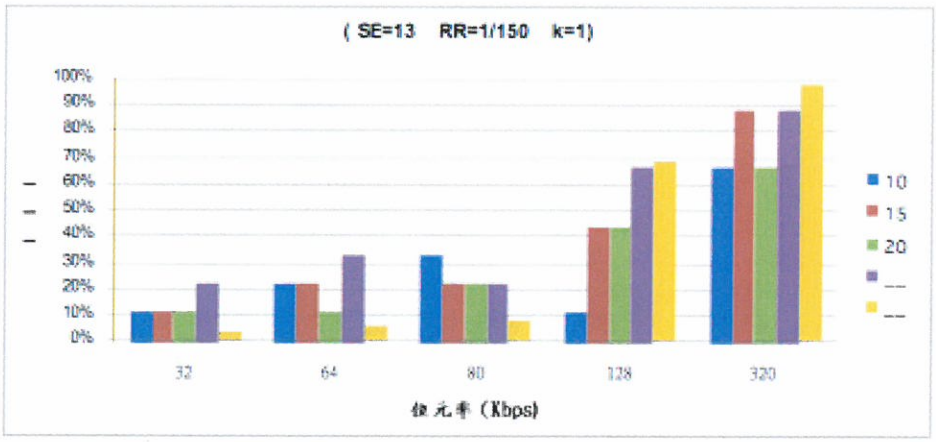

圖十九：查詢長度與位置，Top-1正確命中率

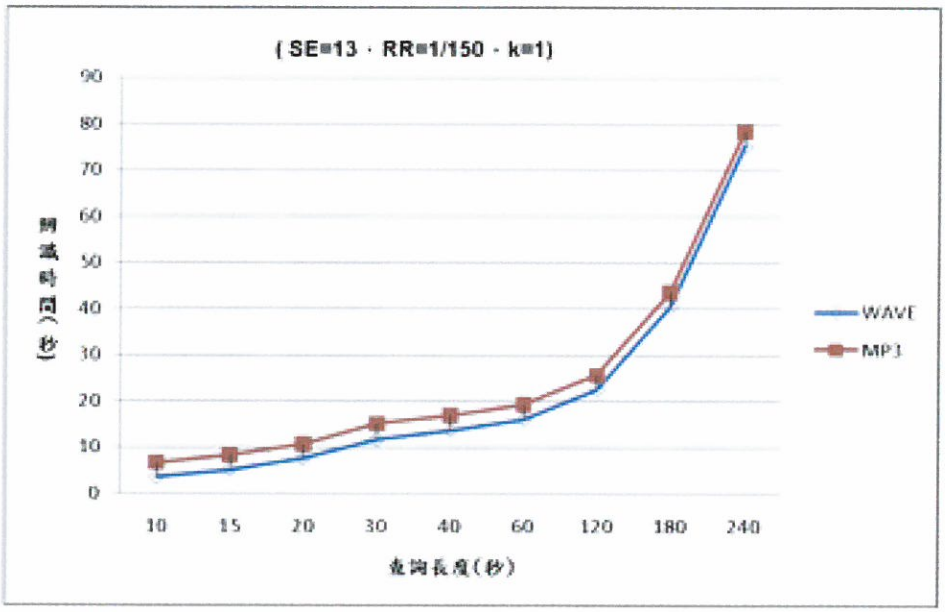

圖二十：不同長度歌曲的查詢時間

6. 結論與未來工作

本論文提出音樂辨識與管理系統(Music Identification Management System) 軟體，命名此系統為 μ zBox，音樂物件以MFCC來當作音樂物件的特徵，我們提出利用Bisecting *K*-means clustering來建立特徵群集，與往常高斯函數模型不同的地方，經音樂特徵(Music feature)縮減資料量並不影響音樂物件的特性，且比高斯函數模型的計算要來的簡單且快速，計算音樂物件之間的相似度結果較為佳，這也是我們提出一個不同的方法與技術，我們整體的比對效能與正確命中率皆表現佳，這也是我們研究目標之一。Bisecting *K*-means clustering中的 值越低代表群集內的點越相似，挑出來越有代表性，但會花較久的時間分群。RR越大越好，可降低資料量，使比對的時間加快，但*k*-NN中*k*投票數太大時，查詢比對時間也會影響，這與資料庫的資料量有關。

最後我們實作一個 μ zBox系統，查詢音樂資訊並且整批的編輯，達到我們硬碟中的音樂整理與分類技術，要讓Top-1的正確命中率最佳時，發現Bisecting *K*-means clustering中的值為11以上，RR=1/100以上和*k*-NN中的*k*只需要設定為3以內，此參數設定值為查詢的正確命中率和效能皆不錯。由實驗當中發現最佳參數設定為*SE*、RR=1/150、*k*=1，此時的查詢正確命中率高且查詢速度也快。

目前就音樂特徵(Music feature)擷取的概念來說，我們利用MFCC特徵參數，未來可以嘗試加入其他特徵參數來提高準確度。MP3位元率低於128Kbps準確度不佳，建置音樂資料庫時，可考慮建置多種位元率的特徵模型，分別以不同位元率模型來辨別，以及將資料庫的音樂數量擴大，納入15張CD全數歌曲，甚至更多的歌曲，提高Top-1實驗的說服度。相似度的計算上，我們是以*k*-NN方法，其準確度很高但效率不理想，因當資料庫的音樂數量越多時，比對的時間就越久。

在未來的工作方面，首先，提昇比對速度與效能，使比對的時間降低且命中率提高，並且將系統以Client-Server的架構、重新實作，以期能在WWW上提供服務。如此，音樂資料庫可由多人提供音樂資訊給Sever端，節省自我建置音樂資料庫的時間與空間。

參考文獻

[Ant00] Antti Eronen, and Anssi Klapuri, "Musical Instrument Recognition Using Cepstral Coefficents and Temoral Features," *in Proceedings of the IEEE International Conference on Acoustics, Speech and Signal Processing* (ICASSP), 2000.

[Gra] http://www.gracenote.com/.

[Ghi95] Asif Ghias, Jonathan Logan, David Chamberlin, and Brian C. Smith, "Query by humming-musical information retrieval in an audio database," *in Proceedings of the ACM International Multimedia Conference* , 1995.

[Gos96] Earl Gose, Richard Johnsonbaugh, and Steve Jost, *Pattern Recognition and Image Analysis*, Prentice Hall Inc., New Jersey, 1996.

[Hig93] L. Higgins, L. G. Bahler, and J. E. Porter, "Voice identification using nearest-neighbor distance measure," *in Proceedings of the IEEE International Conference on Acoustics, Speech and Signal Processing* (ICASSP), 1993.

[Hsu00] W. -H. Hsu, "Survey and Implementation of Pattern Recognition," MS Thesis, National Tsing Hua University, Taiwan, R.O.C., 2000.

[ISO93] ISO/IEC 11172-3:1993, "Information Technology - Coding of Moving Pictures and Associated Audio for Digital Storage Media at up to about 1.5 Mbit/s - Part 3: Audio."

[Jua93] B. H. Juang and L. Rabiner, "Fundamental of speech recognition," Prentice-Hall Signal Processing , 1993.

[Jan00] J.-S. Roger Jang and Ming-Yang Gao, "A Query-by-Singing System based on Dynamic Programming," *in Proceedings of International Workshop on Intelligent Systems Resolutions* (the 8th Bellman Continuum), 2000.

[Jea02] Jean-Julien Aucouturier, and Francois Pachet,"Music Similarity Measures : What's the Use?" *in Proceedings of International Symposium on Music Information Retrieval*(ISMIR), 2002.

[Jea04] Jean-Julien Aucouturier, and Francois Pachetn ,"Improving Timbre Similarity : How high's the sky?"*Journal of Negative Results in Speech and Audio Sciences, 1(1)*, 2004.

[Kos99] N. Kosugi, Y. Nishihara, T. Sakata, M. Yamamuro, and K. Kushima, "Music retrieval by humming" *in Proceedings of IEEE Pacific Rim Conference Communications, Computers, Signal Process., Victoria Canada*, 1999.

[Kat04] Katie Dean , "The House That Music Fans Built," 2004. (http://www.wired.com/entertainment/music/news/2004/07/64033)

[Kyu05] Kyu-Sik Park, Won-Jung Yoon, Kang-Kue Lee, Sang-Heon Oh and Ki-Man Kim, "MRTB Framework: A Robust Content-Based Music Retrieval and Browsing," *Transactions on Consumer Electronics,* Vol. 51, No. 1, Feb. 2005.

[Liv] http://www.liveplasma.com/

[Liu02a] C.C. Liu, and C. S. Huang, "A singer identification technique for content-based classification of MP3 music objects," *in Proceedings of the 11th International Conference on Information and Knowledge Management*,2002.

[Liu02b] C.C. Liu, P. J. Tsai, "Content-Based Retrieval of MP3 Music Objects," *in Proceedings of the 11th International Conference on Information and Knowledge Management*, 2002.

[Mam96] R. J. Mammone, X. Zhang, and R. P. Ramachandran, "Robust speaker recognition: A feature-based approach," *Signal Processing Mag.*, vol. 13, pp. 58-71, 1996.

[Mus] http://www.musicovery.com/.

[Mic04] V. Michael , "The Magic Behind the Music," 2004. (http://money.cnn.com/magazines/business2/business2_archive/2004/03/01/363577/index.htm)

[Mys] http://www.mystikmedia.com/.

[Pan] http://www.pandora.com/.

[Sav01] S.M. Savaresi, D. Boley, "On the performance of bisecting k-means and PDDP", *1st SIAM International Conference on Data Mining*, 2001.

[Sav04] S. M. Savaresi and D. L. Boley. "A comparative analysis on the bisecting k-means and the pddp clustering algorithms", I*ntell. Data Analysis*, 2004.

[Sup] http://www.supermbox.com.tw/AllContentAP/Default.aspx

[Tou74] J. T. Tou, and R. C. Gonzalez, *Pattern Recognition Principles*, Addison-Wesley Publishing Company, 1974.

[Tsu06] Tsung-Han Tsai and Jui-Hung Hung,"Content-based retrieval of MP3 songs for one singer using quantization tree indexing and melody-line tracking method," in *Proceedings of the* IEEE ICASSP,2006.

[Vel88] G. Velius, "Variants of cepstrum based speaker identify verification" in *Proceedings of the* IEEE ICASSP, 1988.

[Win] http://www.windac.de/

[Yua90] Z. X. Yuan, B. L. Xu, and C. Z. Yu, "Binary quantization of feature vectors for robust text-independent speaker identification," in *Proceedings of the IEEE Speech and Audio Processing*, 1990.

[王04] 王小川, 語音訊號處理, 全華圖書，2004。

[楊00] 楊永泰," 隱藏式馬可夫模型應用於中文語音辨識之研究"，中原大學資訊工程研究所碩士論文，2000。

Received October 20 ,2009
Revised December 20 ,2009
Accepted December 23 ,2009

μ zBox: Music identification and management system[3]

Tzu -Wen Yu and Jia-Lien Hsu
Department of Computer Science and Information Engineering
Fu Jen Catholic University

Abstract

In the research of content-based music information retrieval, one of the most important issues is to provide music identification and management service for handling a large amount of music objects. In this paper, we design a music identification system, called μ zBox, to identify music, to compile music meta-data, and to cluster music.

We first extract features from music objects. In this paper, we choose MFCCs as the main features to represent music objects. To reduce the amount of features size, we propose a feature reduction process in which the MFCCs will be clustered by applying Bisecting *K*-means Algorithm, and then those clusters be will sampled accordingly. Therefore, a music will be represented by a set of reference feature points in the vector space.

To identify music objects, we apply k-Nearest Neighbor searching processing. The voting method is simple, but effective. We implement a system prototype to demonstrate our approach, and carry of a series of experiments to show the efficiency and effectiveness of our approach.

Key Words : Content-based music information retrieval、Music identification、Music feature、MFCC(Mel-scale frequency cepstral coefficients)、Bisecting *K*-means clustering、*k*-nearest neighbor classifier。

---

[3] This research was supported by Fu Jen Catholic University, Project No. 409731044039
[4] Corresponding author. Email: alien@csie.fju.edu.tw

Efficient Transmission Range Adjustment and Load-balanced Routing in Wireless Sensor Networks

Chun-Hsien Lu and San-Yi Hung

Dept. of Computer Science and Information Engineering
Fu Jen Catholic University
jonlu@csie.fju.edu.tw

Abstract

Wireless sensor networks use many sensor nodes with limited energy and capabilities to detect and collect data in the monitored environment. It is an important task that wireless sensor networks should employ an efficient routing protocol that reduces the energy consumption of sensor nodes to prolong the system life time. In this work, we propose a new routing algorithm that utilizes transmission range adjustment and load balancing techniques to achieve this. We calculate the expected life time of a sensor node from its transmission range and residual energy. Each sensor node then does a probabilistic selection of routes to achieve load balancing by trying not to overload any intermediate sensor. When a sensor is low on energy, its upstream neighbors will try to forward packets to another node in order to extend the system lifetime maximally. Simulation results show that our proposed scheme can provide a system life time 25% longer than two other schemes [14][18].

keywords: Sensor network, routing algorithm, load balancing, transmission range adjustment

1. Introduction

The rapid advance of wireless communications technologies has made possible many new applications, among which wireless sensor network is an important one [1-4]. In wireless sensor networks, many factors such as environment, weather, or hardware could all impact the operation of the sensors. Most sensors have limited power and memory. A sensor network should possess good fault tolerance characteristic such that a few broken sensor nodes will not seriously impact its operation. Because a sensor usually does not have sophisticated control units capable of a lot of calculation, the routing algorithm employed should not be complicated. In addition, a sensor network often consists of hundreds or thousands of sensor nodes. Each sensor node should be able to send its data packets to the sink node smoothly without congestion or packet loss. In this paper, we would like to propose a distributed routing algorithm with the characteristics of fault tolerance, scalability, and efficient energy consumption. We try to consider load balance, energy consumption, and transmission range adjustment altogether at the same time. We will specifically focus on the energy consumption in order to prolong the system lifetime as much as possible. We also want to minimize the delay for the sink node to collect all the information from the sensors.

The rest of the paper is organized as follows: Section two reviews the related work on the routing protocols for wireless sensor networks. Our proposed mechanism is presented in section three. Section four displays the simulation results, and section five gives the conclusion.

2. Related Work

Hierarchical Energy Efficient Topology Control Protocol (HETCP) [5] and Scheduled Channel Polling (SCP) [6] both suggest that a sensor should enter a sleep phase when it is not transmitting or receiving to decrease the energy consumption. HETCP proposes a sleep scheduling method in which each sensor can be in one of the active, listen, or sleep states. A sensor node in the active state can send or receive packets. Sensors in the listen state probe the

network to decide whether they should switch to the active or sleep state. Sensors in the sleep state completely shut themselves down except leaving a timer on to wake up at a later time. The state transition diagram of HETCP is shown in figure 1. In SCP, all sensor nodes are synchronized. When a node has a packet to send, it will first transmit a short request in the contention period to try to reserve the next slot to send the packet, and only one sender will succeed. During next slot, all the nodes except the intended receiver will go to sleep, thus saving energy.

Several schemes have suggesting node clustering to improve data transmission efficiency [7-11]. In LEACH [13], each cluster head controls the cluster operation and collects data packets from the member sensor nodes, then sends aggregated data to the sink node. In this way, each sensor node can avoid sending data packets to the sink node directly using a large transmission range. This also reduces the chance of packet collision at the sink node.

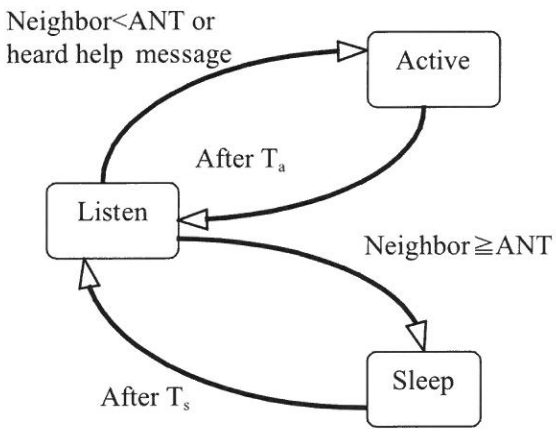

Figure 1. HETCP state transition

A simple way to reduce the energy consumption is for each sensor node to always send packets along the shortest route to the sink node. However, this may cause certain hot spot nodes to consume energy fast if traffic imbalance and collision are not carefully considered.

The Efficient and Reliable Routing Protocol (EAR) [12] solves this problem by using two metrics in route selection: the number of hops a route takes to reach the sink node, and the route score calculated based on the energy level of the next hop node and the link quality to the next hop. A higher route score indicates a better route. When a packet is far away from the sink node, it will take a route with higher energy. Otherwise, it simply selects the shortest route with minimum number of hops since the packet is already close to the sink node.

Longer transmission range provides better reachability but requires more energy [13][14][15]. Both EOBTRA [16] and DPA [17] try to adjust the transmission ranges dynamically in order to reduce energy consumption. A sensor node located close to the sink node would have to help many other nodes forward their packets, so it should try to use a transmission range as small as possible. In EOBTRA, such a sensor node will set its transmission range based on a formula calculated using the neighborhood density and energy consumption rate. Then an adjustment algorithm is applied to fine tune the calculated transmission range of each sensor node. DPA considers a linear network which contains several candidate nodes. A sensor node will first send a packet to a candidate, and the candidate would forward the packet to the next candidate. This process repeats until the packet reaches the sink node. Every candidate uses a different transmission range. A candidate closer to the sink node uses a shorter transmission range while a far away candidate would use a longer transmission one. EOBTRA and DPA both employ this idea to minimize the energy use.

3. Proposed Mechanism

In wireless sensor networks, every sensor node should use the shortest transmission range to forward packets to the next node whenever possible. Here we propose a Transmission range Adjustment and Load-balance Routing (TALR) algorithm to achieve such a goal. Our system consists of one sink node and many sensor nodes. The sink node is responsible for collecting data packets from all the sensor nodes. We assume that a sensor node can adjust its transmission range to communicate to other sensor nodes at various distances.

3.1 Routing Algorithm

A. Establishing Neighbor Information Table

Each sensor tries to find information about its neighbors by first emitting several Neighbor Search Messages (NSM), each with a different transmission range. An NSM contains the source node ID and the transmission range used. A receiving sensor will record these two values in its neighbor information table, from which a sensor node can learn how far away each of its neighbors is located. In figure 2, for example, a sensor node sends out three different NSMs with transmission ranges of X, X+Y, and X+2Y, respectively. In figure 3, node B can receive node A's NSM with transmission range X+2Y only, but it can receive both NSMs from node C with transmission ranges of X+Y and X+2Y. It then records each neighbor's ID and minimum distance, i.e., (A, X+2Y) and (C, X+Y), in its neighbor information table.

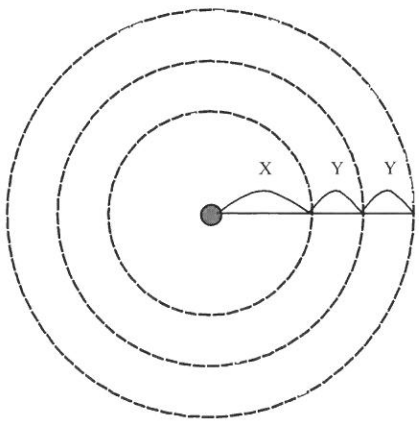

Figure 2. A node sends NSMs with differernt transmission ranges.

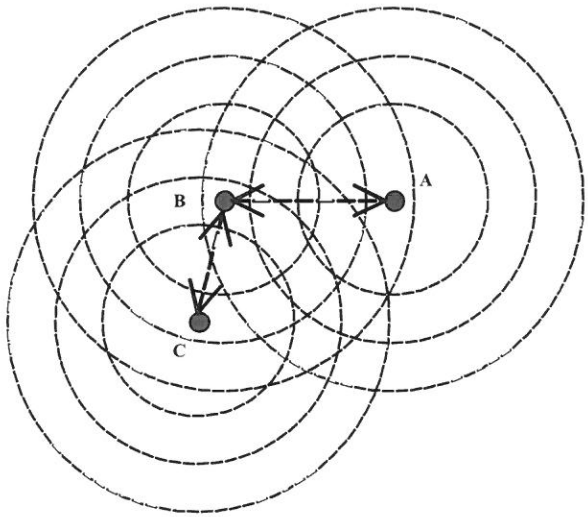

Figure 3. Sensor node receives NSMs from neighbors.

B. Route Discovery

When the sink node receives an NSM from a neighboring sensor node X, it would reply with a Neighbor Response Message (NRM) which contains three fields: sink node's ID, transmission range used, and X's ID. Upon receiving an NRM, node X realizes that it can communicate with the sink directly. It would then broadcast to its neighbors an advertisement packet (ADV) containing three fields: sender ID, *fi*, and number of hops to sink. The *fi* value is an estimate of the remaining lifetime of node i. The *fi* value is calculated as follows:

$$f_i = \frac{E}{R^2 \times (W_h \times Hop + W_d \times Degree)} \quad (1)$$

E: Residual energy of the sensor node
R: The transmission range set by the sensor node
Hop: Number of hops to sink node
Degree: Number of direct upstream sensor nodes
W_h: The weighting factor on number of hops
W_d: The weighting factor on degree

The residual energy is an important metric since a node with higher residual energy can transmit more data packets. A large number of hops for a sensor to reach the sink makes it a bad choice to server as the next hop for its upstream neighbors. The larger a node's degree is, the more packets a sensor node needs to help forwarding, which consumes more energy. The *fi* value indicates how good a sensor node can serve as the intermediate node to forward packets to the sink.

Upon receiving ADV packets from its neighbors, a sensor node could simply select the one with the largest *fi* to be its next hop (called its *bridge* node) to the sink. However, this would create a hot spot because the sensor nodes in the same neighborhood will all select the same bridge node. In our design, a sensor node *A* would select node *i* as its bridge node with probability *fi* /sum(*fi*), where sum(*fi*), represents the sum of the fi values of its neighbors that are closer to the sink node than node *A* itself. Figure 4 shows an example where a neighboring sensor node would select node X with probability 0.5, node Y with probability 0.3, and node Z with probability 0.2, respectively.

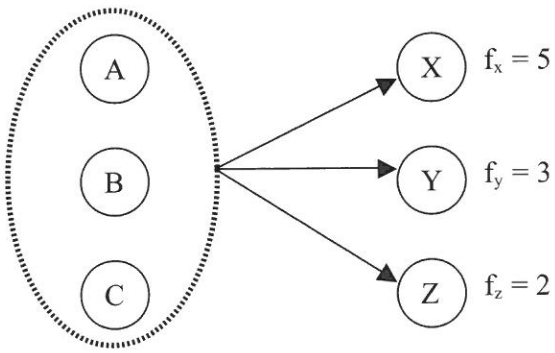

Figure 4. Example of bridge selection.

After selecting the bridge node, each sensor then compares its own *fi* with the *fi* of the bridge node and places the smaller one in an ADV packet to be broadcast to its upstream neighbors. This process repeats until all the sensor nodes find a route to the sink node.

3.2 Route Maintenance and Pruning

In TALR, we use probability distribution to prolong the lifetime of the sensor network. A sensor node is called a heavy node if it is only one hop away from the sink node. When the residual energy of a heavy node drops below 20% of its original level, it would broadcast a help message using the maximum transmission range. The help message contains its ID and *fi* value. When a sensor node receives a help message, it would record the *fi* in the table and reselect the bridge node accordingly. If the new bridge node is different than before, it then again broadcasts a help message to its upstream nodes to indicate the routing change.

A sensor node will also broadcast a help message to its neighbor nodes when its residual energy is below a predetermined level. It would put an extremely small value of *fi* in the help message to prevent the other nodes from selecting it as the bridge node. This will help direct traffic to the nodes with higher energy left.

4. Performance Evaluation

We have implemented a simulator in JAVA platform to evaluate the performance of our proposed design. In our simulation, we assume that all nodes are static nodes. The network area is 1000m° × 1000m, where 300 and 500 nodes, respectively, are randomly distributed. The sink node is assumed to be located at the center. Every node has 50J of energy at the beginning and each node can set its transmission range from 50m to 150m. For power consumption, we use the following formulas:

- Transmission power consumption:

  $E_t = k \times E_c + k \times C \times d^2$

- Reception power consumption:

  $E_r = k \times E_c$

where k denotes the data packet length fixed at 1KB. E_c represents the fixed energy consumption on either transmitting or receiving, d is the transmission range used, and C is the transmission amplifier. The simulation parameters are shown in table 1.

Table 1. Simulation parameters

Parameter	Value
Network Size	1000m×1000m
Number of n odes	300, 500
Adjustable transmissi on range, d	50m, 100m, 150m
Initial energy level	50J
Packet Size, k	1KB
Fixed energy consumption, E_c	125 μJ/bit
Transmission amplifier, C	0.05 μJ/bit/m2
Simulation Time	500 Rounds

We run the simulation for 500 rounds, where in every round each node generates a data packet to the sink node. We compare our TALR to the EAR [14] and the EARWSN [18] methods, where the transmission ranges of EAR and EARWSN are set to 100m (Labeled EAR-100 and EARWSN-100) and 150m (labeled EAR-150 and EARWSN-150) in two different cases, respectively. Figure 5 and Figure 6 show that TALR has better performance in both cases of 300 nodes and 500 nodes. From round 100 to 200, the number of connected nodes in EAR-100 decreases rapidly, and drops to zero in round 250. The case EAR-150 has more connected nodes, but still fewer than TALR and EARWSN. After 500 rounds, TALR still has 35% connected nodes, better than the 17% for EAR-150.

Figure 7 and figure 8 plot the total residual energy of all the sensor nodes at the end of simulation. We note that for the EAR-100 case, almost all the nodes are disconnected from the sink node by round 250 because those nodes close to the sink node (i.e., the heavy nodes) run out of energy fast. The residual energy stays unchanged after that since the system basically stops operating at that point. Because EAR-150 uses a longer transmission range, there will be more nodes in the sink node's neighborhood to share the load of forwarding

packets to the sink node. Thus it operates longer than EAR-100. All the systems except EAR-10 a are still operating by round 500, but TALR has maximum energy left in the end because paths to the sink node are dynamically switched to fully utilize the energy.

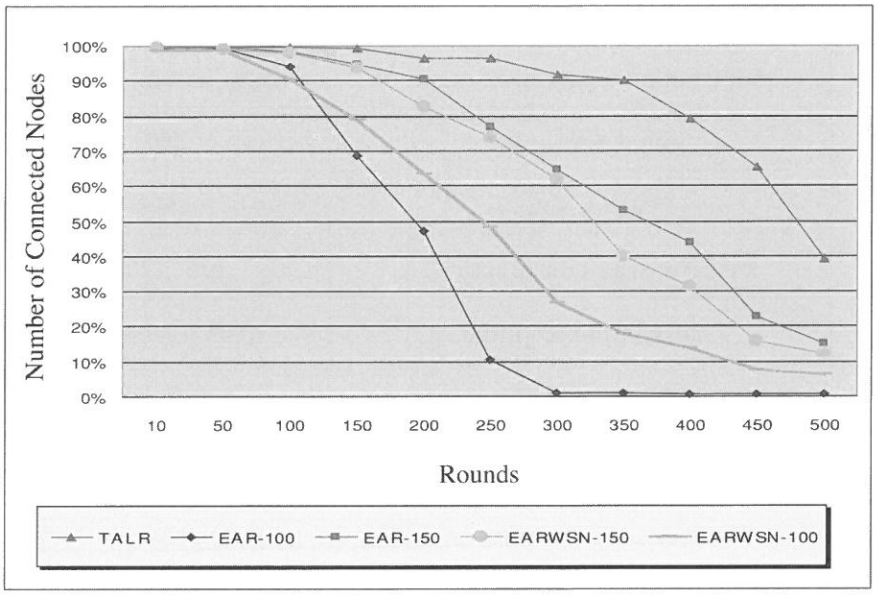

Figure 5. System lifetime with 300 nodes

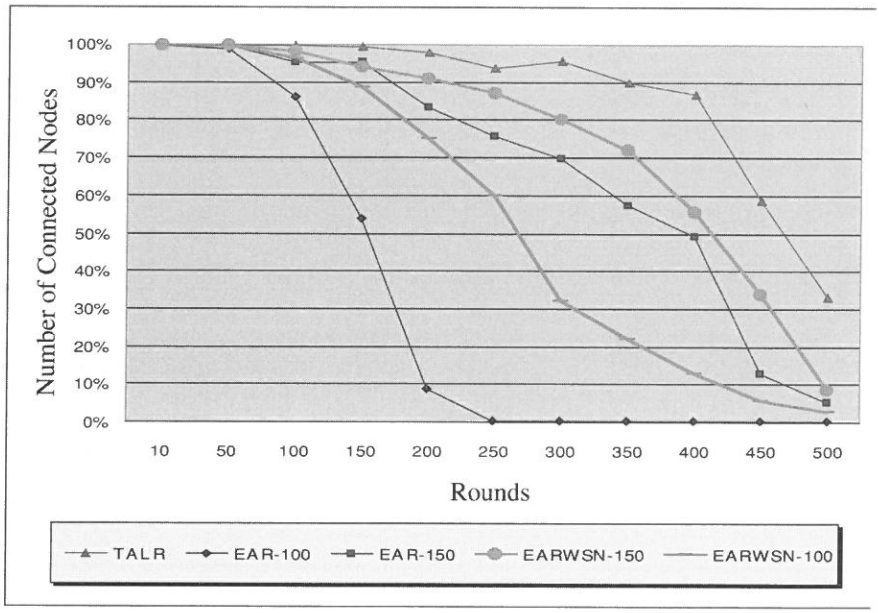

Figure 6. System lifetime with 500 nodes

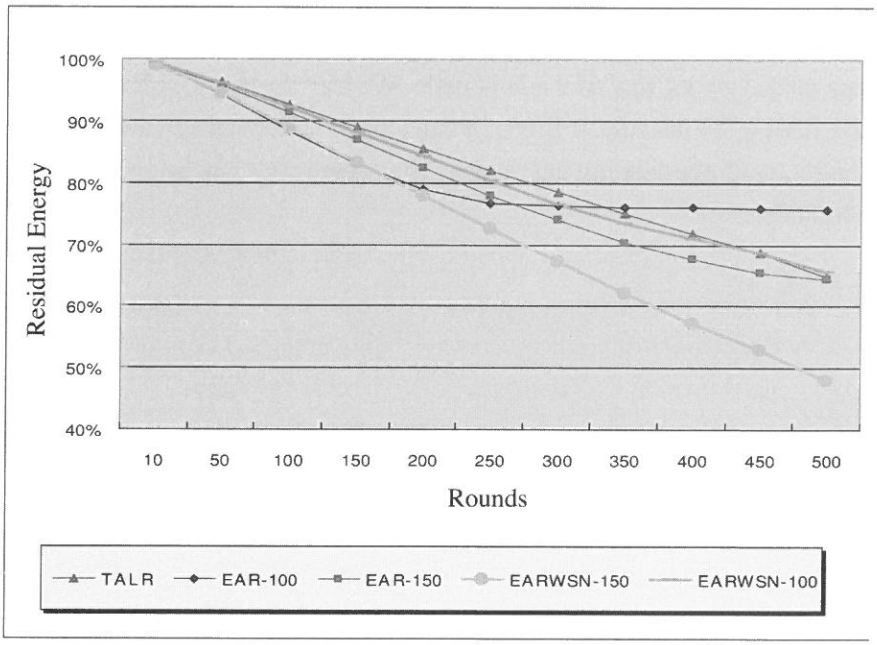

Figure 7. Residual energy by 300 nodes

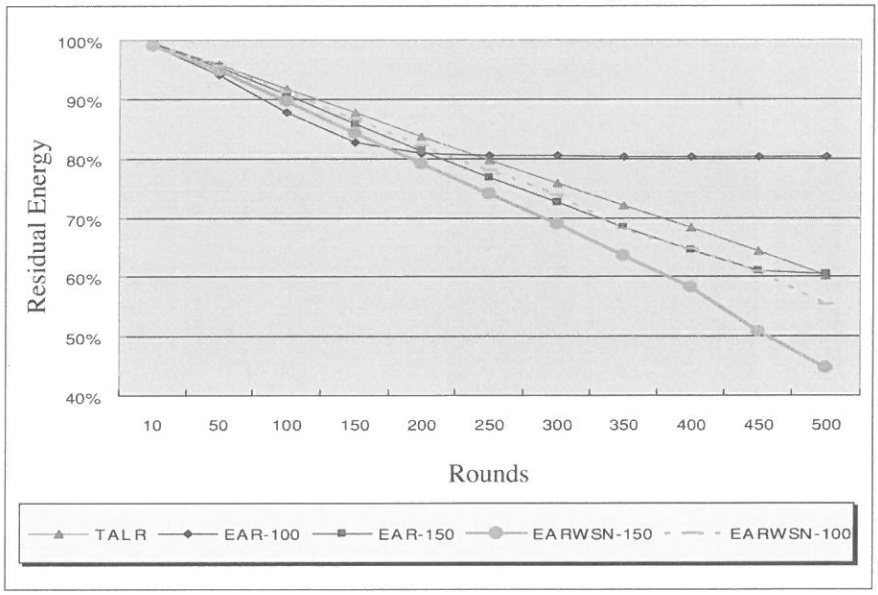

Figure 8. Residual energy by 500 nodes

Figure 9 display the average number of hops and the average delay spent by each successful data packet on its way to the sink node. We can see that TALR has a smaller value than EAR and EARWSN because it favors shorter paths and balances the loads when doing route selection to avoid overloading any nodes. The same result can be seen in both the cases of 300 and 500 nodes.

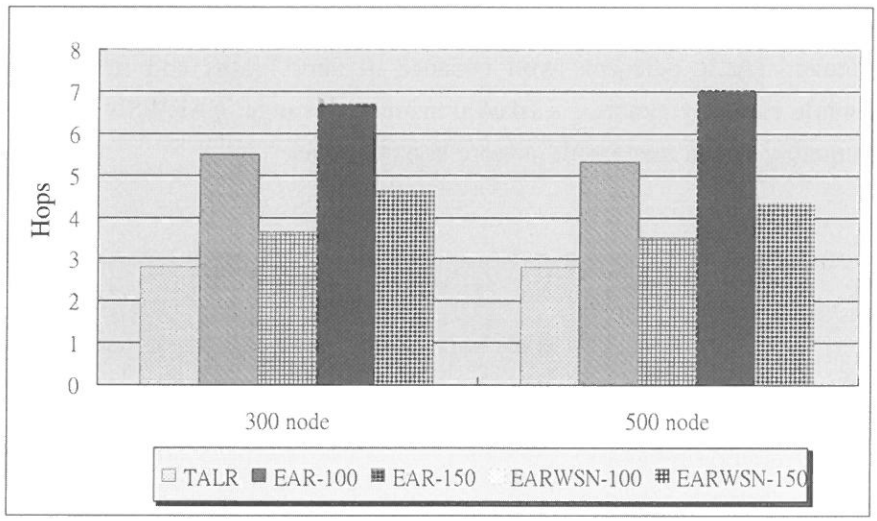

Figure 9. Average number of hops by successful packets

In figure 10, we show the total number of successful packets delivered to the sink node. TALR have more successful packets than EAR and EARWSN. As explained earlier, the EAR-100 can only carry a very small amount of packets because the heavy nodes die out quickly. Our TALR can carry packets about 1.3 times more than EAR-150 and EARWSN-150 because of better load balancing.

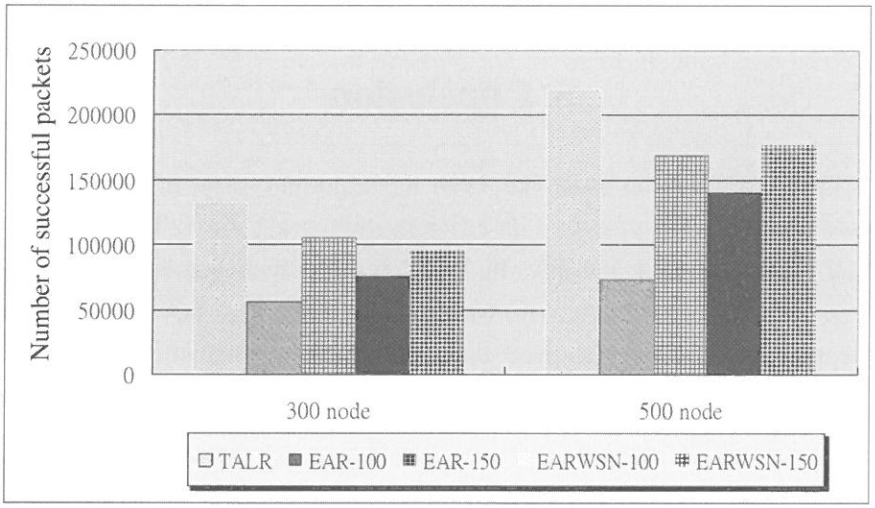

Figure 10. Number of successful packets

Figure 11 plots the amount of energy each successful data packet consumes excluding control overhead. TALR performs well because of short paths and transmission range adjustment, while EAR always uses a fixed transmission range. EARWSN would select the route of high quality which may result in more hops to travel.

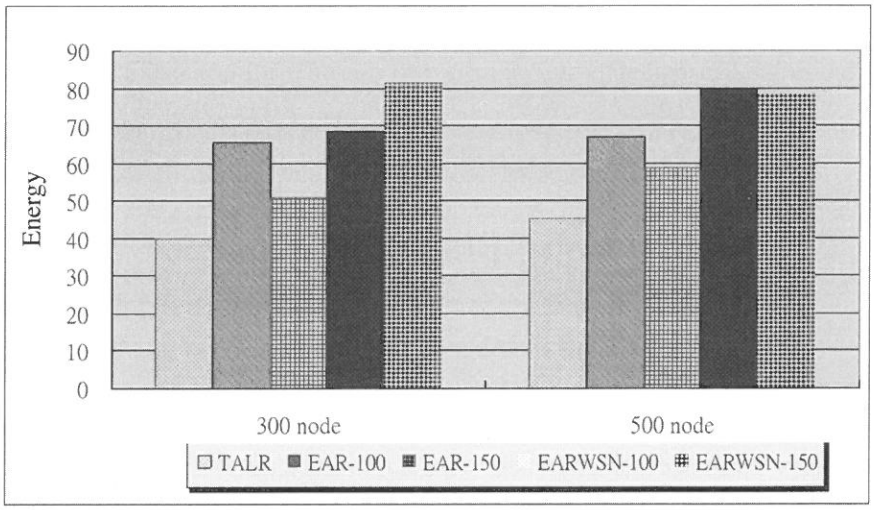

Figure 11. Consumed energy per successful packet

5. Conclusion

The energy consumption issue has been an important issue in routing packets in a wireless sensor networks. We proposed an efficient routing algorithm TALR to provide fault tolerance, load balance, and scalability. In TALR, each sensor can adjust its transmission range to the next hop to a minimum, and tries to choose a bridge node with a high lifetime estimate. The simulation results showed that our TALR mechanism has a better system lifetime compared to the other schemes.

References

[1] J.L. Lu, F. Valois, and D. Barthel, "Low-Energy Self-organization Scheme for Wireless Ad Hoc Sensor Networks," *Fourth Annual Conference on Wireless on Demand Network Systems and Services*, Jan. 2007.

[2] A. Raja and X. Su, "A Mobility Adaptive Hybrid Protocol for Wireless Sensor Networks," *IEEE Consumer Communications and Networking Conference*, Jan. 2008.

[3] S.S. Chiang, C.H. Huang, and K.C. Chang, "A Minimum Hop Routing Protocol for Home Security Systems Using Wireless Sensor Networks," *IEEE Transactions on Consumer Electronics*, vol. 53, no. 4, pp. 1483-1489, Nov. 2007.

[4] S. Hong, Y.J. Choi, and S.J. Kim, "An Energy Efficient Topology Control Protocol in Wireless Sensor Networks," *International Conference on Advanced Communication Technology*, Feb. 2007.

[5] D. Kejun, Z. Xingshe, Z. Xingguo, and L. Zhigang, "HETCP°GA Hierarchical Energy Efficient Topology Control Protocol for Wireless Sensor Networks," *International Conference on Wireless Communications, Networking and Mobile Computing*, Sep. 2006.

[6] W. Ye, F. Silva, and J. Heidemann, "Ultra-low duty cycle mac with scheduled channel polling," *International Conference on Embedded Networked Sensor Systems*, 2006.

[7] A.P. Chandrakasan, W.B. Heinzelman, and HariBalakrishnan, "An Application-Specific Protocol Architecture for Wireless Microsensor Networks," *IEEE Transactions on Communications*, vol. 1, no. 4, pp. 660-670, Oct. 2002.

[8] H. Chen, C.S. Wu, Y.S. Chu, C.C. Cheng, and L.K. Tsai, "Energy Residue Aware (ERA) Clustering Algorithm for Leach-based Wireless Sensor Networks," *International Conference on Systems and Networks Communications*, Aug. 2007.

[9] D. Xia and N. Vlajic, "Near-Optimal node Clustering in Wireless Sensor Networks for Environment Monitoring," *Canadian Conference on Electrical and Computer Engineering*, May 2006.

[10] B.L. Yin, H.C. Shi, and Y. Shang, "Analysis of Energy Consumption in Clustered Wireless Sensor Networks," *International Symposium on Wireless Pervasive Computing*, Feb. 2007.

[11] B. Huang, F. Hao, H. Zhu, Y. Tanabe, and T. Baba, "Low-Energy Static Clustering Scheme for Wireless Sensor Network," International Conference on Wireless Communications, Networking and Mobile Computing, Sep. 2006.

[12] P.K.K. Loh, S.H. Long, and Y. Pan, "An Efficient and Reliable Routing Protocol for Wireless Sensor Networks," *Sixth IEEE International Symposium on a World of Wireless Mobile and Multimedia Networks*, pp. 512-516, Jun. 2005.

[13] H. Su and X. Zhang, "Optimal Transmission Range for Cluster-Based Wireless Sensor Networks With Mixed Communication Modes," *International Symposium on World of Wireless, Mobile and Multimedia Networks*, Jun. 2006.

[14] L. Zhang and A. Lim, "Improving Lifetime in Maximum Residual Energy Routing with Increased Transmission Distance and Retransmission," *International Conference on Circuits and Systems*, pp.1438-1442, Jun. 2006.

[15] B. Huang, F. Hao, H. Zhu, Y. Tavabe, and T. Baba, "Low-Energy Static Clustering Scheme for Wireless Sensor Network," *International Conference on Wireless Communications, Networking and Mobile Computing*, Sep. 2006.

[16] E. Zhao, Q. Zhang, J. Zhang, and B. Yi, "Energy Optimized and Balanced by Transmission Range Adjustment in Wireless Sensor Networks," *International Conference on Wireless Communications, Networking and Mobile Computing*, Sep. 2007.

[17] E. Zhao, B. Yi, H.Y. Li, and J. Yao, "Transmission Range Adjustment in WSNs Based on Dynamic Programming Algorithm," International Conference on Wireless Communications, Networking and Mobile Computing, Sep. 2006.

[18] R. Vidhyapriya and P.T. Vanathi, "Energy Aware Routing for Wireless Sensor Networks," *International Conference on Signal Processing, Communications and Networking*, Feb. 2007.

Received October 20 ,2009
Revised December 20 ,2009
Accepted December 23 ,2009

在感測網路中有效率的傳輸半徑與負載平衡路徑調整

呂俊賢　洪三益

輔仁大學資訊工程系

jonlu@csie.fju.edu.tw

摘　要

無線感測網路藉由許多的感測裝置收集感測環境裡的環境數據，再傳送資料給基地台，這當中的感測裝置便需要感測資料、無線通訊及處理資訊的能力。如何去維持一個無線感測網路的運作、每個感測裝置之間的通訊方式以及如何傳輸資料都是需要仔細研究的課題。在本篇論文之中，我們提出一個新的傳輸半徑以及負載平衡路徑的調整方式，有效地應用在感測裝置的傳輸資料方式上，達到改善系統效能的目的。我們利用可以調整的傳輸半徑以及節點的現有電量，來計算出感測裝置預計可以存活時間，再加上機率分配來選擇路徑以達到平衡負載，避免有些感測裝置消耗電量過於快速。當某一感測器的剩餘電量過低時，其上游感測器便會改將封包送往其他節點，以企圖延長系統整體壽命。模擬實驗的數據顯示我們所提出來的方法確實能達到減少電量消耗以及延長系統生存時間的目的，系統生存時間比起其他兩種協定[14][18]多出了25%。

關鍵字： 感測網路、路由演算法、負載平衡、傳輸距離調整

Exact Error Probability for MMSE Combining and Comparison with Maximal Ratio Combining for Digital Radio with Cochannel Interference

Sheng-Chou Lin* Ching-Wen Chen

Department of Electronic Engineering, Fu-Jen Catholic University
510 Chung-Cheng Rd. Hsin-Chuang, Taipei 24205, Taiwan, R.O.C.
e-mail: sclin@ee.fju.edu.tw

Abstract

The exact performance analysis of MMSE (minimum-mean-square-error) combining for space diversity reception is studied in the presence of a single and multiple cochannel interference (CCI) sources, and compared to maximum-ratio combining (MRC). This paper considers digital cellular mobile radio systems with quadrature amplitude modulation (QAM) transmission and two diversity antennas in both nonfading and flat Rayleigh fading environments. Our analysis accounts for pulse waveform and modulation of the desired signal, as well as cochannel interference (CCI). The phase and symbol timing offsets between the desired signal and CCI, which can result in ISI, are taken into account. The fading of individual channels was generated by Monte Carlo simulation. The error probability for each fading channel is estimated fast and accurately using Gauss quadrature rules (GQR) which can approximate the probability density function (pdf) of the residual ISI produced by the CCI.

keywords: Cochannel interference (CCI); Space Diversity; MMSE (minimum-mean-square) combining; Maximum-ratio combining (MRC); Gauss quadrature rules (GQR)

1. Introduction

Mobile radio transmission is mainly subject to multipath fading and co-channel interference (CCI). Space diversity provides an attractive means to combat multipath fading of the desired signal and reduces the relative power of co-channel interfering signals. A practical and simple diversity combining technique is maximal ratio combining (MRC), which is optimal in the presence of spatially white Gaussian noise. MRC mitigates fading, however, it ignores CCI. Optimum combining (OC) can resolve both problems of multipath fading of the desired signal and the presence of CCI, thus increasing the performance of mobile radio systems. The combiner weights of OC need to be adjusted according to MMSE (minimum-mean-square-error) criterion to minimize interference-plus-noise conditioned on the fixed desired signal. Another similar approach, MMSE diversity combining, adjusts the weights based on the criterion to minimize the mean-square error between the receiver's estimate of the desired source and the source actually transmitted.

Performance analysis of OC and comparison with other combining for binary phase shift keying (BPSK) has been an active research area. The performance of OC was studied for both nonfading [1] and fading [2]-[8] communication systems. Performance of MMSE combining was studied for the fading case in [9]. The emphasis is on obtaining closed-form expressions. The case of a single interference source was studied in [2] and [3]. In [2], Rayleigh fading is assumed for the desired signal, but mean values, rather than actual distributions, are used to represent fading effects on the interference. With taking into account Rayleigh fading of the CCI, the exact expressions (requiring integration) are developed. Closed-form expressions of the bit-error probability for this case were obtained in [4]. The case of multiple cochannel interference was presented [5]-[9]. For this case, it is assumed that the number of interferers exceeds the number of antenna elements, and the antenna array is unable to cancel every interfering signal. Closed form expressions of the bit error probability (BEP) were developed in [5] and the comparison with MRC was studied in [6] by neglecting thermal noise. With non-negligible thermal noise, closed form expressions of the statistical distribution of the signal-to-interference-plus-noise ratio (SINR) and the outage probability were derived in [7][9]. The case of MRC was considered in [8].

Knowledge of the SINR distribution enables analytical computation of performance measures such as outage probability and average BER, assuming that the interference plus noise is Gaussian. Multiple interference meets the conditions of the central limit theorem, hence, it can be assumed Gaussian. The noise approximation model is simplistic, but was shown to be inaccurate for the case of a few dominant interferers. All of the early work mentioned above did not consider pulse waveform and the modulation characteristics of the signal of interest, as well as CCI. The symbol timing and phase offsets between the desired and cochannel interference were also not taken into account, such that the effects of ISI produced by CCI were neglected. In [10][11], the BER of PSK in several different flat fading environments in the presence of CCI was analyzed using the precise cochannel interference model. The performances of dual-branch equal gain combining (EGC) and dual-branch selection combining (SC) were investigated by them. However, the performances of MRC, OC and MMSE combining were not considered.

This paper studies the exact average BER of MMSE combining and provides the comparison with MRC using the precise channel model when channels of the desired signal and interference are subject to nonfading and Rayleigh fading. A single dominant cochannel interferer is often the case in TDMA mobile systems. Both the cases of a single and six interferers are analyzed in this paper. Two diversity antennas, which is often used in current cellular systems, are considered. With the ISI-like CCI, it is expected that the simulation is fairly tedious and time-exhausting. The error probability for each fading channel is estimated fast and accurately using Gauss quadrature rules (GQR) which can approximate the probability density function (pdf) of the CCI.

2. Systen models

The system is modeled assuming that cochannel sources transmitting QAM signal over the fading channel to a K-branch space diversity receiver. The system operates in the presence of L cochannel interferers and thermal noise. The transmitted QAM baseband signal from the ith cochannel source can be expressed in the form

$$s_i(t) = \sum_n c_{i,n}\ g_T(t - nT) \tag{1}$$

where $c_{i,n} = a_{i,n} + jb_{i,n}$ is the sequence of complex data symbols and T is the symbol interval. The data symbols $a_{i,n}$ and $b_{i,n}$ on the in-phase and quadrature paths define the signal constellation of the QAM signal with points. In the constellation, we take $a_{i,n}, b_{i,n} = \pm 1, \pm 3, \ldots, \pm(\sqrt{M+1})$. The transmitter filter gives a pulse $g_T(t)$ having the square-root raised-cosine spectrum with a rolloff factor. The desired signal is indexed by $i = 0$, and the CCI sources by $i > 0$. The diversity branches are indexed by $k = 1, \ldots, K$.

The users experience flat Rayleigh fading, which is spatially independent provided that antenna spacing is sufficiently large. The complex channel gain between the ith source and kth diversity path can be represented by $\lambda_{i,k} e^{j\theta_{i,k}}$, where $\lambda_{i,k}$ is the envelope with Rayleigh distribution having variance $\sigma_i^2 = E\left[\lambda_{i,k}^2\right]$; phase $\theta_{i,k}$ has a uniform distribution in $[0, 2\pi]$. With zero-mean information symbols, the average received power of the ith cochannel signal received by the kth diversity antenna is derived as $\sigma_i^2 \sigma_c^2 / T$, where $\sigma_c^2 = E[|c_{i,n}|^2]$ represents the data symbol variance for all cochannel sources. For a M-QAM system, $\sigma_c^2 = 2(M-1)/3$. The noise power measured in the Nyquist band is N_0 / T . Therefore, for Rayleigh fading channels, the average value of the SNR on each diversity path is defined as $\sigma_s^2 \sigma_c^2 / N_0$, where $\sigma_S^2 = E\left[\lambda_{0,k}^2\right]$ Equal average power is assumed for all received interferers, and therefore, we set $\sigma_S^2 = \sigma_d^2$ for $i = 1, \ldots, L$. The signal-to-interference power ratio (SIR) can be denoted by $\mathrm{SIR} = \sigma_S^2 / \sigma_d^2$.

We assume the frequency and phase tracking as well as symbol synchronization are perfect for the desired signal. Sampling the filtered received signal at $t = lT$ on the kth diversity path, we obtain

$$z_k(lT) = \lambda_{0,k} \sum_n c_{0,n} g(lT - nT) + \sum_{i=1}^{L} \lambda_{i,k} e^{j\phi_{i,k}} \sum_n c_{i,n} g(lT - nT - \tau_i) + n_k(lT) \tag{2}$$

where $\phi_{i,k} = \theta_{i,k} - \theta_{0,k}$ and τ_i represent the relative carrier phase and symbol timing offsets between the desired signal and the ith interfering signal. $\phi_{i,k}$ and τ_i are uniformly distributed the interval of $[0, 2\pi]$ and $[0, T]$, respectively. Pulse response $g(t)$ having the raised-cosine spectrum is the combined transmitter and receiver filters which have the same response.

The sampled signals at the K antennas can be represented by as a $K\times 1$ vector $z=[z_1, z_2,.., z_K]^T$ which is processed with a spatial weight vector $\mathbf{w}=[w_1,....,w_K]^T$. With the phase relative to the desired signal, the channel vector of the ith cochannel interfering signal can be defined as $\mathbf{h}_i = [\lambda_{i,1}e^{j\phi_{i,1}}, \lambda_{i,2}e^{j\phi_{i,2}}, ..., \lambda_{i,K}e^{j\phi_{i,K}}]^T$. The vector of the corresponding envelope is given by $\lambda_\mathbf{i} = [\lambda_{i,1},..., \lambda_{i,K}]^T$. The combiner's output for estimating the symbol is then given by $\hat{c}_{0,l} = \mathbf{w}^T\mathbf{z}$ at $t = lT$. The weight vector $\mathbf{w}$ is determined using MMSE and MRC methods in this paper.

As shown in Fig. 1, when the antennas outputs are combined according to MRC, the weight vector is given by $\mathbf{w}=|\lambda_0|^T$. The weight vector that minimize the MMSE at the output is given by the well known relation

$$\mathbf{w} = \mathbf{R}^{-1}\lambda_0, \tag{3}$$

where $\mathbf{R}$ is the covariance matrix of the received signal across the antenna elements. It is assumed that the fading is fixed over the time interval of interest. $\mathbf{R}$ given by

$$\mathbf{R} = \frac{N_0}{\sigma_c^2}\mathbf{I} + E[\mathbf{z}\mathbf{z}^\dagger] \tag{4}$$

is a k × k matrix, where the superscript † denotes the complex conjugate transpose. With the random relative carrier phase and symbol timing offsets, we can show that $E[\mathbf{z}\mathbf{z}^\dagger] = \lambda_0\lambda_0^\dagger + (1-\beta/4)\mathbf{h}\mathbf{h}^\dagger$, where we define $\mathbf{h} = [\mathbf{h}_1,...,\mathbf{h}_L]$ which is a matrix [6]. $\mathbf{I}$ is the identity matrix of dimension K. The output of the combiner is then written as

$$\hat{c}_{0,l} = \mathbf{w}^T\mathbf{z} = \sum_{k=1}^{K}\left[s_{0,k}(lT) + \sum_{i=1}^{L} s_{i,k}(lT) + v_k(lT) \right] \tag{5}$$

where the part of the desired signal on the *k*th path, can be written as

$$s_k(lT) = w_k \lambda_{0,k} \sum_n c_{0,n} g(lT - nT) \tag{6}$$

and $s_{i,k}(lT)$, the ith interfering signal on the kth path, can be written as

$$s_{i,k}(lT) = w_k \lambda_{i,k} e^{j\phi_{i,k}} \sum_n c_{i,n} g(lT - nT - \tau_i) \tag{7}$$

We can define $w_k = w_{I,k} + jw_{Q,k}$. The combined signal can be written as

$$\hat{c}_{0,l} = (a_0 + jb_0) g_s + (\xi + j\eta) + v_l \tag{8}$$

where g_s is given by the sum of $\lambda_{0,k} w_k$ on all paths. Hence,

$$(a_0 + jb_0) g_s = \sum_{k=1}^{K} \lambda_{0,k} [(a_0 w_{I,k} - b_0 w_{Q,k}) + j(a_0 w_{Q,k} + b_0 w_{I,k})] \tag{9}$$

With defining $g_{i,n} = g(nT + \tau_i)$, the combined ISI in the in-phase rail due to the *i*th CCI is denoted by

$$\xi = \sum_{i=1}^{L} \left(\sum_n a_{i,n} p_{i,-n} - \sum_n b_{i,n} q_{i,-n} \right) \tag{10}$$

where we define the sampled pulse response of the *i*th CCI source as

$$\begin{aligned} p_{i,n} &= \sum_{k=1}^{N} \lambda_{i,k} (w_{I,k} \cos\phi_{i,k} - w_{Q,k} \sin\phi_{i,k}) g_{i,-n} \\ q_{i,n} &= \sum_{k=1}^{N} \lambda_{i,k} (w_{I,k} \sin\phi_{i,k} + w_{Q,k} \cos\phi_{i,k}) g_{i,-n} \end{aligned} \tag{11}$$

The ISI corresponding to the quadrature channel is denoted by η . With a slight change in indexing the signal, we denote above pulse responses in the in-phase and quadrature channels, respectively, as

$$\xi = \sum_{i=1}^{L}\left(\sum_{n} a_{i,n}p_{i,n} + \sum_{n} b_{i,n}q_{i,n}\right)$$
$$\eta = \sum_{i=1}^{L}\left(\sum_{n} a_{i,n}q_{i,n} + \sum_{n} b_{i,n}p_{i,n}\right) \quad (12)$$

Next, we consider the kth weighted noise which can be derived as $v_k(t) = w_k n_k(t)e^{-j\theta_{0,k}}$. The input noise $n_k(t)$ is a zero-mean AWGN with two-sided power spectral density of N_0 W/Hz. The power spectra of the filtered noise is $|w_k|^2 N_0 G(f)$ and hence resulting in the output power (variance) $\sigma_{v_k}^2 = (w_{I,k}^2 + w_{Q,k}^2)N_0/T$, where $G(f)$ has a raised cosine spectral characteristic. The variance of the noise at the output of the combiner can expressed as

$$\sigma_v^2 = \frac{N_0}{T}\sum_{k=1}^{K}\sigma_{v_k}^2 = \frac{N_0}{T}\sum_{k=1}^{K} w_{I,k}^2 + w_{Q,k}^2 \quad (13)$$

We define $v = v_I + jv_Q$ where v_I and v_Q with equal power (variance), $\sigma^2 = \sigma_v^2/2$.

3. Error probability estimation

Since the distribution density functions of quantities ξ and ξ are symmetric to zero, the interferers in the in-phase and quadrature parts have identical probability distribution. It has been shown that the average symbol error probability for each set of channel parameters can be bounded tightly by

$$P_M = 2E[P_I(\xi)] = 2\left(1 - \frac{1}{\sqrt{M}}\right)E\left[erfc(\frac{R_s + \xi}{\sqrt{2}\sigma})\right] \quad (14)$$

Since ξ is a random variable whose distribution is not known explicitly, the evaluation of $E[P_I(\xi)]$ is performed by computing the conditional error probability of each of all possible sequences of the desired signal and CCI, and then averaging over all those sequences. This approach is referred to as the fast semi-analytical technique [12][13]. The corresponding average bit error are $P_M/\sqrt{M}$

While the fast semi-analytical technique is computationally very efficient compared to the Monte-Carlo method, the computational load increases significantly if the memory length of the system and/or the order of the modulation scheme increases, especially when dealing with low error rates and high order communication systems. Thus, such a method becomes extremely time-consuming, in particular, when we consider the random-valued symbols and the carrier timing offsets of CCI, as well as the diversity scenario. Some techniques can be used for evaluation of numerical approximations to the average $E[g(\xi)]$. For (14), $g(\cdot)$ is given by $erfc(\cdot)$. One efficient approach called the Gaussian quadrature rule (GQR) approximation will be addressed for the numerical evaluation of (14), which depends on knowing the moments of ξ , up to an order that depends on the accuracy required.

Using the Gaussian quadrature rule, the averaging operation in (14) can be approximated by

$$E[g(\xi)] = \int_a^b g(x) f_\xi(x) dx \cong \sum_{i=1}^{N} w_i g(x_i) \tag{15}$$

a linear combination of values of the function $g(\cdot)$, where $f_\xi(x)$ denotes the probability function of the random variable ξ with range $[a,b]$. The weights (or coefficients) w_i , and the abscissas (or points or nodes) x_i , $i = 1, 2, ..., N$ can be calculated from the knowledge of the first $2N+1$moments of ξ. Since ξ is the sum of a finite number of random variables and the moment of each of these random variables can be determined, a recursive algorithm which can be used to determine the moments of all order of ξ was discussed in [12]. We compute the average in (15) by means of the classic GQR's suggested in [12] [13].

4. Simulation results

We only exhibit the simulation results with 4-QAM. The rolloff factor β is set to 0.5 . We study MMSE diversity combining when the signal or interferers are subject to nonfading or Rayleigh fading. Average error rate due to fading can be evaluated by averaging the error rate over all possible varying channel parameters. A single dominant CCI and six strongest interferers are considered individually. We only consider the case of two diversity antennas.

In our test, we find that MMSE combining can eliminate CCI efficiently while CCI is strong enough relative to the noise. When both the desired signal and CCI are unfaded (only the amplitude), Fig. 2 shows that MMSE combining is better than MRC combining for the value of SIR less than 6dB when SNR = 30dB. We find that noise is enhanced for a certain instantaneous value of the phase difference between the cochannel interferers received by the two antennas, when MMSE combining intends to suppress CCI, and thus leading to a degradation to the average performance. Figs. 3-4 demonstrate the average bit error probabilities versus SNR when the desired signal is not faded at SIR = 10dB. As CCI is unfaded, Fig. 3 indicates that MMSE diversity is inferior to MRC for the case of a single interferer when SNR is higher than 10dB.

The figure also indicates that the performance becomes worse when there are six interferers. With 6 interferers MMSE combining becomes better than MRC. The possible reason is that the noise enhancement effect is reduced since no interferers can be eliminated for interferers more than receive antennas. As the interferer is subjected to fading, Fig. 4 shows that the performance becomes worse in comparison to Fig. 3. For this case, MMSE combining is better than MRC combining for a single and six interference sources. The reason is that the probability of the low instantaneous SIR becomes great, and thus MMSE combining increases the chances of interference cancellation, as compared to MRC. The error probability floors are caused by the low instantaneous SIR. Fig. 4 also reveals that the performance with multiple interferers is better than that with the single interferer. The explanation is that when they have equal total average interference power, the probability that at least one of the interferers is strongly faded in the case of multiple interferers is smaller, thus leading to a smaller error rate. Note that for SNR>25dB MMSE diversity is better for the case of a single interferer, since CCI becomes dominant and can be efficiently eliminated at this time.

When the desired signal is subject to fading, the results are plotted in Figs. 5-6. It is noted that the average error probabilities become relatively high due to the fading effect of the desired signal. The curves clearly show that the fading effect on CCI seems not to degrade the performance significantly. The average error probability floors caused by cochannel interference are evident for MRC combining. Because the instantaneous SIR has a better

chance to take on low values with the fading effect on the desired signal, MMSE combining can largely cancel CCI for the case of a single interferer and results in no irreducible error floor. With a single and 6 interferers, MRC has similar performance, but is slightly worse than MMSE combining with 6 interferers. Similar to the results in Fig. 3, Fig. 5 shows that the performance is slightly worse with six interferers for MRC when CCI is not unfaded. Similar to Fig. 4, Fig. 6 shows that the performance of MRC becomes slightly better when six interferers are subject to fading. Generally, when both signal and interference are subject to Rayleigh fading, MMSE combining with 6 interferers has similar performance to MRC with a single or 6 interferers and appears irreducible since the interference can not be cancelled using two antennas. In general, our results is higher than the results presented in [2] where CCI is not faded, but is lower than the results in several previous work [3]-[6] in terms of QPSK.

5. Conclusion

We successfully apply the Gaussian Quadrature rule (GQR) to calculate the probability of error in the presence of ISI caused by cochannel interferers. Random-valued phase and timing offsets between the desired signal and CCI are considered in the optimization of MMSE combining and the computation of the probability of error. When the desired signal and CCI are unfaded and SIR is higher, MMSE combining is inferior to MRC for the case of a single interferer due to the noise enhancement resulted from the effect of phase offsets. When the desired signal is subject to fading, our results show that MMSE combining is much better than MRC for the case of a single CCI. When the number of CCI sources exceeds the number of antennas, MMSE combining is only slightly better than MRC.

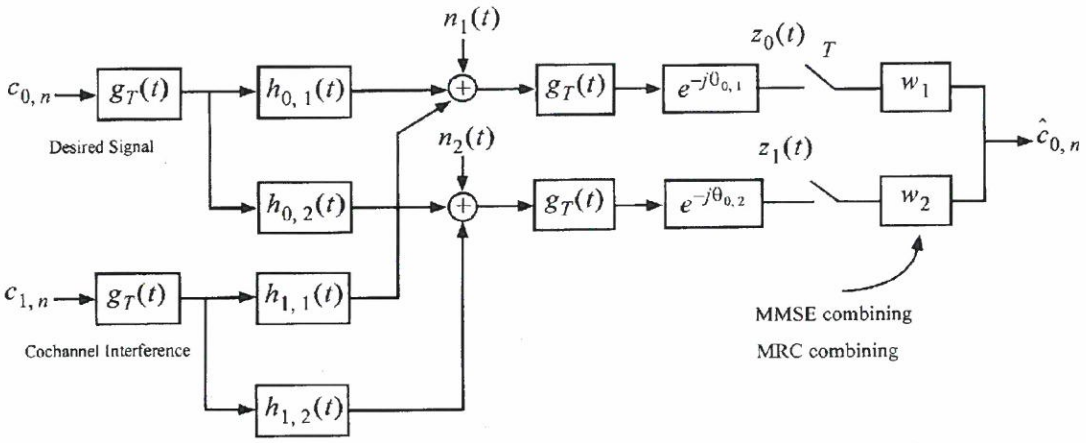

Fig. 1 Block diagram of the diversity receiver over a channel with CCI.

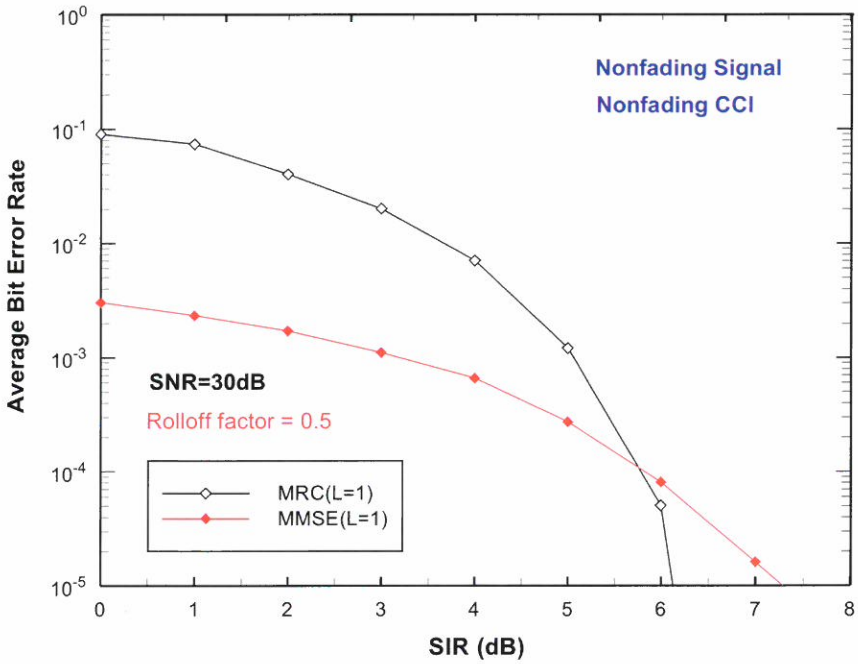

Fig. 2 Average error probability versus SIR for 4-QAM with MMSE combining and MRC combining at SNR=30dB (nonfading signal, nonfading CCI).

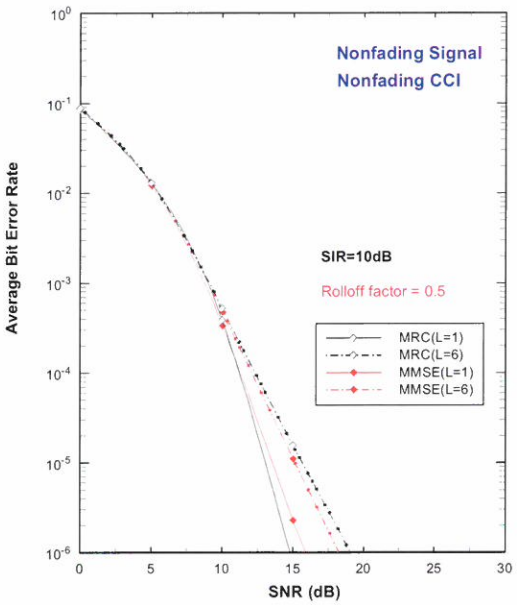

Fig. 3 Average error probability versus SNR for 4-QAM with MMSE combining and MRC combining at SIR=10dB (nonfading signal, nonfading CCI).

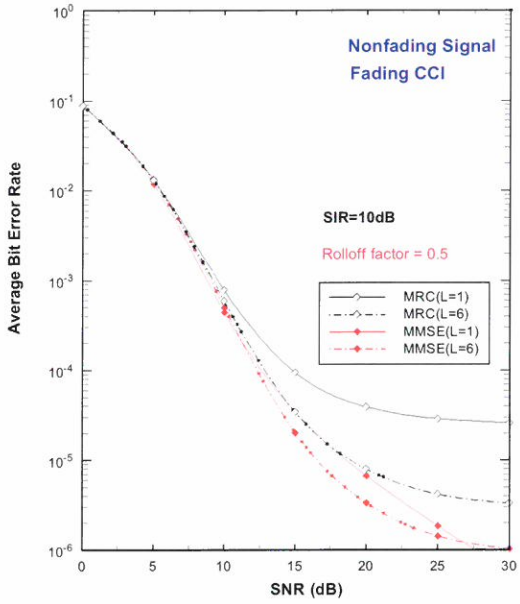

Fig. 4 Average error probability versus SNR for 4-QAM with MMSE combining and MRC combining at SIR=10dB (nonfading signal, fading CCI).

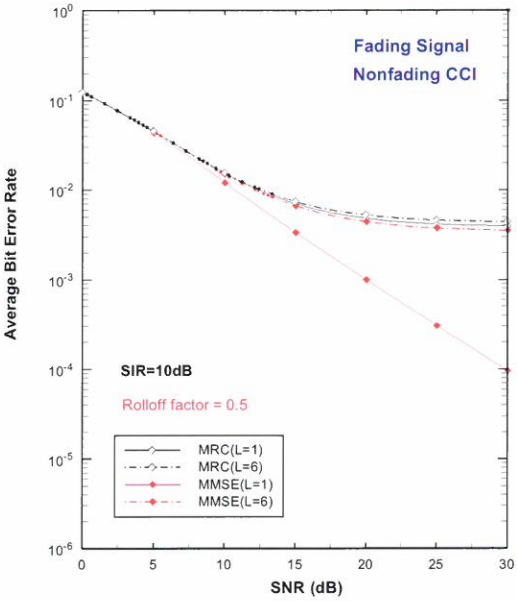

Fig. 5 Average error probability versus SNR for 4-QAM with MMSE combining and MRC combining at SIR=10dB (fading signal, nonfading CCI).

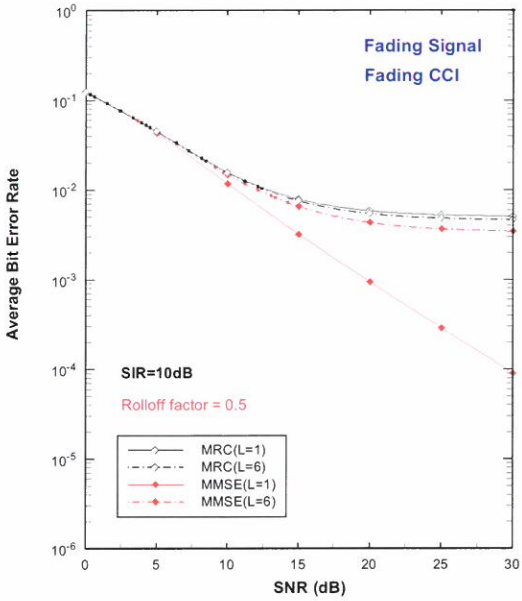

Fig. 6 Average error probability versus SNR for 4-QAM with MMSE combining and MRC combining at SIR=10dB (fading signal, fading CCI).

References

[1] R. A. Monzingo and T. W. Miller, introduction to Adaptive Arrays, New York: Wiley, 1980.

[2] J. H. Winter, "Optimum combining in digital mobile radio with cochannel interference,"

[3] IEEE J. Select. Areas Commun, Vol. 2, pp528-539, July 1984.
Shah, A. M. Haimovich, M. K. Simon and M.-S. Alouini, "Exact bit-error probability for optimum combining with a Rayleigh fading Gaussian cochannel interference," IEEE Trans. Commun., vol. 48, pp.908-912, June 2000.

[4] V. A. Aalo and J. Zhang, "Performance of antenna array systems with optimum combining in a Rayleigh fading environment," IEEE Commun. Lett., vol. 4, pp. 125-127, Apr. 2000.

[5] Shah and A. M. Haimovich, "Performance analysis of optimum combining in wireless communications with Rayleigh fading and cochannel interference," IEEE Trans. Veh. Comm., vol. 46, no. 4, pp. 473-479, Apr. 1998.

[6] Shah and A. M. Haimovich, "Performance analysis of maximal ratio combining and comparison with optimum combining for mobile radio communications with cochannel interference," IEEE Trans. Veh. Comm., vol. 49, no. 4, pp. 1454-1463, Jul. 2000.

[7] Y. Tokgoz, B. D. Rao, M. Wengler, B. Judson, "Performance analysis of optimum combining in antenna array systems with multiple interferers in flat Rayleigh fading," IEEE Trans. Commun., vol. 52,no. 6. pp. 1047 - 1050, July 2004.

[8] Y. Tokgoz, B. D. Rao, M. Wengler, B. Judson, "The Effect of Imperfect Channel Estimation on the Performance of Maximum Ratio Combining in the Presence of Cochannel Interference," IEEE Trans. Commun., vol. 55, no. 5, pp. 1527 - 1534, Sep. 2006.

[9] H. Gao, P. J. Smith, M. V. Clark, "Theoretical reliability of MMSE linear diversity combining in Rayleigh-fading additive interference channel," IEEE Trans. Commun., vol. 46, no. 5, pp. 666-672, May, 1998.

[10] A. Abu-dayya and N. C. Beaulieu, "Diversity MPSK receivers in cochannel interference," IEEE Trans. Comm., vol. 48, no. 6, pp. 1959-1965, Nov. 1999.

[11] A. Abu-dayya and N. C. Beaulieu, "Diversity π/4-DQPSK microcellular interference," IEEE Trans. on Comm., vol. 44, no. 10, pp. 1289-1297, Oct. 1996.

[12] M. C. Jeruchim, P. Balaban and K. S. Shanmugan, Simulation of Communication Systems, Plenum Press, N. Y., 2000.

[13] W. H. Tranter, K. S. Shanmugan and T. S. Rappaport, and K. L. Kosbar, Principles of Communication Systems Simulation with Wireless Applications, Prentice-Hall, N. J., 2004.

Received October 30 ,2009
Revised December 18 ,2009
Accepted December 29 ,2009

MMSE合併分集於具同頻干擾之數位無線電下的準確錯誤率及與MRC合併分集之比較

林昇洲
陳靜雯
輔仁大學電機工程系

摘　要

本研究討論在單一和多個同頻干擾(Cochannel interference，CCI)下，最小均方誤差(Minimum mean-square-error, MMSE)分集接收機(diversity receiver)之準確表現分析及與最大比例合併分集接收機(Maximum-ratio combining，MRC)之比較。本論文考慮正交振幅調變(quadrature amplitude modulation，QAM)兩路天線接收於無衰退(nonfading)及平坦衰退fading)環境下之數位蜂巢式行動系統。我們的分析將想要信號及同頻干擾之脈波波型及調變列入考慮，相鄰符號干擾(Intersymbol Interference，ISI) 導因於想要信號及同頻干擾間之相位差及符號間差也被加以考量。我們使用蒙地卡羅模擬法(Monte Carlo simulation)產生各別衰退通道，同時利用高斯正交規則(Gaussian quadrature rule，GQR)取得同頻干擾導致之相鄰符號干擾的近似的機率密度函數(probability density function，pdf)以準確及快速的運算每個衰退通道之錯誤率。

可應用於RFID具任意輸入位元能力之並行循環冗餘檢查碼晶片設計*

洪玉城、洪翰均、謝韶徽

國立勤益科技大學 電子工程系

ychung@ncut.edu.tw, s970002c@lida.ee.ncut.edu.tw

摘　要

本文提出改善並行CRC電路架構並以TSMC CMOS 0.35 μm製程實現晶片。近年隨著電路設計工作頻率需求越來越快，且所需要處理的資料位元數也持續增加，而一般的串列結構CRC電路已漸無法滿足快速處理大量資料的需求。因此，我們採用文獻之並行架構以提升資料處理速度，並設計一組開關切換電路，改善原文獻電路不能處理任意位元資料的缺點。此改良電路以CRC-8作設計，此改良後之並行CRC電路已能處理任意資料位元，經晶片實體量測可運作於58 MHz@3.3V.

關鍵字：循環冗餘檢查碼、CRC、RFID

Corresponding author : Tel : (04)2392-4505-7374 Fax : (04)2392-6610
E-mail address : ychung@ncut.edu.tw

1.前　言

近年RFID(Radio Frequency Identification)的應用越來越廣泛，相較於條碼技術使用上更為便利。由於RFID 具備跨越一段距離之識別能力，不需瞄準條碼就可快速達到辨識功能。RFID 技術除可幫助物流產業快速管理貨物，亦可應用於門禁系統管理、人員看護、寵物晶片及圖書藏書管理等用途。隨著RFID廣泛應用，以及電路實現技術逐漸被改良，使得人們對RFID 的需求量大增。但無線射頻辨識系統中，標籤（Tag）和讀取器（Reader）之間的資料傳送可能會因為外在環境的干擾而發生錯誤。因此，需在接收端加一層查核機制，以確定所接收到的資料與傳送端的資料完全吻合時，該筆資料才可進一步利用。圖1為RFID標籤內部架構圖，當天線接收到一筆資料後會經由錯誤查核機制CRC (Cyclic Redundancy Check Code)來確認所接收的資料是否正確。相同的，當標籤欲回傳一筆資料給讀取端也需經由CRC編碼後，此筆資料再經由後續電路單元進行處理如:曼徹斯特編碼器與調變器等等，調變過的資料再由天線回傳至讀取器。

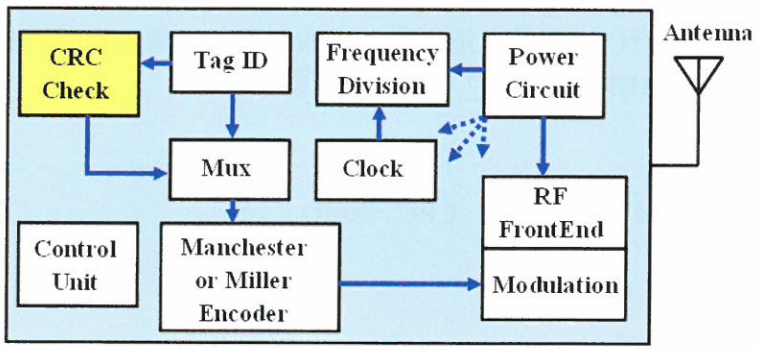

圖1.：RFID標籤(Tag)內部架構

循環冗餘檢查碼CRC是較有效率的錯誤偵測碼之一。CRC的計算方式是將待傳輸的資料區塊視為一堆連續位元所構成的一數值，並將此數值除以一特定除數，除數值位元數依照所要得到的CRC位元數目而定。過去文獻普遍探討將CRC電路應用於高速的傳輸設備中，例如:乙太網路間的傳輸及硬體之間的有線傳輸等技術。1992年由培(Pei)等人[6]首先提出CRC平行處理的概念，1996年布郎(Braun)等人[7]提出改善之矩陣計算方式並以FPGA技術實現32-bit的並行CRC電路，在那之後就陸續有文獻提出各種不同的平行設計架構，如2001年邁克爾(Michael)等人[3]提出使用Combinatoral network

的並行電路架構、2007年塞澤爾(Sezer)等人[8]提出可任意更換輸入port數、CRC多項式及位元數的Programmable電路架構。同年程超(chao cheng)等人[5]提出使用Unfolding、Pipelining、Retiming的CRC電路架構。因此，從過去文獻之探討，大都使用平行處理演算法及電路架構來提升資料運算速度。但上述CRC文獻所提出的平行設計，其電路運作速度雖快但其龐大的功率消耗及晶片面積並不適用於RFID的晶片設計。因此，本文以平行設計為出發點，但同時也以低功率、小面積做為本電路設計基礎。因為在其電路的運作速度、功率消耗及成本上需找到一個平衡點，使我們的設計是適宜應用於RFID的系統。

在現今電路高資料傳輸率的需求下，一般以串列形式所實現的CRC電路已漸不足以應付高速的資料傳輸。相較於串列CRC電路架構，並行CRC架構可以更快及更有效率的去處理每一筆資料運算。雖然並行架構在硬體的成本上會比串列架構來的高，但在現今高資料量處理需求下，並行架構的設計是有其必要性。本文採用文獻[3]之架構，針對其架構只能處理某些固定位元數資料的缺點加以改善。經過我們設計後，此改良之CRC電路架構已能處理任意位元數資料。

2. CRC運算

本節簡單說明錯誤檢查碼之工作原理。一般常使用的資料偵錯技術有同位檢查、縱向冗餘檢查(Longitudinal Redundancy Check)、CRC檢查法等方式。其中CRC檢查法為最常使用的方法之一，以下簡單說明CRC檢查法整合於RFID電路之運算流程。

2.1 RFID資料偵錯流程

如圖2(a)所示，當RFID發送端欲傳送一筆資料，需將資料送到CRC編碼器運算，進而產生一組CRC值，再將此CRC運算值利用多工器(MUX)加在資料後面才傳送至接收端。當接收端收到發送端的資料，如圖2(b)所示，將此筆資料再進行CRC的運算。觀察運算結果，若餘數不為零則代表資料在傳送過程發生錯誤，需通知發送端重新發送此筆資料。若餘數為零則代表資料傳輸成功。

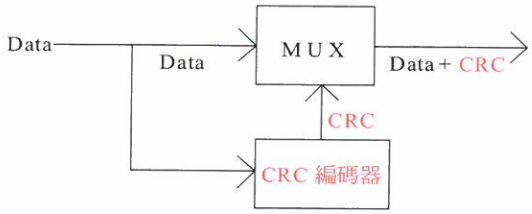

圖2(a)：CRC編碼發送端

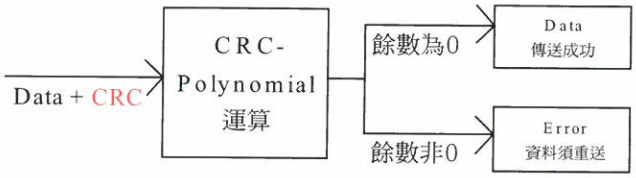

圖2(b)：CRC編碼接收端

2.2 CRC運算原理

CRC演算法的計算是一種循環計算過程，因輸出端暫存器值會拉回輸入端與輸入資料做互斥或比較，每一次所產生的暫存器值皆會影響到下一個Clock輸入時的暫存器值。CRC碼的計算包括了要計算其CRC值的資料位元組，以及所有前面已計算過的資料位元組之CRC值。從數學角度觀察，CRC檢查法可視為利用一組事先已定義好之產生多項式去除資料位元組所組成之多項式。而CRC值即為相除後所得餘項。表1為常用的CRC產生多項式。

表1. 常用的CRC產生多項式

產生多項式 CRC-4	X^4+X+1
產生多項式 CRC-8	$X^8+X^4+X^3+X^2+1$
產生多項式 CRC-16	$X^{16}+X^{15}+X^2+1$
產生多項式 CRC-16/CCITT	$X^{16}+X^{12}+X^5+1$

我們舉例說明計算一個8-bit資料位元組值為01110001。為了計算8位元的CRC值，首先需把資料位元組左移8個位元，即補8個零於資料後。而本篇所採用的產生多項式為$X^8 + X^4 + X^3 + X^2 + 1$ (100011101)，如圖3(a)所示進行CRC的運算。經過一連串互斥或運算後所得到的餘數01000100，即為所要的CRC值。最後我們再將此餘數附加在欲傳送的資料後面，藉由發送端將此已附加CRC值的資料串傳送至接收端，當接收端收到資料後，再進行一次CRC的運算如圖3(b)所示。若運算結果餘數為0，代表所得到的資料與傳送端的資料相同，表傳送成功。

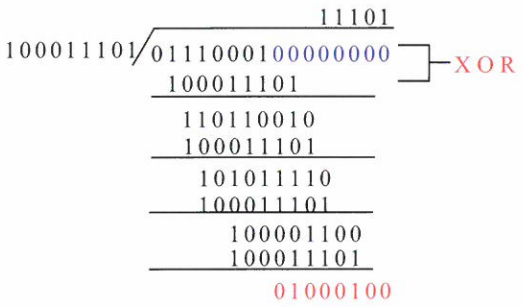

圖3(a) CRC碼的產生

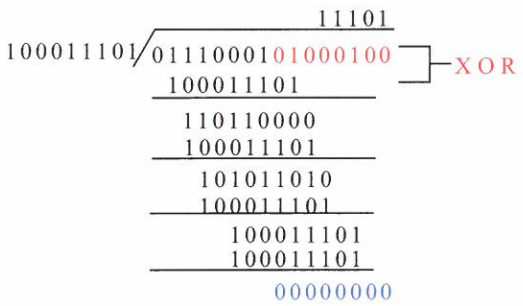

圖3(b) 接收端的CRC錯誤驗證

3. 並行CRC電路設計

在現今電路資料處理量越來越大的情況下，一般所使用的串列式CRC架構已漸漸無法滿足其需求。因此我們需要的是能快速處理資料的電路架構，此並行架構CRC電路設計是有其必要性。

3.1 並列式相較於串列式架構

如圖4所示為一般使用LFSR(Linear Feedback Shift Register)的3-bit串列式CRC電路架構，假設所使用的產生多項式為X^3+X^2+1。當電路開始工作時，資料須以串列形式輸入，直到資料完全輸入暫存器後，此時三個暫存器的值即是我們所要的CRC值。因此假設處理一4-bit資料則需要4個Clock的時間。相較於文獻[3]採用資料並行輸入CRC之電路架構，如圖5所示。圖5所用的產生多項式亦為X^3+X^2+1，四個輸入端採用並列方式輸入，當電路開始工作時資料以並列形式同時丟入i0-i3。因此，同樣處理一組4-bit資料只需要1個Clock的時間。

在比較一般串列式架構及文獻[3]所提出之並行式架構後，以串列架構處理*n-bit*資料至得到CRC值時間需為*n*個Clock，而文獻[3]提出的並行式架構處理*n-bit*資料時間為n/m(m:輸入端並列個數)。因此，並行式架構處理資料速度明顯比串列式快，但在硬體的成本上也相對較高。

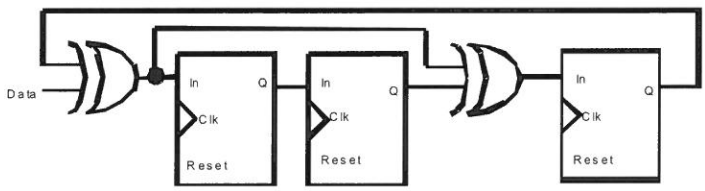

圖4. 使用LFSR之串列CRC電路 (X^3+X^2+1)

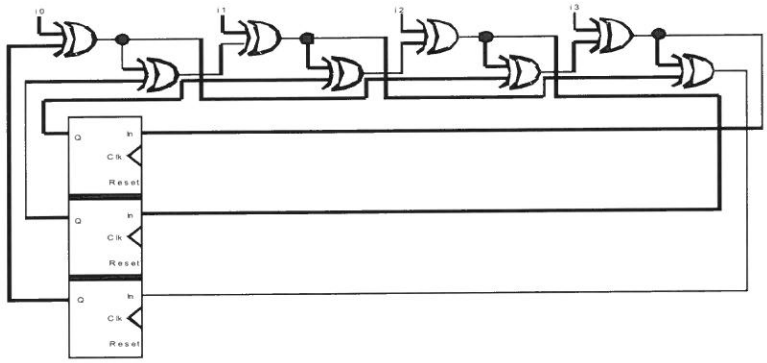

圖5. 文獻[3]所提出之並行式CRC電路 (X^3+X^2+1)

3.2 改良之並行式CRC電路

在文獻[3]所提出之並行式CRC電路架構相較於串列式CRC架構可以更快速的處理資料。但在硬體的實現上會面臨到一個嚴重問題，即為資料只能以輸入端並列個數的倍數輸入。舉例說明當電路輸入端並列數為四個，如圖5所示，則資料僅能以4、8、12、16...等四的倍數輸入資料。因為當資料不為輸入端的並列個數輸入時，勢必會造成某些輸入端沒有資料輸入，進而造成產生錯誤的CRC值。

本文所提出的改良並行式電路則由文獻[3]所提出單一輸入Port的8位元模組衍伸設計而來。如圖6所示，虛線裡包含互斥或閘所產生的Combinatoral network(CN)代表我們所選用的產生多項式，分別從上至下代表著高位元至低位元。我們可任意去選擇不同的產生多項式，藉由不同的互斥或閘擺放位置，擺放互斥或閘的點則代表產生多項式裡每一項的次方數存在與否，圖6表達多項式即為$X^8 + X^4 + X^3 + X^2 + 1$。如圖7所示CN的每一項輸出則對應至下一個狀態(狀態S_{n+1})，暫存器S_n(S7-S0)的輸出則分別對應至產生多項式的相同輸入。因此，藉由增加CN我們可以任意增加電路輸入端的個數。同樣的，藉由增加暫存器的個數我們也可以任意增加CRC餘數值的位元數。

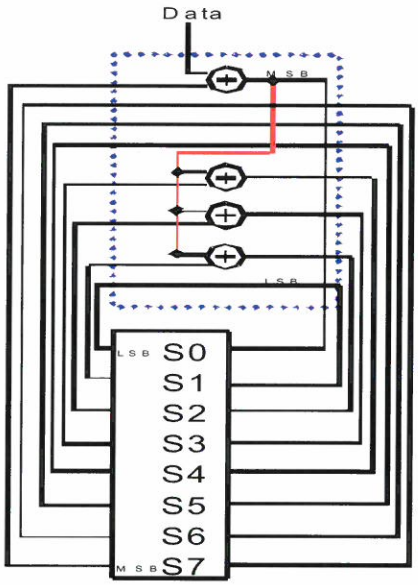

圖6. 單一輸入的8-bit並行CRC模組

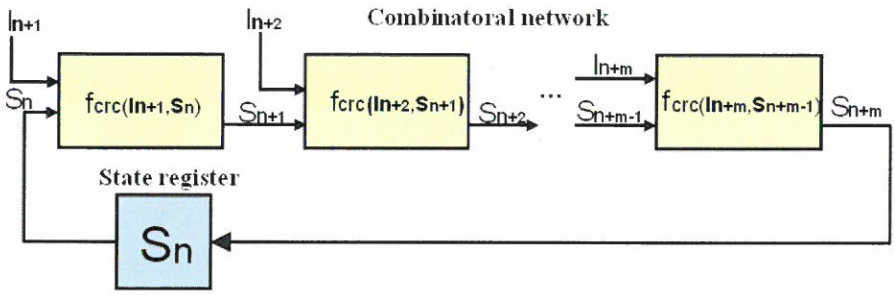

圖7. 文獻[3]所提出的m-bit並行回授網路

為了解決上述資料不為輸入端整數倍所產生錯誤CRC餘數值的問題，本文提出新的並行式CRC電路架構如圖8所示。我們採用文獻[3]之電路架構，並加以擴充至8-bit以增加電路的偵錯能力。所採用的產生多項式為$X^8 + X^4 + X^3 + X^2 + 1$，並在每個輸入端之間增加一組開關切換電路，再利用C0、C1及C2控制線控制其輸出。如圖9所示，我

們所設計開關切換電路每一路徑僅以1顆NMOS作為開關以取代傳輸閘，以達到最省電晶體數目的。雖然NMOS開關操作時會產生弱1信號，但由於我們所用的電壓為3.3伏特，弱信號大約為2.5~2.6伏特，此弱信號依然可以被暫存器正常取樣。並藉由控制線(Control)來控制開關的切換，當控制線輸入1時，輸入端In1~In8訊號經由Out1~Out8輸出；當控制線輸入0時，輸入端訊號經由Out_1~Out_8輸出。

我們在每個輸入端的節點加了我們設計的開關切換電路後，此電路功能將可以藉由開關切換以接受任意bit數的資料輸入。例如當輸入資料bit數為3之倍數時，可設定C0及C1為1，C2及C3為0。此時訊號將會從Switch 3的Out_1~Out_8輸出至暫存器。換句話說，我們藉由控制輸入端的並列數來對應到輸入資料的bit數，只要輸入資料的bit數能被輸入端的並列數整除，資料就能正常的輸入，進而產生正確的CRC值。整體開關控制功能整理至表2所列。而我們在最後一級輸入i3的邏輯閘輸出端又加了一組開關的目的，則是要避免當開關並列數切換至3以下時，最後一級的邏輯閘因CMOS電路浮接可能會產生不正確輸出，因此我們加了開關來隔離最後一級邏輯閘的輸出，確保暫存器能取樣到正確值。

表2. 開關控制訊號表

C0	C1	C2	C3	允許的資料輸入 bit數
1	1	1	1	4-bit 倍數輸入
1	1	0	0	3-bit 倍數輸入
1	0	1	0	2-bit 倍數輸入
0	1	1	0	1-bit 倍數輸入

表3. 本篇電路與過去文獻比較 (m:輸入端並列數)

	電路 bit 數	處理 N-bit 資料時間	電晶體數	能處理的資料bit數
傳統 LFSR架構	4-bit	*N* clock	64	任意 bit數
	8-bit	*N* clock	128	任意 bit數
	16-bit	*N* clock	226	任意 bit數
文獻 [3]	4-bit	*N*/*m* clock	148	m倍數
	8-bit	*N*/*m* clock	200	m倍數
	16-bit	*N*/*m* clock	304	m倍數
本文	4-bit	*N*/*m* clock	210	任意 bit數
	8-bit	*N*/*m* clock	262	任意 bit數
	16-bit	*N*/*m* clock	366	任意 bit數

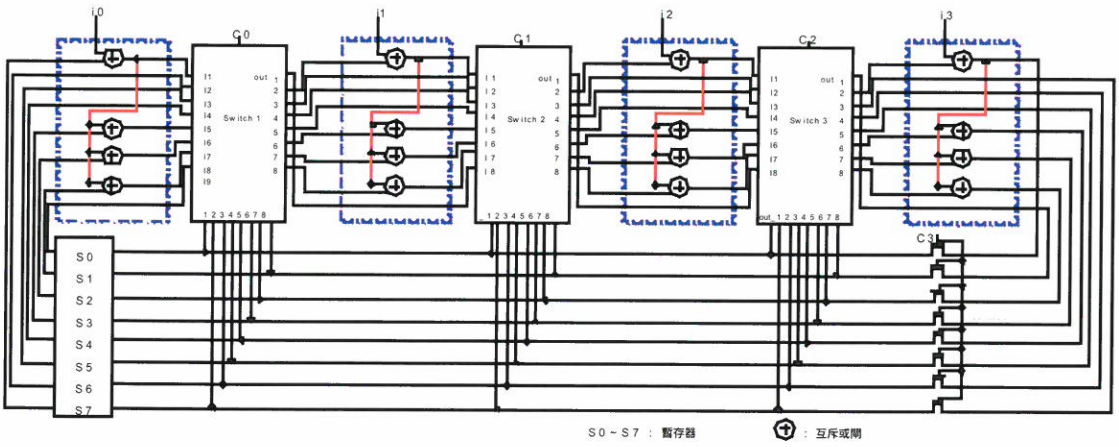

圖 9. NMOS開關切換電路

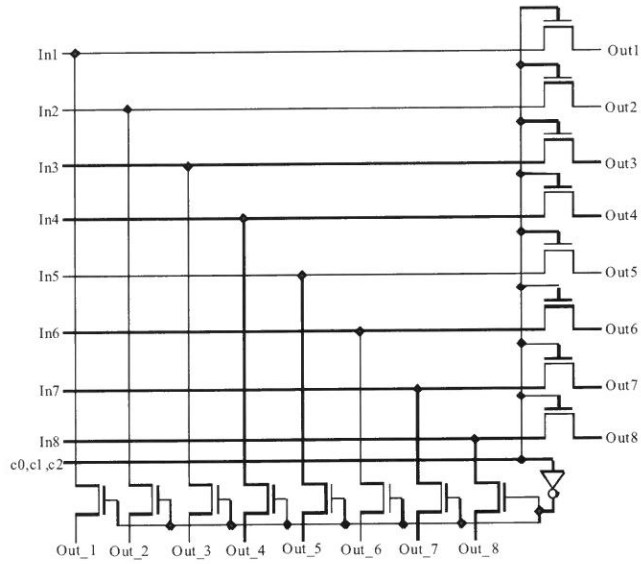

圖 8. 本文所提出之8-bit CRC電路

我們將文獻[3]及一般LFSR串列型電路與本篇電路做比較，電路均使用產生多項式為表1之常用多項式，整理如表3。顯示本電路處理資料速度比一般串列型快，並且我們改善了文獻[3]電路資料輸入只能以並列數倍數輸入的缺點。

4. 模擬及實體量測結果

本篇所使用的模擬參數為TSMC 0.35 μ m Mixed-Signal 2P4M Polycide 3.3/5V製程，使用模擬軟體為HSPICE，驗證軟體為Calibre。電晶體尺寸均為（W/L）$_{NMOS}$=1um/0.35um 與（W/L）$_{PMOS}$ = 2um / 0.35um，工作電壓為3.3V。輸入訊號為基本時脈CLK、i0(MSB)、i1、i2、i3(LSB)，控制訊號有C0、C1、C2、C3，輸出訊號為S0(LSB)~S7(MSB)。

圖10為電路後端模擬結果，輸入測試訊號為並列輸入100100100101的12-bit資料，C0~C1控制訊號皆設為邏輯1(3.3V)因此可以在第4個時脈(Clock)後由輸出端S7~S0得到11111000(虛線顯示部份)的CRC值。本篇所使用的D型暫存器為正緣觸發形式。

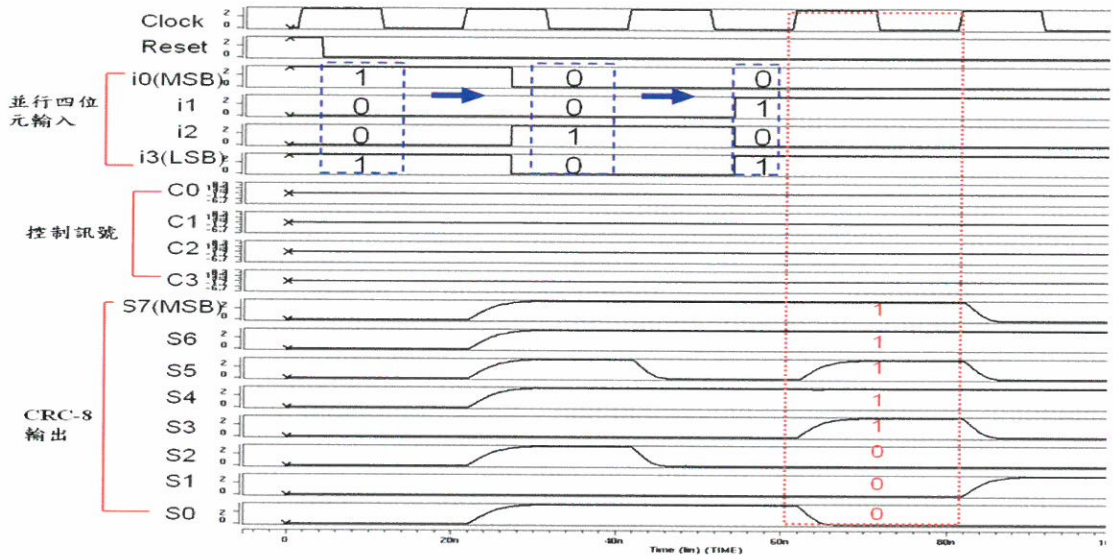

圖10. 電路後端模擬結果

本文所設計之實體IC已製作完成，所使用的量測機台為CIC所提供之Agilent 93000測試平台如圖11(左)所示。測試晶片被放置至48pin IC腳座，再由Agilent 93000機台下方測試板(圖11右)直接送信號至待測晶片。圖12為本文電路佈局圖及晶片實照圖，核心電路面積為229 ×124 μm^2。圖13為晶片實測結果，所使用的測試向量檔與圖10一樣，輸入亦為100100100101的12-bit資料，並將其分為3部份1001,0010,0101依序由3個Clock分別送入晶片之四個輸入接腳。每一個時脈結束時8個暫存器亦會產生一組餘數值，再經由回授(feedback)的方式，回授至電路的第一組CN再與其第二個Clock輸入資料作互斥或運算，直到第3個Clock結束後8個暫存器值S7~S0依序為11111000 (紅色虛線部份)即為晶片輸出之CRC值。將圖13與圖10後端模擬結果作比對為完全相同，證實本晶片功能實作無誤。圖14為Agilent 93000系統所量測晶片最大頻率，圈選部份顯示本晶片最大工作頻率達58 MHz，晶片規格整理至表4。

表4. 晶片規格表

核心電路面積	0.229 × 0 .124 mm^2
電晶體數	262 個
工作電壓	3.3 V
平均功率消耗	2.08 mW @3.3 V
最高工作頻率	58 MHz

圖11. Agilent 93000測試平台

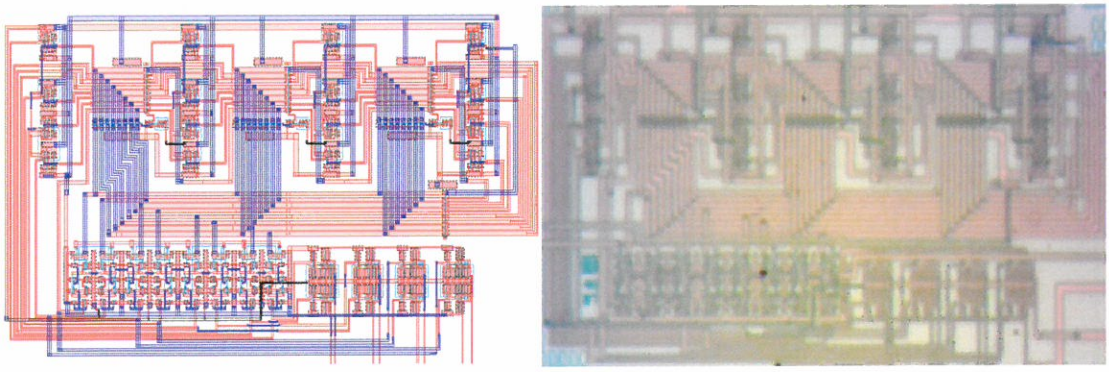

圖12. 晶片佈局圖(左)及實照圖(右)

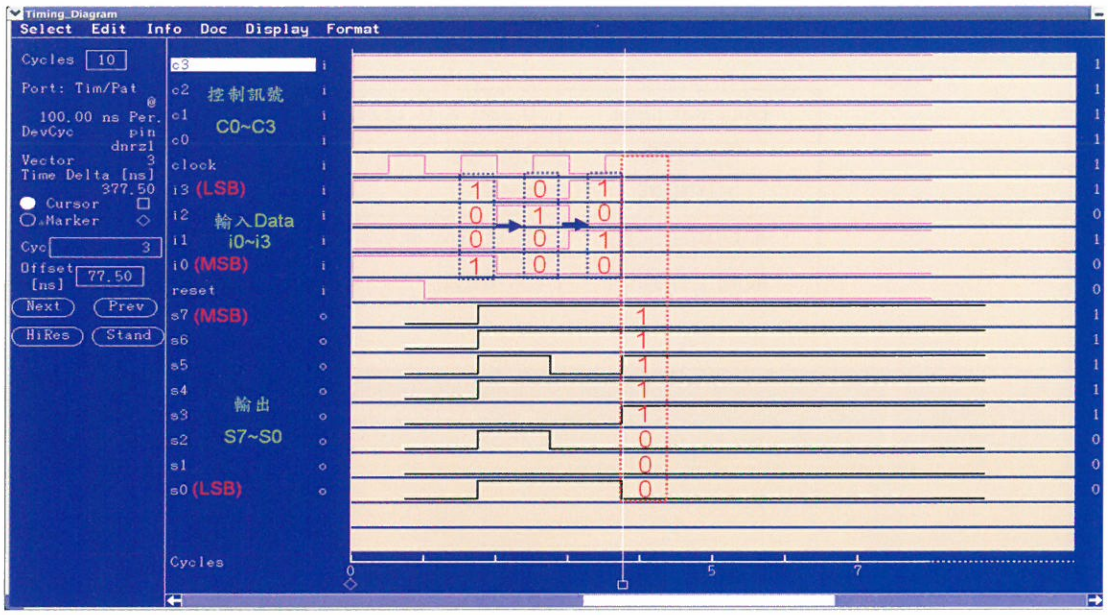

圖13. 晶片量測結果

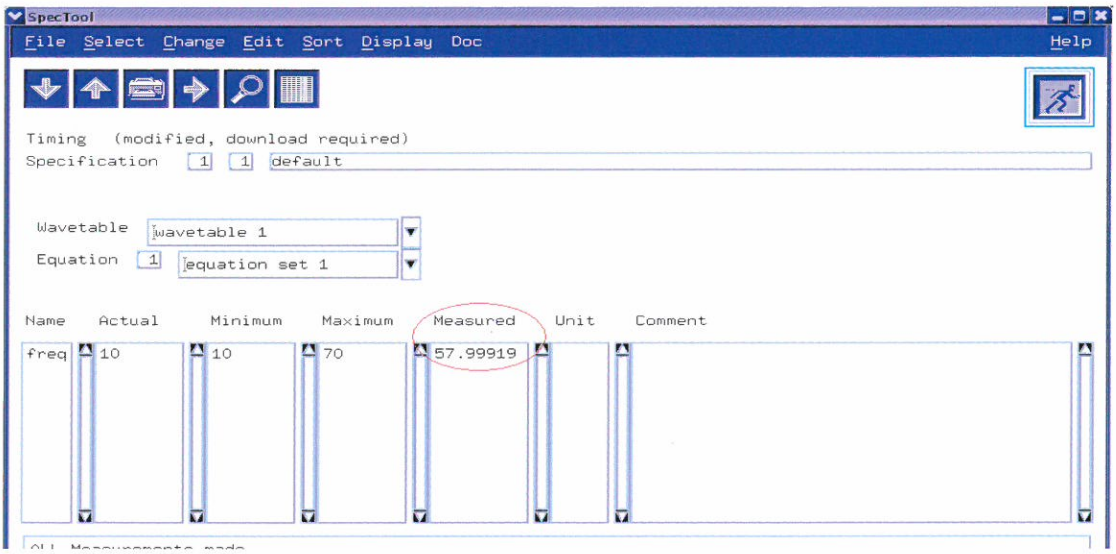

圖14. 晶片實測最大頻率

5. 結論

本文我們已經成功改良出並行結構的CRC電路，在處理資料的速度及效率優於一般使用串列結構的CRC電路。我們採用了文獻[3]之電路架構，經由我們設計一組開關切換電路後，已改善文獻[3]電路不能處理任意位元數資料的缺點。我們更進一步將電路設計至8-bit以提升電路的偵錯能力，最後將我們的設計經由CIC下線得到晶片。量測結果顯示本晶片可達預期之功能，此任意位元數處理之彈性架構有利於RFID後續之整合應用。

參考文獻

[1] 陳俊彥，“可規劃平行循環冗餘檢查電路和攪散器設計及其自動產生”，全國碩博士論文，2006，雲林。

[2] Klaus Finkenzeller 原著，吳曉峰、陳大才 譯， RFID手冊，2007，台北。

[3] Michael Sprachmann, “Automatic Generation of Parallel CRC Circuits,” IEEE Design&Test of computers , vol.18, pp 108-114 , no.3 , May-June. 2001.

[4] Giuseppe Campobello, Giuseppe Patane` , Marco Russo, “ Parallel CRC Realization,” IEEE Transactions on Computers, vol. 52, pp 1312-1319, no.10 , Oct 2003.

[5] Chao Cheng, Keshab K. Parhi, “ High-Speed Parallel CRC Implementation Based on Unfolding, Pipelining, and Retiming,” IEEE Transactions on Circuit and Systems-II, vol. 53, pp 1017-1021 , no. 10 , Oct 2006.

[6] T.-Bi-Pei and C. Zukowski, “ High-Speed Paralell CRC circuits in VLSI,” IEE Transactions on Communication, vol. 40,pp 653-657, April 1992.

[7] M. Braun, J, Freidich, T, Grun and J, Lembert “ Parallel CRC Computation in FPGAs,” The International Conference on Field Programmable Logic, Reconfigurable Computing, and Applications, Universitat des Saarlands , 1996.

[8] Toal Ciaran, Sezer Sakir. Xin Yang, McLaughlin Kieran, Burns Dwayne, Seceleanu Tiberiu, “ Programmable CRC circuit architecture,” IEEE International SOC Conference, pp 123-126 , Sept 2007.

Received October 30 ,2009
Accepted December 29 ,2009

A New Arbitrarily-Input CMOS CRC-8 Chip for RFID Application

Hung, Yu-cherng, Hung, han-jun and Shieh, shao-hui

Abstract

In this paper, the architecture of CRC circuit was improved, and the CMOS chip realization was achieved. With the circuit design, the operation frequency of CRC chip is getting faster and faster in recent years; moreover, circuit needs to deal with increased number of data bits. The structure of the conventional serial CRC circuit will unable to meet the rapid demand for processing large amounts of data. Therefore, based on the parallel structure proposed in previous literature, a new circuit design is proposed to enhance data processing speed. The circuit uses a set of switches to improve the shortcomings of original literature, which can not be dealt with any bit of input data. Based on CRC-8 algorithm, our design has processing capability of any bit of data. The experimental chip had fabricated by using TSMC CMOS 0.35-μm technology. The measured result of the experimental chip shows that the chip functions successfully and works at 58-MHz @ 3.3 V.

Key Words : RFID, Cyclic Redundancy Check Code, CRC

One Synthetic Compound, HDT-1, Inhibits Human Peripheral Blood Mononuclear Cells Proliferation

Shiu-Huey Chou[1], Shang-Shing P. Chou[2], Yih-Fong Liew[3], Jyh-Yih Leu[1], Su-Jane Wang[4], Rwei-Fen S. Huang[3], Woan-Fang Tzeng[1], Yuh-Chi Kuo[1,*]

[1]Department of Life Science, [2]Department of Chemistry, [3]Department of Nutritional Science, [4]School of Medicine, Fu-Jen University, Hsinchuang, Taiwan, ROC

Abstract

In the present study, peripheral blood mononuclear cells (PBMC) isolated from human peripheral blood were used as target cells. Effects of one newly synthetic compound 3, 4, 4a, 5, 8, 8a-hexahydro-6,7-dimethyl-4a-(phenylsulfonyl)-2-tosylisoquinolin-1(2*H*)-one (HDT-1), on PBMC proliferation and interferon-γ (IFN-γ) production were determined by the tritiated thymidine uptake and enzyme-linked immunosorbent assay (ELISA), respectively. The results indicated that HDT-1 inhibited PBMC proliferation activated with phytohemagglutinin (PHA; 5μg/ml) and its effect was compatible with positive control cyclosporine A. The 50% inhibition activity (IC_{50}) of HDT-1 on PBMC proliferation is 64.4±2.7 μM. The inhibitory action of HDT-1 did not involve direct cytotoxicity. The data from ELISA demonstrated that HDT-1 decreased IFN-γ production in PBMC induced by PHA with a dose-dependent manner. We suggest that HDT-1 may be an immunomodulatory agent.

keywords: Keywords:HDT-1, PBMC, Proliferation, IFN-γ

* Correspondent Author and Address:
Prof. Yuh-Chi KuoLS212, Laboratory of Molecular PharmacologyDepartment of Life Science, Fu-Jen UniversityN0. 510, Chung-Cheng Rd., Hsinchuang,Taipei Hsien 242, Taiwan, R.O.C.Telephone Number: 886-2-29053591Fax Number: 886-2-29052193E-mail: 021553@mail.fju.edu.tw

1. Introduction

Tissue inflammation is a harmful immune response that produces tissue injury and may cause serious diseases including asthma and rheumatoid arthritis [1]. There is now convincing evidence that cytokines secreted by T cells such as interferon-γ (IFN-γ) in response to antigen stimulation play a role in lung inflammation and asthma [2]. In patients with asthma or rheumatoid arthritis, the levels of T cells and cytokines have been shown to significantly elevate in bronchoalveolar lavage fluids and rheumatoid synovium, respectively, suggesting a possible pathological role for T cells and substances [3]. One of the therapeutic objectives in tissue inflammation is to reduce T cells proliferation and IFN-γ production [4].

The activation and clonal expansion of T cells play important roles in generation of immune responses [5]. Interaction of T cells with antigens initiates a cascade of biochemical events and gene expression that induces resting T cells to proliferate and differentiate [6]. It has been demonstrated in many previous studies with T cells that cytokines such as IFN-γ are pivotal in the growth of T lymphocytes induced by antigens [7]. Thus, regulation of T lymphocyte activation and proliferation and cytokine production has been shown to be one of actions of immunomodulatory agents [8].

Recently, a new piperidine compound 3, 4, 4a, 5, 8, 8a-hexahydro-6,7-dimethyl-4a-(phenylsulfonyl)-2-tosylisoquinolin-1 (2H)-one (HDT-1) has been synthesized by Prof. Chou [9]. It has been proved that HDT-1 can block glutamate release from rat neuron cells [10]. However, there has been relatively scarce definitive evidence to prove its pharmacological activities. Herein, we utilized HDT-1 to investigate its immunopharmacological activities. In order to investigate the immunomodulatory actions of HDT-1, PBMC, which contain T lymphocytes, were used as target cells [11]. To elucidate the effects of HDT-1 on PBMC proliferation, the tritiated thymidine uptake method was utilized to detect total cellular DNA synthesis in the cultures. In addition, we determined the effect of HDT-1 on IFN-γ production in PBMC by enzyme-linked immunosorbent assay (ELISA). We elucidated that HDT-1 affected cell proliferation and IFN-γ production in PBMC.

2. Materials and methods

2.1. Preparation of HDT-1

The HDT-1 compound was prepared and characterized according to the method published by Prof. Chou [9]. HDT-1 was obtained by heating a toluene solution of 4-(phenylsulfonyl)-1-tosylpyridin-2(1H)-one with 1-methoxy-3-(trimethylsilyloxy)-1,3-butadiene in a sealed tube at 140 °C for 24 hr. Its structure is shown in Fig. 1. HDT-1 was dissolved in dimethylsulfoxide (DMSO) to a concentration of 100 mM and then stored at 4 °C for use.

2.2. Human Subjects

Twenty-two healthy male subjects (26 to 36 yr, mean age 29 yr) were chosen for this investigation. The experimental protocol had been reviewed and approved by the institutional human experimentation committee. Written informed consent was obtained from each subject.

2.3. Preparation of PBMC

Heparinized human peripheral blood (35 ml) was obtained from healthy donors. PBMC was isolated by the Ficoll-Paque (specific gravity 1.077) gradient density method as described previously [12]. The 35 ml peripheral blood was centrifuged at 850 x g, 4 °C for 10 min to remove the plasma. Blood cells were diluted with phosphate-buffered saline (PBS; pH7.2) then centrifuged in a Ficoll-Paque discontinuous gradient at 420 x g for 30 min. The PBMC layer was collected and washed with cold distilled water and 10X Hanks' buffer saline solution (HBSS) to remove red blood cells. The cells were resuspended to a concentration of 2×10^6 cells/ml in RPMI-1640 medium supplemented with 2% fetal bovine serum (FBS), 100 U/ml penicillin, and 100 μg/ml streptomycin.

2.4. Lymphoproliferation test

The lymphoproliferation test was modified from previously described [13]. 100 μl of cell suspension (2×10^6 cells/ml) was applied into each well of a 96-well flat-bottomed plate (Nunc 167008, Nunclon, Raskilde, Denmark). Cyclosporine A (CsA; 2.5 μM; Sigma) was used as a positive control [14]. PHA (5 μg/ml) or varying concentrations of HDT-1 (6.25 to 100 μM) were added to the cells. The plates were incubated in 5 % CO_2-air humidified atmosphere at 37 °C for 3 days. Subsequently, tritiated thymidine (1 μCi/well, NEN) was

added into each well. After a 16 hr incubation, the cells were harvested on glass fiber filters by an automatic harvester (Dynatech, Multimash 2000, Billingshurst, U.K.). Radioactivity in the filters was measured by a scintillation counting. The inhibitory activity of HDT-1 on PBMC proliferation was calculated by the following formula:

$$\text{Inhibitory activity (\%)} = \frac{\text{Control Group}_{(CPM)} - \text{Experiment group}_{(CPM)}}{\text{Control group}_{(CPM)}} \times 100$$

2.5. *Determination of IFN-* γ *production*

PBMC (2×10^5 cells/well) were cultured with PHA (5 μg/ml) or varying concentrations of HDT-1 (6.25 to 100 μM) for 3 days. The cell supernatants were then collected and assayed for IFN-γ concentrations by ELISA (R&D systems, Minneapolis, USA).

2.6. *Determination of cell viability*

Approximately 2×10^5 PBMC were cultured with medium, vehicle (0.1% DMSO), or various concentration of HDT-1 (6.25 to 100 μM) for 3 days. Total, viable, and non-viable cell numbers were counted under the microscope with the help of a hemocytometer following staining by trypan blue. The percentage of viable cells was calculated:

$$\text{Viability (\%)} = \frac{\text{Viable Cell Number}}{\text{Total Cell Number}} \times 100$$

2.7. *Statistical analysis*

Data were presented as mean±SD, and the differences between groups were assessed with student's t test at a significant level of $p < 0.05$.

3. Results

3.1. Effects of HDT-1 on PBMC proliferation

To study the effects on PBMC proliferation, resting cells or cells activated with PHA were treated with various concentrations of HDT-1 (6.25 to 100 μM), after which cell proliferation was determined on the basis of uptake of tritiated thymidine. As shown in Fig 2, cyclosporine A blocked PBMC proliferation activated with PHA. Whereas HDT-1 had mild or little effects on resting PBMC proliferation, HDT-1 decreased the cells proliferation stimulated with PHA. The inhibitory effects of HDT-1 on PHA activated PBMC proliferation were concentration dependent. The 50% inhibitory concentration (IC_{50}) of HDT-1 was 64.4±2.7 μM. These results indicated that HDT-1 reduced PBMC proliferation induced by PHA and this effect was similar to cyclosporine A.

3.2. Viability of PBMC treated with HDT-1

To realize that the inhibitory mechanisms of HDT-1 on PBMC proliferation were not related to direct cytotoxicity, we determined the viability of PBMC in the presence of 6.25, 12.5, 25, 50, and 100 μM HDT-1 for 3 days. As shown in Fig. 3, the viability of PBMC was not significantly decreased after treatment with HDT-1 for 3 days. Comparison with the medium treated group, the viability of PBMC was not reduced by the vehicle group (0.1% DMSO). We suggest that HDT-1 impairments of PBMC proliferation were not through direct cytotoxicity.

3.3. Effects of HDT-1 on IFN- γ production in PBMC

To study whether HDT-1 affected IFN- γ production in PBMC, the cells were incubated with or without various concentration of HDT-1 (6.25 to 100 μM) for 3 days. Supernatants were then collected, and the IFN- γ productions were assayed by ELISA. . As shown in Fig. 4, comparison with resting cells, PHA significantly increased IFN- γ production in PBMC ($p < 0.001$). At 12.5 to 100 μM, the production of IFN- γ in activated PBMC were significantly suppressed by HDT-1 in a concentration-dependent manner ($p < 0.001$). At 100 μM, the stimulated production of IFN- γ in activated PBMCs were completely blocked by HDT-1, and IFN- γ concentrations were almost the same as those in resting cells. It indicated that HDT-1 reduced IFN- γ production in PBMC activated with PHA.

4. Discussion

In the present study, HDT-1, a new synthetic compound, was subjected to biological activity assay. The results indicated that HDT-1 suppressed proliferation in PBMC activated by PHA. The stimulated IFN-γ production in PHA activated PBMC was significantly decreased by HDT-1. This effect was not related to cytotoxicity. It suggests that HDT-1 inhibiting immune responses may be related to decreasing of cell proliferation and IFN-γ production in PBMC.

Many bioactive compounds have a piperidine structure [15]. For example, (S)-armepavine inhibits the proliferation of PBMC activated with PHA by regulation of IFN-γ production and improves tissue inflammation in mice [16,17]. Bortezomib is a proteasome inhibitor and used for treatment multiple myeloma [18]. This is the first immunomodulatory action on PBMC described for HDT-1. PBMC viability was not changed by DMSO. Therefore, the inhibitory function of HDT-1 was unlikely related to DMSO.

PHA is a mitogen for T lymphocytes. It binds to N-acetylgalactosamine glycoproteins expressed on the surface of T cells then activates the cells to proliferate [17]. In the present study, T cells were major proliferating cells in PBMC cultures activated with PHA. Thus, inhibitory effects of HDT-1 on PHA activated PBMC proliferation could be suggested as suppression on T cells proliferation. Many previous studies indicate a series of cytokines such as IFN-γ is included in a carefully controlled order as T cells pass through cell proliferation [5]. Although, the molecular mechanisms involved in regulating passage through cell proliferation in T cells stimulated with PHA remain largely unknown, the events that affect the T cells proliferation are ultimately likely to act by controlling the expression of IFN-γ [19].

From the present results, we have proved that HDT-1 inhibited PBMC proliferation and IFN-γ production. Thus, these results indicate that HDT-1 may also have acted to reduce tissue inflammation-in part by inhibiting PBMC proliferation and IFN-γ production. Although in vitro studies do not necessarily predict in vivo outcomes, such studies have provided insights into molecular targets, as illustrated by the effects of IFN-γ proteins. The relative contributions of these activities to the potent immunosuppressive by HDT-1 in vivo remain to

be elucidated. The action mechanisms of HDT-1 are subjected for further study.

Acknowledgements

This study was partially supported by grants-in aid from Fu-Jen University (9991A15/10963104995-4;9991A15/10973104995-4;9991A15/10983104995-4),The National Science Council (NSC96-2320-B-030-006-MY3), Committee on Chinese Medicine and Pharmacy (CCMP96-RD-207), and Council of Agriculture, Republic of China (97-1.2.1-a1-22).

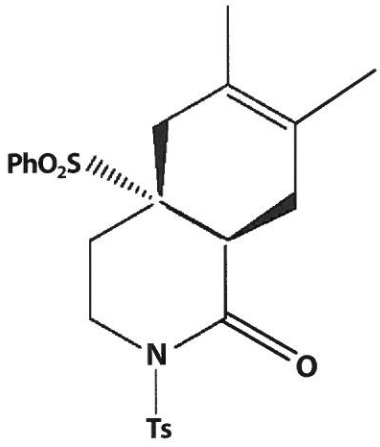

Fig. 1: The structure of HDT-1.

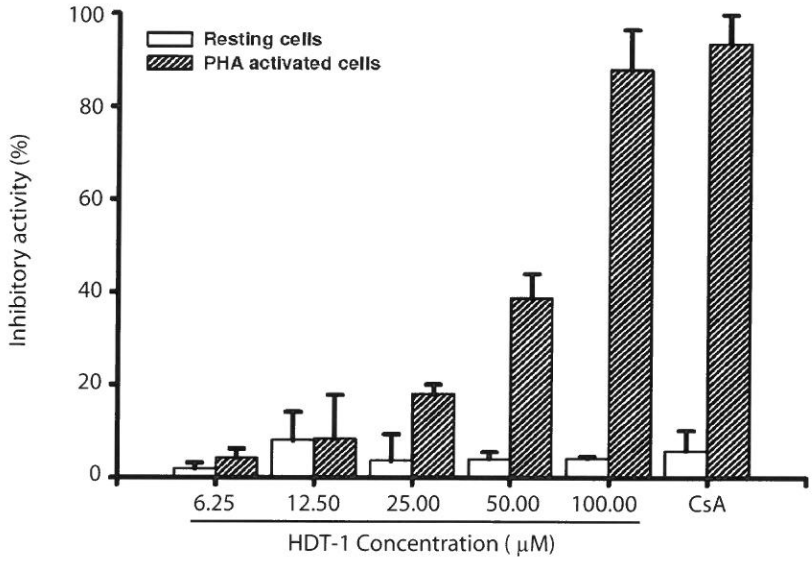

Fig. 2: HDT-1 suppressed PBMC proliferation in a concentration-dependent manner. PBMC (2×10^5/well) were treated with 6.25, 12.5, 25, 50, or 100 μM of HDT-1 with or without PHA (5 μg/ml) for 3 days. The CsA (2.5 μM) was used as a positive control. The Cell proliferation was detected on the basis of uptake of tritiated thymidine uptake. After a 16 hr incubation, the cells were harvested with an automatic harvester, after which radioactivity was measured with a scintillation counting. The inhibitory percentage was calculated with the formula described in Materials and Methods. Bars represent the mean±SD of three independent experiments.

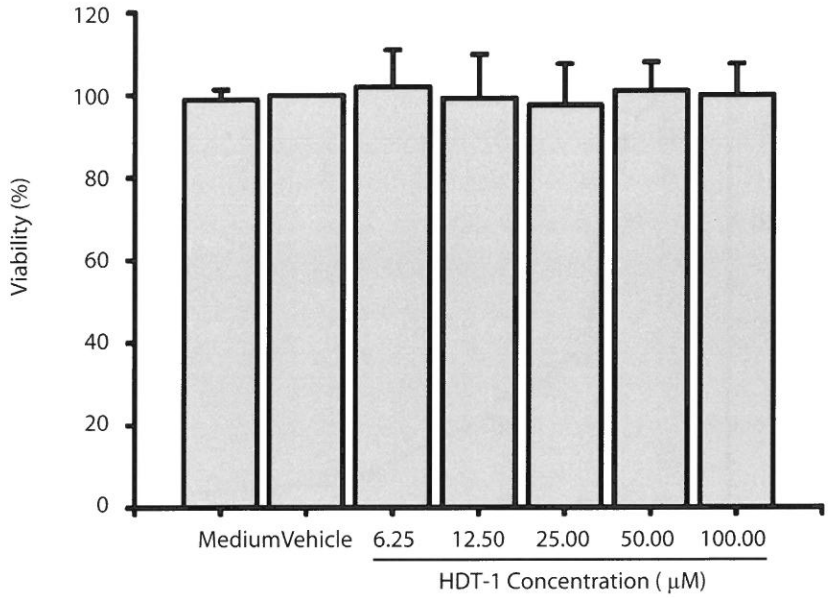

Fig. 3: Viability of PBMC treated with the HDT-1.

PBMC (2×10^5) were treated with medium, vehicle (0.1% DMSO), or the indicated concentration of HDT-1 for 3 days. Numbers of total, viable, and nonviable cells were counted after trypan blue staining. Bars represent the mean±SD of three independent experiments.

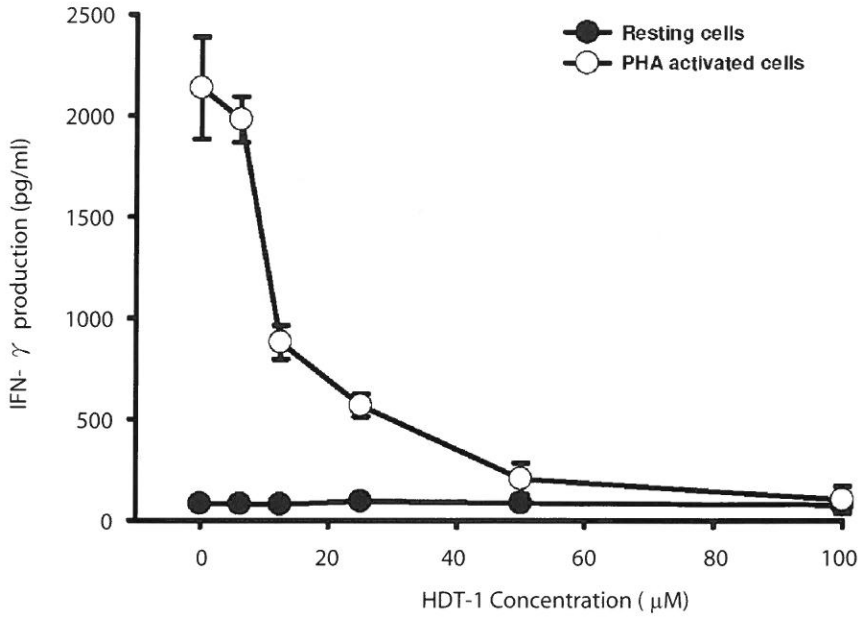

Fig. 4: Impairments of IFN- γ production in PBMC treated with HDT-1.
Resting or PHA (5 μg/ml) activated PBMC (2×10^5 / well) were in the presence or absence of 6.25, 12.5, 25, 50, and 100 μM HDT-1 for 3 days. Next, cell supernatants were collected and IFN- γ concentrations were determined with an ELISA. Each point is the mean±SD of three independent experiments.

References

[1] HanadaT and Yoshimura A. Regulation of cytokine signaling and inflammation. Cytokine Growth Factor Rev. 13:413-421 (2002).

[2] GoodmanRB, Sterieter RM, Martin DP, Steinberg KP, Milberg JA, Maunder RJ, Kunkel SL, Walz A, Hudson LD, and Martin TR. Inflammatory cytokines in patients with persistence of the acute respiratory distress syndrome. Am. J. Respir. Crit. Care. Med. 154:602-611 (1996).

[3] Szabo SJ, Sullivan BM, Peng SL, and Glimcher LH. Molecular mechanisms regulating TH1 immune responses. Annu. Rev. Immunol. 21:713-758 (2003).

[4] Arai K, Lee F, and Miyajima A. Cytokines: Coordinators of immune and inflammatory response. Annu. Rev. Biochem. 59:783-836 (1990).

[5] Janeway CA, Jr and Travers P, editors. Immunobiology: The immune system in health and disease. Oxford: Blackwell Scientific Publications p. 7:1-7:49 (1994).

[6] Ferreia V, Sidenius N, Tarantino N, Hubert P, Chatenoud L, Blasi F, and Körner M. In vivo inhibition of NF-κB in T-lineage cells leads to a dramatic decrease in cell proliferation and cytokine production and to increased cell apoptosis in response to mitogen stimuli, but not to abnormal thymopoiesis. J. Immunol. 162:6442-6450 (1999).

[7] Young HA. Regulation of interferon-gamma gene expression. J. Interf. Cytok. Res. 16:563-568 (1996).

[8] ChenYC, Tsai WJ, Wu MH, Lin LC, and Kuo YC. Suberosin inhibits human peripheral blood mononuclear cells proliferation through the modulation of NF-AT and NF-κB transcription factors. Brit J. Pharmacol. 150:298-312 (2007).

[9] Chou SSP and Chen PW. Cycloaddition reactions of 4-sulfur-substituted dihydro-2-pyridones and 2-pyridones with conjugated dienes. Tetrahedron 64:1879-1887 (2008).

[10] Wang SJ, Chou SH, Kuo YC, Chou SS P, Tzeng WF, Leu CY, Huang RF S, and Liew YF. HDT-1, a new synthetic compound, inhibits glutamate release in rat cerebral cortex nerve terminals (synaptosomes). Acta Pharmacologica Sinica 29:1289-1295 (2008).

[11] Charles AJ, Jr., Paul T, Hunt S, and Walport M, editors. Immunobiology. New York: Current Biology Ltd (1997).

[12] Wu MH, Tsai WJ, Don MJ, Chen YC, and Kuo YC. Tanshinlactone A from *Salvia miltiorrhiza* modulates interleukin-2 and interferon-γ gene expression. J. Ethnopharmacol. 113:210-217 (2007).

[13] Kuo YC, Yang NS, Chou CJ, Lin LC, and Tsai WJ. Regulation of cell proliferation, gene expression, production of cytokines, and cell cycle progression in primary human T lymphocytes by piperlactam S isolated from *Piper kadsura*. Mol. Pharamcol. 58:1057-1066 (2000).

[14] ChenYC, Chang SC, Wu MH, Chuang KA, Wu JY, Tsai WJ, and Kuo YC. Norcantharidin reduced cyclins and cytokines production in human peripheral blood mononuclear cells. Life Sci. 84:218-226 (2009).

[15] Numata A, Ibuka I. (1987) Alkaloids from ants and other insects. In The Alkaloids, Brossi A., editor. New York: Academic Press. p. 193-203.

[16] Liu CP, Kuo YC, Lin YL, Liao JF , Shen CC, Chen CF, and Tsai WJ. (S)-Armepavine inhibits human peripheral blood mononuclear cells activation by regulating Itk and PLC γ activation in a PI3K-dependent manner. J. Leukocyte. Biol. 81:1276-1286 (2007).

[17] Liu CP, Tsai WJ, Lin YL, Liao JF , Shen CC, Chen CF, and Kuo YC. Inhibitory effects of (S)-armepavine from *Nelumbo nucifera* on autoimmune disease of MRL *lpr/lpr* mice. Eur. J. Pharmacol. 531:270-279 (2006).

[18] San Miguel JF, Schlag R, Khuageva NK, Dimopoulos MA, Shpilberg O, Kropff M, Spicka I, Petrucci MT, Palumbo A, Samoilova OS, Dmoszynska A, Abdulkadyrov KM, Schots R, Jiang B, Mateos MV, Anderson KC, Esseltine DL, Liu K, Cakana A, van de Velde H, Richardson PG, and VISTA Trial Investigators. Bortezomib plus melphalan and prednisone for initial treatment of multiple myeloma. N. Engl. J. Med. 359:906-917 (2008).

[19] Ajchenbaum F, Ando K, DeCaprio JA, and Griffin JD. Independent regulation of human D-type cyclin gene expression during G_1 phase in primary human T lymphocytes. J. Biol. Chem. 268:4113-4119 (1993).

Received October 31 ,2009
Accepted December 30 ,2009

合成化合物HDT-1仰制人類周邊血單核細胞增生

周秀慧[1]周善行[2]劉奕方[3]呂誌翼[1]王素珍[4]
許瑞芬[3]曾婉芳[1]郭育綺[1]

[1]生命科學系 [2]化學系 [3]營養科學系 [4]醫學系
中華民國 台灣 新莊市 輔仁大學

摘 要

在此研究中，以取自人類周邊血之周邊血單核細胞做為標的細胞，利用氚胸嘧啶吸收法檢測新的合成化合物 3, 4, 4a, 5, 8, 8a-hexahydro-6,7-dimethyl-4a-(phenylsulfonyl)-2-tosylisoquinolin-1 (2H)-one(HDT-1)對於細胞增生的影響，以酵素連結免疫吸附法分析HDT-1對於丙種干擾素產生之影響。實驗結果顯示，於植物血球凝集素刺激下，HDT-1可抑制周邊血單核細胞之增生，其結果與正對照組 Cyclosporine A相當，HDT-1抑制 50% 細胞增生之濃度為 64.4 ±2.7 μM，而此抑制活性與直接細胞毒殺作用無關。藉由酵素連結免疫吸附法分析數據顯示，HDT-1可效降低周邊血單核細胞中，由植物血球凝集素所引起之丙種干擾素產生。依據此些研究結果，我們認為HDT-1可能是一種免疫調控劑。

關鍵字：HDT-1、周邊血單核細胞、增生、丙種干擾素

從三角面多邊形到非凸三角面多面體之摺黏

呂克明
亞洲大學資訊工程學系教授

陳啟豐　張文蒼
亞洲大學資訊工程學系研究生

摘　要

拿破崙紙積木基本型，有領結、眼淚、翅膀、巧克力條、船型、星型、山形袖章與鯉魚等8型以及衍生型46型，總共54型。結合24個拿破崙紙積木基本型，又有拿破崙紙燈籠與虧格數研究的發表。我們不禁要問，是否還有其他基本型的存在？衍生型是否相等於基本型？就凸面多面體存在性與獨特性問題的解答，柯西與亞歷山大洛夫，曾經發表理論。今天擴展這些理論，我們藉動態規劃的技巧，證明非凸面16三角面多面體，存在13型，而衍生型相等於這些基本型。

在藉助演算法求解非凸面16三角面多面體基本型存在性與獨特性之前，我們將介紹凸面多面體相關定理以及非凸三角多面體擴展面臨問題的討論，然後藉動態規劃的演算法解答一個實例：三角紙積木建構13個非凸16三角面多面體。我們未來的工作，將是非凸32三角面多面體的拿破崙紙積木的基本型存在性與獨特性的研究。

關鍵詞：摺黏、三角面多邊形、非凸三角面多面體、凸面多面體、展開、柯西堅硬定理、亞歷山大洛夫獨特定理、動態規劃、同胚、黏接樹

Corresponding author : Tel : (04)2332-3456　Fax : (04)2330-5737
E-mail address : KLU@asia.edu.tw

1.前　言

在過去十年，學術界開啟一系列跨兩千年幾何研究的熱潮。主題從古希臘凸面多面體到今天尖端幾何的研究。這些議題看似基礎，但其知識卻可以在教室內於寬廣的教育層次中，獲得豐盛的成果。

拿破崙紙積木基本型，有領結、眼淚、翅膀、巧克力條、船型、星型、山形袖章與鯉魚等8型以及衍生型46型總共54型。(Lu，2006) 結合24個拿破崙紙積木基本型，又有拿破崙紙燈籠與虧格數研究的發表。(Lu，2007) 我們不禁要問，是否還有其他基本型的存在？衍生型是否根本就是基本型的翻版？或者應該僅算基本型？就這些問題的解答，柯西與亞歷山大洛夫，曾經發表凸面多面體存在性與獨特性的理論。今天，我們將他們的理論擴展到屬於非凸16面三角面多面體。我們將使用動態規劃的方法，證明非凸16面三角面多面體的基本型存在13型，而這些獨特的基本型建構其他的衍生型。

在藉助演算法求解非凸16面三角面多面體基本型存在性與獨特性之前，我們將介紹凸面多面體相關定理以及非凸三角面多面體擴展面臨問題的討論，然後藉動態規劃的演算法解答一個實例：三角紙積木建構13個非凸16面三角面多面體。

1.1名詞解釋

我們研究的主題，簡單地說：什麼樣的多邊形，可以摺黏成凸面體(polytope)？在未進入討論之前，我們先解釋五個名詞。

首先，三角面多邊形(polyiamond) P，是一個多個等邊三角形所構成的等邊多邊形。它是一個使用剪刀切割下來的紙片。

其次，三角面多面體(deltahedra) D，是類似於2維三角面多邊形的3D多面體。它是佔有空間的立體，外表是多個三角面所構成的多邊形。我們所關注的是D的表面而不是其固體。

其三，凸面三角面多面體(convex deltahedra)的表面沒有凹陷。凸面三角面多面體，總共有4、6、8、10、12、14、16與20面等八個凸面三角面多面體。(Freudenthal,1947)請注意：內含偶數個等邊三角形的三角面多邊形才能建構成三角面多

面體。這點我們可以做以下的證明，假設n個等邊三角形，於是有面數 F=n，以及3n個邊，每個邊均被兩個面共用，所以三角面多面體的邊數E=3n/2，根據歐拉龐加萊的公式：V+F-E=2-2g，將面數F=n與邊數E=3n/2代入化簡可得V=(3n/2)-n+2-2g=(n/2)+2-2g，因為角頂數V、面數n與虧格數g必須是大於0或等於0的整數，n/2是整數，故n是偶數。因此，這八個凸面三角面多面體均是偶數個等邊三角形。三角面多面體有無窮多個(Trigg,1978)，除了這八個凸面三角面多面體之外，均是非凸面三角面多面體。(Whiteley,1994)本文所關注的是非凸面三角面多面體。

其四，三角面多邊形P建構成非凸面三角面多面體D的摺黏。摺黏，是摺三角面多邊形P的邊痕，然後精確地黏貼建構成三角面多面體D。這個動作不容許紙片的重疊與留下任何空隙。從另外一個角度來說，假若一個三角面多面體D能夠切開然後平面展開成一個三角面多邊形P，就稱這個三角面多邊形P，可以摺黏成三角面多面體D。

其五，當找出合法黏接路徑，我們可以依序畫出黏接樹（Gluing Tree）。畫黏接樹的目的有兩個：其一是做出三角面多面體的實體黏接，其二是算出秩數（valence或degree），就是交會在角頂的邊的個數。我們藉用秩數與角頂數，來查核動態規劃整個過程的正確性。

1.2三角面多邊形

三角面多邊形，英文稱polyiamond，又稱謂polyamond或簡單為iamond，它是由正三角形基本形狀結合而成的全面多邊形polyform。英文字polyiamond源自鑽石diamond，因為diamond通常被用來描述兩個正三角形底邊相連接的形狀，「 di-」是希臘字首代表「二」的意思。三個、四個、五個或六個正三角形連結成的多邊形分別稱謂Triamond、Tetriamond、Pentiamond與Hexiamond。三個、四個、五個或六個正三角形，分別有1、3、4與12個不同的樣式。隨著正三角形數量的增加，其樣式的數量也隨之增加。其數列為A000577。(Sloane and Plouffe,1995)三角面多邊形有凸面形與非凸面形之分。隨後，我們分別有非凸面形與凸面形摺黏成三角面多面體D，使用動態規劃的演算法不遺漏地搜尋所有三角面多面體。

2.數學定義與公式

提到主題：什麼樣的多邊形，可以摺黏成凸面多面體？我們會面臨凸面多面體存在性與唯一性的問題。在這兩個議題上，我們會提到法國數學家柯西（Augustin

Louis Cauchy,1789-1857）與俄國數學家亞歷山大洛夫（Aleksandr Danilovich Aleksandrov，1912-1999）。

2.1柯西堅硬定理(Cauchy's rigidity theorem)

1813年，柯西證明一個基本的定理：假若兩個凸面多面體有組合的相同結構，以及對應的面是全等的，則凸面多面體是全等的。(Whiteley, 1994)柯西定理要求摺黏線。定理的證明，請參考 MIT 任教的Erik Demaine 教授網站。

2.2 亞歷山大洛夫獨特定理 (Alexandrov's uniqueness theorem)

1950年，亞歷山大洛夫則將要求摺黏線的條件除去，延伸柯西定理。亞歷山大洛夫獨特定理：一個在球面上非負曲面「多面體的刻度(polyhedral metric)」可以建構一個經過移動，也僅有一個多面體。「多面體的刻度」指定多面體一個點的圓碟，以此圓碟為底的圓錐，它的角頂環繞的「完全角（complete angle）」小於2π。(Pogorelov, 1952)「完全角」是凸面多面體角頂所有入射角和。定理的證明，請同樣地參考 Erik Demaine 教授網站。

一個方法解釋這個定理成為一種形式是經過亞歷山大洛夫，匹配邊對或符合以下三個條件的多邊形集合的概念：

1. 每一個邊匹配多邊形的邊長。
2. 對於每個角頂的入射角和不多於2π。
3. 摺黏後的複合體與球面同胚。

條件一：多邊形的一個邊e_i與另外一個邊e_j的邊長相等，因而產生「匹配邊對（edge matching）」，我們使用$e_i \equiv e_j$或(e_i,e_j) 來代表。條件二：每個角頂的入射角和不多於2π是亞歷山大洛夫的創新，他與柯西堅硬定理小於2π的嚴格要求不同。條件三：撇開柯西堅硬定理當中，兩個凸多面體相等狹隘的觀念，亞歷山大洛夫提出凸多面體與球面同胚。在拓樸學中，同胚(homeomorphic)是兩個拓樸空間之間的雙連續函數。同胚是拓樸空間範疇中的同構；也就是說，它們是保持給定空間的所有拓樸性質的映射。如果兩個空間之間存在同胚，那麼這兩個空間就稱為同胚的，從拓樸學的觀點來看，兩個空間是相同的。

我們將在第3節提出動態規劃公式，並討論演算法的複雜度。第4節舉出三角紙積

木實例，推導出13個模型，第5節將使用亞歷山大洛夫的第二條，舉出三角紙積木的4個型，雖然屬於非凸三角面多面體的情況下，仍然合乎亞歷山大洛夫獨特定理。

3. 動態規劃公式

Lubiw與O'Rourke建議將亞歷山大洛夫的三個條件為基礎，藉用動態規劃的遞迴關係(recurrence relation)與列表式運算(tabular computation)的技巧，不遺漏地搜尋凸多面體(polytope)的摺黏。(Lubiw & O'Rourke, 1996; O'Rourke, 2007)同樣地，我們將亞歷山大洛夫的三個條件中的第一條與第三條為基礎，藉用動態規劃的遞迴關係與列表式運算的技巧，不遺漏地搜尋非凸三角面多面體的摺黏。

當我們寫下$v_i \equiv v_j$的意思，是兩個角頂v_i與v_j相同的。有一個和$v_i \equiv v_j$相關的關鍵值是 路徑(i,j)值。路徑(i, j) 值的非正式定義：首先，路徑(i, j)=∞是代表P〔i, j〕之間連結的線段鏈中，至少有一個非合法的摺黏，我們以∞表示不存在的摺黏；其次，假若在P〔i, j〕之間連結的線段鏈當中，沒有一個不合法的摺黏，則路徑(i, j)是$v_i=v_j$線段鏈當中所有合法路徑的集合。我們將應用動態規劃的遞迴關係計算路徑(i, j) 表格。路徑(i, j)正式的定義如下：

A.D1：｜i-j ｜是奇數，必會留下一個邊線，找不到邊匹配，故路徑(i,j)= ∞。

B.D2： i＝j，則路徑(i, j)代表所有路徑的集合。

C.D3：｜i-j ｜大於或等於2的偶數，同時k是從i開始$i < k \leq j-1$可能的配對，即k是從i+1直到j-1之間的奇數或偶數，要看i是偶數或奇數。路徑(i, j)是$v_i=v_j$線段鏈當中，所有k當中邊線與邊線的匹配$e_i \equiv e_k$所能建構成的路徑。假若邊線長度不等，即$l_i \neq l_j$，代表兩個邊線不匹配，則路徑(i, j)= ∞。否則的話，這個匹配創造出兩個次問題，請參照圖一。

1.$v_i+1 = v_k$。假若i+1=k，這個次問題如圖一內的1的部分是空集合，代表產生一個轉折點。合法路徑為(e_i,e_i+1) (i+1,j)，次路徑(i+1,j)則從前面的表格產生。假若$i+1 \neq k$，合法路徑將由第二個次問題來決定。

2.$v_k+1=v_j$。假若k+1=j，則(e_i,e_k)(i+1,k)。否則的話，假若$k < j$，(i,k)(k+1,j)，k=i+1,i+3,...j-3。次路徑(i,k)與次路徑(k+1,j)，則從前面的表格產生。

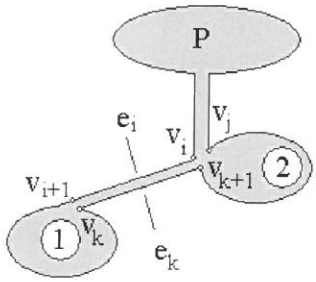

圖一：對所有可能的黏貼$e_i \equiv e_k$，匹配邊對 $\{ v_i, v_k \}$ 創造出兩個次問題。

藉助動態規劃，對於任何i與 j，非常明顯地，我們可以求出合法的路徑(i,j)值。令 $| i-j | =d$，我們可以按d=0,2,4,6,8,10,...,n-2的順序，將路徑 (i, j)的值求出來。接著，我們就可以藉助路徑 (i, j)值的表格，算出所有可能的合法路徑(0,0)的集合。經過重複模型剔除與同形模型的辨識，找出一組路徑的集合。每個路徑經過黏接樹的角頂數目與秩數的查核，最終完成3D作圖。

3.1 演算法的複雜度

我們要知道整個演算法的複雜度（complexity）需要算出所有可能的合法路徑(0,0)的集合。假設：n邊三角面多邊形P，角頂的集合V ＝ $\{ v_0, v_1, ...v_{n-1} \}$ 從v_0開始，逆時鐘方向排列至v_{n-1}止。從角頂v_i，到角頂v_{i+1}所連接的邊e_i，所有邊的集合E= $\{ e_0, e_1, ...e_{n-1} \}$ 。角頂v_i與角頂v_j之間的間距，$| i-j | =d$，d=0,2,4,6,8,10, ...,n-2。同時，k值由小而大搜尋合法路徑（i,j），k=i+1, i+3, ..., j-3,j-1。合法路徑 (i, j)的值，可以從D3的公式求出來：

k=i+1, 路徑 (i, i+2) (i+2, j)
k=i+3, 路徑 (i, i+4) (i+4, j)
...
k= j-3, 路徑 (i, j-2) (j-2, j)
k= j-1, 路徑 (e_i,e_k) (i+1, k)

最後，n邊三角面多邊形，合法路徑(0,0)的集合，可以將i=0與j=0代入以上的公式得到：

k= 1, 路徑 (0, 2) (2, 0)
k= 3, 路徑 (0, 4) (4, 0)
...
k= n-3, 路徑 (0,n-2) (n-2,0)

k= n-1, 路徑 (e_0,e_{n-1}) (1, n-1)

整個演算法的複雜度是以上計算的總合。為了計算複雜度，現在我們先定義m是匹配對數，F(m) 是｜i-j｜ = d=2m的計算次數。因為k= 1，路徑(0, 2) 的d=2，其計算次數可以寫成F(1) ，同樣地路徑(2, 0)的d=n-2，其計算次數可以寫成F(m-1) 。然後，k= 3，路徑(0, 4) 的d=4，其計算次數可以寫成F(2)，同樣地路徑(4, 0)的d=n-4，其計算次數可以寫成F(m-2) 。我們可以連續下去到k= n-3，路徑(0,n-2)的d=n-2，其計算次數可以寫成F(m-1) ，同樣地路徑(n-2,0)的d= 2，其計算次數可以寫成F(1) 。最後，路徑 (e_0,e_{n-1})的計算僅有一次，而(1, n-1)的d=n-2計算次數可以寫成F(m-1) 。所以以上的式子的計算次數可以寫成：

k= 1, 計算次數 F(1) xF(m-1)
k= 3, 計算次數 F(2) xF(m-2)
...
k= n-3, 計算次數F(m-1)x F(1)
k= n-1, 計算次數1xF(m-1)

接著我們要從計算F(m) 。初值化的結果，路徑(0, 2) 僅有一個算法，而且｜i-j｜= d=2 的計算次數F(1)=1。然後將F(1)=1代入公式D3則｜i-j｜= d=4 的計算次數F(2)=2。當m=3，k= 1, 3, 5。（0, 4）的計算次數F（3）為
k= 1, 路徑 (0, 2) (2, 0)，計算次數 F(1) xF(2)
k= 3, 路徑 (0, 4) (4, 0)，計算次數 F(2) xF(1)
k= 5, 路徑(e_0,e_5) (1, 5)計算次數1xF(2)

然後將F(1)=1與F(2)=2代入F(3)= F(1) xF(2)＋F(2) xF(1)＋1xF(2)＝1x2 + 2x1 + 1x2=6。然後， F(4)= F(1) xF(3)＋F(2) xF(2)＋F(3) xF(1)+1xF(3)＝1x6 + 2x2 + 6x1 + 1x6 = 2x2 +3x6 = 22。同樣地，F(5)= F(1) xF(4)＋F(2) xF(3)＋F(3) xF(2)+ F(4)x F(1) +1xF(4) ＝1x22 + 2x6 + 6x2 + 22x1+1x22 =(2x6 + 6x2)+ 3x22 =90。我們可以將計算次數的遞歸公式的一般式，表示如下：

$$F(m) = \Sigma F(i)F(m-i) + F(m-1)，i=1,2,...,m-1或$$
$$F(m) = \Sigma F(i)F(m-i) + 3F(m-1)，i=2,...,m-2$$

由上述計算演算次數的公式中，因為有乘積的關係，每個合法路徑（i,j）的複雜度為$O(m^2)$或$O(n^2)$。但是，需要將合法路徑（i,j）填入m列的表格，因此，整個演算法的複雜度為$O(m^3)$或$O(n^3)$ 。

4.三角紙積木實例

三角紙積木為16個三角面建成的多邊形(如圖二)摺黏成的16面三角面多面體。多數個16面三角面多面體，可以結合成橢圓球體。(Lu & Tsaur, 2008)。16三角面多邊形有12個角頂，即n=12。角頂集合V＝｛$v_0,v_1,...v_{11}$｝的順序是逆時鐘方向增加，它們的內角，如表一。16面三角面多邊形的角頂之間有摺痕連接。它有12個邊的集合E=｛$e_0,e_1,...e_{11}$｝。

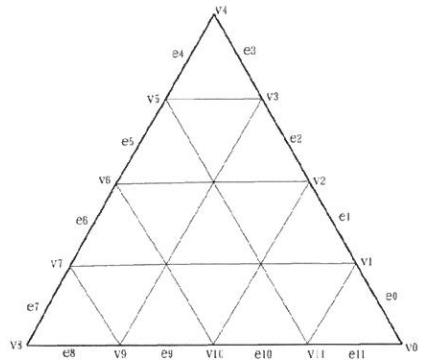

圖二：三角紙積木為16三角面多邊形

表一 16面三角多邊形的12個內角

i	0	1	2	3	4	5	6	7	8	9	10	11
內角	60	180	180	180	60	180	180	180	60	180	180	180

因為16面三角面多邊形的邊線均等，令邊長l_i=1。我們藉用前一節動態規劃的方法，設定對邊匹配的原則：

設定角頂v_i與角頂v_j之間的間距，｜i-j｜= d，d=2,4,6,...n-2。按k值由小而大搜尋合法路徑（i,j），k=i+1,i+3,...j-3, j-1。

｜i-j｜= d，角頂v_i與角頂v_j之間的合法路徑（i,j）為所有不同k值計算，合法路徑的組合，其公式如下：

假若k＜j，(i,k+1)(k+1,j)，k=i+1,i+3,...j-3；假若k=j-1，(e_i,e_k) (i+1,k)。

4.1 間距為2的合法路徑

首先，我們設定角頂v_i與角頂v_j之間的間距，｜i-j｜=d=2。因為(3,5)、(7,9)與(11,1)無合法路徑，路徑(e_3,e_4)、路徑(e_7,e_8)與路徑(e_{11},e_0) =∞。請參閱表二｜i-j｜= 2 ，合法路徑。

表二 ｜i-j｜= 2 ，合法路徑

(0,2)	(4,6)	(8,10)
(e_0,e_1)	(e_4,e_5)	(e_8,e_9)
(1,3)	(5,7)	(9,11)
(e_1,e_2)	(e_5,e_6)	(e_9,e_{10})
(2,4)	(6,8)	(10,0)
(e_2,e_3)	(e_6,e_7)	(e_{10},e_{11})
(3,5)	(7,9)	(11,1)
$(e_3,e_4)=\infty$	$(e_7,e_8)=\infty$	$(e_{11},e_0)=\infty$

4.2 間距為4的合法路徑

設定角頂v_i與角頂v_j之間的間距，｜i-j｜= d=4，12個間距為4的合法路徑分別在4.2.1至4.2.12節中求解。

4.2.1 求解(0,4)的合法路徑：

當k=1，$(0,2)(2,4)=(e_0,e_1)(e_2,e_3)$。當k=3，$(e_0,e_3)(1,3)=(e_0,e_3)(e_1,e_2)$。

4.2.2 求解(1,5)的合法路徑：

當k=2，$(1,3)(3,5)=(e_1,e_2)\infty=\infty$。當k=4，$(e_1,e_4)(2,4)=(e_1,e_4)(e_2,e_3)$。

4.2.3 求解(2,6)的合法路徑：

當k=3，$(2,4)(4,6)=(e_2,e_3)(e_4,e_5)$。當k=5，$(e_2,e_5)(3,5)=(e_2,e_5)\infty=\infty$。

4.2.4 求解(3,7)的合法路徑：

當k=4，$(3,5)(5,7)=\infty(e_5,e_6)=\infty$。當k=6，$(e_3,e_6)(4,6)=(e_3,e_6)(e_4,e_5)$。

4.2.5 求解(4,8)的合法路徑：

當k=5，$(4,6)(6,8)=(e_4,e_5)(e_6,e_7)$。當k=7，$(e_4,e_7)(5,7)=(e_4,e_7)(e_5,e_6)$。

4.2.6 求解(5,9)的合法路徑：

當k=6，$(5,7)(7,9)=(e_5,e_6)\infty=\infty$。當k=8，$(e_5,e_8)(6,8)=(e_5,e_8)(e_6,e_7)$。

4.2.7 求解(6,10)的合法路徑：

當k=7，$(6,8)(8,10)=(e_6,e_7)(e_8,e_9)$。當k=9，$(e_6,e_9)(7,9)=(e_6,e_9)\infty=\infty$。

4.2.8 求解(7,11)的合法路徑：

當k=8，$(7,9)(9,11)=\infty(e_9,e_{10})=\infty$。當k=10，$(e_7,e_{10})(8,10)=(e_7,e_{10})(e_8,e_9)$。

4.2.9 求解(8,0) 的合法路徑：

當k=9，(8,10)(10,0)=(e_8,e_9)(e_{10},e_{11})。當k=11，(e_8,e_{11}) (9,11)= (e_8,e_{11})(e_9,e_{10})。

4.2.10 求解(9,1) 的合法路徑：

當k=10，(9,11)(11,1)=(e_9,e_{10})$\infty = \infty$。當k=0，(e_9,e_0) (10,0)= (e_9,e_0)(e_{10},e_{11})。

4.2.11 求解(10,2) 的合法路徑：

當k=11，(10,0)(0,2)=(e_{10},e_{11})(e_0,e_1)。當k=1，(e_{10},e_1) (11,1)= (e_{10},e_1) $\infty = \infty$。

4.2.12 求解(11,3) 的合法路徑：

當k=0，(11,1)(1,3)=∞(e_1,e_2)$= \infty$。當k=2，(e_{11},e_2) (0,2)=(e_{11},e_2)(e_0,e_1)。

我們將上述合法路徑依序填入表三。請參閱表三，｜i-j｜= 4，合法路徑。

表三 ｜i-j｜= 4 ，合法路徑

(0,4)	(4,8)	(8,0)
(e_0,e_1)(e_2,e_3)	(e_4,e_5)(e_6,e_7)	(e_8,e_9)(e_{10},e_{11})
(e_0,e_3)(e_1,e_2)	(e_4,e_7)(e_5,e_6)	(e_8,e_{11})(e_9,e_{10})
(1,5)	(5,9)	(9,1)
(e_1,e_2)(e_3,e_4) =∞	(e_5,e_6)(e_7,e_8) =∞	(e_9,e_{10})(e_{11},e_0) =∞
(e_1,e_4)(e_2,e_3)	(e_5,e_8)(e_6,e_7)	(e_9,e_0)(e_{10},e_{11})
(2,6)	(6,10)	(10,2)
(e_2,e_3)(e_4,e_5)	(e_6,e_7)(e_8,e_9)	(e_{10},e_{11})(e_0,e_1)
(e_2,e_5)(e_3,e_4) =∞	(e_6,e_9)(e_7,e_8) =∞	(e_{10},e_1)(e_{11},e_0) =∞
(3,7)	(7,11)	(11,3)
(e_3,e_4)(e_5,e_6) =∞	(e_7,e_8)(e_9,e_{10}) =∞	(e_{11},e_0)(e_1,e_2) =∞
(e_3,e_6)(e_4,e_5)	(e_7,e_{10})(e_8,e_9)	(e_{11},e_2)(e_0,e_1)

4.3 間距為6的合法路徑

設定角頂v_i與角頂v_j之間的間距，｜i-j｜= d=6，則｛(0,6)、(1,7)、(2,8)、(3,9)｝在4.3.1至4.3.4節中求解。

4.3.1 **求解**(0,6) **的合法路徑**：i=0，j=6，k=1, 3, 5。

當k=1，(0,2)(2,6)=(e_0,e_1)(e_2,e_3)(e_4,e_5)。當k=3，(0,4)(4,6)= {(e_0,e_1)(e_2,e_3)，(e_0,e_3)(e_1,e_2)} (e_4,e_5)。當k=5，(e_0,e_5)(1,5)=(e_0,e_5)(e_1,e_4)(e_2,e_3)。因為路徑(e_0,e_1)(e_2,e_3)(e_4,e_5)與k=1的路徑重複，僅取一個。我們將(e_0,e_1)(e_2,e_3)(e_4,e_5)、(e_0,e_3)(e_1,e_2)(e_4,e_5)與(e_0,e_5)(e_1,e_4)(e_2,e_3)等三個合法路徑填入表四的(0,6)欄位下。

4.3.2 **求解**(1,7) **的合法路徑**：i=1，j=7，k=2, 4, 6。

當k=2，(1,3)(3,7)= (e_1,e_2)(e_3,e_6)(e_4,e_5)。當k=4，(1,5)(5,7)= (e_1,e_4)(e_2,e_3)(e_5,e_6)。當k=6，(e_1,e_6)(2,6)=(e_1,e_6)(e_2,e_3)(e_4,e_5)。我們將(e_1,e_2)(e_3,e_6)(e_4,e_5)、(e_1,e_4)(e_2,e_3)(e_5,e_6)與(e_1,e_6)(e_2,e_3)(e_4,e_5)等三個合法路徑填入表四的(1,7)欄位下。

4.3.3 **求解**(2,8) **的合法路徑**：i=2，j=8，k=3, 5, 7。

當k=3，(2,4)(4,8)=(e_2,e_3) {(e_4,e_5)(e_6,e_7)，(e_4,e_7)(e_5,e_6)} 。當k=5，(2,6)(6,8)=(e_2,e_3)(e_4,e_5)(e_6,e_7)。當k=7，(e_2,e_7)(3,7)=(e_2,e_7)(e_3,e_6)(e_4,e_5)。因為路徑(e_2,e_3)(e_4,e_5)(e_6,e_7)與k=3重複，僅取一個。我們將(e_2,e_3)(e_4,e_5)(e_6,e_7)、(e_2,e_3)(e_4,e_7)(e_5,e_6)與(e_2,e_7)(e_3,e_6)(e_4,e_5)等三個合法路徑填入表四的(2,8)欄位下。

4.3.4**求解**(3,9) **的合法路徑**：i=3，j=9，k=4, 6, 8。

當k=4，(3,5)(5,9)=∞(e_5,e_8)(e_6,e_7)=∞。當k=6，(3,7)(7,9)=(e_3,e_6)(e_4,e_5)∞=∞。當k=8，(e_3,e_8)(4,8)=(e_3,e_8) {(e_4,e_5)(e_6,e_7)，(e_4,e_7)(e_5,e_6)} 。因為(e_3,e_8)(e_4,e_7)(e_5,e_6)為不合法路徑，我們將一個合法路徑(e_3,e_8)(e_4,e_5)(e_6,e_7)填入表四的(3,9)欄位下。

然後求解 {(4,10)、(5,11)、(6,0)、(7,1)} 與 {(8,2)、(9,3)、(10,4)、(11,5)} 等合法路徑和上述 {(0,6)、(1,7)、(2,8)、(3,9)} 的計算方式相類似，我們不重複地贅述。請參照 | i-j | =6 的合法路徑，如表四。

表四 | i-j | = 6 ，合法路徑

(0,6)	(4,10)	(8,2)
$(e_0,e_1)(e_2,e_3)(e_4,e_5)$	$(e_4,e_5)(e_6,e_7)(e_8,e_9)$	$(e_8,e_9)(e_{10},e_{11})(e_0,e_1)$
$(e_0,e_3)(e_1,e_2)(e_4,e_5)$	$(e_4,e_7)(e_5,e_6)(e_8,e_9)$	$(e_8,e_{11})(e_9,e_{10})(e_0,e_1)$
$(e_0,e_5)(e_1,e_4)(e_2,e_3)$	$(e_4,e_9)(e_5,e_8)(e_6,e_7)$	$(e_8,e_1)(e_9,e_0)(e_{10},e_{11})$
(1,7)	(5,11)	(9,3)
$(e_1,e_2)(e_3,e_6)(e_4,e_5)$	$(e_5,e_6)(e_7,e_{10})(e_8,e_9)$	$(e_9,e_{10})(e_{11},e_2)(e_0,e_1)$
$(e_1,e_4)(e_2,e_3)(e_5,e_6)$	$(e_5,e_8)(e_6,e_7)(e_9,e_{10})$	$(e_9,e_0)(e_{10},e_{11})(e_1,e_2)$
$(e_1,e_6)(e_2,e_3)(e_4,e_5)$	$(e_5,e_{10})(e_6,e_7)(e_8,e_9)$	$(e_9,e_2)(e_{10},e_{11})(e_0,e_1)$
(2,8)	(6,0)	(10,4)
$(e_2,e_3)(e_4,e_5)(e_6,e_7)$	$(e_6,e_7)(e_8,e_9)(e_{10},e_{11})$	$(e_{10},e_{11})(e_0,e_1)(e_2,e_3)$
$(e_2,e_3)(e_4,e_7)(e_5,e_6)$	$(e_6,e_7)(e_8,e_{11})(e_9,e_{10})$	$(e_{10},e_{11})(e_0,e_3)(e_1,e_2)$
$(e_2,e_7)(e_3,e_6)(e_4,e_5)$	$(e_6,e_{11})(e_7,e_{10})(e_8,e_9)$	$(e_{10},e_3)(e_{11},e_2)(e_0,e_1)$
(3,9)	(7,1)	(11,5)
$(e_3,e_8)(e_4,e_5)(e_6,e_7)$	$(e_7,e_0)(e_8,e_9)(e_{10},e_{11})$	$(e_{11},e_4)(e_0,e_1)(e_2,e_3)$

4.4 間距為8的合法路徑

設定角頂v_i與角頂v_j之間的間距，｜i-j｜=d=8，則｛(0,8)、(1,9)、(2,10)、(3,11)｝在4.4.1至4.4.4節中求解。

4.4.1求解(0,8)的合法路徑：i=0，j=8，k=1, 3, 5, 7。

當k=1，$(0,2)(2,8)=(e_0,e_1)$｛$(e_2,e_3)(e_4,e_5)(e_6,e_7)$、$(e_2,e_3)(e_4,e_7)(e_5,e_6)$、$(e_2,e_7)(e_3,e_6)(e_4,e_5)$｝等三個路徑。當k=3，$(0,4)(4,8)=$｛$(e_0,e_1)(e_2,e_3)$、$(e_0,e_3)(e_1,e_2)$｝｛$(e_4,e_5)(e_6,e_7)$、$(e_4,e_7)(e_5,e_6)$｝等四個路徑，其中$(e_0,e_1)(e_2,e_3)(e_4,e_5)(e_6,e_7)$與$(e_0,e_1)(e_2,e_3)(e_4,e_7)(e_5,e_6)$與k=1的兩個路徑重複，剩下$(e_0,e_3)(e_1,e_2)(e_4,e_5)(e_6,e_7)$與$(e_0,e_3)(e_1,e_2)(e_4,e_7)(e_5,e_6)$等兩個路徑。當k=5，$(0,6)(6,8)=$｛$(e_0,e_1)(e_2,e_3)(e_4,e_5)$、$(e_0,e_3)(e_1,e_2)(e_4,e_5)$、$(e_0,e_5)(e_1,e_4)(e_2,e_3)$｝$(e_6,e_7)$等三個路徑，其中$(e_0,e_1)(e_2,e_3)(e_4,e_5)(e_6,e_7)$與$(e_0,e_3)(e_1,e_2)(e_4,e_5)(e_6,e_7)$分別與k=1和k=3兩個路徑重複，剩下$(e_0,e_5)(e_1,e_4)(e_2,e_3)(e_6,e_7)$一個路徑。當k=7，$(e_0,e_7)(1,7)=(e_0,e_7)$｛$(e_1,e_2)(e_3,e_6)(e_4,e_5)$、$(e_1,e_4)(e_2,e_3)(e_5,e_6)$、$(e_1,e_6)(e_2,e_3)(e_4,e_5)$｝等三個路徑。我們將3+2+1+3=9個合法路徑填入表五的(0,8)欄位下。

4.4.2 **求解**(1,9) **的合法路徑**：i=1，j=9，k=2, 4, 6, 8。

當k=2，$(1,3)(3,9)=(e_1,e_2)(e_3,e_8)(e_4,e_5)(e_6,e_7)$一個路徑。當k=4，$(1,5)(5,9)=(e_1,e_4)(e_2,e_3)(e_5,e_8)(e_6,e_7)$一個路徑。當k=6，$(1,7)(7,9)=(1,7)\infty=\infty$。當k=8，$(e_1,e_8)(2,8)=(e_1,e_8)$｛$(e_2,e_3)(e_4,e_5)(e_6,e_7)$、$(e_2,e_3)(e_4,e_7)(e_5,e_6)$、$(e_2,e_7)(e_3,e_6)(e_4,e_5)$｝三個路徑。我們將1+1+0+3=5個合法路徑填入表五的(1,9)欄位下。

4.4.3 **求解**(2,10) **的合法路徑**：i=2，j=10，k=3, 5, 7, 9。

當k=3，$(2,4)(4,10)=(e_2,e_3)$｛$(e_4,e_5)(e_6,e_7)(e_8,e_9)$、$(e_4,e_7)(e_5,e_6)(e_8,e_9)$、$(e_4,e_9)(e_5,e_8)(e_6,e_7)$｝三個路徑。當k=5，$(2,6)(6,10)=(e_2,e_3)(e_4,e_5)(e_6,e_7)(e_8,e_9)$。與k=3的路徑重複。無路徑。當k=7，$(2,8)(8,10)=$｛$(e_2,e_3)(e_4,e_5)(e_6,e_7)$、$(e_2,e_3)(e_4,e_7)(e_5,e_6)$、$(e_2,e_7)(e_3,e_6)(e_4,e_5)$｝$(e_8,e_9)$三個路徑。其中｛$(e_2,e_3)(e_4,e_5)(e_6,e_7)$、$(e_2,e_3)(e_4,e_7)(e_5,e_6)$｝$(e_8,e_9)$與k=3的兩個路徑重複。剩下一個路徑。當k=9，$(e_2,e_9)(3,9)=(e_2,e_9)(e_3,e_8)(e_4,e_5)(e_6,e_7)$一個路徑。我們將3+0+1+1=5個合法路徑填入表五的(2,10)欄位下。

4.4.4 **求解**(3,11) **的合法路徑**：i=3，j=11，k=4, 6, 8, 10。

當k=4，$(3,5)(5,11)=\infty(5,11)=\infty$。當k=6，$(3,7)(7,11)=(e_3,e_6)(e_4,e_5)(e_7,e_{10})(e_8,e_9)$一個路徑。當k=8，$(3,9)(9,11)=(e_3,e_8)(e_4,e_5)(e_6,e_7)(e_9,e_{10})$一個路徑。當k=10，$(e_3,e_{10})(4,10)=(e_3,e_{10})$｛$(e_4,e_5)(e_6,e_7)(e_8,e_9)$、$(e_4,e_7)(e_5,e_6)(e_8,e_9)$、$(e_4,e_9)(e_5,e_8)(e_6,e_7)$｝三個路徑。我們將0+1+1+3=5個合法路徑填入表五的(3,11)欄位下。

然後求解｛(4,0)、(5,1)、(6,2)、(7,3)｝與｛(8,4)、(9,5)、(10,6)、(11,7)｝等合法路徑和上述｛(0,8)、(1,9)、(2,10)、(3,11)｝的計算方式相類似，我們不重複地贅述。請參照｜i-j｜=8的合法路徑，如表五。

表五 ｜i-j｜ = 8 ，合法路徑

(0,8)	(4,0)	(8,4)
$(e_0,e_1)(e_2,e_3)(e_4,e_5)(e_6,e_7)$	$(e_4,e_5)(e_6,e_7)(e_8,e_9)(e_{10},e_{11})$	$(e_8,e_9)(e_{10},e_{11})(e_0,e_1)(e_2,e_3)$
$(e_0,e_1)(e_2,e_3)(e_4,e_7)(e_5,e_6)$	$(e_4,e_5)(e_6,e_7)(e_8,e_{11})(e_9,e_{10})$	$(e_8,e_9)(e_{10},e_{11})(e_0,e_3)(e_1,e_2)$
$(e_0,e_1)(e_2,e_7)(e_3,e_6)(e_4,e_5)$	$(e_4,e_5)(e_6,e_{11})(e_7,e_{10})(e_8,e_9)$	$(e_8,e_9)(e_{10},e_3)(e_{11},e_2)(e_0,e_1)$
$(e_0,e_3)(e_1,e_2)(e_4,e_5)(e_6,e_7)$	$(e_4,e_7)(e_5,e_6)(e_8,e_9)(e_{10},e_{11})$	$(e_8,e_{11})(e_9,e_{10})(e_0,e_1)(e_2,e_3)$
$(e_0,e_3)(e_1,e_2)(e_4,e_7)(e_5,e_6)$	$(e_4,e_7)(e_5,e_6)(e_8,e_{11})(e_9,e_{10})$	$(e_8,e_{11})(e_9,e_{10})(e_0e_3)(e_1,e_2)$
$(e_0,e_5)(e_1,e_4)(e_2,e_3)(e_6,e_7)$	$(e_4,e_9)(e_5,e_8)(e_6,e_7)(e_{10},e_{11})$	$(e_8,e_1)(e_9,e_0)(e_{10},e_{11})(e_2,e_3)$
$(e_0,e_7)(e_1,e_2)(e_3,e_6)(e_4,e_5)$	$(e_4,e_{11})(e_5,e_6)(e_7,e_{10})(e_8,e_9)$	$(e_8,e_3)(e_9,e_{10})(e_{11},e_2)(e_0,e_1)$
$(e_0,e_7)(e_1,e_4)(e_2,e_3)(e_5,e_6)$	$(e_4,e_{11})(e_5,e_8)(e_6,e_7)(e_9,e_{10})$	$(e_8,e_3)(e_9,e_0)(e_{10},e_{11})(e_1,e_2)$
$(e_0,e_7)(e_1,e_6)(e_2,e_3)(e_4,e_5)$	$(e_4,e_{11})(e_5,e_{10})(e_6,e_7)(e_8,e_9)$	$(e_8,e_3)(e_9,e_2)(e_{10},e_{11})(e_0,e_1)$
(1,9)	(5,1)	(9,5)
$(e_1,e_2)(e_3,e_8)(e_4,e_5)(e_6,e_7)$	$(e_5,e_6)(e_7,e_0)(e_8,e_9)(e_{10},e_{11})$	$(e_9,e_{10})(e_{11},e_4)(e_0,e_1)(e_2,e_3)$
$(e_1,e_4)(e_2,e_3)(e_5,e_8)(e_6,e_7)$	$(e_5,e_8)(e_6,e_7)(e_9,e_0)(e_{10},e_{11})$	$(e_9,e_0)(e_{10},e_{11})(e_1,e_4)(e_2,e_3)$
$(e_1,e_8)(e_2,e_3)(e_4,e_5)(e_6,e_7)$	$(e_5,e_0)(e_6,e_7)(e_8,e_9)(e_{10},e_{11})$	$(e_9,e_4)(e_{10},e_{11})(e_0,e_1)(e_2,e_3)$
$(e_1,e_8)(e_2,e_3)(e_4,e_7)(e_5,e_6)$	$(e_5,e_0)(e_6,e_7)(e_8,e_{11})(e_9,e_{10})$	$(e_9,e_4)(e_{10},e_{11})(e_0,e_3)(e_1,e_2)$
$(e_1,e_8)(e_2,e_7)(e_3,e_6)(e_4,e_5)$	$(e_5,e_0)(e_6,e_{11})(e_7,e_{10})(e_8,e_9)$	$(e_9,e_4)(e_{10},e_3)(e_{11},e_2)(e_0,e_1)$
(2,10)	(6,2)	(10,6)
$(e_2,e_3)(e_4,e_5)(e_6,e_7)(e_8,e_9)$	$(e_6,e_7)(e_8,e_9)(e_{10},e_{11})(e_0,e_1)$	$(e_{10},e_{11})(e_0,e_1)(e_2,e_3)(e_4,e_5)$
$(e_2,e_3)(e_4,e_7)(e_5,e_6)(e_8,e_9)$	$(e_6,e_7)(e_8,e_{11})(e_9,e_{10})(e_0,e_1)$	$(e_{10},e_{11})(e_0,e_3)(e_1,e_2)(e_4,e_5)$
$(e_2,e_3)(e_4,e_9)(e_5,e_8)(e_6,e_9)$	$(e_6,e_7)(e_8,e_1)(e_9,e_0)(e_{10},e_{11})$	$(e_{10},e_{11})(e_0,e_5)(e_1,e_4)(e_2,e_3)$
$(e_2,e_7)(e_3,e_6)(e_4,e_5)(e_8,e_9)$	$(e_6,e_{11})(e_7,e_{10})(e_8,e_9)(e_0,e_1)$	$(e_{10},e_3)(e_{11},e_2)(e_0,e_1)(e_4,e_5)$
$(e_2,e_9)(e_3,e_8)(e_4,e_5)(e_6,e_7)$	$(e_6,e_1)(e_7,e_0)(e_8,e_9)(e_{10},e_{11})$	$(e_{10},e_5)(e_{11},e_4)(e_0,e_1)(e_2,e_3)$
(3,11)	(7,3)	(11,7)
$(e_3,e_6)(e_4,e_5)(e_7,e_{10})(e_8,e_9)$	$(e_7,e_{10})(e_8,e_9)(e_{11},e_2)(e_0,e_1)$	$(e_{11},e_2)(e_0,e_1)(e_3,e_6)(e_4,e_5)$
$(e_3,e_8)(e_4,e_5)(e_6,e_7)(e_9,e_{10})$	$(e_7,e_0)(e_8,e_9)(e_{10},e_{11})(e_1,e_2)$	$(e_{11},e_4)(e_0,e_1)(e_2,e_3)(e_5,e_6)$
$(e_3,e_{10})(e_4,e_5)(e_6,e_7)(e_8,e_9)$	$(e_7,e_2)(e_8,e_9)(e_{10},e_{11})(e_0,e_1)$	$(e_{11},e_6)(e_0,e_1)(e_2,e_3)(e_4,e_5)$
$(e_3,e_{10})(e_4,e_7)(e_5,e_6)(e_8,e_9)$	$(e_7,e_2)(e_8,e_{11})(e_9,e_{10})(e_0,e_1)$	$(e_{11},e_6)(e_0,e_3)(e_1,e_2)(e_4,e_5)$
$(e_3,e_{10})(e_4,e_9)(e_5,e_8)(e_6,e_7)$	$(e_7,e_2)(e_8,e_1)(e_9,e_0)(e_{10},e_1)$	$(e_{11},e_6)(e_0,e_3)(e_1,e_4)(e_2,e_3)$

4.5 間距為10的合法路徑

設定角頂v_i與角頂v_j之間的間距，｜i-j｜=d=10，則｛(0,10)、(1,11)、(2,0)、(3,1)｝分別在4.5.1至4.5.4節中求解。

4.5.1 **求解**(0,10) **的合法路徑**：i=0，j=10，k=1, 3, 5, 7, 9。

當k=1，(0,2)(2,10)=(e_0,e_1) {(e_2,e_3)(e_4,e_5)(e_6,e_7)(e_8,e_9)、(e_2,e_3)(e_4,e_7)(e_5,e_6)(e_8,e_9)、(e_2,e_3)(e_4,e_9)(e_5,e_8)(e_6,e_7)、(e_2,e_7)(e_3,e_6)(e_4,e_5)(e_8,e_9)、(e_2,e_9)(e_3,e_8)(e_4,e_5)(e_6,e_7)} 等五個路徑。當k=3，(0,4)(4,10)= {(e_0,e_1)(e_2,e_3)、(e_0,e_3)(e_1,e_2)} {(e_4,e_5)(e_6,e_7)(e_8,e_9)、(e_4,e_7)(e_5,e_6)(e_8,e_9)、(e_4,e_9)(e_5,e_8)(e_6,e_7)} 等六個路徑，其中(e_0,e_1)(e_2,e_3) {(e_4,e_5)(e_6,e_7)(e_8,e_9)、(e_4,e_7)(e_5,e_6)(e_8,e_9)、(e_4,e_9)(e_5,e_8)(e_6,e_7)} 等三個路徑與k=1的三個路徑重複，剩下(e_0,e_3)(e_1,e_2) {(e_4,e_5)(e_6,e_7)(e_8,e_9)、(e_4,e_7)(e_5,e_6)(e_8,e_9)、(e_4,e_9)(e_5,e_8)(e_6,e_7)} 等三個路徑。當k=5，(0,6)(6,10)= {(e_0,e_1)(e_2,e_3)(e_4,e_5)、(e_0,e_3)(e_1,e_2)(e_4,e_5)、(e_0,e_5)(e_1,e_4)(e_2,e_3)} (e_6,e_7)(e_8,e_9)等三個路徑，其中(e_0,e_1)(e_2,e_3)(e_4,e_5)(e_6,e_7)(e_8,e_9)與(e_0,e_3)(e_1,e_2)(e_4,e_5)(e_6,e_7)(e_8,e_9)兩個路徑分別與k=1和k=3的路徑重複，剩下(e_0,e_5)(e_1,e_4)(e_2,e_3)(e_6,e_7)(e_8,e_9)一個路徑。當k=7，(0,8)(8,10)= {(e_0,e_1)(e_2,e_3)(e_4,e_5)(e_6,e_7)、(e_0,e_1)(e_2,e_3)(e_4,e_7)(e_5,e_6)、(e_0,e_1)(e_2,e_7)(e_3,e_6)(e_4,e_5)、(e_0,e_3)(e_1,e_2)(e_4,e_5)(e_6,e_7)、(e_0,e_3)(e_1,e_2)(e_4,e_7)(e_5,e_6)、(e_0,e_5)(e_1,e_4)(e_2,e_3)(e_6,e_7)、(e_0,e_7)(e_1,e_2)(e_3,e_6)(e_4,e_5)、(e_0,e_7)(e_1,e_4)(e_2,e_3)(e_5,e_6)、(e_0,e_7)(e_1,e_6)(e_2,e_3)(e_4,e_5)} (e_8,e_9)等九個路徑，其中 {(e_0,e_1)(e_2,e_3)(e_4,e_5)(e_6,e_7)、(e_0,e_1)(e_2,e_3)(e_4,e_7)(e_5,e_6)、(e_0,e_1)(e_2,e_7)(e_3,e_6)(e_4,e_5)、(e_0,e_3)(e_1,e_2)(e_4,e_5)(e_6,e_7)、(e_0,e_3)(e_1,e_2)(e_4,e_7)(e_5,e_6)、(e_0,e_5)(e_1,e_4)(e_2,e_3)(e_6,e_7)} (e_8,e_9)六個路徑分別與k=1、k=3和k=5的3+2+1=6個路徑重複，剩下 {(e_0,e_7)(e_1,e_2)(e_3,e_6)(e_4,e_5)、(e_0,e_7)(e_1,e_4)(e_2,e_3)(e_5,e_6)、(e_0,e_7)(e_1,e_6)(e_2,e_3)(e_4,e_5)} (e_8,e_9)三個路徑。

當k=9，(e_0,e_9)(1,9)=(e_0,e_9) {(e_1,e_2)(e_3,e_8)(e_4,e_5)(e_6,e_7)、(e_1,e_4)(e_2,e_3)(e_5,e_8)(e_6,e_7)、(e_1,e_8)(e_2,e_3)(e_4,e_5)(e_6,e_7)、(e_1,e_8)(e_2,e_3)(e_4,e_7)(e_5,e_6)、(e_1,e_8)(e_2,e_7)(e_3,e_6)(e_4,e_5)} 等五個路徑。我們將5+3+1+3+5=17個合法路徑填入表六的(0,10)欄位下。

4.5.2 **求解**(1,11) **的合法路徑**：i=1，j=11，k=2, 4, 6, 8, 10。

當k=2，(1,3)(3,11)=(e_1,e_2) (3,11) 不合法路徑。當k=4，(1,5)(5,11)= (e_1,e_4) (5,11) 不合法路徑。當k=6，(1,7)(7,11)= (1,7) (e_7,e_{10})(e_8,e_9) 不合法路徑。當k=8，(1,9)(9,11)= (1,9) (e_9,e_{10})不合法路徑。當k=10，(e_1,e_{10})(2,10)=∞ (2,10) =∞。我們將∞填入表六的(1,11)欄位下。

4.5.3 **求解**(2,0) **的合法路徑**：i=2，j=10，k=3, 5, 7, 9, 11。

當k=3，(2,4)(4,0)=(e_2,e_3) {(e_4,e_5)(e_6,e_7)(e_8,e_9)(e_{10},e_{11})、(e_4,e_5)(e_6,e_7)(e_8,e_{11})(e_9,e_{10})、(e_4,e_5)(e_6,e_{11})(e_7,e_{10})(e_8,e_9)、(e_4,e_7)(e_5,e_6)(e_8,e_9)(e_{10},e_{11})、(e_4,e_7)(e_5,e_6)(e_8,e_{11})(e_9,e_{10})、

$(e_4,e_9)(e_5,e_8)(e_6,e_7)(e_{10},e_{11})$、$(e_4,e_{11})(e_5,e_6)(e_7,e_{10})(e_8,e_9)$、$(e_4,e_{11})(e_5,e_8)(e_6,e_7)(e_9,e_{10})$、$(e_4,e_{11})(e_5,e_{10})(e_6,e_7)(e_8,e_9)$｝九個路徑。當k=5，$(2,6)(6,0)=(e_2,e_3)(e_4,e_5)$｛$(e_6,e_7)(e_8,e_9)(e_{10},e_{11})$、$(e_6,e_7)(e_8,e_{11})(e_9,e_{10})$、$(e_6,e_{11})(e_7,e_{10})(e_8,e_9)$｝。與k=3的三個路徑重複。無路徑。當k=7，$(2,8)(8,0)=$｛$(e_2,e_3)(e_4,e_5)(e_6,e_7)$、$(e_2,e_3)(e_4,e_7)(e_5,e_6)$、$(e_2,e_7)(e_3,e_6)(e_4,e_5)$｝｛$(e_8,e_9)(e_{10},e_{11})$、$(e_8,e_{11})(e_9,e_{10})$｝3x2=6個路徑。其中｛$(e_2,e_3)(e_4,e_5)(e_6,e_7)$、$(e_2,e_3)(e_4,e_7)(e_5,e_6)$｝｛$(e_8,e_9)(e_{10},e_{11})$、$(e_8,e_{11})(e_9,e_{10})$｝分別與k=3的四個路徑重複。剩下$(e_2,e_7)(e_3,e_6)(e_4,e_5)$｛$(e_8,e_9)(e_{10},e_{11})$、$(e_8,e_{11})(e_9,e_{10})$｝二個路徑。當k=9，$(2,10)(10,0)=$｛$(e_2,e_3)(e_4,e_5)(e_6,e_7)(e_8,e_9)$、$(e_2,e_3)(e_4,e_7)(e_5,e_6)(e_8,e_9)$、$(e_2,e_3)(e_4,e_9)(e_5,e_8)(e_6,e_7)$、$(e_2,e_7)(e_3,e_6)(e_4,e_5)(e_8,e_9)$、$(e_2,e_9)(e_3,e_8)(e_4,e_5)(e_6,e_7)$｝$(e_{10},e_{11})$五個路徑。其中｛$(e_2,e_3)(e_4,e_5)(e_6,e_7)(e_8,e_9)$、$(e_2,e_3)(e_4,e_7)(e_5,e_6)(e_8,e_9)$、$(e_2,e_3)(e_4,e_9)(e_5,e_8)(e_6,e_7)$、$(e_2,e_7)(e_3,e_6)(e_4,e_5)(e_8,e_9)$｝$(e_{10},e_{11})$分別與k=3的三個和k=7的一個路徑重複。剩下一個路徑。當k=11，$(e_2,e_{11})(3,11)=(e_2,e_{11})$｛$(e_3,e_6)(e_4,e_5)(e_7,e_{10})(e_8,e_9)$、$(e_3,e_8)(e_4,e_5)(e_6,e_7)(e_9,e_{10})$、$(e_3,e_{10})(e_4,e_5)(e_6,e_7)(e_8,e_9)$、$(e_3,e_{10})(e_4,e_7)(e_5,e_6)(e_8,e_9)$、$(e_3,e_{10})(e_4,e_9)(e_5,e_8)(e_6,e_7)$｝等1x5=5個路徑。我們將9+0+2+1+5=17個合法路徑填入表六的(2,0)欄位下。

4.5.4 **求解(3,1) 的合法路徑**：i=3，j=1，k=4, 6, 8, 10, 0。

當k=4，$(3,5)(5,1)=\infty(5,1)=\infty$。當k=6，$(3,7)(7,1)=(e_3,e_6)(e_4,e_5)(e_7,e_0)(e_8,e_9)(e_{10},e_{11})$一個路徑。當k=8，$(3,9)(9,1)=(e_3,e_8)(e_4,e_5)(e_6,e_7)(e_9,e_0)(e_{10},e_{11})$一個路徑。當k=10，$(3,11)(11,1)=(3,11)\infty=\infty$無路徑。當k=0，$(e_3,e_0)(4,0)=(e_3,e_0)$｛$(e_4,e_5)(e_6,e_7)(e_8,e_9)(e_{10},e_{11})$、$(e_4,e_5)(e_6,e_7)(e_8,e_{11})(e_9,e_{10})$、$(e_4,e_5)(e_6,e_{11})(e_7,e_{10})(e_8,e_9)$、$(e_4,e_7)(e_5,e_6)(e_8,e_9)(e_{10},e_{11})$、$(e_4,e_7)(e_5,e_6)(e_8,e_{11})(e_9,e_{10})$、$(e_4,e_9)(e_5,e_8)(e_6,e_7)(e_{10},e_{11})$、$(e_4,e_{11})(e_5,e_6)(e_7,e_{10})(e_8,e_9)$、$(e_4,e_{11})(e_5,e_8)(e_6,e_7)(e_9,e_{10})$、$(e_4,e_{11})(e_5,e_{10})(e_6,e_7)(e_8,e_9)$｝九個路徑。其中三個路徑$(e_3,e_0)$｛$(e_4,e_{11})(e_5,e_6)(e_7,e_{10})(e_8,e_9)$、$(e_4,e_{11})(e_5,e_8)(e_6,e_7)(e_9,e_{10})$、$(e_4,e_{11})(e_5,e_{10})(e_6,e_7)(e_8,e_9)$｝不合法，剩下六個路徑。我們將0+1+1+0+6=8個填入表六的(3,1)欄位下。

然後求解｛(4,2)、(5,3)、(6,4)、(7,5)｝與｛(8,6)、(9,7)、(10,8)、(11,9)｝等合法路徑和上述｛(0,10)、(1,11)、(2,0)、(3,1)｝的計算方式相類似，我們不重複地贅述。請參照｜i-j｜=10 的合法路徑，如表六。

表六 ｜i-j｜= 10 ，合法路徑

(0,10)	(4,2)	(8,6)
$(e_0,e_1)(e_2,e_3)(e_4,e_5)(e_6,e_7)(e_8,e_9)$	$(e_4,e_5)(e_6,e_7)(e_8,e_9)(e_{10},e_{11})(e_0,e_1)$	$(e_8,e_9)(e_{10},e_{11})(e_0,e_1)(e_2,e_3)(e_4,e_5)$
$(e_0,e_1)(e_2,e_3)(e_4,e_7)(e_5,e_6)(e_8,e_9)$	$(e_4,e_5)(e_6,e_7)(e_8,e_{11})(e_9,e_{10})(e_0,e_1)$	$(e_8,e_9)(e_{10},e_{11})(e_0,e_3)(e_1,e_4)(e_2,e_3)$
$(e_0,e_1)(e_2,e_3)(e_4,e_9)(e_5,e_8)(e_6,e_7)$	$(e_4,e_5)(e_6,e_7)(e_8,e_1)(e_9,e_0)(e_{10},e_{11})$	$(e_8,e_9)(e_{10},e_{11})(e_0,e_5)(e_1,e_4)(e_2,e_3)$
$(e_0,e_1)(e_2,e_7)(e_3,e_6)(e_4,e_5)(e_8,e_9)$	$(e_4,e_5)(e_6,e_{11})(e_7,e_{10})(e_8,e_9)(e_0,e_1)$	$(e_8,e_9)(e_{10},e_3)(e_{11},e_2)(e_0,e_1)(e_4,e_5)$
$(e_0,e_1)(e_2,e_9)(e_3,e_8)(e_4,e_5)(e_6,e_7)$	$(e_4,e_5)(e_6,e_1)(e_7,e_0)(e_8,e_9)(e_{10},e_{11})$	$(e_8,e_9)(e_{10},e_5)(e_{11},e_4)(e_0,e_1)(e_2,e_3)$
$(e_0,e_3)(e_1,e_2)(e_4,e_5)(e_6,e_7)(e_8,e_9)$	$(e_4,e_7)(e_5,e_6)(e_8,e_9)(e_{10},e_{11})(e_0,e_1)$	$(e_8,e_{11})(e_9,e_{10})(e_0,e_1)(e_2,e_3)(e_4,e_5)$
$(e_0,e_3)(e_1,e_2)(e_4,e_7)(e_5,e_6)(e_8,e_9)$	$(e_4,e_7)(e_5,e_6)(e_8,e_{11})(e_9,e_{10})(e_0,e_1)$	$(e_8,e_{11})(e_9,e_{10})(e_0,e_3)(e_1,e_2)(e_4,e_5)$
$(e_0,e_3)(e_1,e_2)(e_4,e_9)(e_5,e_8)(e_6,e_7)$	$(e_4,e_7)(e_5,e_6)(e_8,e_1)(e_9,e_0)(e_{10},e_{11})$	$(e_8,e_{11})(e_9,e_{10})(e_0,e_5)(e_1,e_4)(e_2,e_3)$
$(e_0,e_5)(e_1,e_4)(e_2,e_3)(e_6,e_7)(e_8,e_9)$	$(e_4,e_9)(e_5,e_8)(e_6,e_7)(e_{10},e_{11})(e_0,e_1)$	$(e_8,e_1)(e_9,e_0)(e_{10},e_{11})(e_2,e_3)(e_4,e_5)$
$(e_0,e_7)(e_1,e_2)(e_3,e_6)(e_4,e_5)(e_8,e_9)$	$(e_4,e_{11})(e_5,e_6)(e_7,e_{10})(e_8,e_9)(e_0,e_1)$	$(e_8,e_3)(e_9,e_{10})(e_{11},e_2)(e_0,e_1)(e_4,e_5)$
$(e_0,e_7)(e_1,e_4)(e_2,e_3)(e_5,e_6)(e_8,e_9)$	$(e_4,e_{11})(e_5,e_8)(e_6,e_7)(e_9,e_{10})(e_0,e_1)$	$(e_8,e_3)(e_9,e_0)(e_{10},e_{11})(e_1,e_2)(e_4,e_5)$
$(e_0,e_7)(e_1,e_6)(e_2,e_3)(e_4,e_5)(e_8,e_9)$	$(e_4,e_{11})(e_5,e_{10})(e_6,e_7)(e_8,e_9)(e_0,e_1)$	$(e_8,e_3)(e_9,e_2)(e_{10},e_1)(e_0,e_1)(e_4,e_5)$
$(e_0,e_9)(e_1,e_2)(e_3,e_8)(e_4,e_5)(e_6,e_7)$	$(e_4,e_1)(e_5,e_6)(e_7,e_0)(e_8,e_9)(e_{10},e_{11})$	$(e_8,e_5)(e_9,e_{10})(e_{11},e_4)(e_0,e_1)(e_2,e_3)$
$(e_0,e_9)(e_1,e_4)(e_2,e_3)(e_5,e_8)(e_6,e_7)$	$(e_4,e_1)(e_5,e_8)(e_6,e_7)(e_9,e_0)(e_{10},e_{11})$	$(e_8,e_5)(e_9,e_0)(e_{10},e_{11})(e_1,e_4)(e_2,e_3)$
$(e_0,e_9)(e_1,e_8)(e_2,e_3)(e_4,e_5)(e_6,e_7)$	$(e_4,e_1)(e_5,e_0)(e_6,e_7)(e_8,e_9)(e_{10},e_{11})$	$(e_8,e_5)(e_9,e_4)(e_{10},e_{11})(e_0,e_1)(e_2,e_3)$
$(e_0,e_9)(e_1,e_8)(e_2,e_3)(e_4,e_7)(e_5,e_6)$	$(e_4,e_1)(e_5,e_0)(e_6,e_7)(e_8,e_{11})(e_9,e_{10})$	$(e_8,e_5)(e_9,e_4)(e_{10},e_{11})(e_0,e_3)(e_1,e_2)$
$(e_0,e_9)(e_1,e_8)(e_2,e_7)(e_3,e_6)(e_4,e_5)$	$(e_4,e_1)(e_5,e_0)(e_6,e_{11})(e_7,e_{10})(e_8,e_9)$	$(e_8,e_5)(e_9,e_4)(e_{10},e_3)(e_{11},e_2)(e_0,e_1)$
(1,11)	(5,3)	(9,7)
∞	∞	∞
(2,0)	(6,4)	(10,8)
$(e_2,e_3)(e_4,e_5)(e_6,e_7)(e_8,e_9)(e_{10},e_{11})$	$(e_6,e_7)(e_8,e_9)(e_{10},e_{11})(e_0,e_1)(e_2,e_3)$	$(e_{10},e_{11})(e_0,e_1)(e_2,e_3)(e_4,e_5)(e_6,e_7)$
$(e_2e_3)(e_4,e_5)(e_6,e_7)(e_8,e_{11})(e_9,e_{10})$	$(e_6,e_7)(e_8,e_9)(e_{10},e_{11})(e_0,e_3)(e_1,e_2)$	$(e_{10},e_{11})(e_0,e_1)(e_2,e_3)(e_4,e_7)(e_6,e_6)$
$(e_2e_3)(e_4,e_5)(e_6,e_{11})(e_7,e_{10})(e_8,e_9)$	$(e_6,e_7)(e_8,e_9)(e_{10},e_3)(e_{11},e_2)(e_0,e_1)$	$(e_{10},e_{11})(e_0,e_1)(e_2,e_7)(e_3,e_6)(e_4,e_5)$
$(e_2e_3)(e_4,e_7)(e_5,e_6)(e_8,e_9)(e_{10},e_{11})$	$(e_6,e_7)(e_8,e_{11})(e_9,e_{10})(e_0,e_1)(e_2,e_3)$	$(e_{10},e_{11})(e_0,e_3)(e_1,e_2)(e_4,e_5)(e_6,e_7)$
$(e_2e_3)(e_4,e_7)(e_5,e_6)(e_8,e_{11})(e_9,e_{10})$	$(e_6,e_7)(e_8,e_{11})(e_9,e_{10})(e_0,e_3)(e_1,e_2)$	$(e_{10},e_{11})(e_0,e_3)(e_1,e_2)(e_4,e_7)(e_5,e_6)$
$(e_2e_3)(e_4,e_9)(e_5,e_8)(e_6,e_7)(e_{10},e_{11})$	$(e_6,e_7)(e_8,e_1)(e_9,e_0)(e_{10},e_{11})(e_2,e_3)$	$(e_{10},e_{11})(e_0,e_5)(e_1,e_4)(e_2,e_3)(e_0,e_7)$
$(e_2e_3)(e_4,e_{11})(e_5,e_6)(e_7,e_{10})(e_8,e_9)$	$(e_6,e_7)(e_8,e_3)(e_9,e_{10})(e_{11},e_2)(e_0,e_1)$	$(e_{10},e_{11})(e_0,e_7)(e_1,e_2)(e_3,e_6)(e_4,e_5)$
$(e_2e_3)(e_4,e_{11})(e_5,e_8)(e_6,e_7)(e_9,e_{10})$	$(e_6,e_7)(e_8,e_3)(e_9,e_0)(e_{10},e_{11})(e_1,e_2)$	$(e_{10},e_{11})(e_0,e_7)(e_1,e_4)(e_2,e_3)(e_5,e_6)$
$(e_2e_3)(e_4,e_{11})(e_5,e_{10})(e_6,e_7)(e_8,e_9)$	$(e_6,e_7)(e_8,e_3)(e_9,e_2)(e_{10},e_{11})(e_0,e_1)$	$(e_{10},e_{11})(e_0,e_7)(e_1,e_6)(e_2,e_3)(e_4,e_5)$
$(e_2e_7)(e_3,e_6)(e_4,e_5)(e_8,e_9)(e_{10},e_{11})$	$(e_6,e_{11})(e_7,e_{10})(e_8,e_9)(e_0,e_1)(e_2,e_3)$	$(e_{10},e_3)(e_{11},e_2)(e_0,e_1)(e_4,e_5)(e_6,e_7)$
$(e_2e_7)(e_3,e_6)(e_4,e_5)(e_8,e_{11})(e_9,e_{10})$	$(e_6,e_{11})(e_7,e_{10})(e_8,e_9)(e_0,e_3)(e_1,e_2)$	$(e_{10},e_3)(e_{11},e_2)(e_0,e_1)(e_4,e_7)(e_5,e_6)$

$(e_2e_9)(e_3,e_8)(e_4,e_5)(e_6,e_7)(e_{10},e_{11})$	$(e_6,e_1)(e_7,e_0)(e_8,e_9)(e_{10},e_{11})(e_2,e_3)$	$(e_{10},e_5)(e_{11},e_4)(e_0,e_1)(e_2,e_3)(e_6,e_7)$
$(e_2e_{11})(e_3,e_6)(e_4,e_5)(e_7,e_{10})(e_8,e_9)$	$(e_6,e_3)(e_7,e_{10})(e_8,e_9)(e_1,e_2)(e_0,e_1)$	$(e_{10},e_7)(e_{11},e_2)(e_0,e_1)(e_3,e_6)(e_4,e_5)$
$(e_2e_{11})(e_3,e_8)(e_4,e_5)(e_6,e_7)(e_9,e_{10})$	$(e_6,e_3)(e_7,e_0)(e_8,e_9)(e_{10},e_{11})(e_1,e_2)$	$(e_{10},e_7)(e_{11},e_4)(e_0,e_1)(e_2,e_3)(e_5,e_6)$
$(e_2e_{11})(e_3,e_{10})(e_4,e_5)(e_6,e_7)(e_8,e_9)$	$(e_6,e_3)(e_7,e_2)(e_8,e_9)(e_{10},e_{11})(e_0,e_1)$	$(e_{10},e_7)(e_{11},e_6)(e_0,e_1)(e_2,e_3)(e_4,e_5)$
$(e_2e_{11})(e_3,e_{10})(e_4,e_7)(e_5,e_6)(e_8,e_9)$	$(e_6,e_3)(e_7,e_2)(e_8,e_{11})(e_9,e_{10})(e_0,e_1)$	$(e_{10},e_7)(e_{11},e_6)(e_0,e_3)(e_1,e_2)(e_4,e_5)$
$(e_2e_{11})(e_3,e_{10})(e_4,e_9)(e_5,e_8)(e_6,e_7)$	$(e_6,e_3)(e_7,e_2)(e_8,e_1)(e_9,e_0)(e_{10},e_1)$	$(e_{10},e_7)(e_{11}e_6)(e_0,e_5)(e_1,e_4)(e_2,e_3)$
(3,1)	(7,5)	(11,9)
$(e_3,e_6)(e_4,e_5)(e_7,e_0)(e_8,e_9)(e_{10},e_{11})$	$(e_7,e_{10})(e_8,e_9)(e_{11},e_4)(e_0,e_1)(e_2,e_3)$	$(e_{11},e_2)(e_0,e_1)(e_3,e_8)(e_4,e_5)(e_6,e_7)$
$(e_3,e_8)(e_4,e_5)(e_6,e_7)(e_9,e_0)(e_{10},e_{11})$	$(e_7,e_0)(e_8,e_9)(e_{10},e_{11})(e_1,e_4)(e_2,e_3)$	$(e_{11},e_4)(e_0,e_1)(e_2,e_3)(e_5,e_8)(e_6,e_7)$
$(e_3e_0)(e_4,e_5)(e_6,e_7)(e_8,e_9)(e_{10},e_{11})$	$(e_7,e_4)(e_8,e_9)(e_{10},e_{11})(e_0,e_1)(e_2,e_3)$	$(e_{11},e_8)(e_0,e_1)(e_2,e_3)(e_4,e_5)(e_6,e_7)$
$(e_3,e_0)(e_4,e_5)(e_6,e_7)(e_8,e_{11})(e_9,e_{10})$	$(e_7,e_4)(e_8,e_9)(e_{10},e_{11})(e_0,e_3)(e_1,e_2)$	$(e_{11},e_8)(e_0,e_1)(e_2,e_3)(e_4,e_7)(e_5,e_6)$
$(e_3,e_0)(e_4,e_5)(e_6,e_{11})(e_7,e_{10})(e_8,e_9)$	$(e_7,e_4)(e_8,e_9)(e_{10},e_3)(e_{11},e_2)(e_0,e_1)$	$(e_{11},e_8)(e_0,e_1)(e_2,e_7)(e_3,e_6)(e_4,e_5)$
$(e_3,e_0)(e_4,e_7)(e_5,e_6)(e_8,e_9)(e_{10},e_{11})$	$(e_7,e_4)(e_8,e_{11})(e_9,e_{10})(e_0,e_1)(e_2,e_3)$	$(e_{11},e_8)(e_0,e_3)(e_1,e_2)(e_4,e_5)(e_6,e_7)$
$(e_3,e_0)(e_4e_7)(e_5,e_6)(e_8,e_{11})(e_9,e_{10})$	$(e_7,e_4)(e_8,e_{11})(e_9,e_{10})(e_0,e_3)(e_1,e_2)$	$(e_{11},e_8)(e_0,e_3)(e_1,e_2)(e_4,e_7)(e_5,e_6)$
$(e_3,e_0)(e_4,e_9)(e_5,e_8)(e_6,e_7)(e_{10},e_{11})$	$(e_7,e_4)(e_8,e_1)(e_9,e_0)(e_{10},e_{11})(e_2,e_3)$	$(e_{11},e_8)(e_0,e_5)(e_1,e_4)(e_2,e_3)(e_6,e_7)$

4.6 間距為12的合法路徑

最後，我們求角頂v_0與角頂v_0之間的間距｜i-j｜=d=12。當(0,0)，k=1, 3, 5, 7, 9, 11。設定k=1，求路徑(0,2) (2,0)，因為從表二得知路徑(0,2) 有1個，以及從表六得知路徑(2,0)有17個，因此路徑(0,2) (2,0)會有1x17個，即17個，列出如表七。模型後括號內標示I與R分別代表「同形的 (isomorphic)」模型與「重複的(repeated)」路徑。

表七 k=1，合法路徑(0,2) (2,0)

k=1，合法路徑(0,2) (2,0)	模型
$(e_0,e_1)(e_2,e_3)(e_4,e_5)(e_6,e_7)(e_8,e_9)(e_{10},e_{11})$	風車
$(e_0,e_1)(e_2,e_3)(e_4,e_5)(e_6,e_7)(e_8,e_{11})(e_9,e_{10})$	飛機
$(e_0,e_1)(e_2,e_3)(e_4,e_5)(e_6,e_{11})(e_7,e_{10})(e_8,e_9)$	右腿
$(e_0,e_1)(e_2,e_3)(e_4,e_7)(e_5,e_6)(e_8,e_9)(e_{10},e_{11})$	飛機(I)
$(e_0,e_1)(e_2,e_3)(e_4,e_7)(e_5,e_6)(e_8,e_{11})(e_9,e_{10})$	巧克力
$(e_0,e_1)(e_2,e_3)(e_4,e_9)(e_5,e_8)(e_6,e_7)(e_{10},e_{11})$	左腿

$(e_0,e_1)(e_2,e_3)(e_4,e_{11})(e_5,e_6)(e_7,e_{10})(e_8,e_9)$	左
$(e_0,e_1)(e_2,e_3)(e_4,e_{11})(e_5,e_8)(e_6,e_7)(e_9,e_{10})$	右
$(e_0,e_1)(e_2,e_3)(e_4,e_{11})(e_5,e_{10})(e_6,e_7)(e_8,e_9)$	鯨魚
$(e_0,e_1)(e_2,e_7)(e_3,e_6)(e_4,e_5)(e_8,e_9)(e_{10},e_{11})$	右腿(I)
$(e_0,e_1)(e_2,e_7)(e_3,e_6)(e_4,e_5)(e_8,e_{11})(e_9,e_{10})$	飛船
$(e_0,e_1)(e_2,e_9)(e_3,e_8)(e_4,e_5)(e_6,e_7)(e_{10},e_{11})$	鯨魚(I)
$(e_0,e_1)(e_2,e_{11})(e_3,e_6)(e_4,e_5)(e_7,e_{10})(e_8,e_9)$	左旋風車
$(e_0,e_1)(e_2,e_{11})(e_3,e_8)(e_4,e_5)(e_6,e_7)(e_9,e_{10})$	左(I)
$(e_0,e_1)(e_2,e_{11})(e_3,e_{10})(e_4,e_5)(e_6,e_7)(e_8,e_9)$	右腿(I)
$(e_0,e_1)(e_2,e_{11})(e_3,e_{10})(e_4,e_7)(e_5,e_6)(e_8,e_9)$	飛船(I)
$(e_0,e_1)(e_2,e_{11})(e_3,e_{10})(e_4,e_9)(e_5,e_8)(e_6,e_7)$	船

設定k=3，求路徑(0,4) (4,0)，因為從表三得知路徑(0,4) 有2個，以及從表五得知路徑(4,0)有9個，因此路徑(0,4)(4,0)會有2x9個，即18個，列出如表八。值得注意的是，有$(e_0,e_3)(e_1,e_2)(e_4,e_{11})$的非法次路徑。

表八 k=3，合法路徑(0,4) (4,0)

k=3，合法路徑(0,4) 4,0)	模型
$(e_0,e_1)(e_2,e_3)(e_4,e_5)(e_6,e_7)(e_8,e_9)(e_{10},e_{11})$	風車(R)
$(e_0,e_1)(e_2,e_3)(e_4,e_5)(e_6,e_7)(e_8,e_{11})(e_9,e_{10})$	飛機(R)
$(e_0,e_1)(e_2,e_3)(e_4,e_5)(e_6,e_{11})(e7,e10)(e_8,e_9)$	右腿(R)
$(e_0,e_1)(e_2,e_3)(e_4,e_7)(e_5,e_6)(e_8,e_9)(e_{10},e_{11})$	飛機(I、R)
$(e_0,e_1)(e_2,e_3)(e_4,e_7)(e_5,e_6)(e_8,e_{11})(e_9,e_{10})$	巧克力(R)
$(e_0,e_1)(e_2,e_3)(e_4,e_9)(e_5,e_8)(e_6,e_7)(e_{10},e_{11})$	左腿(R)
$(e_0,e_1)(e_2,e_3)(e_4,e_{11})(e_5,e_6)(e_9,e_{10})(e_8,e_9)$	左(R)
$(e_0,e_1)(e_2,e_3)(e_4,e_{11})(e_5,e_8)(e_6,e_7)(e_9,e_{10})$	右(R)
$(e_0,e_1)(e_2,e_3)(e_4,e_{11})(e_5,e_{10})(e_6,e_7)(e_8,e_9)$	鯨魚(R)
$(e_0,e_3)(e_1,e_2)(e_4,e_5)(e_6,e_7)(e_8,e_9)(e_{10},e_{11})$	飛機(I)
$(e_0,e_3)(e_1,e_2)(e_4,e_5)(e_6,e_7)(e_8,e_{11})(e_9,e_{10})$	巧克力(I)
$(e_0,e_3)(e_1,e_2)(e_4,e_5)(e_6,e_{11})(e_7,e_{10})(e_8,e_9)$	飛機(I)
$(e_0,e_3)(e_1,e_2)(e_4,e_7)(e_5,e_6)(e_8,e_9)(e_{10},e_{11})$	巧克力(I)

$(e_0,e_3)(e_1,e_2)(e_4,e_7)(e_5,e_6)(e_8,e_{11})(e_9,e_{10})$	四面體
$(e_0,e_3)(e_1,e_2)(e_4,e_9)(e_5,e_8)(e_6,e_7)(e_{10},e_{11})$	飛船(I)
$(e_0,e_3)(e_1,e_2)(e_4,e_{11})(e_5,e_6)(e_7,e_{10})(e_8,e_9)$	非法黏接
$(e_0,e_3)(e_1,e_2)(e_4,e_{11})(e_5,e_8)(e_6,e_7)(e_9,e_{10})$	非法黏接
$(e_0,e_3)(e_1,e_2)(e_4,e_{11})(e_5,e_{10})(e_6,e_7)(e_8,e_9)$	非法黏接

設定k=5，求路徑(0,6) (6,0)，因為從表四得知路徑(0,6) 有3個，以及從表四得知路徑(6,0)有3個，因此路徑(0,6)(6,0)會有3x3個，即9個，列出如表九。

表九 k=5，合法路徑(0,6) (6,0)

k=5，合法路徑(0,6) 6,0)	模型
$(e_0,e_1)(e_2,e_3)(e_4,e_5)(e_6,e_7)(e_8,e_9)(e_{10},e_{11})$	風車(R)
$(e_0,e_1)(e_2,e_3)(e_4,e_5)(e_6,e_7)(e_8,e_{11})(e_9,e_{10})$	飛機(R)
$(e_0,e_1)(e_2,e_3)(e_4,e_5)(e_6,e_{11})(e_7,e_{10})(e_8,e_9)$	右腿(R)
$(e_0,e_3)(e_1,e_2)(e_4,e_5)(e_6,e_7)(e_8,e_9)(e_{10},e_{11})$	飛機(I、R)
$(e_0,e_3)(e_1,e_2)(e_4,e_5)(e_6,e_7)(e_8,e_{11})(e_9,e_{10})$	巧克力(I、R)
$(e_0,e_3)(e_1,e_2)(e_4,e_5)(e_6,e_{11})(e_7,e_{10})(e_8,e_9)$	飛船(I、R)
$(e_0,e_5)(e_1,e_4)(e_2,e_3)(e_6,e_7)(e_8,e_9)(e_{10},e_{11})$	左腿(I)
$(e_0,e_5)(e_1,e_4)(e_2,e_3)(e_6,e_7)(e_8,e_{11})(e_9,e_{10})$	飛船(I)
$(e_0,e_5)(e_1,e_4)(e_2,e_3)(e_6,e_{11})(e_7,e_{10})(e_8,e_9)$	船(I)

設定k=7，求路徑(0,8) (8,0)，因為從表五得知路徑(0,8) 有9個，以及從表三得知路徑(8,0)有2個，因此路徑(0,8) (8,0)會有9x2個，即18個，列出如表十。值得注意的是，有$(e_0,e_7)(e_1,e_6)$與 $(e_8,e_{11})(e_9,e_{10})$的非法次路徑。

表十 k=7，合法路徑(0,8) (8,0)

k=7，合法路徑(0,8)(8,0)	模型
$(e_0,e_1)(e_2,e_3)(e_4,e_5)(e_6,e_7)(e_8,e_9)(e_{10},e_{11})$	風車(R)
$(e_0,e_1)(e_2,e_3)(e_4,e_7)(e_5,e_6)(e_8,e_9)(e_{10},e_{11})$	飛機(I、R)
$(e_0,e_1)(e_2,e_7)(e_3,e_6)(e_4,e_5)(e_8,e_9)(e_{10},e_{11})$	右腿(I、R)
$(e_0,e_3)(e_1,e_2)(e_4,e_5)(e_6,e_7)(e_8,e_9)(e_{10},e_{11})$	飛機(I、R)

$(e_0,e_3)(e_1,e_2)(e_4,e_7)(e_5,e_6)(e_8,e_9)(e_{10},e_{11})$	巧克力(I、R)
$(e_0,e_5)(e_1,e_4)(e_2,e_3)(e_6,e_7)(e_8,e_9)(e_{10},e_{11})$	左腿(I、R)
$(e_0,e_7)(e_1,e_2)(e_3,e_6)(e_4,e_5)(e_8,e_9)(e_{10},e_{11})$	左(I)
$(e_0,e_7)(e_1,e_4)(e_2,e_3)(e_5,e_6)(e_8,e_9)(e_{10},e_{11})$	右(I)
$(e_0,e_7)(e_1,e_6)(e_2,e_3)(e_4,e_5)(e_8,e_9)(e_{10},e_{11})$	鯨魚(I)
$(e_0,e_1)(e_2,e_7)(e_3,e_6)(e_4,e_5)(e_8,e_{11})(e_9,e_{10})$	飛機(R)
$(e_0,e_1)(e_2,e_3)(e_4,e_7)(e_5,e_6)(e_8,e_{11})(e_9,e_{10})$	巧克力(R)
$(e_0,e_3)(e_1,e_2)(e_4,e_5)(e_6,e_{11})(e_7,e_{10})(e_8,e_9)$	飛船(R)
$(e_0,e_3)(e_1,e_2)(e_4,e_5)(e_6,e_7)(e_8,e_{11})(e_9,e_{10})$	巧克力(I、R)
$(e_0,e_3)(e_1,e_2)(e_4,e_7)(e_5,e_6)(e_8,e_{11})(e_9,e_{10})$	四面體(R)
$(e_0,e_5)(e_1,e_4)(e_2,e_3)(e_6,e_7)(e_8,e_{11})(e_9,e_{10})$	飛船(I、R)
$(e_0,e_7)(e_1,e_2)(e_3,e_6)(e_4,e_5)(e_8,e_{11})(e_9,e_{10})$	左(I)
$(e_0,e_7)(e_1,e_4)(e_2,e_3)(e_5,e_6)(e_8,e_{11})(e_9,e_{10})$	右(I)
$(e_0,e_7)(e_1,e_6)(e_2,e_3)(e_4,e_5)(e_8,e_{11})(e_9,e_{10})$	非法黏接

設定k=9，求路徑(0,10) (10,0)，因為從表六得知路徑(0,10) 有17個，以及從表二得知路徑(10,0)有1個，因此路徑(0,10) (10,0)會有17x1個，即17個，列出如表十一。

表十一 k=9，合法路徑(0,10) (10,0)

k=9，合法路徑(0,10) (0,0)	模型
$(e_0,e_1)(e_2,e_3)(e_4,e_5)(e_6,e_7)(e_8,e_9)(e_{10},e_{11})$	風車(R)
$(e_0,e_1)(e_2,e_3)(e_4,e_7)(e_5,e_6)(e_8,e_9)(e_{10},e_{11})$	飛機(R)
$(e_0,e_1)(e_2,e_3)(e_4,e_9)(e_5,e_8)(e_6,e_7)(e_{10},e_{11})$	左腿(R)
$(e_0,e_1)(e_2,e_7)(e_3,e_6)(e_4,e_5)(e_8,e_9)(e_{10},e_{11})$	右腿(I、R)
$(e_0,e_1)(e_2,e_9)(e_3,e_8)(e_4,e_5)(e_6,e_7)(e_{10},e_{11})$	鯨魚(I、R)
$(e_0,e_3)(e_1,e_2)(e_4,e_5)(e_6,e_7)(e_8,e_9)(e_{10},e_{11})$	飛機(I、R)
$(e_0,e_3)(e_1,e_2)(e_4,e_7)(e_5,e_6)(e_8,e_9)(e_{10},e_{11})$	巧克力(I、R)
$(e_0,e_3)(e_1,e_2)(e_4,e_9)(e_5,e_8)(e_6,e_7)(e_{10},e_{11})$	飛船(I、R)
$(e_0,e_5)(e_1,e_4)(e_2,e_3)(e_6,e_7)(e_8,e_9)(e_{10},e_{11})$	左腿(I、R)
$(e_0,e_7)(e_1,e_2)(e_3,e_6)(e_4,e_5)(e_8,e_9)(e_{10},e_{11})$	左(I、R)
$(e_0,e_7)(e_1,e_4)(e_2,e_3)(e_5,e_6)(e_8,e_9)(e_{10},e_{11})$	右((I、R)

$(e_0,e_7)(e_1,e_6)(e_2,e_3)(e_4,e_5)(e_8,e_9)(e_{10},e_{11})$	鯨魚(I、R)
$(e_0,e_9)(e_1,e_2)(e_3,e_8)(e_4,e_5)(e_6,e_7)(e_{10},e_{11})$	右(I)
$(e_0,e_9)(e_1,e_4)(e_2,e_3)(e_5,e_8)(e_6,e_7)(e_{10},e_{11})$	右旋風車
$(e_0,e_9)(e_1,e_8)(e_2,e_3)(e_4,e_5)(e_6,e_7)(e_{10},e_{11})$	左腿(I)
$(e_0,e_9)(e_1,e_8)(e_2,e_3)(e_4,e_7)(e_5,e_6)(e_{10},e_{11})$	飛船(I)
$(e_0,e_9)(e_1,e_8)(e_2,e_7)(e_3,e_6)(e_4,e_5)(e_{10},e_{11})$	船(I)

設定k=11，因為k+1=12，路徑(e_0, e_{11}) (1,11)，因為從表二得知$(e_{11},e_0) =\infty$，因此路徑(e_0, e_{11}) (1,11)沒有合法路徑。

4.7 三角紙積木模型與黏接樹

從表七至表十二等五個表，我們將17+15+9+17+17=75個合法黏接路徑，除去重複剩下17+6+3+5+5=36個，然後除去同形的(isomorphic)模型6+5+3+5+4=23個，最後剩下11+1+0+0+1=13個模型。請見表十二中13個模型的「匹配邊對」。

4.8 三角紙積木模型與黏接樹

我們將畫出表十二中，13個模型的「黏接樹(gluing tree)」。目的是想藉助這些「黏接樹」提供的角頂與角頂，以及邊對之間的資訊，來計算每個模型的「角頂數」與各個角頂的「秩（valence或degree）數」，秩就是交會在這個角頂的邊的個數。我們有13個模型，每個模型均有6組「匹配邊對」路徑。黏接樹，通常是在空白紙的右下角的位置，從第一組「匹配邊對」開始「反時鐘方向」畫起，有時候為了追求美感，在啟始點位置與其角度會適當地調整，但是「反時鐘方向」的原則是不變的。

第一組匹配邊對為(e_0,e_i)。假如i=1，則第一組匹配邊對(e_0,e_1)以及第二組邊對(e_2,e_k)。因為第一組匹配邊對(e_0,e_1)，代表（v_0,v_2）之間有個轉折點，一個動作完成一個匹配邊對(e_0,e_1)。我們通常先找尋六組邊對中，所有連號的「匹配邊對」，先把這些轉折點的匹配邊對畫好。假如$i\neq 1$，則j=1，第二組邊對為(e_1,e_K)。我們從v_0開始，向右的方向畫（v_0,v_1）之間的邊線，然後停在v_1的角頂；接著在v_1的上方選一個點v_i，從vi開始向左與（v_0,v_1）邊線「平行地」畫匹配邊（v_i,v_i+1），然後停在v_0的上方是為v_i+1。接著畫第二組邊對(e_j,e_k)。隨著i=1或$i\neq 1$，第二組邊對(e_j,e_k)會有(e_2,e_k)或 (e_1,e_k)兩種情況。我們不要擔心i、j與k三者之間的關係，只要順著路徑走下去。直到第六組畫完了結束。

4.8.1. **風車模型黏接路徑** $(e_0,e_1)(e_2,e_3)(e_4,e_5)(e_6,e_7)(e_8,e_9)(e_{10},e_{11})$

按照黏接路徑，我們可以依序畫出黏接樹，如圖三。首先，有0-2-4-6-8-10六角頂共點，其內角總合為60+180+60+180+60+180=720，共有1個720/60=12秩。有6個180° (3秩)轉折點，共有180x6=1080，即6個3秩。故，角頂數為1+6=7；秩數為12x1+3x6=30；總內角和為720+1080=1800。請注意，角頂數與秩數分別為7與30。

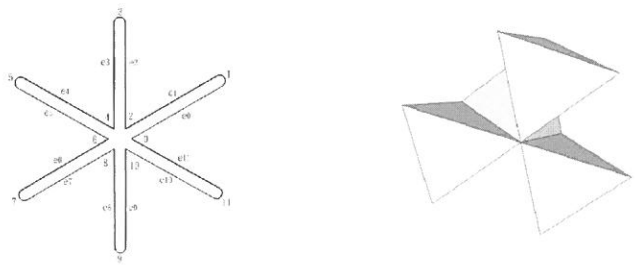

圖三：風車黏接樹與模型

4.8.2. **飛機模型黏接路徑** $(e_0,e_1)(e_2,e_3)(e_4,e_5)(e_6,e_7)(e_8,e_{11})\ (e_9,e_{10})$

按照黏接路徑，我們可以依序畫出黏接樹，如圖四。0-2-4-6-8五角頂共點，其角度總合為60+180+60+180+60=540，共有一個540/60=9秩。有5個180° (3秩)轉折點，共有180x5=900，即5個3秩，以及9-11共點的角和為180x2=360，即一個360/60=6秩，總內角和為540+900+360=1800。

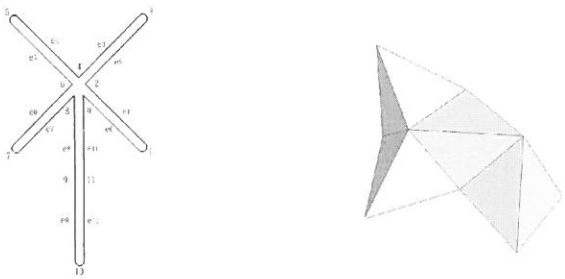

圖四：飛機黏接樹與模型

4.8.3. **左模型黏接路徑** $(e_0,e_1)(e_2,e_3)(e_4,e_{11})(e_5,e_6)(e_7,e_{10})(e_8,e_9)$

按照黏接路徑，我們可以依序畫出黏接樹，如圖五。5-7-11三角頂共點，其角度總合為180+180+180=540，有一個540/60=9秩。0-2-4三角頂共點，其角度總合為60+180+60=300，有一個300/60=5秩。有4個180°(3秩)轉折點，共有180x4=720，即4個3秩，以及8-10共點的角和為60+180=240，即一個240/60=4秩，總內角和為540+300+720+240=1800。

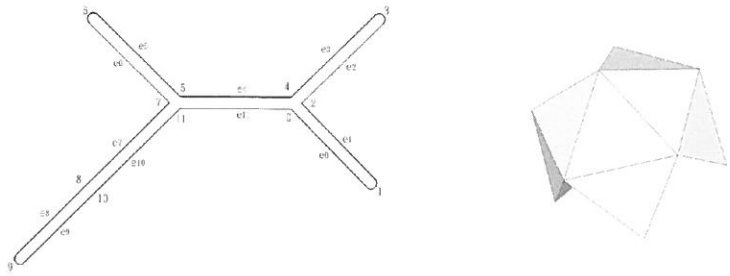

圖五：左黏接樹與模型

4.8.4. **右模型接路徑** $(e_0,e_1)(e_2,e_3)(e_4,e_{11})(e_5,e_8)\ (e_6,e_7)\ (e_9,e_{10})$

按照黏接路徑，我們可以依序畫出黏接樹，如圖六。5-9-11三角頂共點，其角度總合為180+180+180=540，有一個540/60=9秩。0-2-4三角頂共點，其角度總合為60+180+60=300，有一個300/60=5秩。有4個180°(3秩)轉折點，共有180x4=720，即4個3秩，以及6-8共點的角和為180+60=240，即一個240/60=4秩，總內角和為540+300+720+240=1800。

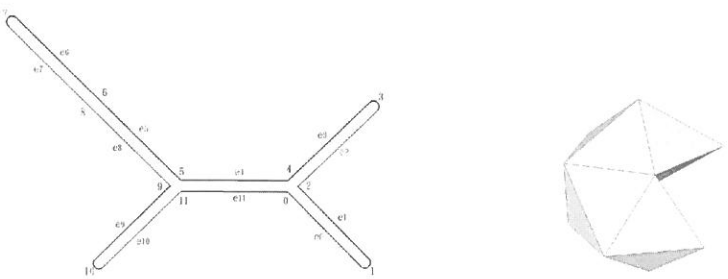

圖六：右黏接樹與模型

4.8.5. **左旋風車模型黏接路徑** $(e_0,e_1)(e_2,e_{11})(e_3,e_6)(e_4,e_5)(e_7,e_{10})(e_8,e_9)$

按照黏接路徑，我們可以依序畫出黏接樹，如圖七。3-7-11三角頂共點，其角度總合為180+180+180=540，有一個540/60=9秩。有3個180° (3秩)轉折點，共有180x3=540，即3個3秩，以及0-2、4-6與8-10共點的角和為(60+180)x3=720，即3個240/60=4秩，總內角和為540+540+720=1800。

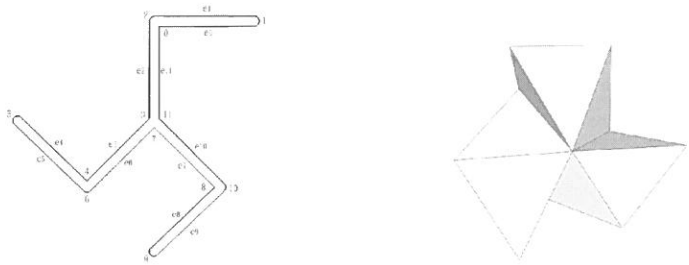

圖七：左旋風車黏接樹與模型

4.8.6. **右旋風車模型黏接路徑** $(e_0,e_9)(e_1,e_4)(e_2,e_3)(e_5,e_8)(e_6,e_7)(e_{10},e_{11})$

按照黏接路徑，我們可以依序畫出黏接樹，如圖八。1-5-9三角頂共點，其角度總合為180+180+180=540，有一個540/60=9秩。有3個180° (3秩)轉折點，共有180x3=540，即3個180/60=3秩，以及0-10、4-2與8-6共點的角和為(60+180)x3=720，即3個240/60=4秩，總內角和為540+540+720=1800。

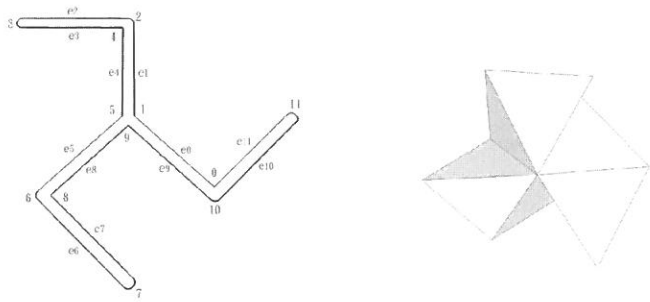

圖八：右旋風車黏接樹與模型

4.8.7. **右腿模型黏接路徑** $(e_0,e_1)(e_2,e_3)(e_4,e_5)(e_6,e_{11})(e_7,e_{10})(e_8,e_9)$

按照黏接路徑，我們可以依序畫出黏接樹，如圖九。0-2-4-6四角頂共點，其角度總合為60+180+60+180=480，有一個480/60=8秩。有4個180° (3秩)轉折點，共有180x4=720，即4個3秩，以及8-10與7-11共點的角和(60+180)+ 180x2 =600，分別為一個(60+180)/60=4秩與一個180x2/60=6秩，總內角和為480+720+600=1800。

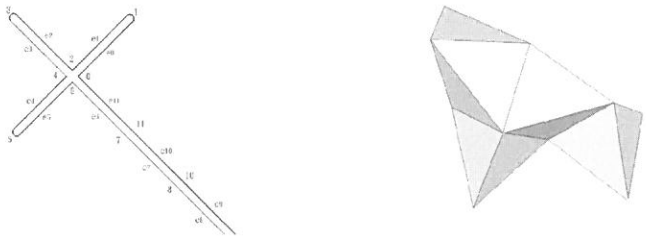

圖九：右腿黏接樹與模型

4.8.8. **左腿模型黏接路徑** $(e_0,e_1)(e_2,e_3)(e_4,e_9)(e_5,e_8)(e_6,e_7)(e_{10},e_{11})$

按照黏接路徑，我們可以依序畫出黏接樹，如圖十。0-2-4-10四角頂共點，其角度總合為60+180+60+180=480，有一個480/60=8秩。有4個180° (3秩)轉折點，共有180x4=720，即4個180/60=3秩，以及6-8與5-9共點的角和(60+180)+ 180x2 =600，分別為一個(60+180)/60=4秩與一個180x2/60=6秩，總內角和為480+720+600=1800。

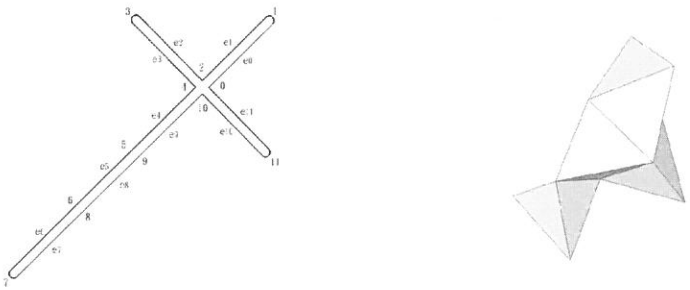

圖十：左腿黏接樹與模型

4.8.9. **鯨魚模型黏接路徑** $(e_0,e_1)(e_2,e_3)(e_4,e_{11})(e_5,e_{10})(e_6,e_7)(e_8,e_9)$

按照黏接路徑，我們可以依序畫出黏接樹，如圖十一。0-2-4與6-8-10兩個三角頂共點，其角度總合分別為60+180+60=300與180+60+180=420，各有一個300/60=5秩與一個420/60=7秩。有4個180° (3秩)轉折點，共有180x4=720，即4個180/60=3秩，以及5-11共點的角和為180x2=360，有一個360/60=6秩。總內角和為300+420+720+360=1800。

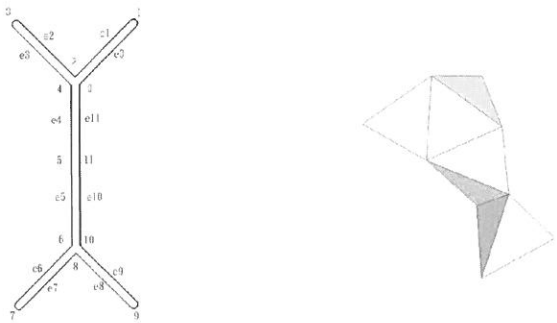

圖十一：鯨魚黏接樹與模型

4.8.10. **四面體模型黏接路徑** $(e_0,e_3)(e_1,e_2)(e_4,e_7)(e_5,e_6)(e_8,e_{11})(e_9,e_{10})$

按照黏接路徑，我們可以依序畫出黏接樹，如圖十二。0-4-8三角頂共點，其角度總合為60+60+60=180，有一個180/60=3秩。有3個180° (3秩)轉折點，共有180x3=540，即3個3秩，加上前面的一個3秩，總共有4個3秩。以及1-3、5-7與9-11共點的角和為180x2x3=1080，有3個360/60=6秩，總內角和為180+540+1080=1800。

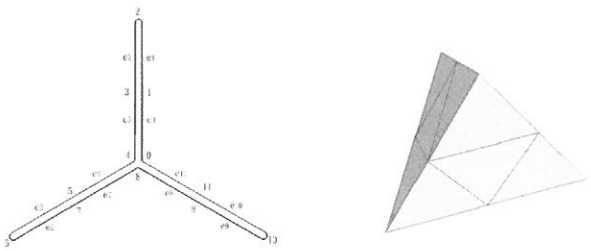

圖十二：四面體黏接樹與模型

4.8.11. **巧克力模型黏接路徑** $(e_0,e_1)(e_2,e_3)(e_4,e_7)(e_5,e_6)(e_8,e_{11})(e_9,e_{10})$

按照黏接路徑，我們可以依序畫出黏接樹，如圖十三。0-2-4-8四角頂共點，其角度總合為60+180+60+60=360，有一個360/60=6秩。有4個180° (3秩)轉折點，共有180x4=720，即4個3秩，以及5-7與9-11共點的角和為180x2x2=720，即2個180x2x2/60=6秩，加上前面的一個6秩，總共有3個6秩。總內角和為360+720+720=1800。

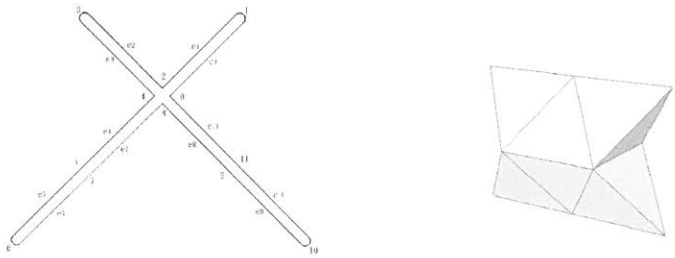

圖十三：巧克力黏接樹與模型

4.8.12. **飛船模型黏接路徑** $(e_0,e_1)(e_2,e_7)(e_3,e_6)(e_4,e_5)(e_8,e_{11})(e_9,e_{10})$

按照黏接路徑，我們可以依序畫出黏接樹，如圖十四。0-2-8三角頂共點，其角度總合為60+180+60=300，有一個300/60=5秩。有3個180° (3秩)轉折點，共有180x3=540，即3個3秩，以及3-7、4-6與9-11共點的角和為180x2+(60+180)+180x2=960，有一個(60+180)/60=4秩與有2個180x2/60=6秩，總內角和為300+540+960=1800。

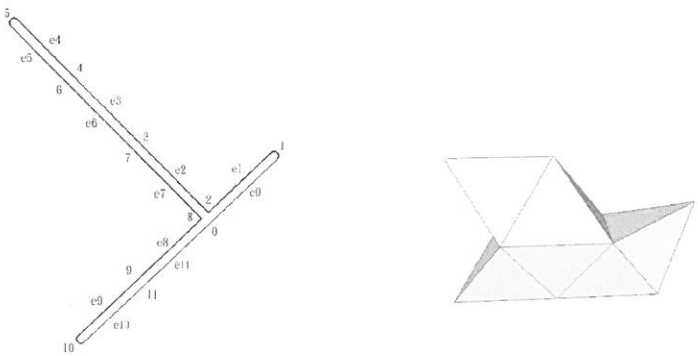

圖十四：飛船黏接樹與模型

4.8.13. **船模型黏接路徑** $(e_0,e_1)(e_2,e_{11})(e_3,e_{10})(e_4,e_9)(e_5,e_8)(e_6,e_7)$

按照黏接路徑，我們可以依序畫出黏接樹，如圖十五。0-2、4-10與8-6三對兩角頂共點，其角度總合為(60+180)x3=720，有三個240/60=4秩。有2個180°(3秩)轉折點，共有180x2=360，即2個180/60=3秩，以及5-7與3-11共點的角和為180x2x2=720，即2個180x2/60=6秩，總內角和為720+360+720=1800。三角紙積木黏貼與角頂數與秩數查核表，請參照表十二。

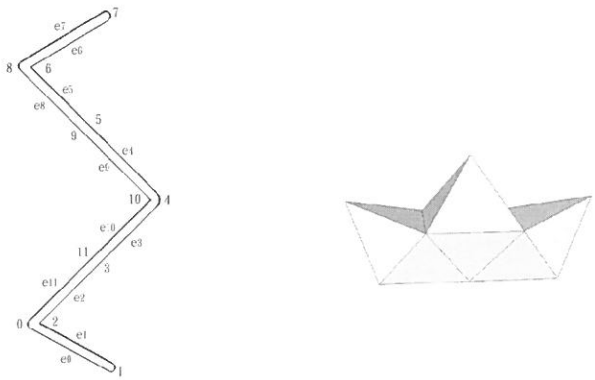

圖十五：船黏接樹與模型

表十二 三角紙積木黏貼與角頂數與秩數查核表

模型	匹配邊對	12	11	10	9	8	7	6	5	4	3	角數	秩數
風車	$(e_0,e_1)(e_2,e_3)(e_4,e_5)(e_6,e_7)(e_8,e_9)(e_{10},e_{11})$	1	0	0	0	0	0	0	0	0	6	7	30
飛機	$(e_0,e_1)(e_2,e_3)(e_4,e_5)(e_6,e_7)(e_8,e_9)(e_{10},e_{11})$	0	0	0	1	0	0	1	0	0	5	7	30
左	$(e_0,e_1)(e_2,e_3)(e_4,e_5)(e_6,e_7)(e_8,e_9)(e_{10},e_{11})$	0	0	0	1	0	0	0	1	1	4	7	30
右	$(e_0,e_1)(e_2,e_3)(e_4,e_5)(e_6,e_7)(e_8,e_9)(e_{10},e_{11})$	0	0	0	1	0	0	0	1	1	4	7	30
左旋風車	$(e_0,e_1)(e_2,e_3)(e_4,e_5)(e_6,e_7)(e_8,e_9)(e_{10},e_{11})$	0	0	0	1	0	0	0	0	3	3	7	30
右旋風車	$(e_0,e_1)(e_2,e_3)(e_4,e_5)(e_6,e_7)(e_8,e_9)(e_{10},e_{11})$	0	0	0	1	0	0	0	0	3	3	7	30
右腿	$(e_0,e_1)(e_2,e_3)(e_4,e_5)(e_6,e_7)(e_8,e_9)(e_{10},e_{11})$	0	0	0	0	1	0	1	0	1	4	7	30
左腿	$(e_0,e_1)(e_2,e_3)(e_4,e_5)(e_6,e_7)(e_8,e_9)(e_{10},e_{11})$	0	0	0	0	1	0	1	0	1	4	7	30
鯨魚	$(e_0,e_1)(e_2,e_3)(e_4,e_5)(e_6,e_7)(e_8,e_9)(e_{10},e_{11})$	0	0	0	0	0	1	1	1	0	4	7	30
四角體	$(e_0,e_1)(e_2,e_3)(e_4,e_5)(e_6,e_7)(e_8,e_9)(e_{10},e_{11})$	0	0	0	0	0	0	3	0	0	4	7	30

巧克力	$(e_0,e_1)(e_2,e_3)(e_4,e_5)(e_6,e_7)(e_8,e_9)(e_{10},e_{11})$	0	0	0	0	0	0	3	0	0	4	7	30
飛船	$(e_0,e_1)(e_2,e_3)(e_4,e_5)(e_6,e_7)(e_8,e_9)(e_{10},e_{11})$	0	0	0	0	0	0	2	1	1	3	7	30
船	$(e_0,e_1)(e_2,e_3)(e_4,e_5)(e_6,e_7)(e_8,e_9)(e_{10},e_{11})$	0	0	0	0	0	0	2	0	3	2	7	30

5. 討論與結論

我們以亞歷山大洛夫的三個條件中的第一條與第三條為基礎，藉用動態規劃的遞迴關係與列表式運算的技巧，不遺漏地搜尋出三角紙積木摺黏，可以建成13個三角面多面體。這些模型，雖然是非凸三角面多面體，但是均合乎亞歷山大洛夫三個條件中的第一條與第三條。特別是其中四面體、巧克力、飛船與船等4個模型的7個角頂的秩數不超過6個，換句話說，合乎亞歷山大洛夫的第二個條件-對於每個角頂的入射角和不多於2π，故，它們是滿足亞歷山大洛夫的三個條件的非凸三角面多面體。我們在表十二內，這4個模型列，特別使用灰底標示出來。值得一提的是，這些模型的總角數均是7，總秩數和為30。

這13個模型，均是從16面三角面多邊形(16-iamond)摺黏建成的16面非凸三角面多面體(nonconvex 16-deltahedra)。這些模型中，左模型與右模型的角秩從12秩數倒序至3秩的序列(0,0,0,1,0,0,0,1,1,4)相同。其他三對模型，如左旋風車與右旋風車模型的序列(0,0,0,1,0,0,0,0,3,3)、左腿與右腿模型的序列(0,0,0,0,1,0,1,0,1,4)以及四面體與巧克力模型的序列(0,0,0,0,0,0,3,0,0,4)。

同形的(isomorphic)模型，有6+5+3+5+4= 23個。風車、左旋風車、右旋風車與四面體等四個模型沒有同形模型，其主要原因是因為它們本身的對稱性。還有是左與右以及左腿與右腿，它們的同形模型數目是相等的。最後是飛船的同形模型數目為5個是所有模型當中最多的模型。我們分別將23個同形模型列出，如表十三 三角紙積木同形模型。

表十三 三角紙積木同形模型

模型	基本型匹配邊對	同型模型型匹配邊對
風車	$(e_0,e_1)(e_2,e_3)(e_4,e_5)(e_6,e_7)(e_8,e_9)(e_{10},e_{11})$	無
飛機	$(e_0,e_1)(e_2,e_3)(e_4,e_5)(e_6,e_7)(e_8,e_9)(e_{10},e_{11})$	$(e_0,e_1)(e_2,e_3)(e_4,e_5)(e_6,e_7)(e_8,e_9)(e_{10},e_{11})$
		$(e_0,e_1)(e_2,e_3)(e_4,e_5)(e_6,e_7)(e_8,e_9)(e_{10},e_{11})$

左	$(e_0,e_1)(e_2,e_3)(e_4,e_5)(e_6,e_7)(e_8,e_9)(e_{10},e_{11})$	$(e_0,e_1)(e_2,e_3)(e_4,e_5)(e_6,e_7)(e_8,e_9)(e_{10},e_{11})$
		$(e_0,e_1)(e_2,e_3)(e_4,e_5)(e_6,e_7)(e_8,e_9)(e_{10},e_{11})$
		$(e_0,e_1)(e_2,e_3)(e_4,e_5)(e_6,e_7)(e_8,e_9)(e_{10},e_{11})$
右	$(e_0,e_1)(e_2,e_3)(e_4,e_5)(e_6,e_7)(e_8,e_9)(e_{10},e_{11})$	$(e_0,e_1)(e_2,e_3)(e_4,e_5)(e_6,e_7)(e_8,e_9)(e_{10},e_{11})$
		$(e_0,e_1)(e_2,e_3)(e_4,e_5)(e_6,e_7)(e_8,e_9)(e_{10},e_{11})$
		$(e_0,e_1)(e_2,e_3)(e_4,e_5)(e_6,e_7)(e_8,e_9)(e_{10},e_{11})$
左旋風車	$(e_0,e_1)(e_2,e_3)(e_4,e_5)(e_6,e_7)(e_8,e_9)(e_{10},e_{11})$	無
右旋風車	$(e_0,e_1)(e_2,e_3)(e_4,e_5)(e_6,e_7)(e_8,e_9)(e_{10},e_{11})$	無
右腿	$(e_0,e_1)(e_2,e_3)(e_4,e_5)(e_6,e_7)(e_8,e_9)(e_{10},e_{11})$	$(e_0,e_1)(e_2,e_3)(e_4,e_5)(e_6,e_7)(e_8,e_9)(e_{10},e_{11})$
		$(e_0,e_1)(e_2,e_3)(e_4,e_5)(e_6,e_7)(e_8,e_9)(e_{10},e_{11})$
左腿	$(e_0,e_1)(e_2,e_3)(e_4,e_5)(e_6,e_7)(e_8,e_9)(e_{10},e_{11})$	$(e_0,e_1)(e_2,e_3)(e_4,e_5)(e_6,e_7)(e_8,e_9)(e_{10},e_{11})$
		$(e_0,e_1)(e_2,e_3)(e_4,e_5)(e_6,e_7)(e_8,e_9)(e_{10},e_{11})$
鯨魚	$(e_0,e_1)(e_2,e_3)(e_4,e_5)(e_6,e_7)(e_8,e_9)(e_{10},e_{11})$	$(e_0,e_1)(e_2,e_3)(e_4,e_5)(e_6,e_7)(e_8,e_9)(e_{10},e_{11})$
		$(e_0,e_1)(e_2,e_3)(e_4,e_5)(e_6,e_7)(e_8,e_9)(e_{10},e_{11})$
四面體	$(e_0,e_1)(e_2,e_3)(e_4,e_5)(e_6,e_7)(e_8,e_9)(e_{10},e_{11})$	無
巧克力	$(e_0,e_1)(e_2,e_3)(e_4,e_5)(e_6,e_7)(e_8,e_9)(e_{10},e_{11})$	$(e_0,e_1)(e_2,e_3)(e_4,e_5)(e_6,e_7)(e_8,e_9)(e_{10},e_{11})$
		$(e_0,e_1)(e_2,e_3)(e_4,e_5)(e_6,e_7)(e_8,e_9)(e_{10},e_{11})$
飛船	$(e_0,e_1)(e_2,e_3)(e_4,e_5)(e_6,e_7)(e_8,e_9)(e_{10},e_{11})$	$(e_0,e_1)(e_2,e_3)(e_4,e_5)(e_6,e_7)(e_8,e_9)(e_{10},e_{11})$
		$(e_0,e_1)(e_2,e_3)(e_4,e_5)(e_6,e_7)(e_8,e_9)(e_{10},e_{11})$
		$(e_0,e_1)(e_2,e_3)(e_4,e_5)(e_6,e_7)(e_8,e_9)(e_{10},e_{11})$
		$(e_0,e_1)(e_2,e_3)(e_4,e_5)(e_6,e_7)(e_8,e_9)(e_{10},e_{11})$
		$(e_0,e_1)(e_2,e_3)(e_4,e_5)(e_6,e_7)(e_8,e_9)(e_{10},e_{11})$
船	$(e_0,e_1)(e_2,e_3)(e_4,e_5)(e_6,e_7)(e_8,e_9)(e_{10},e_{11})$	$(e_0,e_1)(e_2,e_3)(e_4,e_5)(e_6,e_7)(e_8,e_9)(e_{10},e_{11})$
		$(e_0,e_1)(e_2,e_3)(e_4,e_5)(e_6,e_7)(e_8,e_9)(e_{10},e_{11})$

除了以上23個同形模型，這些16面非凸三角面多面體基本型，可以產生無數的衍生型。諸如四面體基本型的四個3秩角頂，分別或不同的組合地壓縮進入四面體(1,1,1,1)的體內，可以建成壓縮一型(0,1,1,1)、壓縮二型(0,0,1,1)、壓縮三型(0,0,0,1)與壓縮四型(0,0,0,0) 等4個衍生型。其他的基本型，也可以產生無數的衍生型。這些衍生型有一個共同點，就是它們與其對應的基本型為同胚(homeomorphic)。

6. 誌謝與未來研究工作

動態規劃演算法的計算，沒有實體模型查核，一定會發生錯誤的。我們要感謝亞洲大學資訊工程學系四年級的陳泰有、侯保丞、張皓淵、陳佑任、林梓平、洪維澤、柯昆廷等七位大學部專題研究生努力地趕製模型，以及負責使用SketchUp畫三角紙積木3D模型。我們未來的工作，將是拿破崙紙積木與非零虧格數三角面多面體基本型存在性與獨特性的研究。

參考文獻

[1] Freudenthal, H. and van der Waerden, B. L. (1947) "On an Assertion of Euclid." Simon Stevin 25, 115-121, 1947.

[2] Lu, Keh-Ming, Tsaur, Alan S, and Chen Mei-Fan (2006),"A Study of Napoleon Paper Building Blocks", Fu Ren Studies (Science and Engineering), Taipei: Fu Ren Catholic University, College of Science and Engineering, Vol. 40, pp. 39-70.

[3] Lu, Keh-Ming and Tsaur, Alan S (2007),"Napoleon Lanterns and Genus", Fu Ren Studies (Science and Engineering), Taipei: Fu Ren Catholic University, College of Science and Engineering, Vol. 41, pp. 71-104.

[4] Lu, Keh-Ming, Tsaur, Alan S, and Chuang, Feng-Tse, (2008), "Triblock Origami Spheroid Workshops", Bridges 2008, July 24-26, 2008.

[5] Lubiw, Anna and O'Rourke, Joseph, (1996), "When Can a Polygon Fold a Polytope?" Technical Report048, Department of Computer Science, Smith Colledge, Northampton, MA,June 1996. Presented at Am. Math. Soc.Conf.,5 October 1996.

[6] O'Rourke, Joseph, (2007),"Folding Polygons to Convex Polyhedra", http://citeseerx.ist.psu.edu/viewdoc/download?doi=10.1.1.89.9845 &rep=rep1 &type=pdf

[7] Pogorelov, A. V. (1952). "Quasi-geodesic lines on a convex surface." Mat. Sb. 25(62):275-306, 1949. English transl., Amer. Math. Soc. Transl. 74, 1952.

[8] Sloane N. J. A. and Plouffe, Simon, (1995).The Encyclopedia of Integer Sequences, Academic Press, 1995 (includes this sequence).

[9] Trigg, C. (1978). An Infinite Class of Deltahedra, Mathematics Magazine, 51 (January 1978) 55-57.

[10] Whiteley, W. (1994) "How to describe or design a polyhedron." J. Intell. Robeotic Systems. 11:135-160, 1994

[11] Erik Demaine教授網站http://courses.csail.mit.edu/6.885/fall07/lectures/

Received October 31 ,2009
Revised December 23 ,2009
Accepted December 31 ,2009

Folding Polyiamonds to Nonconvex Deltahedra

Keh-Ming Lu, Chi-Feng Chen and Wen-Tsang Chang

Abstract

Napoleon paper building blocks were comprised of Bowtie, Teardrop, Wing, Bar, Boat, Star, Chevron, and Carp basic models as well as derivative models. Having attached the modules built by 24 units of the same models of building, we developed cage-like models. We need find the answers for the questions: whether there exist any more basic models? Whether the derivative models are topological copies of basic models? Should they be counted as basic models? To respond these issues, Cauchy and Alexandrov answered the existence and uniqueness of polytopes. We will then extend these theorems from the ploytopes to the nonconvex 16-deltahedra. Applying dynamic programming, we will find 13 basic models and these basic models are deduced into other derivative models.

Before exploring the number of the nonconvex 16-deltahedra, we will introduce the theorems of polytopes and discuss the extension issues of folding polyiamonds to the nonconvex deltahedra. We then resolve the problems by using dynamic programming folding 16-iamond to 16-deltahedron. We will perform the further studies on folding the 32-iamond to the Napoleon paper building blocks.

Key Words : Folding, Polyiamonds, Nonconvex Deltahedra, Polytope, Unfolding, Cauchy's Rigidity Theorem , Alexandrov's Uniqueness Theorem, Dynamic Programming, Homeomorphic, Gluing tree